

**Experimental Fabrication and Characterisation  
of Textile Metamaterial Structures  
for Microwave Applications**

**Berit Greinke**

b.greinke@qmul.ac.uk

Submitted in partial fulfilment  
of the requirements of the  
Degree of Doctor of Philosophy

Queen Mary University of London

November, 2016

## Statement of Originality

I, Berit Greinke, confirm that the research included within this thesis is my own work or that where it has been carried out in collaboration with, or supported by others, that this is duly acknowledged. Previously published material is also acknowledged below. I attest that I have exercised reasonable care to ensure that the work is original, and does not to the best of my knowledge break any UK law, infringe any third party's copyright or other Intellectual Property Right, or contain any confidential material. I accept that the College has the right to use plagiarism detection software to check the electronic version of the thesis. I confirm that this thesis has not been previously submitted for the award of a degree by this or any other university.

The copyright of this thesis rests with the author and no quotation from it or information derived from it may be published without the prior written consent of the author.

Signature:

Date:

### Details of collaboration and publications:

- Greinke, B., Candotti, M., Alomainy, A., & Parini, C. (2013). Parameters Extraction of Three-Dimensional Structures for Graded Textile Cloaking Materials. In *Loughborough Antennas & Propagation Conference (LAPC)* (pp. 7–10). Loughborough, UK.
- Greinke, B., Alomainy, A., & Parini, C. G. (2014). Towards Meta-textiles with a Negative Refractive Index. In *Proceedings of Ambience'14 & 10i3m*. Tampere, Finland
- Greinke, B., Alomainy, A., & Parini, C. G. (2014). Meta-textiles: An experimental “material-preferential” approach for prototyping electromagnetic periodic textile surfaces. In *Proceedings of Transition: Re-thinking Textiles and Surfaces*. Huddersfield, UK.

## **Abstract**

This thesis presents an investigation of fabrication technologies and electromagnetic characterisation of textile metamaterials in the microwave frequency range. Interdisciplinary in nature, the work bridges textile design practice and electromagnetic engineering. The particular ambition was to explore a number of surface techniques prevalent in the textile design field, and map their suitability for the construction of metatextiles for microwave operation.

Two different classes of metatextiles, all-dielectric and dielectric with electrically conductive patterns, were examined.

First, five structures of all-dielectric textiles and papers are reported; three textiles with graded embroidered and screen printed patterns, and two papers embellished with regular and irregular laser cut patterns. Permittivities for these materials were measured in a purpose-built test chamber and shown to be similar to permittivity ranges exhibited by solid discrete metamaterial cells previously reported in the scientific literature. Importantly these metatextiles were realised within one textile surface and one fabrication process, bypassing the need to assemble large numbers of isotropic material cells. This reveals the potential for rapid and low-cost manufacture of graded textile materials to produce anisotropic ground plane cloaks.

Secondly, three studies are presented that examine the use of electrically conductive patterned textile materials in the design of metatextiles which exhibit negative refractive index over a narrow frequency band. A range of e-textile (electronic textile) fabrication technologies were explored to assess their suitability for prototyping splitting and wire arrays, resonating in a narrow region between 3 - 10 GHz. Designs utilised a repeated unit cell pattern on a two-dimensional textile surface and were subsequently pleated into the required three-dimensional structure. A small negative refractive index was achieved for an embroidered prototype at 4.9 GHz, and two 'printed and plated' prototypes at, 7.5 GHz and 9.5 GHz respectively.

In summary the thesis demonstrates a set of guidelines for the fabrication of textile metamaterials for microwave frequencies, derived through a practice-led and interdisciplinary method based on material experimentation.

## **Acknowledgements**

I would very much like to thank my primary supervisor Prof. Clive G. Parini for the unique opportunity to undertake this research and, in particular, for his continued advice, positive and sustained support and excellent guidance throughout my Ph.D.

I also offer my gratitude to my second supervisor Dr. Akram Alomainy and annual review examiner Dr. Sara Robertson for their feedback and advice along the way.

Thanks go to Ho Huen and Dr. Massimo Candotti for their invaluable enthusiasm and support with the fabrication, measurement and documentation of the textiles.

Thanks to my colleagues and friends for their support and encouragement: Richard Kelly, Nanda Khaorapapong, Sam Duffy, Doon MacDonald, Pollie Barden, and Jonathan Winfield. Thank you to my colleagues in the Antennas & Electromagnetics group, for patiently and capably sharing their knowledge. Thanks also to Sam Duffy for proofreading this thesis for the purposes of spelling and grammar.

Finally, I would especially like to thank my family and dearest for their endless support, patience and encouragement along my way.

This work is supported by the Media and Arts Technology programme, EPSRC Doctoral Training Centre EP/G03723X/1.

# Table of Contents

<b>List of Figures .....</b>	<b>11</b>
<b>List of Tables .....</b>	<b>22</b>
<b>1 Introduction .....</b>	<b>23</b>
1.1 Motivation and Aims.....	23
1.2 Structure of the Thesis.....	24
1.3 Contributions of the Thesis .....	25
<b>2 Background.....</b>	<b>27</b>
2.1 Electromagnetic Metamaterials .....	28
2.1.1 Seminal Publications.....	28
2.1.2 Transformation Optics as a Design Tool .....	30
2.1.3 Negative Refractive Index Metamaterials .....	31
2.1.4 Dielectric Metamaterials.....	38
2.1.5 Textile Metamaterials .....	40
2.2 Electromagnetic Textiles.....	43
2.2.1 Electromagnetic Engineering.....	44
2.2.2 E-Textile Design .....	49
2.3 Summary and Implications.....	50
<b>3 Design Methodology .....</b>	<b>53</b>
3.1 Material-based Design.....	54
3.2 Skills Advancement.....	60
3.3 Analytical Measures .....	61
3.4 Conclusions .....	63
<b>4 Material Parameter Identification .....</b>	<b>66</b>
4.1 Material Property Overview .....	66
4.1.1 Relative Permittivity .....	67
4.1.2 Dielectric Loss .....	68

4.1.3	Relative Permeability.....	68
4.1.4	Refractive Index.....	69
4.1.5	Impedance.....	70
4.2	Scattering Parameters.....	70
4.3	Material Parameter Retrieval.....	73
4.3.1	Parameter Extraction from S-parameters.....	73
4.3.2	Parameter Extraction from Capacitance.....	74
4.3.3	Refractive Index Extraction from Transmission Phase Data.....	74
4.4	Discussion.....	74
<b>5</b>	<b>Material as Structural Form.....</b>	<b>77</b>
5.1	Material Geometry.....	77
5.1.1	Scale.....	78
5.1.2	Two-dimensional Surface Pattern.....	80
5.1.3	Three-dimensional Architecture.....	82
5.2	Material Performance.....	83
5.2.1	Effective Medium Theory.....	83
5.2.2	Dielectrics.....	84
5.2.3	Composites.....	85
5.2.4	Periodic Structures and Repeat Patterns.....	86
5.2.5	Resonating Surfaces.....	86
5.2.6	Artificial Dielectrics.....	87
5.2.7	Functional Directivity.....	89
5.2.8	Graded Materials.....	90
5.3	Conclusion.....	91
<b>6</b>	<b>Materials, Fabrication Techniques and Experimental Analysis.....</b>	<b>93</b>
6.1	Introduction and Objectives.....	93
6.2	Materials.....	94
6.2.1	Fabric Substrates.....	94
6.2.2	Conductive Fabrics.....	96
6.2.3	Paper and Films.....	96
6.2.4	Adhesive ('Iron-on') and Stabiliser Fabrics.....	98
6.2.5	Embroidery Threads.....	98

6.2.6	Conductive Embroidery Threads .....	98
6.2.7	Dielectric Printing Inks .....	99
6.2.8	Conductive Printing Inks .....	99
6.2.9	Resists .....	100
6.2.10	Other Materials .....	100
6.3	Surface Design Techniques .....	100
6.3.1	Digital Embroidery .....	100
6.3.2	Screen Printing .....	104
6.3.3	Vacuum Deposition .....	106
6.3.4	Inkjet Printing .....	107
6.3.5	Off-site Fabrication: 'Print and Etch' .....	108
6.3.6	Chemical Etching .....	109
6.3.7	Laser Engraving .....	110
6.3.8	Silver Leafing .....	111
6.3.9	Assembly: Pleating and Heat Bonding .....	111
6.4	Measurements of S-Parameters of Textile Samples .....	112
6.4.1	Mechanical and Electrical Evaluation .....	113
6.4.2	Waveguide Measurements .....	113
6.4.3	Free Space .....	115
6.4.4	Parallel Plate Capacitance .....	121
6.4.5	Discussion .....	123
6.5	Numerical Modelling .....	125
6.5.1	Unit Cells, Periodic Structures and Perfect Boundary Conditions in CST .....	125
6.6	Material Parameter Retrieval .....	127
6.6.1	Agilent 85071E Material Measurement Software .....	127
6.6.2	Nicolson-Ross-Weir Algorithm .....	128
6.6.3	Refractive Index Retrieval with Transmission Phase Results .....	129
6.7	Summary .....	129
<b>7</b>	<b>Dielectric Textiles .....</b>	<b>131</b>
7.1	Introduction and Objectives .....	131
7.2	Manipulating Dielectric Properties of Textiles .....	133
7.3	Study 1: Embroidered Dielectric Textiles .....	135

7.3.1	Two-dimensional Embroidered Textiles with Graded Permittivity .....	135
7.3.2	Three-dimensional Embroidered Textiles with Graded Permittivity.....	137
7.4	Study 2: Screen Printed Dielectric Textile .....	148
7.4.1	Two-dimensional Screen Printed Textile with Graded Permittivity .....	148
7.5	Study 3: Patterned Paper Cut-outs.....	150
7.5.1	Two-dimensional Symmetric and Randomised Patterns .....	150
7.6	Conclusion.....	154
<b>8</b>	<b>Negative Refractive Index Textiles .....</b>	<b>157</b>
8.1	Introduction and Objectives .....	157
8.2	Textile Unit Cell.....	158
8.3	Study 1: Applying Resonator Arrays to Textile Substrates .....	163
8.3.1	Screen Printing.....	164
8.3.2	Vacuum Deposition .....	165
8.3.3	Ink-jet Printed Silver Ink with Nanoparticles .....	168
8.3.4	Chemical Etching.....	169
8.3.5	Laser Engraving .....	171
8.3.6	Digital Embroidery .....	172
8.3.7	Silver Leafing .....	173
8.3.8	Summary .....	175
8.4	Study 2: Pleated Prototypes to Study Single-layer Transmission Behaviour ....	176
8.4.1	Milled FR-4 Circuit Boards for Comparative Analysis.....	176
8.4.2	Screen printed and Pleated Paper and Fabric.....	178
8.4.3	Laser Engraved and Pleated Cotton.....	181
8.4.4	Embroidered and Pleated Cotton .....	183
8.4.5	Summary .....	185
8.5	Study 3: Negative Refractive Index Textiles .....	186
8.5.1	Printed Circuit Boards for Comparative Analysis .....	186
8.5.2	Embroidered Cotton and Polyester Fabric.....	188
8.5.3	Printed and Plated Polycarbonate Woven Fabric (PEL).....	189
8.5.4	Summary .....	194
8.6	Conclusion.....	194



<b>9</b>	<b>Conclusions and Future Work</b> .....	<b>198</b>
9.1	Overview .....	198
9.2	Research Findings .....	199
9.2.1	All-dielectric Graded Materials .....	200
9.2.2	Negative Refractive Index Textile Metamaterials .....	202
9.2.3	Measurement and Analysis.....	202
9.3	Design Methodology and Interdisciplinary Contribution .....	203
9.4	Future Work .....	204
9.4.1	Optimisation of Textiles .....	204
9.4.2	Accessible Computational Tools .....	205
9.4.3	Design Scenarios.....	206
9.5	Closing Remark.....	208
	<b>References</b> .....	<b>209</b>
	<b>Appendix A</b> .....	<b>224</b>
A.1	Publications .....	224
A.2	Workshops and Outreach.....	225
	<b>Appendix B</b> .....	<b>227</b>
B.1	Definitions of Metamaterial.....	227
	<b>Appendix C</b> .....	<b>231</b>
C.1	Material Resources .....	231
C.2	Datasheets.....	236
	<b>Appendix D</b> .....	<b>244</b>
D.1	Index of Samples .....	244
	<b>Appendix E</b> .....	<b>266</b>
E.1	Anechoic Chamber Design Documentation .....	266
	<b>Appendix F</b> .....	<b>273</b>
F.1	Conceptual Drawings of Cloaking Mechanisms.....	273

<b>Appendix G .....</b>	<b>276</b>
G.1 Conceptual Samples for the Purpose of Illustration .....	276
<b>Appendix H .....</b>	<b>280</b>
H.1 Agilent 85071E Materials Measurement Software: Technical Overview.....	280

## List of Figures

Figure 2.1: (a) Positive refractive index as occurring in natural materials (b) Negative refractive index as predicted by Veselago (1968). .....	28
Figure 2.2: Flat lens using a slab of left-handed substance, thickness $d$ , as suggested by Veselago (1968). .....	28
Figure 2.3: The path of the wave in A is diverted, by distortion of the coordinate system as in B (Pendry et al., 2006). .....	30
Figure 2.4: Illustration of the invisibility cloak as proposed by Pendry (2006). (a) A two-dimensional cross section, with radius of the cloaked area ( $R_1$ ) and radius of cloak ( $R_2$ ). (b) Depiction of the cloak as 3D view. ....	31
Figure 2.5: First prototype for a metamaterial with a negative refractive index, resonating frequency 4.2-4.8 GHz. (Smith, Padilla, Vier, Nemat-Nasser, et al., 2000) .....	31
Figure 2.6: Second publication of a negative-refractive-index metamaterial (NIM) (Shelby, Smith, & Schultz, 2001; Smith, Padilla, Vier, Shelby, et al., 2000). (a) Material wedge to demonstrate NIM behaviour (b) Close-up of three- dimensional SRR and wire medium (c) Measurement demonstrates negative region of refractive index between 10.2 – 10.8 GHz (black dotted), corresponding to theory (red), and in contrast to Teflon that exhibits a positive refractive index (blue). .....	32
Figure 2.7: (a) and (b) Bulk metamaterial with omega-shaped inclusions. (c) Both real parts of permittivity and permeability are below 0 around 13.2 GHz (Lheurette et al., 2008). .....	33
Figure 2.8: First example of NIM for near-optical frequencies, using a nano-rod structure (Shalaev et al., 2005) (a) schematic of parallel nanorods, (b) image with dimensions (c) negative real part of refractive index ( $n'$ ) demonstrated at around 210 – 270 THz .....	34
Figure 2.9: Near-infrared NIM made from a sandwich structure of two perforated silver films and a ceramic dielectric (Shuang Zhang, Fan, Panoiu, et al., 2005). (a) Schematic of the structure. For this given polarisation and propagation direction, the regions acting in the E-field are marked black, regions acting in	

the H-field are marked hatched. (b) SEM picture of the structure	
(c) Refractive index retrieved from measurement and simulation shows a negative region at around 150 THz. ....	34
Figure 2.10: Fishnet structure for optical frequencies (Dolling et al., 2006)	
(a) Structural unit cell (b) Microscopic view (c) Retrieved permittivity, permeability and refractive index $n$ (solid lines = $n'$ , dashed lines = $n''$ ). ....	35
Figure 2.11: (Valentine et al., 2008): (a) Schematic and (b) SEM image of fishnet structure, fabricated from multiple layers of silver and magnesium fluoride ( $MgF_2$ ). (c) Region of negative refractive index for simulation (black line) and measurement (circles). ....	
	35
Figure 2.12: Distribution of field around perturbation and cloak (a) Simulation with cloak (b) Experiment without cloak (c) Experiment with cloak. (Averitt, 2013) .....	
	36
Figure 2.13: First invisibility cloak, hiding a circular region in the centre at 8.5 GHz (Schurig et al., 2006). (a) Fabricated cloak with illustrated wave path (b) View of the measurement set up with cutout for illustration purpose. Microwaves are introduced with a waveguide; absorbers placed around represent free space. An antenna probe fixed to the upper plate records the field. ....	
	37
Figure 2.14: Real part of the electric field with an indication of direction of the wave path (black lines) from left to right. (a) Simulation of ideal cloak at frequency of 8.5 GHz (b) Simulation of cloak considering real-life factors such as reduced number of cells. (c) Measurement of uncloaked copper structure. (d) Measurement of cloaked copper structure. ....	
	37
Figure 2.15: First experimental verification of a ground plane cloak (Liu et al., 2009). (a) Cloak with indicated element size distribution. (b) Varying index of $n$ in relation to inclusion geometry. ....	
	38
Figure 2.16: Measured E-field at 14 GHz of (a) incident on ground plane without cloak, (b) incident on uncloaked metal perturbation, (c) incident on cloaked perturbation, showing strong resemblance to the reflection on the ground plane. ....	
	38

Figure 2.17: (a) 3D printed binary cloak (Urzhumov et al., 2013). (b) E-field distribution at 9.9 GHz as measured (top) and simulated (bottom), showing a low loss undisturbed field. ....	39
Figure 2.18: Key features related to the wearable antenna design process, adapted from Salonen & Rahmat-Samii (2006). Qualities which have been considered in this thesis are marked in blue. ....	45
Figure 2.19: Illustration of an integrated approach to metamaterial research promoting interdeisciplinary knowledge exchange. ....	52
Figure 3.1: The interdependance of the four factors of product design, which equally contribute to proposed design solutions (Ashby, 1999). ....	54
Figure 3.2: New materials are commonly developed in labs first, then processed by material suppliers, and only in the last step used in design (Ashby, 2010). ....	57
Figure 3.3: An illustration of material-based design using development of an NIM metatextile as an example. ....	59
Figure 4.1: Refractive index. ....	69
Figure 4.2 : Magnitude (amplitude) and phase of an electromagnetic wave. ....	71
Figure 4.3: S-parameter matrix in two-port network. ....	71
Figure 5.1: Illustration showing comparisons of sizes with matching scales (Addington & Schodek, 2005). ....	78
Figure 5.2: The electromagnetic spectrum. While the human eye can only perceive the small spectrum of ‘visible light’ (430–790 THz), electromagnetic devices are designed for specific frequency bands located in various parts of the spectrum. ....	80
Figure 5.3: Simple woven coil for textile loudspeaker. ....	81
Figure 5.4: Dynamic colour pattern enabled by e-textiles and thermochromic dyes (Calder, 2014). ....	82
Figure 5.5: Kock’s lightweight lenses. a) Copper foil disks on polystyrene, b) metal spraying on polystyrene sheets, c) conductive spheres mounted on insulated rods, d) steel balls mounted on polystyrene board. ....	88

Figure 5.6: Fashion designer Kunihiro Morinaga’s collection ‘Focus’ reflects conceptually on the use of electromagnetic shielding and frequency selective bandwidth patterns (Morinaga, 2013).....	89
Figure 5.7: Patented FSS wallpaper, printed with silver ink to block out WiFi signals (De Barros, Eymin-Petot-Tourtollet, Lemaitre-Auger, & Vuong, 2011). .....	89
Figure 6.1: Sashiko fire fighter uniform, c. 1870. Reinforced and decorative embroidery.....	101
Figure 6.2: Lockstitch technique for embroidery.....	102
Figure 6.3: Embroidery tests with conductive threads, with complete samples on the left, and detail on the right. (a) Statex thread, tests for thread tension, embedding into surrounding thread to maintain shape geometry (b) Front of embroidery shows the overlay of threads occurring. Tests to find stitching path that allows later separation of shapes. (c) Small sample of stitched SRR with Liberator thread, after separation of shapes.....	103
Figure 6.4: Vacuum deposition chamber .....	107
Figure 6.5: First test of vacuum deposition on polyester sample resulted in high conductivity. (a) Sample c.8x5 cm (b) Detail.....	107
Figure 6.6: Inkjet printed silver traces with circuit stickers (Hodges et al., 2014). .....	108
Figure 6.7: An example of Neltex® fabric by PEL. ....	109
Figure 6.8: (a) Accordion pleat (b) Box pleat (c) U-fold, as used to design three-dimensional NIMs from one piece of flat textile.....	112
Figure 6.9: For measuring thickness, a digital handheld micrometer was used. The probe has a diameter of 5 mm. ....	113
Figure 6.10: Measurement set up with waveguides, The material under test (MUT) is locked in between the two openings of the waveguides. A vector network analyse (VNA) is used to record the s-parameters. ....	114
Figure 6.11: Permittivity retrieved from measured s-parameters in waveguide (blue) and free space (red) set ups.....	114
Figure 6.12: Free space measurements. The material under test (MUT) is fixed in between the two opening of the horn antennas.....	115

Figure 6.13: The boundary of the far field is determined by the Fraunhofer Distance, and describes the distance at which the wave front behaves like a plane wave. The radiation pattern in the far field does not change shape. ....	116
Figure 6.14: Custom-built anechoic chamber, to measure samples with graded permittivity in a free space set up. Horn antennas for either X band (8.2 – 12.4 GHz) or wideband horn antennas (c. 4 – 16 GHz) can be installed. ....	117
Figure 6.15: FR-4 measurement results from measurement in the free space chamber. Agilent Materials Software was used for retrieval, applying the NIST algorithm. While permittivity results are smooth and comply with values given in the data sheet ( $\epsilon = 4.8$ at 1 MHz), dielectric losses are inconsistent. ....	119
Figure 6.16: Measurements of viscose felt, polycotton and card in the free space chamber. Retrieval of permittivity and dielectric losses show that, while permittivity results are sufficiently smooth, inconsistencies in dielectric loss results become less reliable with thinner materials. ....	120
Figure 6.17: A typical parallel plate capacitor configuration. ....	121
Figure 6.18: Test fixture Agilent 16451B. ....	122
Figure 6.19: FR-4 results, Parallel Plate capacitance method, 50Hz – 5MHz. ....	123
Figure 6.20: Polycotton results, Parallel Plate capacitance method, 50Hz – 5MHz. ....	123
Figure 6.21: A typical set up a unit cell with a shifted phase offset. Material is repeated in Y and Z direction. (a) Propagation direction is X, electric field (E-field) is Y direction and magnetic field (H-field) in Z direction. (b) The infinite array is set up in x and y direction. ....	127
Figure 6.22: Partitioning into tetrahedrons for meshing. ....	127
Figure 7.1: All-dielectric cloak by Bao (2012). (a) High resolution map of permittivity blocks (b) Lower resolution map (c) Fabricated cloak from BaTiO <sub>3</sub> blocks. ....	132
Figure 7.2: Manipulation of permittivity of woven textile. (a) 75% fibre, 25% air (b) 88.8% fibre, 11.1% air (c) 75% fibre soaked with ink, 25% ink. ....	133
Figure 7.3: Two ways of designing graded patterns. (a) Dot matrix with varying unit size. (b) Pattern with one-directional scaling factor. ....	134
Figure 7.4: Sample 1 with a length of 360 mm. Complete design as a vector graphic. ....	135

Figure 7.5: Results of Sample 1: dielectric two-dimensional embroidery with increasing line density. (a) Permittivity range measured, with red line showing least dense end, and blue line showing most dense end of the sample. (b) Loss tangent measured, with red line showing least dense end, and blue line showing most dense end of the sample. (c) Permittivity range measured at 11 GHz. Permittivity gradients over length of the sample, experimental results.....	136
Figure 7.6: Illustration of Sample 2 as a vector graphic. Circles show the five regions, which were stitched separately for electromagnetic analysis (Figure 7.7).....	139
Figure 7.7: Sample 2: Five stitched disks that represent five regions of the graded sample. Disks were used for capacity measurements in the parallel plate set up. Five larger tiles (120 x 120mm) with the same stitch densities, not shown in the figure, were used for free space measurements. ....	139
Figure 7.8: Embroidered Sample 2. (a) Loosely folded (~45°). (b) Tightly folded (~170°).....	140
Figure 7.9: (a)-(b) Parallel plate measurements for disks of Sample 2. (c)-(d) Free space measurements for tiles of Sample 2. ....	141
Figure 7.10: Gradient Sample 2. (a) Permittivity gradient and (b) dielectric loss, plotted against stitch density.....	141
Figure 7.11: Shape experimentation utilising ‘smocking’, Sample 2.....	142
Figure 7.12: Sample 3: Illustration of embroidery with locations of five sections (see Figure 7.13) which were measured as disks and tiles.....	143
Figure 7.13: Sample 3: Five stitched disks that represent five regions of the graded sample. Disks were used for capacity measurements in parallel plate set up. Two larger tiles (120 x 120mm) with the same stitch densities, not shown in the figure, were used for free space measurements. ....	144
Figure 7.14: Results of Sample 3 (a-b) Parallel plate measurements for disks (c-d) Free space measurements for tiles. ....	145
Figure 7.15: Results for embroidered Sample 3 (a) Graded permittivity and (b) dielectric loss tangent.....	146
Figure 7.16: Smocking process of Sample 3.....	146



Figure 7.17: Shape experimentation, Sample 3 .....	147
Figure 7.18: Screen printed dot matrix over a sample length of 560 mm. Dot diameters vary between 0.1 - 5.0 mm.....	148
Figure 7.19: The unit cell modelled using CST to obtain a predicted permittivity for a matrix of screen printed dots. (a) Front view and (d) side view with dimensions. ....	149
Figure 7.20: Permittivity range for screen printed Sample 1. Permittivity gradient for diameter dot change. Measured (red) and simulated (blue) results. ....	149
Figure 7.21: Laser cut card, screen printed with BaTiO <sub>3</sub> ink. One pattern was created as two versions, a symmetric pattern with equal repeats and a manual adaptation using a hand drawn version of the pattern. (a) symmetric (b) asymmetric. ....	151
Figure 7.22: Tiles of BaTiO <sub>3</sub> screen printed and cut out card. Each tile is 5.5 cm wide and 6 cm high.....	151
Figure 7.23: Results of permittivity and dielectric losses for measurements of directional change (isotropy) of the sample, to investigate the possibility to design asymmetric isotropic samples. ....	152
Figure 7.24: Results ‘consistency over length’ measurements at three different locations on the sample, to indicate whether the asymmetric pattern could be used as an alternative for the symmetric pattern. (a) Symmetric pattern permittivity and (b) dielectric losses. (c) Asymmetric pattern permittivity and (d) dielectric losses. ....	153
Figure 8.1: NIM unit cell as presented by Smith, Vier, & Koschny (2005). The cell has been used as starting point and guide for NIM designs presented in this chapter. The cell is designed for X band frequencies, with an overall cell dimension of 2.50 mm. ....	159
Figure 8.2: Simulations confirming S <sub>21</sub> magnitude and phase of the original ‘Smith cell’. Note the slope of phase in the transmitted wave, which is an indicator of the presence of a negative refractive index at that frequency band. ....	159
Figure 8.3: Material parameters from the original simulated ‘Smith cell’, retrieved using the NRW method. ....	160

Figure 8.4: ‘Smith cell’ adapted to textile fabrication. (a) SRR, wire and high dielectric substrate are applied to a flat textile, prepared for pleating in mountain folds (red) and valley folds (blue). (b) Pleated unit cell as simulated in CST. ....	161
Figure 8.5: Simulations showing $S_{21}$ magnitude (left) and phase (right) of the transmitted wave for a generic textile unit cell. Note the slope in phase, which is an indicator of the presence of a negative refractive index at that frequency band.....	161
Figure 8.6: Material parameters from simulated pleated textile unit cell. Retrieval using the NRW method. ....	162
Figure 8.7: Manually screen printed SRRs on $TiO_2$ coated cotton textile. (a) Small assembled structure (b) Detail. ....	165
Figure 8.8: Steps of vacuum deposition process. (a) Copper laid onto both mask and textile surface after deposition. (b) and (c) Careful removal of latex mask. ....	166
Figure 8.9: Four samples produced on waterproof or water-repellent fabrics using a latex mask, which varied in their geometric accuracy. (a) - (b) Microfibre: mask bonded with substrate and was non-removable (c) - (d) Polycotton Chintz: mask bonded with substrate and was non-removable (e) - (f) 100% Polyester: Mask was easily removable and SRR geometry was accurate. Resistance for outer SRR: 1 M $\Omega$ (g) - (h) 100% Nylon: Mask was easily removable and SRR geometry was accurate. Resistance for outer SRR: similar to copper but inconsistent with broken traces. ....	167
Figure 8.10: Inkjet printed silver ink onto $TiO_2$ -coated cotton. Although care was taken to achieve a smooth and non-absorbent substrate surface, no conductive traces were achieved. ....	168
Figure 8.11: Sample of waterproof fabric inkjet printed with nano-particle silver ink. ....	169
Figure 8.12: Copper tape bonded onto cotton fabrics. Complete samples (left), details (right). Mask applied with screen printed petroleum jelly. Chemical etching results in clear geometries and high conductance, but bonding fabric results in adhesive residue. ....	170
Figure 8.13: Testing chemical etching on a larger sample resulted in uneven design. Adhesive residues hindered pleating. Large sample (left), detail (right).....	170

Figure 8.14: Two small samples of laser engraved silver cotton fabric.	
(a) First sample and (b) detail. (c) Two rows of SRRs and (d) detail.....	172
Figure 8.15: Examples of embroidered SRR and wire designs. (a) - (b) Form finding process and testing of dimensions achievable with the embroidery machine.	
(c) - (d) Liberator thread, using lower top thread tension (e) - (f) Statex thread, which delivered more accurate corners, however the gap size was difficult to maintain evenly.....	173
Figure 8.16: Samples of silver leafing (a) - (b) Hahnemühle filter paper (c) - (d) Polycotton Chintz fabric (e) - (f) Polyester (g) - (h) Polyester microfiber (i) - (j) Polycotton .....	175
Figure 8.17: Study 2: Unit cell for PCB milling .....	177
Figure 8.18: Milled geometry on strips of FR-4 (a) PCB strips on notched cardboard (b) Assembly detail (c) PCB strip detail.....	177
Figure 8.19: (a) $S_{21}$ magnitude and (b) $S_{21}$ phase of the simulated cell (red line) and measured sample (blue line) for a milled circuit board. ....	177
Figure 8.20: Unit cell for screen print.....	179
Figure 8.21: Three prototypes of screen printed papers and fabric, assembled in three-dimensional architectures. (a) Technical filter paper (b) White card (c) Polycotton.....	179
Figure 8.22: Assembled sample of screen printed white card .....	180
Figure 8.23: Magnitude and phase of $S_{21}$ for screen printed samples, simulation (red) and measurements of the white card (green line), polycotton (blue line) and filter paper (black line).....	180
Figure 8.24: Unit cell for laser engraving.....	181
Figure 8.25: Laser-engraved silver cotton. Assembled prototype (left), detail (right). ....	181
Figure 8.26: Perspective view of assembled and pleated sample of laser engraved silver cotton. ....	182
Figure 8.27: Magnitude and phase of $S_{21}$ for laser-engraved sample, simulation (red) and measurements (blue). ....	183
Figure 8.28: Embroidery unit cell as modeled in CST. ....	183

Figure 8.29: Samples embroidered with Statex thread. Assembled prototype (left) and detail (right). (a) Cotton (b) Polycotton .....	184
Figure 8.30: Magnitude and phase of $S_{21}$ for the embroidered sample. Simulation results are shown in red, measurement results shown in blue. For the latter a sample was loosely assembled from two smaller samples, to obtain an area large enough to fill the illumination area in the measurement set up.....	184
Figure 8.31: Study 3: Etched PCB strips (a) Front of PCB with SRR array (b) Detail of SRR (c) Assembled structure with six layers.....	186
Figure 8.32: Three layers of PCB SRR/wire designs. Transmission results (a) magnitude (b) phase (c) retrieved refractive index. ....	187
Figure 8.33: Embroidered samples (a) One layer (b) Detail of non-conductive top thread stitch. (c) Stacked three-layer prototype.....	188
Figure 8.34: Three layers of embroidered designs. Transmission results (a) magnitude (b) phase (c) retrieved refractive index. ....	189
Figure 8.35: Unit cell design for larger SRR/wire structure, aimed for ‘print and etch’ fabrication technique. ....	190
Figure 8.36: Unit cell design for smaller SRR and wire structure, aimed for ‘print and etch’ fabrication technique.....	191
Figure 8.37: Prototypes ‘print and etch’. The circuits were produced by PEL on polycarbonate woven textile. Two sizes were designed, of which one was designed for negative refractive index at (a) - (b) 7 GHz and one for (c) - (d) 9 GHz. (e) Assembled and stacked samples. Irregularities in the frequencies of folds are the result of the handmade pleating and assembling process. The aim was to achieve precise arrays, some irregularities were tolerated as part of textile behaviour. ....	192
Figure 8.38: Results for ‘print and etch’ prototype 1, larger design. The flat designs were fabricated by PEL Ltd. And subsequently printed with TiO <sub>2</sub> ink, pleated and assembled.....	192
Figure 8.39: PEL ‘print and etch’ prototype with larger design. Measured result was retrieved by calculating the refractive index from the negative phase shift. ....	193
Figure 8.40: Results for ‘print and etch’ prototype 2, smaller design. The flat designs were fabricated by PEL and subsequently printed with TiO <sub>2</sub> ink,	

pleated and assembled. The measured results show a deviation of 0.4 GHz to the simulated results, and the resonance is weaker than the simulations. ....	193
Figure 8.41: PEL ‘print and etch’ prototype with smaller design. Measured result was retrieved by calculating the refractive index from the negative phase shift. ....	193
Figure 8.42: Three studies were presented in chapter 8. In the first study (left column), seven textile techniques were tested. The three most successful samples were then used to produce single-layer samples in the second study (centre column), compared to an industrially produced sample (print and etch). In the third study (right column), three samples were constructed in multiple layers (two ‘print and etch’ structures with different dimensions, and one embroidered structure) and negative refractive indices verified. PCB structures were designed for comparison in each study. ....	195
Figure A.1: Poster design for INNOVATE UK annual conference 2014 .....	225
Figure B.1: Geometry of material arrangement in electromagnetic engineering and textile design. ....	230
Figure C.1: Pure Copper Polyester Taffeta Fabric (LessEMF) .....	236
Figure C.2: Datasheet SaniSilver™ Fabric (LessEMF).....	237
Figure C.3: Datasheet NB-TP-3GU100 PET film (Mitsubishi) .....	238
Figure C.4: Datasheet Silver coated thread 234/34 4-ply (Statex) .....	239
Figure C.5: Datasheet Liberator 40 (Syscom Advanced Materials) .....	240
Figure C.6: Datasheet BT-101 (Conductive Compounds).....	241
Figure C.7: Datasheet CuPro-Cote™ (LessEMF).....	242
Figure C.8: Datasheet Silver Nano Particle Ink (Mitsubishi) .....	243

## List of Tables

Table 4.1: Common material measurement techniques, including recommendations for suitability, measured parameters and retrievable properties. ....	72
Table 5.1: Frequency bandwidths and wavelengths relevant to this thesis (IEEE Standard 521 – 1984).....	79
Table 6.1: Screen printing techniques used to achieve various functionalities. ....	106
Table 6.2: Optimisation applied before, during and after free space measurement.....	118
Table 7.1: Summary of techniques applied in chapter 7, stating success and challenges encountered when prototyping and analysing samples.....	156
Table 8.1: Summary Results Study 3: Negative Refractive Index Textiles.....	194
Table 8.2: Summary of techniques applied in chapter 8, including success and challenges encountered when prototyping small and large samples. ....	197
Table B.1: Definitions of term ‘metamaterials’ found in literature .....	227
Table C.1: List of material resources .....	231
Table D.1: Index of produced samples that utilise conductive materials. ....	244
Table E.1: Anechoic chamber design process .....	266
Table F.1: Conceptual drawings of cloaking mechanisms .....	273
Table G.1: List of conceptual samples.....	276

# Chapter 1

## Introduction

### 1.1 Motivation and Aims

This thesis presents an exploration of the potential of textile materials, prototyping technologies and textile design methods for fabrication of electromagnetic metamaterials in the microwave range. The motivation behind this work is to demonstrate how pairing a practice-led textile design approach with electromagnetic engineering theory and procedures, can contribute to the development of textile metamaterials.

The central questions of this thesis are:

1. How can functional advanced electromagnetic metamaterials for the microwave range be fabricated using textile materials and textile design techniques?
2. Can a practice-led textile design approach provide more options for material selection in metamaterials research?

Metamaterials, a class of materials that can manipulate electromagnetic fields in precisely controlled and often unusual ways, are characterised by both their periodic structural composition and electromagnetic properties. They constitute an engineering solution for a number of pioneering and futuristic applications, amongst them an invisibility cloak (Pendry, Schurig, & Smith, 2006) and a lens with sub-wavelength resolution (Pendry, 2000).

Metamaterials have received significant research interest since 2000, partly due to the development of negative refractive index materials. Whilst early research focused on exploring theoretical framework and numerical procedures, a second field of work emerged that was concerned with the engineering practices of the complex anisotropic and graded materials. A third field investigates the potential of new materials and fabrication technologies. Specifically this last area is motivated and driven by advances in computer-aided design (CAD) and manufacturing (CAM) technologies, which provide an exciting opportunity for engineers to bridge the theory and practice of designing and building metamaterial devices.

It is this field that may benefit from the skillset of textile designers. Combinations of materials and structural composition are already prevalent in traditional areas of textile design, which supports this prospect. Advantages are the pre-existence of industrial infrastructure, specialised equipment, and the possibility of extending the fabrication portfolio through the integration and adaptation of more recent digital prototyping technologies. By reviewing existing textile technologies and suggesting how these can be adapted, textile designers could make significant contributions to the development of microwave metamaterial fabrication.

## **1.2 Structure of the Thesis**

This thesis presents empirical data from a series of studies in the field of textile metamaterials. It promotes a practice-led approach based on material experimentation, with the aim to extend the choice of materials and fabrication techniques available to electromagnetic engineers.

Chapter 2 provides the foundation of the thesis, delivering a review of research in the fields of metamaterials, e-textiles (in particular, their use for the design of wearable antennas) and electromagnetic textiles, and the use of e-textiles for electromagnetic applications in the design community.

Chapter 3 reflects on the interdisciplinary path taken for this thesis, identifying key positions in science-design collaborative approaches to illustrate the decision-making process.



Chapter 4 delivers the terminology used to describe material behaviour in electromagnetic engineering.

Chapter 5 identifies relevant aspects of material theory and specifications as applied in electromagnetic engineering and textile design, presenting an overview of how ‘structure’ is practically understood and applied in both fields.

Chapter 6 describes the textile materials and techniques used in the experimental studies. It further details work done to develop measurement techniques for textile properties and presents the methods used to derive electromagnetic material properties.

Chapter 7 and chapter 8 document the empirical studies including analysis of experimental data. While chapter 7 is concerned with dielectric textiles, exploring their usability for both fabricating all-dielectric metatextiles as well as further utilisation in resonant metatextiles, chapter 8 demonstrates the experiments that have been conducted in order to prototype three-dimensional textiles with a negative refractive index in microwave frequencies.

Chapter 9 presents and reviews the outcomes of the thesis in relation to the research questions. Conclusions of this work are provided, and limitations and improvements are discussed. Potential future implications of this work are given, including design scenarios broken down into short-term-, mid-term, and long-term prospects.

### **1.3 Contributions of the Thesis**

This thesis is relevant to metamaterial engineers and e-textile designers who have an interest in interdisciplinary collaboration, and to researchers and practitioners studying new materials for the design of electromagnetic devices.

The key contributions of the work presented in this thesis can be summarised as follows:

- Evaluation of the suitability of traditional textile techniques for the fabrication of graded dielectric substrates.
- Empirical evidence of three-dimensional textiles with a negative refractive index at microwave frequencies.

- Evaluation of a range of e-textile techniques to produce small, non-conductive and conductive structures with manual and semi-automated fabrication.
- Design and fabrication of a free space anechoic chamber built to measure graded-permittivity substrates between 4 – 12 GHz.
- An extended selection of available materials and fabrication techniques for textile prototyping in metamaterial and electromagnetic engineering, including:
- A set of design guidelines for textile metamaterials, derived through a practice-led and interdisciplinary method that is grounded in material experimentation.
- Transferability of fabrication guidelines to other textile and non-textile electromagnetic devices.

## **Chapter 2**

### **Background**

The approach of this thesis is interdisciplinary and related to three research fields in particular: firstly, research in the field of electromagnetic engineering, secondly, electronic textile (e-textile) and electromagnetic textile engineering research, and thirdly, fabrication techniques and general design methods adopted from practice in e-textile experimental design and crafts. A review of the three fields is provided in this chapter, illustrating the ground on which the thesis is based.

Section 2.1 covers literature from the field of electromagnetic metamaterials. Section 2.1.1 describes the field and related seminal publications. In section 2.1.2, the theoretical design tool Transformation Optics is introduced. The next two sections give an overview of two types of metamaterials; metamaterials with a negative refractive index in section 2.1.3, and all-dielectric metamaterials in section 2.1.4. Textile metamaterials of both types are discussed in section 2.1.5.

Section 2.2 presents an outline of the field of e-textiles, with a focus on electromagnetic applications in textile engineering and electromagnetic engineering in section 2.2.1. It also explores the e-textile areas impacting electromagnetic functionality, which are relevant to textile designers at the current time in section 2.2.2.

The final section 2.3 builds the bridge between the disciplines and discusses the implications of an interdisciplinary approach. It identifies how a practice-led e-textile design approach can serve as a vehicle to develop innovative textile metamaterials.

## 2.1 Electromagnetic Metamaterials

### 2.1.1 Seminal Publications

Reviewing the historical development of electromagnetic metamaterials, the field can be narrowed down to five seminal publications that build the foundation of this research area.

In 1968 physicist Viktor Veselago formulated a theory for materials that have both a negative permittivity and negative permeability (Veselago, 1968). Introducing the term “left-handed substance” as a synonym for “substance with negative group velocity”, he showed that, if it were possible to engineer such a substance, it would have a negative refractive index. Figure 2.1 illustrates a positive refractive index, common in all naturally occurring materials, compared to a negative refractive index.

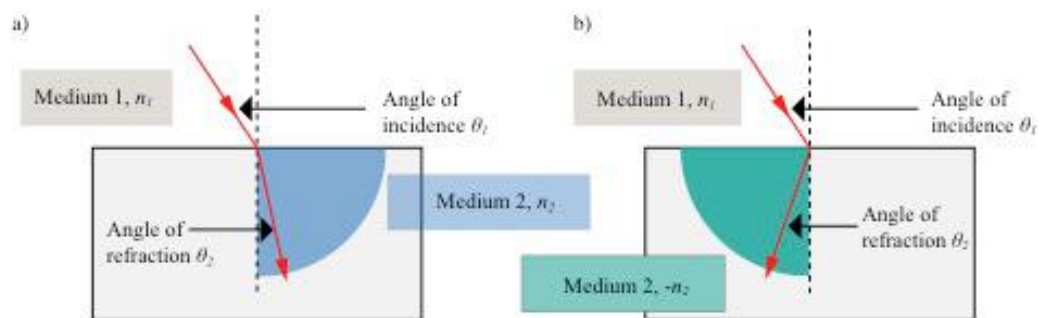


Figure 2.1: (a) Positive refractive index as occurring in natural materials (b) Negative refractive index as predicted by Veselago (1968).

Making use of a plate of negative refractive index material, he proposed the concept of a flat lens that bundles radiation originating from a point source, into a focal point. This principle is shown in Figure 2.2, where the plate is of thickness  $d$ .

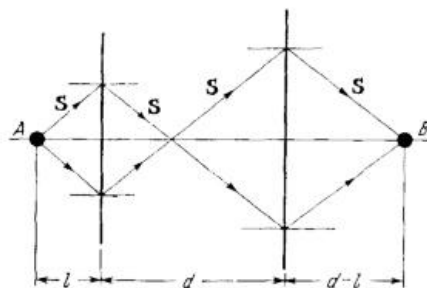


Figure 2.2: Flat lens using a slab of left-handed substance, thickness  $d$ , as suggested by Veselago (1968).

It took more than 30 years after the publication of this theory, until Smith et al. (2000) devised a medium that allowed to actually engineer negative refraction. By pairing a matrix of split-ring-resonators that produces a negative permeability with an array of wires that results in negative permittivity for a small frequency band, Smith and his team inverted Snell's law by creating a cell-based material with a negative refractive index at about 4.2 - 4.6 GHz. In-depth experimental verification followed a year later in the third seminal paper (Shelby, Smith, & Schultz, 2001).

In between these two publications, and vastly increasing the interest in this phenomenon within the research community, theoretical physicist Pendry demonstrated in a review letter the concept of a "perfect lens" making use of the "focal point to focal point" refraction illustrated by Veselago. He suggested a lens that could focus wavelengths smaller than visible light (so called "sub wavelength imaging"), delivering a compelling application for negative refractive index materials in optics (Pendry, 2000).

The fifth paper named these new structures "metamaterials" (Walser, 2001), acknowledging the complexity of composites that result in increased electromagnetic performance, not known to exist in natural materials up to this date. According to Walser, metamaterials are "macroscopic composites having a man-made, three dimensional, periodic cellular architecture designed to produce an optimized combination, not available in nature." Although this description has been shifted and adapted many times<sup>1</sup>, his original definition is still regularly used for classification. It considers any group of objects to be a metamaterial, as long as the size and spacing of its elements display some form of geometrical order and are much smaller than the wavelength of interest, so the grouped elements can be described as an effective medium (section 5.2.1).

---

<sup>1</sup> A collection of definitions extracted from articles and published interviews included in Appendix B.

### 2.1.2 Transformation Optics as a Design Tool

In 2006, two simultaneous publications introduced the theory of Transformation Optics (and Transformation Electromagnetics for a larger wavelength scale), which enabled new possibilities for electromagnetic designs in the whole range of the electromagnetic spectrum (Leonhardt, 2006; Pendry et al., 2006).

The theory of Transformation Optics as developed by Pendry et al. (2006) makes use of the fact that a free space can be distorted and the path of a wave diverted, while still satisfying Maxwell's equations. The spatial distortions are then represented by variant material properties, which facilitate a physical implementation. The path of the wave is directed by varying the material properties across the composite, making use of the potential given by possibility to precisely engineer metamaterials. Original and distorted spaces are shown in Figure 2.3.

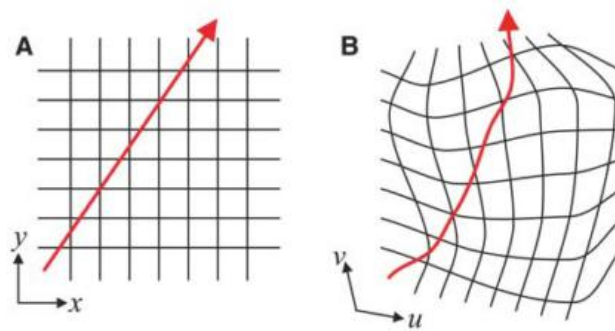


Figure 2.3: The path of the wave in A is diverted, by distortion of the coordinate system as in B (Pendry et al., 2006).

Whilst the theory to translate distorted space into material properties had been suggested in previous pioneering publications, Pendry's clear demonstration of Transformation Optics as a practical "design tool" promoted the need for new and precisely engineered materials. Representing a compelling application, the concept of an 'invisibility cloak' helped to accelerate research in this field. An invisibility cloak is a metamaterial structure that hides an area in space by compressing material blocks around it, thus guiding an electromagnetic wave around a 'hole' created within a small part of the electromagnetic spectrum. Figure 2.4 (a) illustrates the principle on a two-dimensional cross section, showing how electromagnetic waves that aim towards a round object, are redirected around the object and led back on the original path.

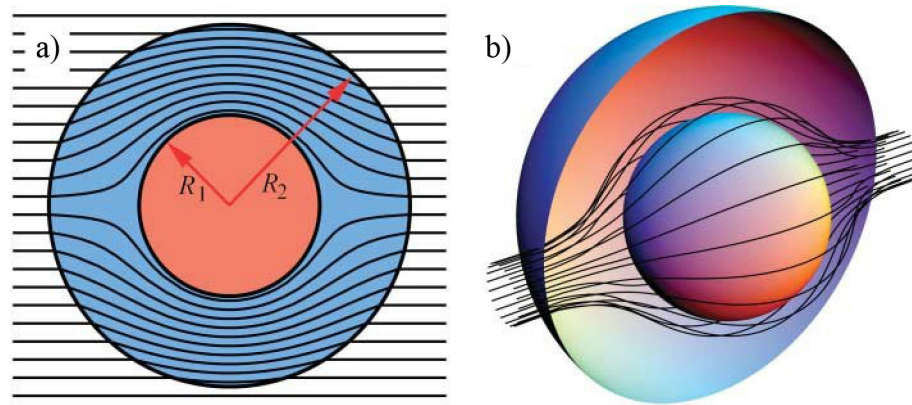


Figure 2.4: Illustration of the invisibility cloak as proposed by Pendry (2006).  
 (a) A two-dimensional cross section, with radius of the cloaked area ( $R_1$ ) and radius of cloak ( $R_2$ ).  
 (b) Depiction of the cloak as 3D view.

### 2.1.3 Negative Refractive Index Metamaterials

Negative refractive index or ‘left-handed’ metamaterials (NIM) refract an electromagnetic wave ‘the wrong way’. NIMs were theoretically formulated nearly 50 years ago by the physicist Veselago (1968), however researchers did not have the technological means to engineer a physical prototype at that time. Thirty years later Smith et al. (2000) designed and built the first material with a negative refractive index in microwave frequencies by pairing a split-ring resonator (SRR) array to cause negative permeability, with a wire array that causes negative permittivity. The anisotropic matrix, as seen in Figure 2.5, was shown to exhibit a negative refractive index in the range of 4.2 – 4.8 GHz.

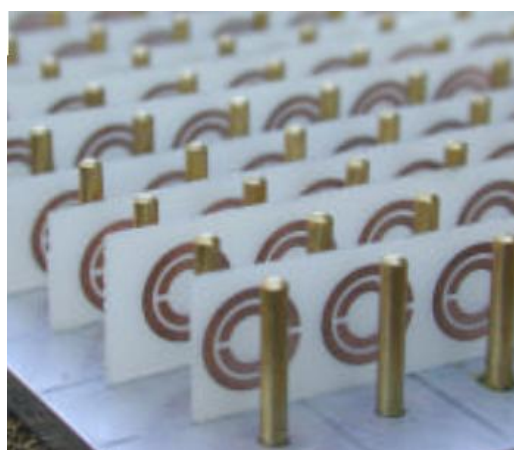


Figure 2.5: First prototype for a metamaterial with a negative refractive index, resonating frequency 4.2-4.8 GHz. (Smith, Padilla, Vier, Nemat-Nasser, et al., 2000)

A second negative refractive index material was developed and experimentally verified by the same team in 2001. The structure, shown in Figure 2.6, was fabricated using standard microwave quality double-sided printed circuit board (PCB) using etching technology, allowing a combined fabrication of both SRR and wire on alternative sides of the PCB surface. Two layers were stacked perpendicularly resulting in multi-directional functionality. This material exhibited a negative refractive index in the range 10.2 – 10.8 GHz (see Figure 2.6 (c)).

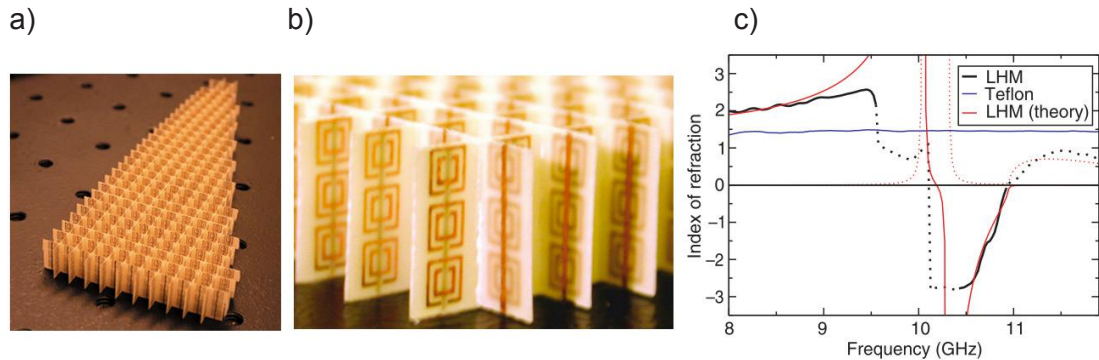


Figure 2.6: Second publication of a negative-refractive-index metamaterial (NIM) (Shelby, Smith, & Schultz, 2001; Smith, Padilla, Vier, Shelby, et al., 2000). (a) Material wedge to demonstrate NIM behaviour (b) Close-up of three-dimensional SRR and wire medium (c) Measurement demonstrates negative region of refractive index between 10.2 – 10.8 GHz (black dotted), corresponding to theory (red), and in contrast to PTFE (Teflon) that exhibits a positive refractive index (blue).

In the following years, researchers were concerned with formulating a robust method for measuring the permittivity and permeability of NIMs (Chen, Grzegorzczuk, Wu, Pacheco, & Kong, 2004; Smith & Schultz, 2002; Smith, Vier, Koschny, & Soukoulis, 2005). Although for standard ‘right-handed’ material techniques such as the Nicolson-Ross-Weir procedure can be used (section 6.6.2), there are ambiguities that need to be addressed. For example choosing the correct branch of the real part of the refractive index, which can be solved iteratively (Chen et al., 2004) providing continuity of the material parameters. This thesis does not pursue the mathematical complexity of parameter retrieval of NIMs, and an alternative method is used for experimental verification that delivers an unambiguous result based on phase shift observation. However it was necessary to enquire about the reasons for ambiguities in results obtained in simulations. This further clarified the importance of experimental precision, highlighting how even small errors in sample thickness measurements or periodical inaccuracy of the structure impacted the method of retrieval.



Shortly after the main theory and parameter retrieval was verified, research began to branch out into various aspects of NIMs. Although real-life applications were not yet elaborated on, an emphasis can be found on solving engineering issues for metamaterials. For example, the geometric form of NIMs came under the spotlight and ways of practically fabricating metamaterials were investigated. Engineers were interested in simplifying the form of the unit cell elements, replacing the split ring and wire design, and exploring the engineering feasibility of NIMs in higher frequency bands and cloaking devices.

The SRR and wire design for negative refractive index metamaterials was pioneering, yet showed disadvantages that needed to be overcome in order to design practical engineering devices. Whilst the problems of the narrow resonating frequency bandwidth, of typically a few per cent, and high-energy loss are inherent to NIMs, the complexity of form could be modified. To enable more simple fabrication an ‘omega’ configuration was suggested, which combined the SRR and wire matrix in one shape (Aydin, Li, Hudlička, Tretyakov, & Ozbay, 2007; Lheurette et al., 2008; Simovski & Sauviac, 2003), reducing the complexity of fabrication from two (or one double-sided) arrays to a single side. An example is shown in Figure 2.7, which achieved a negative refractive index at around 13.2 GHz (Lheurette et al., 2008).

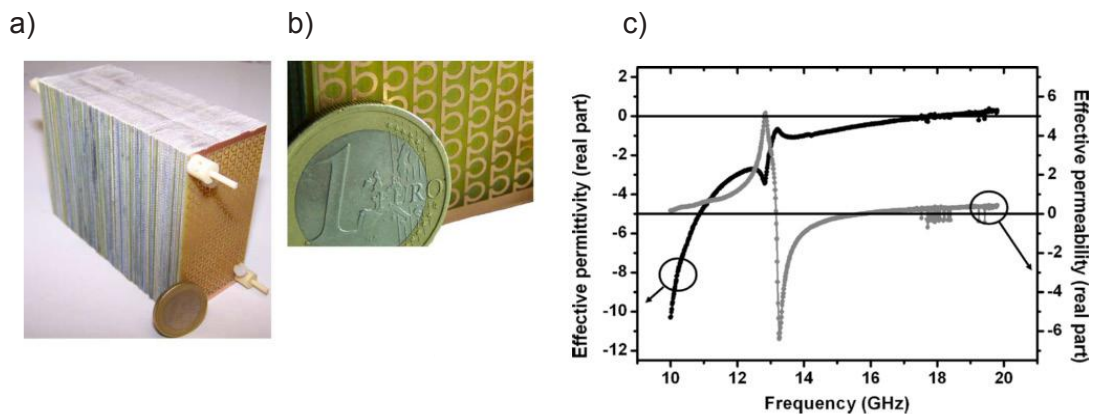


Figure 2.7: (a) and (b) Bulk metamaterial with omega-shaped inclusions. (c) Both real parts of permittivity and permeability are below 0 around 13.2 GHz (Lheurette et al., 2008).

With the development of the “fishnet” structure, possible frequency ranges were pushed towards the optical spectrum (Shuang Zhang, Fan, Malloy, et al., 2005; Shuang Zhang, Fan, Panoiu, et al., 2005). The first experimental verification of negative refractive index materials in optical frequencies was developed by Shalaev et al. (2005) using a

doubled array of pairs of parallel nano-rods (see Figure 2.8). Several variations of other structural metamaterials also demonstrated functionality in the visible spectrum (Dolling, Enkrich, Wegener, Soukoulis, & Linden, 2006; Valentine et al., 2008; Shuang Zhang et al., 2006), as seen in Figure 2.9 to Figure 2.11.

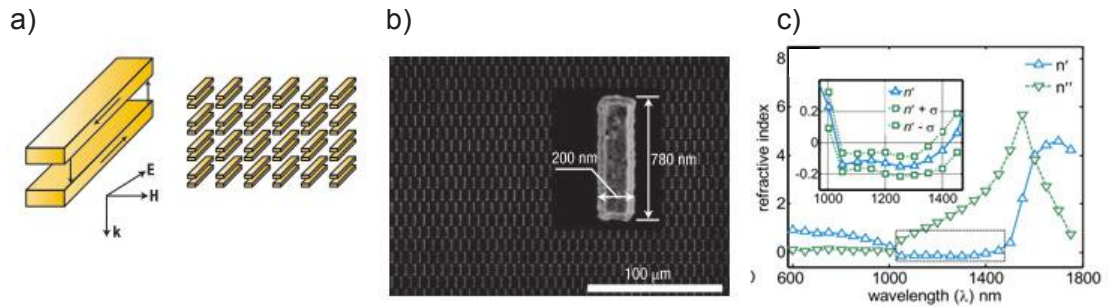


Figure 2.8: First example of NIM for near-optical frequencies, using a nano-rod structure (Shalaev et al., 2005) (a) schematic of parallel nanorods, (b) image with dimensions (c) negative real part of refractive index ( $n'$ ) demonstrated at around 210 – 270 THz

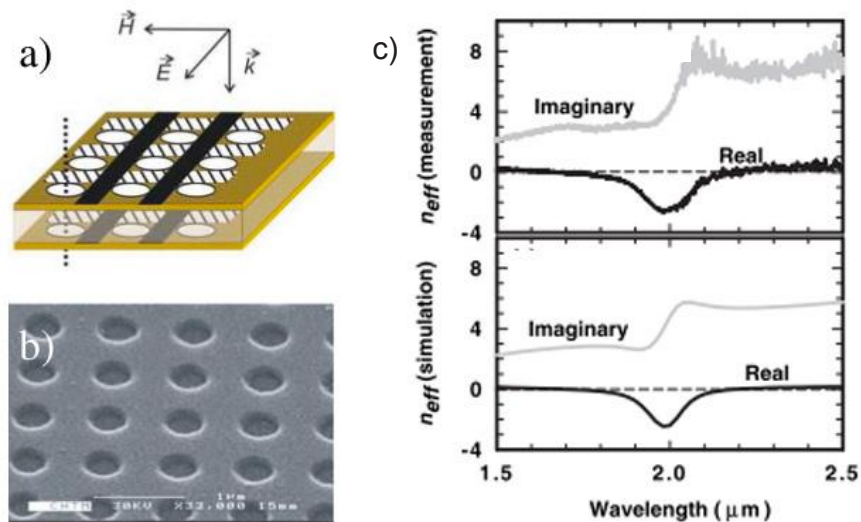


Figure 2.9: Near-infrared NIM made from a sandwich structure of two perforated silver films and a ceramic dielectric (Shuang Zhang, Fan, Panoiu, et al., 2005). (a) Schematic of the structure. For this given polarisation and propagation direction, the regions acting in the E-field are marked black, regions acting in the H-field are marked hatched. (b) SEM picture of the structure (c) Refractive index retrieved from measurement and simulation shows a negative region at around 150 THz.

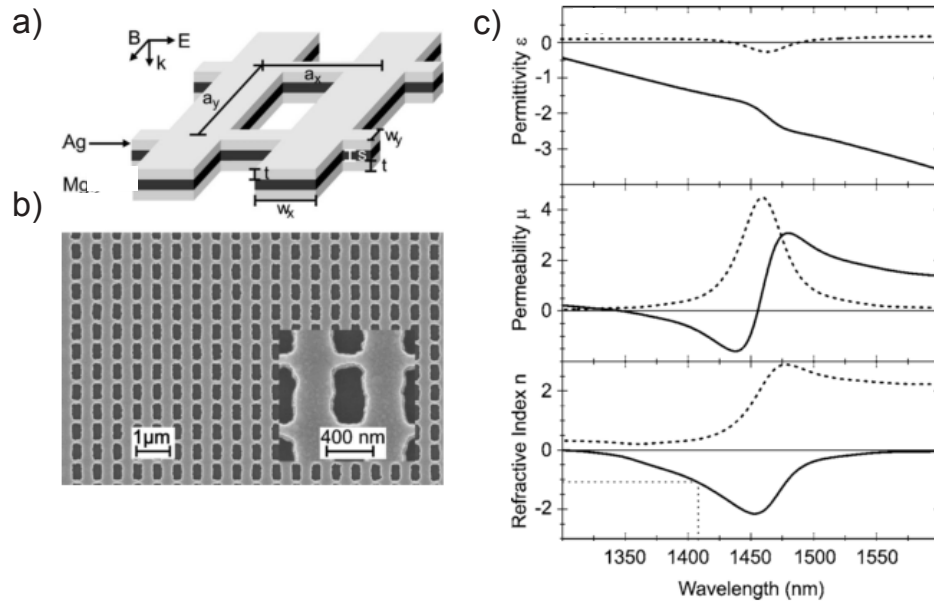


Figure 2.10: Fishnet structure for optical frequencies (Dolling et al., 2006) (a) Structural unit cell (b) Microscopic view (c) Retrieved permittivity, permeability and refractive index  $n$  (solid lines =  $n'$ , dashed lines =  $n''$ ).

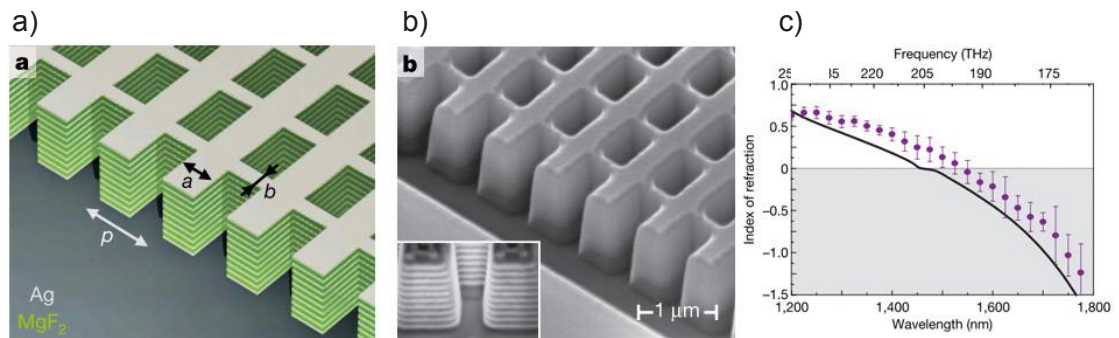


Figure 2.11: (Valentine et al., 2008): (a) Schematic and (b) SEM image of fishnet structure, fabricated from multiple layers of silver and magnesium fluoride ( $\text{MgF}_2$ ). (c) Region of negative refractive index for simulation (black line) and measurement (circles).

Due to the invention of Transformation Optics, the interest in new applications became more prevalent. These made use of pre-existing electromagnetic tools, such as lenses (Pendry, 2000), artificial magnets (Pendry, Holden, Robbins, & Stewart, 1999), and flat antennas (Tang, Hao, & Mittra, 2012). Some devices have been commercialised, for example flat metamaterial panels that can replace bulky and heavy satellite dishes in space communication applications (Billings, 2013), antennas with beam direction

adaptability<sup>2</sup>, detection technology for security applications<sup>3</sup>, and thin and light radar antennas<sup>4</sup>.

As detailed in the previous section, the concept of a metamaterial free-space invisibility cloak made headlines as an application for Transformation Optics, both theoretically (Pendry et al., 2006), and in practice (Schurig et al., 2006). The principle is shown in Figure 2.12, illustrating the distribution of the electromagnetic field around a perturbation. In Figure 2.12 (a) a perfect cloaking is shown in a simulated set up, Figure 2.12 (b) shows the electric field around a perturbation only, and Figure 2.12 (c) the perturbation with a cloak (Averitt, 2013).

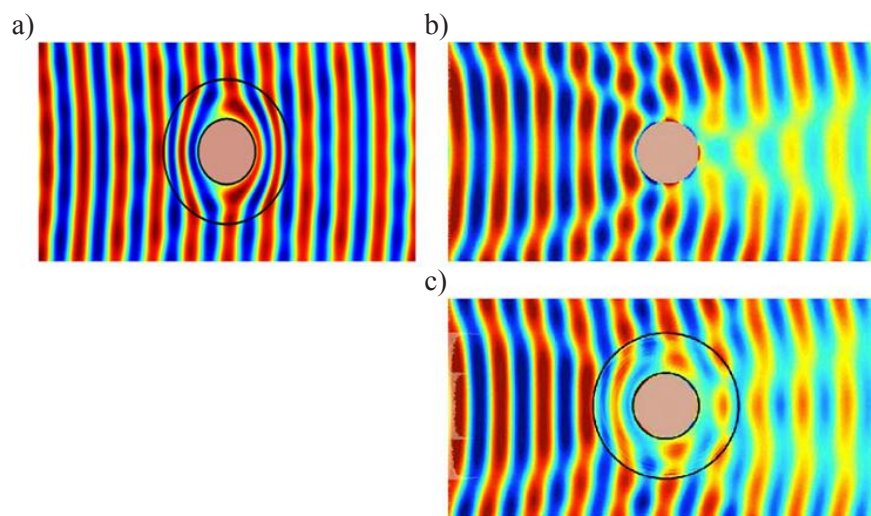


Figure 2.12: Distribution of field around perturbation and cloak (a) Simulation with cloak (b) Experiment without cloak (c) Experiment with cloak. (Averitt, 2013)

The first experimental verification of a cloaking device was achieved by Schurig et al. (2006). This cloak, shown in Figure 2.13 (a), demonstrated an operating frequency of 8.5 GHz and worked two-dimensionally. Rings of NIMs guide the waves around the circular free space in the centre of the cloak and then back to their original path, rendering the centre part invisible to the impinging wave. In order to verify the theory, a waveguide apparatus was designed (see Figure 2.13 (b)), in which the cloak was fixed

---

<sup>2</sup> <https://www.kymetacorp.com/technology/mtenna/> accessed 6/11/2015

<sup>3</sup> <http://www.intellectualventures.com/news/press-releases/iv-spins-out-evolv-to-commercialize-metamaterials-security-imaging-technolo/> accessed 6/11/2015

<sup>4</sup> <http://echodyne.com/technology/> accessed 6/11/2015

between two parallel metal plates surrounded by absorbers to represent free space. A field was introduced by a waveguide, and electric field measurements were conducted in a band of frequencies using a field probe inserted into the upper plate. Figure 2.14 shows results at 8.5 GHz, with the black lines indicating the course of the wave from left to right. Figure 2.14 (d) demonstrates that a plane wave on the right hand side of the cloak is nearly undisturbed, as opposed to the field shown in Figure 2.14 (c), in which the wave front is shifted in the region of the copper cylinder.

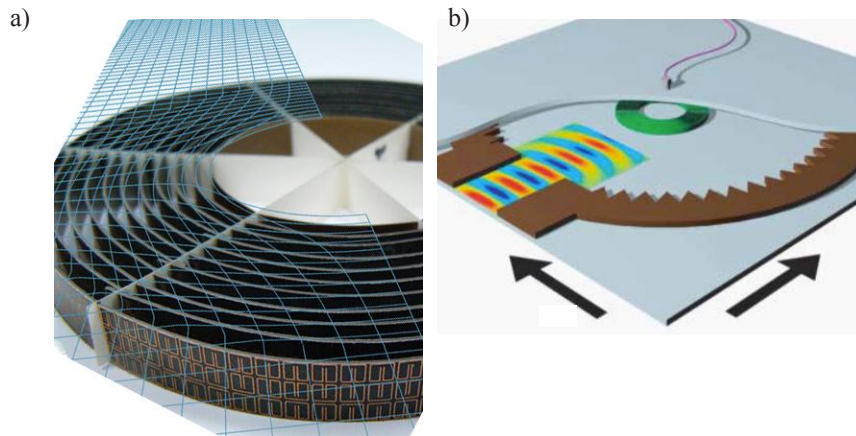


Figure 2.13: First invisibility cloak, hiding a circular region in the centre at 8.5 GHz (Schurig et al., 2006). (a) Fabricated cloak with illustrated wave path (b) View of the measurement set up with cutout for illustration purpose. Microwaves are introduced with a waveguide; absorbers placed around represent free space. An antenna probe fixed to the upper plate records the field.

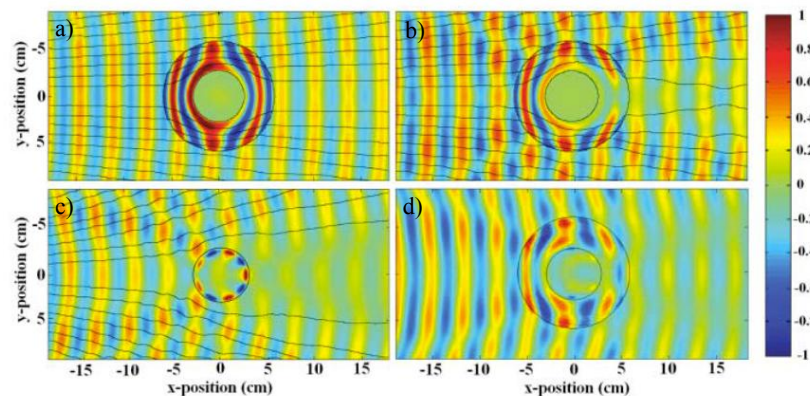


Figure 2.14: Real part of the electric field with an indication of direction of the wave path (black lines) from left to right. (a) Simulation of ideal cloak at frequency of 8.5 GHz (b) Simulation of cloak considering real-life factors such as reduced number of cells. (c) Measurement of unclocked copper structure. (d) Measurement of cloaked copper structure.

Utilising the universality of Transformation Optics, various remarkable cloak models employing NIMs have been developed since, such as the space-time cloak, combining

spatial and temporal capability in the same device (Fridman, Farsi, Okawachi, & Gaeta, 2012; McCall, Favaro, Kinsler, & Boardman, 2011), or an illusionary cloak in which an object can appear to have a different shape (Jiang & Cui, 2011).

#### 2.1.4 Dielectric Metamaterials

The concept of ground plane cloaking was introduced theoretically by J. Li & Pendry (2008) with a subsequent experimental verification in the following year (Liu et al., 2009, see Figure 2.15). A ground plane cloak, also named “carpet cloak”, imitates a ground plane by reflecting the radiation just as it would be reflected from a flat conductive surface. This cloaking strategy reduces fabrication challenges because it only requires isotropic dielectric material elements, instead of complex anisotropic resonating metamaterials. Further advantages of this cloaking method are the broadening of the operational frequency band, as well as low energy losses. Whilst free-space cloaks are restricted to two-dimensional functionality, carpet cloaks can be made for all incident angles, simply by rotating the permittivity map around its centre point.

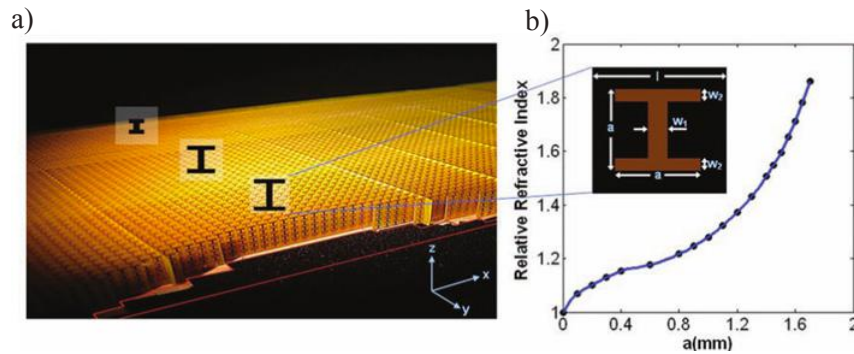


Figure 2.15: First experimental verification of a ground plane cloak (Liu et al., 2009). (a) Cloak with indicated element size distribution. (b) Varying index of  $n$  in relation to inclusion geometry.

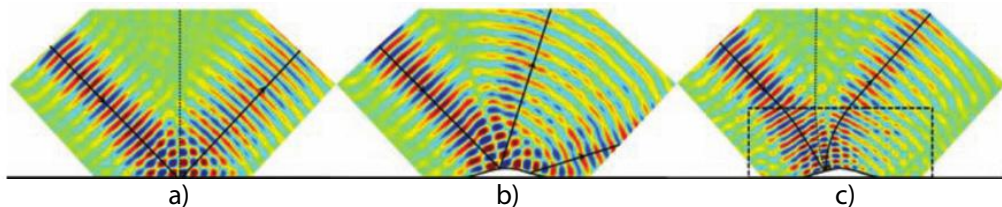


Figure 2.16: Measured E-field at 14 GHz of (a) incident on ground plane without cloak, (b) incident on uncloaked metal perturbation, (c) incident on cloaked perturbation, showing strong resemblance to the reflection on the ground plane.

Following the introduction of this new method, researchers were then able to suggest further adaptations to simplify design and physical implementation. One main goal was more cost-effective fabrication, which was achieved using a quantised version of the desired continuous graded permittivity structure (Kallos, Argyropoulos, & Hao, 2009). The solution proposed by Bao (Bao, 2012; Bao et al., 2011), described in detail in chapter 7, was used as a starting point to examine textile fabrication technologies for the production of finely graded dielectric materials.

A different approach for simplification of cloak realisation was suggested by (Urzhumov, Landy, Driscoll, Basov, & Smith, 2013). The authors proposed a free space cloak design computed through an iterative algorithmic process, and implementing a binary configuration from a low loss ABS (Acrylonitrile butadiene styrene) material and air. This cloak, shown in Figure 2.17 (a), was fabricated with a 3D printer in one single process, significantly reducing costs and production time of previous dielectric metamaterials. It works at a band between 9.7 - 10.1 GHz and whilst not perfect, visibility is reduced by four times. This showed that generative design techniques paired with computer-aided-manufacturing (CAM) processes and using commercially available materials, are a viable option for cloak fabrication.

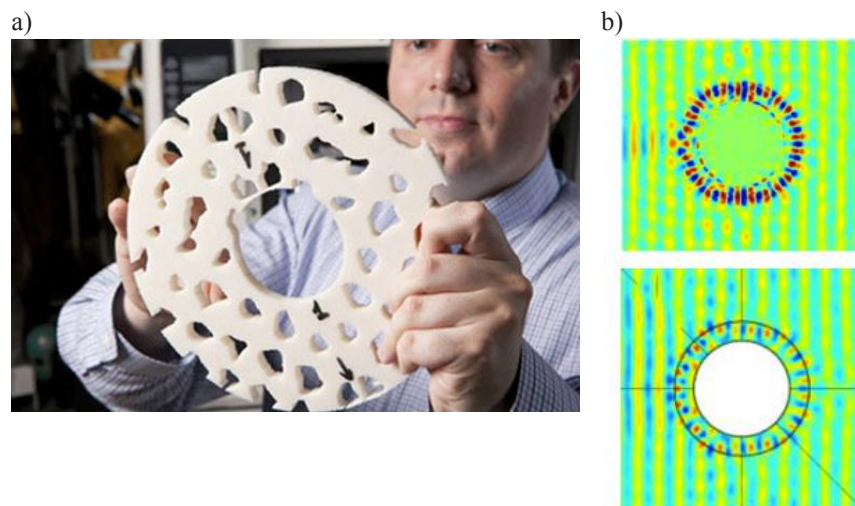


Figure 2.17: (a) 3D printed binary cloak (Urzhumov et al., 2013). (b) E-field distribution at 9.9 GHz as measured (top) and simulated (bottom), showing a low loss undisturbed field.

Based on the same principle as Transformation Optics, waves other than electromagnetic waves can also be directed in the same way, and it has been suggested that Transformation Acoustics would be appropriate to control sound waves (Cummer,

Rahm, & Schurig, 2008; Cummer & Schurig, 2007; Torrent & Sánchez-Dehesa, 2008), and other surface waves (Mitchell-Thomas, McManus, Quevedo-Teruel, Horsley, & Hao, 2013). While the prospect of invisibility was seen as a compelling application and generated wide interest in the research community and media, the approach shifted to specific real-life applications for cloaking devices. Engineers started to design isotropic material transformation for a range of operational designs, such as cloaking sensors (Alù & Engheta, 2009), and flat antennas and lenses (Tang, Argyropoulos, Kallos, & Hao, 2010; Tang, Argyropoulos, Kallos, Song, & Hao, 2010; Tang et al., 2012).

### **2.1.5 Textile Metamaterials**

The majority of metamaterial research makes use of established fabrication technologies such as PCB techniques, including chemical etching and circuit board milling. In recent years, interest in alternative fabrication technologies has increased, driven by the identification of new applications (such as biomedical materials) or advancements in fabrication technology (such as 3D printing). In addition, novel technologies in nano-engineering permit fabrication for much higher frequency bands, including visible light.

The challenges of metamaterial fabrication vary with the target frequency. As the single unit cell is required to be significantly smaller than the wavelength (see section 5.2.1), physical implementation becomes more difficult in bands of smaller wavelengths. While large unit cells intended for microwave applications are comparably straightforward to fabricate with circuit board technology, smaller structures intended for the terahertz regions require specialist nano-fabrication equipment.

Metamaterials quickly lose their unusual properties if geometry and material content are not accurate. For NIM designs, the conductivity of the split ring resonators must be high; the dielectric substrate must have low losses and the geometry must be precise to achieve the cooperation between the cells to yield the desired bulk property.

High anisotropy is regarded as a fabrication issue, requiring finely graded surfaces made from isotropic blocks. Although not made explicit in most publications, it is often assumed that, apart from 3D-printed prototypes, cloaks are modular and require assembly. Based on the grounds that capabilities of both computing and digital fabrication technologies are increasing, this thesis argues that modularity can be replaced by one-piece designs.



Textile metamaterials have rarely been directly reported in literature. The identification of textile metamaterials is not a clear-cut task, partly due to the inconsistent definition of metamaterials in the first place. On one hand, authors focus on the novelty of using textiles to fabricate metamaterials while defining their characteristics broadly, or they use ‘textile-inspired’ technologies for the simulation of near perfect structures. On the other hand, considering the structural aspect as the defining characteristic of a metamaterial, one could argue that almost any textile material could be seen as a metamaterial. In order to identify relevant literature for this section, only textiles that were defined specifically for an electromagnetic function were considered. In addition, the following categories were found to be relevant:

- Textile structures that demonstrate negative permeability.
- Textile bandgap structures that present novel fabrication methods, demonstrating potential for fabricating metatextiles.
- Textile antennas that make use of placed metamaterial arrays demonstrating novel antenna functionality.

One of the first textile metamaterial arrays was reported in Seager, Chauraya, & Vardaxoglou (2008). A 2x2 and 2x3 spiral cell was included in an antenna design in order to minimise dimensions and disturbance between the antenna and human body. A textile antenna presented by Joshi, Pattnaik, & Devi (2012) used an SRR cell to provide an impedance match that counteracted the effects of bending the antenna. The SRR cell was independently assessed and produced a negative permeability between 8.35 GHz and 8.7 GHz. Similar to the antenna reported by Seager, Chauraya, & Vardaxoglou (2008), results show that the embedded cells reduce the required size of patch antennas. In a later publication, Joshi, Pattnaik, & Devi (2013) discuss a wearable antenna design that uses light-weight polypropylene as a substrate material and a four-cell SRR array to reduce size and match impedance. For all three antennas, a copper patch was simply glued onto a fabric substrate. Although this is a simple and quick technique that also ensures high conductivity of the copper parts, the antenna is not embedded into the textile and therefore sensitive to mechanical force and abrasion. While this was a common technique before e-textile materials and techniques became common for electromagnetic engineering, more recent research embeds the conductive parts using textile materials and techniques (see section 2.2.1).

Another example of a textile antenna that utilises metamaterial behaviour can be found in Yan, Vandenbosch, & Soh (2014). The proposed wearable WLAN antenna makes use of both 'left-handed' and 'right-handed' behaviour in adjacent frequency bands to produce a dual-band mode (Dong & Itohdan, 2012), indicating that through fine-tuning the resonating frequencies, novel characteristics in antennas can be achieved. The material used is a conductive nickel fabric that is fixed to a thick felt substrate using iron-on fabric. This is a manual prototyping method enabled by the commercial availability of e-textiles and adoption of common textile techniques in design and crafts.

An interesting use of materials and techniques is presented in Tao et al. (2010). The authors use a combination of scattering patterns made from gold and a silk substrate to demonstrate a biocompatible material that resonates at around 0.9 THz. The gold SRR structure was sprayed using electron-beam evaporation after placing micro-stencils onto the substrate. This technique has the advantage that flexible materials with good mechanical robustness and low abrasion rate can be produced on large areas. Although a film and not a textile, further development of nano-woven silk structures could be feasible. Additionally, it was demonstrated that silk-based sub-wavelength structures are suitable for detecting biological activities in the body (Tsioris et al., 2011) or can even achieve electromagnetic responses in various bands by stretching (Lee et al., 2012).

Woven textiles were coated with titanium by Esen et al. (2014) using vacuum deposition. The authors show that the technique results in textile absorbers, which are lightweight and independent from the incident angle of the impinging wave. Absorption rate is stated as 98% at 4.42 GHz. Unlike typical metamaterial designs, here the metal is distributed randomly via means of vacuum deposited nano particles. This leads to the assumption that resonance frequency would be difficult to control for applications that require precise frequency values or graded surfaces, as are needed for cloak designs. However, this work demonstrates a similar design approach to the work presented in this thesis, which is based on the exploration of capabilities of materials and fabrication techniques (detailed in section 3.1).

Ghebrebrhan et al. (2014) present two textile prototypes of which one is woven and the other knitted with a yarn composed of polyester and copper. The authors found that careful configuration of woven or knitted structures resulted in textiles, which can be tuned through structural changes and absorption of electromagnetic waves. Although

they do not report negative-refractive-index performance, the variety of thread arrangement suggested indicates the potential of textile fabrication for metamaterials. This was followed by Burgnies, Lheurette, & Lippens (2015), who proposed a textile-inspired configuration which produced NIM behaviour in simulations between 18 - 38 GHz. Again, through careful adjustments of the lattice period and geometrical positioning of the threads, the resonating frequency is tuneable. These two publications also demonstrate the challenges of textile metamaterials. While the first discusses the fabrication method including both the potential of thread architecture and the limits of structural robustness, resulting in electromagnetic inaccuracies, the latter assumes a perfect production method. This theoretically leads to finely tuneable and accurate electromagnetic behaviour, but disregards material and fabrication aspects.

## **2.2 Electromagnetic Textiles**

Fibres that conduct electricity are at the centre of a wide field of research that spans textile engineering, electronic engineering, textile design, fashion design, applied physics and chemistry. Conductivity is achieved by either coating fibres with conductive metals or polymers, or by winding conductive thin ribbons or metal threads around a core (Cork, 2015). Although some techniques have been used for centuries to apply decorative value to textile products, thin flexible fibres came only widely into electrical operation in the form of the filament in the electrical lamp (Edison, 1880).

Section 2.2.1 provides an overview of the current state of technical development and use of e-textiles to produce electromagnetic behaviour. While textile and electromagnetic engineering is taking the lead here, section 2.2.2 focuses on the larger involvement of designers in the development of electronic products, as a result of the emergence of digital technology in the past 30 years. Wearable computing (Weiser, 1991) has created a demand for electronics embedded into textile intermediate products. E-textiles and Wearable Computing is on the way to becoming an established field in design research, in which designers investigate possibilities for electronically responsive textiles in interactive scenarios for clothing, interior and architectural products. 'Smart' materials inspire textile designers to develop electrically activated design artefacts that question and potentially redefine their relationship to functional objects in daily use. In the past decade, a range of products has been introduced to the

commercial market, accelerating the development of e-textiles and applications even further. In addition, conductive, resistive and piezoresistive properties have become widely available in the form of coatings, paints and yarns. While in this chapter, the focus is given to projects that utilise e-textiles to influence electromagnetic properties, in order to provide the thematic context for textile metamaterials, chapter 6 will detail the design materials and techniques for e-textiles, on which the practical part of this thesis is built.

### **2.2.1 Electromagnetic Engineering**

Electronic textiles (e-textiles) have developed from a niche research area to an important and widely acknowledged field in the past 15 years. Growing availability of conductive fibres has stimulated creation of a range of fabrics and textile products. In return, this has accelerated research not only in technical textiles, but also adjacent fields such as electronic and electromagnetic engineering, as well as textile and fashion design. This section introduces key research that makes use of e-textiles in order to design electromagnetic textiles, and provides an overview of recent development in this field.

#### **Textile antennas**

Textile and wearable antennas constructed from conductive yarns, threads and coated fabrics have been of interest since the late 1990s. Applications include functional clothing utilising the advantages of textiles being flexible (sports), hidden (military) or non-disruptive (healthcare). Previously, large-scale foldable antennas for space applications have been developed, which deploy only when situated in space (Bloom, Park, & Hill, 1985)

The first wearable antenna was presented in 1999 by Salonen, Sydanheimo, Keskilammi, & Kivikoski (1999). While it was not made from textile materials, it was designed small enough to be placed on the body, and separated from the other electronics in a way that allowed the antenna to be embedded in a wearable system. In 2001 an antenna was proposed from a flexible substrate for single or dual-band operation in the Bluetooth neighbourhood (2.4 GHz), which could be embedded in a sleeve (Salonen, Keskilammi, & Sydanheimo, 2001). Although the authors did not specify the type of material used, its dielectric constant of 3.29 suggests that it was not a textile material, since textile materials usually have low dielectric constants, similar to

that of air. An antenna made from textile materials entirely is mentioned by Tanaka, (2003). The operating frequency is 2.5 GHz. The authors describe the challenges of embedding, including the impractical size of common microwave SMA (SubMiniature version A) connectors and finding a suitable location for embedding.

The book “Antennas and propagation for body-centric wireless communications” (Salonen & Rahmat-Samii, 2006) provides a comprehensive summary of potentials and challenges related to purely textile antennas. The authors identify the key features of wearable antenna design, as shown in Figure 2.18. Relevant qualities are marked blue to highlight their importance for textile metamaterials as investigated in this thesis.

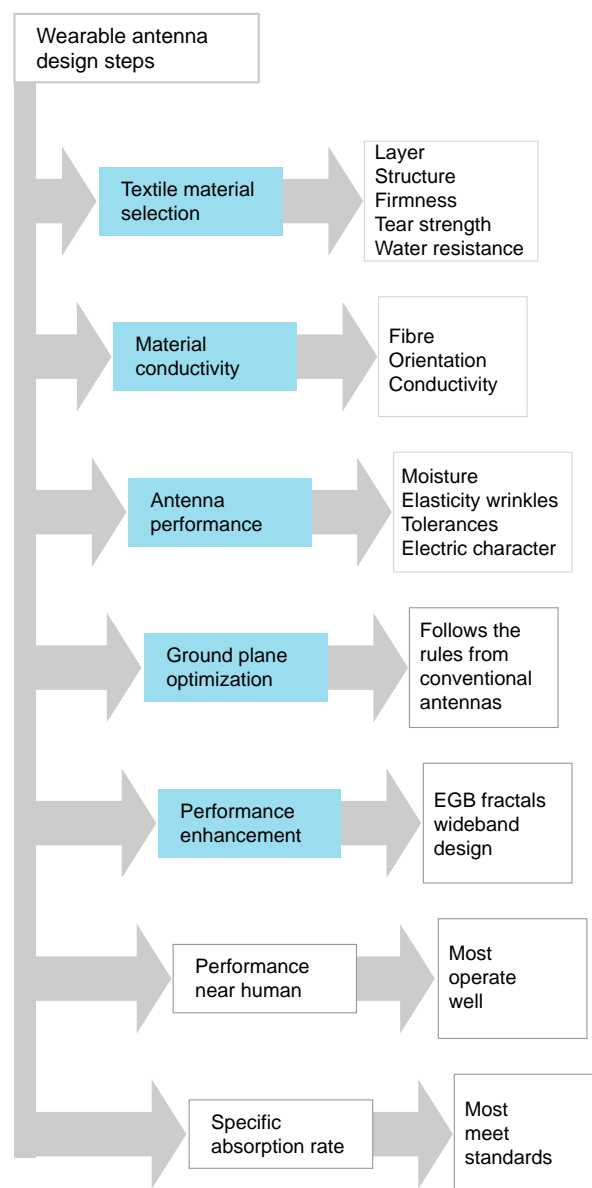


Figure 2.18: Key features related to the wearable antenna design process, adapted from Salonen & Rahmat-Samii (2006). Qualities which have been considered in this thesis are marked in blue.

Regarding the choice of suitable fabric materials for antennas, a few specific examples are discussed by the authors. They suggest using water-repellent fabrics since, due to the high dielectric constant of water, antenna performance changes significantly when the substrate absorbs water. A variety of commercially available conductive fabrics, and copper tape have been employed. The authors conclude that while high conductivity is important and less conductive fabrics do not perform as well, they note that as long as the surface is conductive and parallel to the surface current, the material does not need to be homogeneous in order to obtain good impedance match and bandwidth. This is promising for future textile development as inhomogeneity is an inherent property of textiles. However there is a conflict that needs to be resolved when designing textile antennas. In order to widen the bandwidth of microstrip antennas, the height of the substrate needs to be thicker, which reduces the flexibility of textile antennas. Hence, aspects of required performance, and size and location of the embedded antenna, need to be assessed and balanced.

A broader and more detailed approach to the design of textile antennas can be found in literature after 2007. Research moved from the first steps of producing functional antennas to detailed aspects of antenna efficiency, bandwidth and radiation patterns. Both textile and antenna engineering literature acknowledge technological developments from stand-alone and self-contained wearable systems, which place emphasis on wearability, to ambient-aware systems that monitor the surroundings and link dynamically with other wearable systems. Publications in the textile domain such as the *Textile Research Journal* discuss textile antennas in relation to fabrication issues such as the importance of the substrate (Hertleer, Tronquo, Rogier, & Van Langenhove, 2008), environmental influences on antenna performance (Hertleer, Van Laere, Rogier, & Van Langenhove, 2009), and nano-structured fabrication (Prabir et al., 2007). Further refining flexibility, Kennedy et al. (2009) describe multiple-antenna communication systems for body-worn applications. They developed a microstrip array constructed from purely textile materials to test robustness in performance when bending occurs. Additionally, they designed a wideband multiple-antenna system tailored to body dimensions and placement. The authors state that both arrays showed stability in antenna gain and wide bandwidth. It should be noted that these systems have only been measured in one body position, and further research about flexibility of the system is required. An advanced study into flexible antenna performance is shown in Bai & Langley (2012). Moulds were fabricated to bend and maintain the antenna in

severe crumpling positions in two perpendicular planes. The authors report significant changes in most cases for both impedance and resonant frequency. They concluded that, based on both free space and on-body measurements, the efficiencies of the antennas varied considerably with the type and plane of crumpling, both in terms of radiation efficiency and the shift in resonant frequency. This is an example of the need to balance the performance of the antenna while maintaining flexibility of the system. It becomes clear that a compromise needs to be made between the thickness, size and location of the antenna on the body to achieve satisfactory results. From a material and fabrication point of view, the work by Zheyu Wang, Zhang, Bayram, & Volakis (2011) is highly relevant. The authors present a fabrication method for embroidered microstrip lines (the basic microwave transmission line), describing a process which coats an embroidered antenna with a polymer enriched with ceramics. This approach uniquely combines a textile technique with the fine tunability of ceramic and polymer composites to yield components that are flexible while maintaining robust performance, without compromising efficiency. The evaluation of a microstrip line indicated that the insertion loss was only insignificantly higher than that of a copper microstrip line. This research shows that further investigation of composites made of textile and inelastic materials, as well as the application of textile fabrication techniques during the process, could be beneficial for the development of flexible yet reliably performing antennas. Moreover, the technique appears to be suitable for a further investigation into the fine manipulation of dielectric constants while maintaining the aesthetics of a textile substrate.

### **Key research groups for textile antennas**

The Wireless Communications Research Group at Loughborough University focuses on development of wearable antennas and the detailed assessment of electromagnetic functionality. Researchers, in collaboration with Nottingham Trent University and Southampton University, investigated and compared novel e-textile fabrication techniques (S. Zhang, Seager, Chauraya, Whittow, & Vardaxoglou, 2014) and developed practical connector solutions for placing antennas on the body (Fonseca, Seager, & Flint, 2015; Seager, Whittow, Vardaxoglou, Chauraya, & Zhang, 2013). In Seager, Bowman et al. (2013) the authors present low-cost fabrication of textile frequency selective surfaces (FSS) using embroidery, as well as weaving and screen printing. Several papers discuss simplification, costs of the fabrication technique and

repeatability of embroidered antennas (Chauraya et al., 2012; Dias et al., 2013; Seager, Zhang, & Chauraya, 2013; S. Zhang et al., 2012; S. Zhang & Chauraya, 2013; Shiyu Zhang, Seager, Chauraya, Whittow, & Vardaxoglou, 2014).

The Advanced Textiles research group, under the leadership of Tilak Dias at Nottingham Trent University had a significant impact on the development of e-textiles across the UK. With a focus on knitted and embroidered electronics, the most notable works are electrically heated textiles and temperature sensors (Husain, Kennon, & Dias, 2014), invisible integration of electronic components in yarns (Dias & Rathnayake, 2015; Rathnayake & Dias, 2015) and embroidered antennas (in partnership with Loughborough University, see above). The group's research provides an intermediate step between the development of raw materials and design applications, often collaborating with other institutions enabling employment of the specialist knitting and embroidery knowledge in various fields.

An area of interest of The School of Electronics and Computer Science (ECS) at the Faculty of Physical Sciences and Engineering at the University of Southampton is printed e-textiles for various applications, including textile antennas and wearable applications. Most notably, ink was developed and commercialised<sup>5</sup> that could be screen printed as a polyurethane-based intermediate layer to even the surface of conventional textiles. The ink produces a non-absorbent but still flexible coating. It was then possible to screen print conductive traces with nanoparticle ink (Komolafe, Torah, Yang, Tudor, & Beeby, 2015; Paul, Torah, Yang, Beeby, & Tudor, 2014; Yang, Freeman, Torah, Beeby, & Tudor, 2014) and inkjet-print antennas (Y. Li, Torah, Beeby, & Tudor, 2012; Whittow et al., 2014).

The Electronics Laboratory and Wearable Computing Group at the Swiss Federal Institute of Technology in Zurich completed a project about textile antennas in 2005, from which three publications were produced. The first describes a circular polarised antenna made from entirely textile products (Klemm, Locher, & Troster, 2004), and the second demonstrates four textile patch antennas including a detailed report of textile-related challenges such as deforming when sewn or soaking when glued (Locher, Klemm, & Kirstein, 2006). The third publication discusses the difficulties associated

---

<sup>5</sup> <http://www.fabinks.com> accessed 14/01/2016



with screen printed textile transmission lines onto common absorbent fabrics (Locher & Troster, 2007).

### **2.2.2 E-Textile Design**

E-textiles have become a popular tool for textile designers, enabling them to propose and implement designs in the field of Human-Computer-Interaction. While electromagnetic principles such as structural colour or wireless data transfer from textile to computer are often discussed; textiles that make calculated use of the electromagnetic field as found in antenna design, are almost non-existent. Applications for the ISM (Industrial, Scientific & Medical) frequency band, such as Bluetooth, Wi-Fi or mobile phones, are often used in experimental e-textile design, and offering an all-textile version would contribute to the common aim of replacing hard components with soft textile materials. The optical range of the spectrum is even more relevant, due to the potential to create dynamic colour effects generated through microscopically structured surfaces. These effects can be visually interesting, for example as seen in dichroic materials. Typically used for large glass surface areas in architecture, and impressively demonstrated in the Lycurgus cup (Freestone, Meeks, Sax, & Higgitt, 2007), this effect can also have a decorative purpose in textiles. Supported by the anisotropy of the fibre, colour effects can be observed when changing the viewing angle of such a textile (Burkinshaw, 2015).

This section will illustrate examples that provide insights into how e-textile design may be transferable to the fabrication of electromagnetic textiles. Due to the high geometric accuracy required for metamaterials, the identification of suitable techniques and concepts is key. Using textiles for electronic applications is challenging. They bend and crumple, are sensitive to humidity, commonly wear out or degrade, and have irregular surfaces that resist standardisation. While these qualities provide advantages for a number of conventional textile applications, e-textiles are usually required to be more robust and controllable. Despite advancements in integration of circuits to fabrics, it is still a challenge to manufacture reliable, stable e-textiles, which will endure usage and handling. E-textiles often function differently from their intended response.

The most tolerant applications for electronic functionality are textile sensors. Readings of the sensors are easy to map and scale using textile materials with digital processing. They provide the largest freedom for designers to test applications on the body and in

interior design products, and are therefore amongst the most popular e-textile applications, resulting in experimental outcomes that are the furthest away from e-textile engineering products. The largest database on Do-it-yourself textile sensors has been developed and published by Satomi & Perner-Wilson<sup>6</sup>, and many of these ideas have been taken further in university design departments and open labs worldwide.

Textile actuators are, amongst other applications, used for controlling electromagnetic function. For example, resistive metal yarns can provide a textile solution to activate temporal colour patterns on textile surfaces. The colour change is generated by change in the alignment of the microstructure, activated by temperature, thus creating a filtering effect that falls into the category of frequency selective surfaces (FSS). Heat sensitive molecules form so-called ‘thermochromic pigments’ that are dispersed in a carrier fluid. This means that they can be screen printed onto textile materials. The mechanism and potential for design has been intensely studied in design textile research, as for example by Robertson (2011) and Worbin (2010). While in this case, conductive textiles are used to trigger an electromagnetic effect on the visible spectrum, there has also been work in which magnetic textiles were employed as part of an electromagnet. Mostly, this was done to produce oscillating textile surfaces to generate sound waves (Coelho, Hall, Berzowska, & Maes, 2009; Leclerc & Berzowska<sup>7</sup>; Satomi & Perner-Wilson<sup>8</sup>), or to form a textile-based servo motor (Perner-Wilson, 2014).

### **2.3 Summary and Implications**

In this chapter, the topic of this thesis was situated within the research fields of metamaterials, and electromagnetic textiles in engineering and textile engineering, as well as e-textiles with electromagnetic implications in design and crafts.

Section 2.1 described how metamaterials have been applied in physics and electromagnetic engineering, noting that the choice of current fabrication technologies is not particularly diverse, due to the novelty of the field. The potential for innovation

---

<sup>6</sup> <http://www.kobakant.at/DIY/> accessed 14/03/2015

<sup>7</sup> <http://xslabs.net/accouphene/> accessed 14/03/2015

<sup>8</sup> <http://www.kobakant.at/DIY/?p=5509> accessed 15/03/2015

using a more diverse range of fabrication technologies could push the possible bandwidth towards higher frequencies in the spectrum.

Section 2.2 introduced a range of uses of textiles in electromagnetic engineering, as well as outlining the use of e-textiles, with implications for electromagnetic use in textile design.

The main conclusion, based on this literature review, is that a large area of overlap can be found between textile design and textile engineering, as well as textile engineering and electromagnetic engineering. However, the overlap between textile design and electromagnetic engineering is currently almost non-existent. E-textile design has brought advancements in sensor and actuator technology, and although there is a large interest in material composition and circuit configuration, designing for the electromagnetic field is less explored.

A growing number of designers are undertaking interdisciplinary work in textile design research using new materials with electronic function. Their wider aim is to not only develop better products, as practiced in commercial design, but to install an interdisciplinary inquiry within academia. The field of e-textiles provides a playground to test these methods, as both design aspects and electronic engineering skills need to be applied in order to develop integrated design solutions. Whilst the next chapter will look in detail at how one goes about conducting this interdisciplinary research, the literature detailed in this chapter highlights implications for the advancement of technical knowledge.

The research gaps identified are:

- So far, metamaterials have been investigated in science and engineering contexts. While fabrication methods have become of interest in recent years, there is still much possibility for applying techniques established in other disciplines.
- Textile technology and materials show potential for the design of all-dielectric metamaterials, using existing skills and equipment, to fabricate fine gradients and small periodic structural patterns.
- Skills and knowledge of textile designers may equip the metamaterial engineer with a new tool set, to not only technically fabricate flexible metamaterials but

also to inspire new possibilities for applications. The latter is illustrated in Figure 2.19, indicating how current isolation of the fields may be exchanged for an integrated approach. This is based on the premise that advancement in fabrication technologies also generates new insights into the workings of metamaterials, potentially accelerating the development of practical engineering devices.

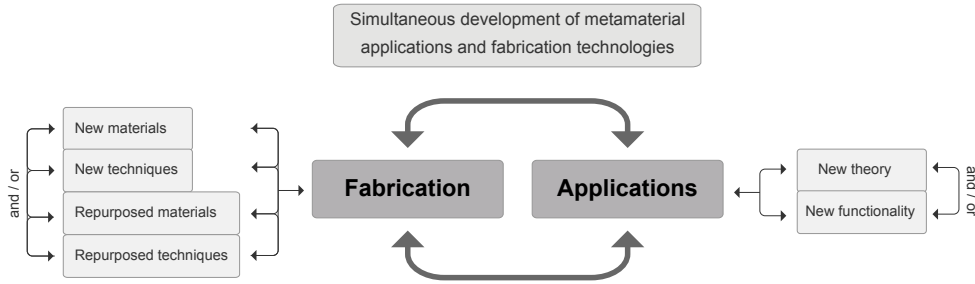


Figure 2.19: Illustration of an integrated approach to metamaterial research promoting interdisciplinary knowledge exchange.

- Whilst a growing number of textile designers are exploring the potential of e-textiles by designing circuitry and textile-based sensors and actuators, electromagnetic textiles have not yet experienced the same level of interest. Despite the fact that many textile designers design *with* the electromagnetic field, most notably using structural colour effects and employing wireless data transfer between textile and computer in wearable computing, the workings behind these mechanisms are mostly disregarded. The potential to use textile structures in order to design devices that enable wireless functionality offer an interesting opportunity for textile designers to apply their skills.

## Chapter 3

# Design Methodology

Bridging textile practice and electromagnetic engineering, this thesis is located in the broad area of science design research. This chapter reflects on relevant key positions in interdisciplinary research in design and applied science, and identifies the potential that arises by applying practice-led methods in electromagnetic engineering.

In section 1.1 the problem was defined as a technical one, and the goal of this thesis set out as a contribution to the field of electromagnetic engineering. However, the process towards achieving this goal differs from the engineering field of technical textiles, in that it follows textile design practice (Albers, 2001) instead of textile engineering proceedings, which typically focus on the rigorous pursuit of a problem-solving task.

This work has followed design stages that share characteristics of “research through practice” defined in the directive for textile design research (Bye, 2010), and creative-production research (Scrivener, 2000). In summary, although the aim was to fabricate textiles that show evidence of metamaterial functionality, the wider aspiration was to explore the potential of textile materials and techniques for metamaterials when used by a textile practitioner. Solutions were informed by experimental textile experience and tacit skills.

Metamaterials are communicated as advanced engineered materials, and currently an in-depth discussion requires an understanding of the specific mathematical and physics principles behind their design and operation. In contrast, this thesis is initiated on the observation that metamaterial engineers and textile designers use similar technical

approaches for constructing designs (albeit having different aims and terminology) that evolve around two- and three-dimensional geometry, pattern, surface and structure. As opposed to choosing from a standardised index of electromagnetic materials for a previously optimised design, it investigates how a practice-led method that uses material experimentation as the primary step can be used to prototype functional metatextiles.

Material experimentation is often described as the driver of knowledge advancement in practice-led research (Frayling, 1993). Pursuing this approach, the presented work can be separated roughly into two stages. The first stage is characterised by specific exploration (Philpott, 2013) and material experimentation with usefulness in mind (Albers, 2001). While this stage requires pre-existing knowledge of electronic textiles and electromagnetic engineering, it is exploratory and aims to gain affirmation for the use of one material rather than another. Using these findings as a basis, the second stage is concerned with the fabrication of prototypes, which are then analysed to validate their electromagnetic functionality.

### 3.1 Material-based Design

In design and engineering fields, materials are one of the building blocks for the development of a new product. They cannot be designed or selected independently from the desired application, the form-finding decisions or the manufacturing technique (Ashby, 1999). Figure 3.1 illustrates the interdependence of function, shape, process and material without prioritising one over the others.

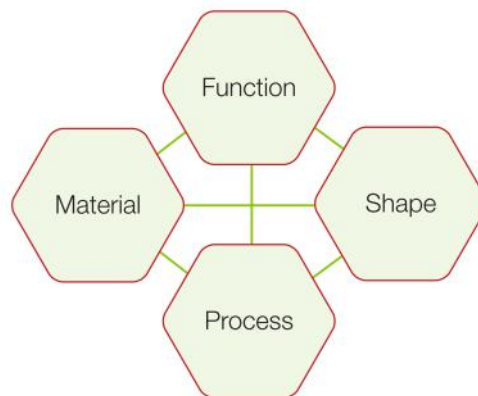


Figure 3.1: The interdependence of the four factors of product design, which equally contribute to proposed design solutions (Ashby, 1999).

In the process of designing and building new devices, the role and place of materials varies, depending on professional preferences, tools, application goals and the designer's expertise. Highly specified material classifications are available to provide information to different groups of professionals and application fields (Addington & Schodek, 2005).

In engineering design, it is desirable to minimise costs whilst ensuring good performance of the new device. An index of standardised materials aids material selection, which describes the process of systematically selecting a material with specific optimal properties for the given application (Ashby, 1999; Charles, 1997). The methodology formed by Ashby provided engineers and industrial designers with "guidance through the forest of complex choices the designer faces." (Ashby, 1999, p.3). Although an iterative process, engineering design has a clearly defined optimisation process with steps evaluated by scientific means (Ertas & Jones, 1993). Ashby separates the design process into three stages, with increasingly detailed knowledge of material properties at each level. In the first stage (conceptual stage) a wide range of materials is considered without the requirement of depth of knowledge about their properties. The second stage (embodiment stage) is marked by optimisation and narrowing down the selection, based on a detailed knowledge about material properties. For the third design stage, highly precise and detailed information needs to be available for the materials selected. Although Ashby acknowledges the potential for disarray of the design process due to iterations and design changes, material selection promotes a linear process for mapping information available, (i.e. known and proven facts about materials under consideration), finalised by the selection of the most suitable material. The means of selection are trade-offs to balance conflicting goals (Ashby, 1999).

Reviewing this method, there is the possibility that it impedes creative material experimentation by disregarding possibilities of interdisciplinary crossovers in the first stage of material review. For example, properties that are desirable for one discipline, (e.g. high dielectric constant in electromagnetic engineering) are not stated in data sheets for materials used in another discipline, (e.g. whiteness of acrylic paints in fine arts), and can thus be easily overlooked in the initial material review if the reviewer lacks comprehensive knowledge of the unfamiliar discipline. As an alternative to material selection a material-based approach is proposed. In contrast to Ashby's

method in which material, shape, function and process have balanced roles, a material-based approach describes how an in-depth exploration of a material initiates the process of designing, and subsequently determines process, shape and function. This approach is frequently used when a designer is involved at an early stage of material development, for example where a material is used that has not yet been fully researched, where designers develop their own materials in a laboratory, or where a fabrication process is altered for a new material. In each case, the boundaries of the design are defined by the capabilities of the chosen materials. This procedure is typically followed in e-textile design research, where the aim is to create and design new materials and structures with special functions and aesthetic value (Kimbell & Street, 2009; Veja, 2014). The starting point of the design process is often an intermediate component, such as a copper-coated fabric, or a silver-coated thread, and the design process is initiated by the availability of this component. The designer considers not only what application these semi-finished components could have, but also how to manipulate the material characteristics and make it act jointly with other materials, to find a new application or an aesthetic style that responds to human senses. The process is often experimental and iterative, driven by material prototyping (Mossé, Gauthier, & Kofod, 2012; Philpott, 2011; Ramsgard Thomsen & Tamke, 2009), until either the desired affect is achieved, or a property previously not considered is exploited (Robertson, 2011).

In a more recent book published by Ashby, one chapter examines this development of designs that are born out of the availability of new materials (Ashby, 2010). Ashby states that using new materials for design is often characterised by both a potential for innovation and a large risk. He further points out that the often “awkward adolescence” of new materials is characterised by two factors; the lack of detailed information, and the language and vocabulary in which the new material is described, which does not have meaning for either the materials developer or the designer. Traditionally, the adoption of new materials follows the direction illustrated in Figure 3.2; once a material has been developed in materials science and research labs, it is then transferred to material manufacturers and suppliers, and reaches the designer only as an endpoint in the supply chain.



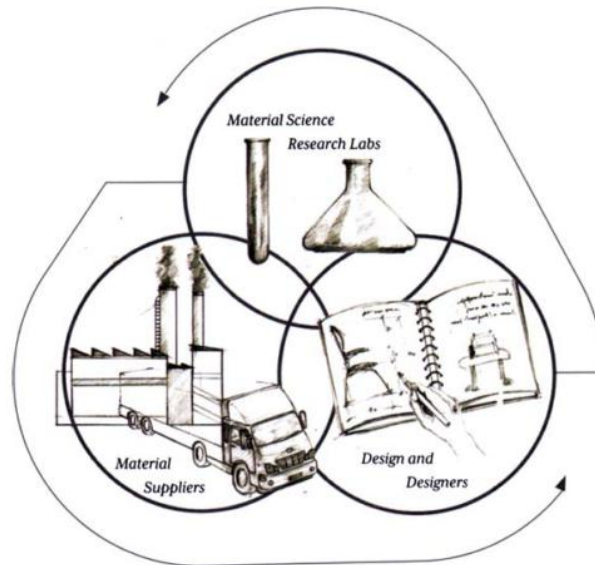


Figure 3.2: New materials are commonly developed in labs first, then processed by material suppliers, and only in the last step used in design (Ashby, 2010).

In the field of smart and electronic materials, an earlier consideration of new materials in design can be observed. A number of researchers, who are often trained in both scientific and artistic disciplines, put material research at the heart of their practice. While this form of research was previously achieved through the pairing of a designer with an industrial partner or cross-institutional collaboration, funding sources are now more widely available to support this level of cross-disciplinarity on a broader scale. Often, the outcomes can be found in architectural disciplines, which intertwine engineering and design objectives and have a longer academic tradition than other design disciplines. Examples of this are the doctoral theses of Babu (2014) and Oxman (2010), which both employ scientific analysis but are centred on questions of design disciplines and pursue a design goal in the longer term. In experimental and commercial textile design, there are a number of designers who aim to close the gap between engineering and textile design, bypassing the materials manufacturer and technical textile engineer. For example, fashion designer Lauren Bowker has developed a carbon emission sensing ink during her studies at Manchester School of Art<sup>9</sup>, applying it in fashion design. Textile design researcher Sara Robertson's doctoral thesis

---

<sup>9</sup> <http://www.dazeddigital.com/fashion/article/12909/1/exclusive-phnx-for-peachoo-krejberg-womenswear-a-w12> accessed 23/03/2014

provides comprehensive knowledge of the workings of thermochromic inks on textiles, with a specific emphasis on liquid crystal dyes that create additive colour mixing effects on textile surfaces (Robertson, 2011). Robertson attributes one of her most significant findings to a “chance discovery”, which became evident through material practice.

Materials-based research is noted by Frayling (1993) in the field of “research through design”, acknowledging the often fundamental contributions that crafts can bring to applied science<sup>10</sup>. Some of the design steps described in this thesis have been based on this process, however some aspects of technical evaluation of the design prototypes are different. In crafts and design professions, learning about a material is traditionally assessed by sensory observation. In textile design, mainly visual and haptic evaluation determines success or failure of a design. For the research presented, it was not possible to rely on these evaluation methods, and outcomes had to be assessed based on the feedback given by instrument based measurement of material properties. In common with other e-textile design projects, over time and through practice the author accumulated a theoretical knowledge of the materials used, for example steel fabrics are less conductive than copper fabrics and thread from company x is less conductive than thread from company y. These were then applied more intuitively to the materials selection process. As a result of repeated handling and growing experience with these textiles, goals for electromagnetic functionality were refined in the second stage of sample production. In particular, this concerned the target frequency of the textiles, as experimentation clarified questions about dimensions achievable for respective textile techniques. For example, dimensions of split-ring resonators (SRRs) were found only through experimentation with equipment and conductive materials available, which then defined the resonating frequency and thus the potential application area for the textile.

To offer a wider range of materials available for selection and thus allow more flexible design decisions, application techniques that separate the electromagnetic function from the textile base material were applied. For instance, the process of screen printing high permittivity ink onto low permittivity textile substrates grants more diversity for base

---

<sup>10</sup> The Lycurgus Cup, crafted around 400 A.D. during the Roman Empire, is an impressive example of how workmanship both advanced the understanding of electromagnetic functionality and generated objects of high value (Freestone et al., 2007).

fabrics. The roots for this design method can be found in the concept of “Kit-of-parts” (Howe, Ishii, & Yoshida, 1999) and Perner-Wilson’s “Kit-of-no-parts” (2011). Whilst the first aims to produce a cheaper and more efficient method of fabrication, the second emphasizes the advantages of craft-based skilled experimentation from raw materials and components.

Figure 3.3 illustrates the process of material-based design, using the development of an NIM metatextile as an example. The first step is given by the material available (conductive silver thread), which then defines the fabrication process, achievable dimensions and thus specific electromagnetic function. The design undergoes iterative changes and information exchange occurs in forward as well as backward direction, influencing design decisions.

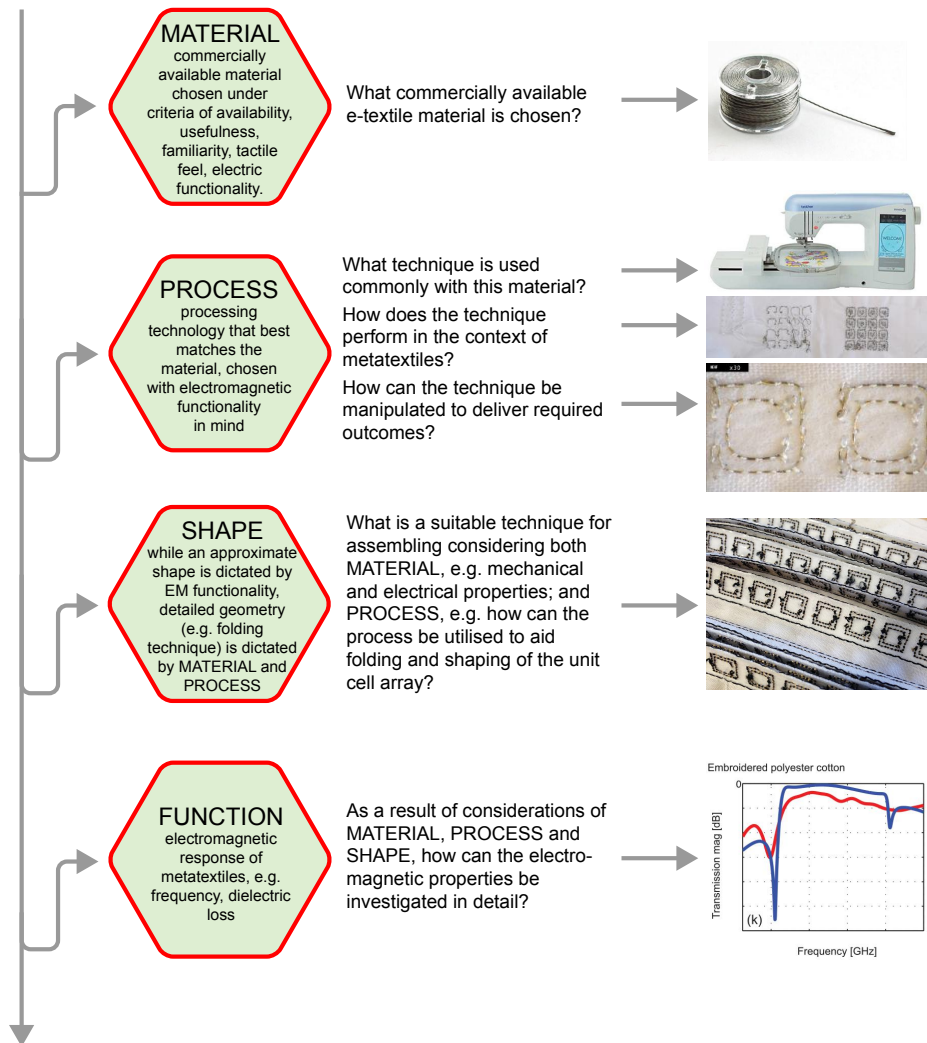


Figure 3.3: An illustration of material-based design using development of an NIM metatextile as an example.

## 3.2 Skills Advancement

The thesis is grounded in experimentation and empirical evidence and the design process was iterative, with each cycle of sample production and measurement producing new insight into the working of textile metamaterials and fabrication aspects.

The concepts of sensemaking, abductive thinking and design synthesis (Kolko, 2010) played an important role for developing designs. They describe how, through the process of data collection, the researcher built connections between apparently unrelated topics and findings. This creative process of adopting practical ideas for the uses of textiles and e-textiles was applied in various design stages.

The setting of professional practice is often seen as the common ground for disciplines in design education and the point of origin for design-led research (Rust, Mottram, & Till, 2007). Over the course of this work, detailed scientific knowledge about how materials respond to electromagnetic fields had to be developed, enabling the author to reach a level of expertise with which materials could be applied in experimental and intuitive ways. Fundamental rules of physics, embedded in engineering methodologies were observed in experimental settings and applied habitually in order to further the research. Advancement of knowledge was closely coupled with an understanding of materials from both the theoretical and practical technological perspectives of design.

An approach encompassing laboratory-based experimentation was chosen for this work, which offered several advantages. First, this approach resembles a textile designer's studio practice where knowledge and skills are acquired through repetition, iteration of manual tasks and reflection. Second, with the laboratory at QMUL being an open space, it allowed the observation of fellow researchers' practice and encouraged discussion. Third, it enabled the understanding of scientific principles in electromagnetics as an embodied approach. An example for this is visiting the three anechoic chambers at QMUL's antenna laboratory, whose design and size help to physically determine the relationship between wavelength and chamber dimensions.

Although limited in its application to textiles, the availability of 3D electromagnetic modelling software provided further aid. The software requires an initial understanding of electromagnetic field distribution, however it enabled the author to understand how to solve electromagnetic problems and pre-test device designs. Models are built as geometric bodies, which are segmented into a mesh. Maxwell's equations are then

solved using a finite element type approach, resulting in both near and far field prognosis. Drawing and 3D paper modelling was another aspect of the learning and communication process (see examples of conceptual drawings in Appendix F). The concepts of spatial distribution of electromagnetic fields were explored and communicated in conversations with academic and technical staff.

### **3.3 Analytical Measures**

With the body of work in practice-led and practice-based research in design-science fields growing, there is a concern about the evaluation of knowledge, which differs from traditional scientific knowledge. Many research projects in this field are the outcome of collaborative approaches between science and textile design stakeholders, in which partners, as experts in their profession, form teams to synthesise knowledge (Geesin, 1995; Robertson, 2011). Pioneering work in the field of e-textile design research primarily looks at technical advancement in applied science, which can be utilised in textile design. Outcomes are often based on a “domain shift” which describes “how a tool initially used for one purpose can be applied to another task, or how the principle guiding one practice can be applied to another activity” (Sennett, 2008, p.125). Although Sennett’s analysis is focused on knowledge distribution within craft fields, this style of activity can open doors for the interdisciplinary design researcher to the unknown discipline in science design partnerships. Domain shifts have been repeatedly applied in this thesis to map out fabrication potential for metatextiles. Some technologies used are located closer to manual textile techniques and materials familiar to the textile designer, such as manual screen printing and embroidery. Others, such as vacuum deposition, inkjet printing of nanofluids or chemical etching, are built upon technologies that are prevalent in electronic engineering and materials science.

When applied on a technical basis, the outcomes of the process are evaluated with technical standards. For e-textiles this would be electrical resistance of the designed and fabricated conductive textiles, which can be roughly assessed with standard tools such as multimeters. Further measures are important to assess textiles for electromagnetic use, such as thickness and permittivity of the textile when used as a substrate. However, growing interest in practice-based design research shows that evaluation of artefacts designed for research has to go further, by including

contributions from e-textile crafts (Perner-Wilson, 2011; Taylor & Robertson, 2014; Tharakan, 2011), interaction design using e-textiles for wearable computing (Baurley, 2004), e-textiles for architecture and interior design (Berzina, 2009; Ramsgard Thomsen & Tamke, 2009; Robertson, 2011; Worbin, 2010), and performance (Lamontagne, 2012). Each category follows a path of evaluation methods, which are often led by the partner discipline, such as Computer Science for Human-Computer-Interaction involving smart and e-textile interfaces, or Performance Studies for Wearable Computing fashion. Common ground is the practice of design making and interest in materials and tool adaptation, as noted in Frayling's concept of "research through art and design" (1993).

In Scrivener's reflection on practice-based doctoral theses that use creative-production research as opposed to problem-solving research, he points out that the evaluation of such work brings up different norms (Scrivener, 2000). He argues that it needs to be assessed based on its contribution to "human experience", with the process of creative production being more important than the knowledge generated by the object itself. In contrast to problem-solving engineering projects, reflection on how to narrow the focus of the problem and its possible solutions plays an inherent part in the progress of this work. According to Scrivener (2000), creative-production research requires rethinking of the setting of objectives, processes, reflection and evidence in doctoral theses. As frequently described in design-led research theses, pursued routes can come to a halt, take a different path, and ultimately lead to different design solutions (Philpott, 2013). Scrivener argues that such "reframing of the problem" (as a result of reflection-in-action) is not only part of the research process which leads to the best-possible solution of a defined goal, but forms an important aspect of the knowledge generation itself. To illustrate this process, this thesis contains documentation of the cycles of the sample fabrication in order to demonstrate the process of refining the selection of materials and techniques. The aim is to undergo a critical review of the validity of using certain techniques for achieving the goal, which considers the constraints of our experiments and acknowledges the originality of creative production.

A further point to consider when evaluating design outcomes is the notion of success and failure. Electromagnetic engineering standards introduce measures against which a device is deemed successful or unsuccessful, and against which textiles have to be assessed. For example, a metamaterial that exhibits a signal loss of -10 dB in

transmitted signal is accounted as failing, or reported as an absorber. While taking into account the thresholds for engineering success, in this thesis the approach of “satisficing”, a term that has been used by Simon (1997) to describe designers’ path of quickly reaching solutions which are “good enough”, was followed. With regard to the fact that materials already commercially available were used, and thus functionalities were delegated to another field of application (from textiles to electromagnetic engineering), satisficing results was not a quick path to easy solutions. Many solutions may be possible for the same problem and optimisation will only be justified in real life settings. In our case, this would concern questions about the specific application for the textile, such as target frequency, absorption rate, and mechanical requirements. Due to the novelty of the field of metamaterials, specifically in textiles, we aimed to define a scope for metatextiles, and then explore how they could be used to initiate more specific and optimised electromagnetic engineering designs.

### **3.4 Conclusions**

The practice-led process presented in this thesis uses cycles of making, measuring and reflective review to produce textile metamaterials that have potential for devices in the microwave bandwidth. Although the goal was to produce textile prototypes with functionality in electromagnetic engineering, the process of research advancement differed from a goal-oriented electromagnetic engineering task.

Knowledge advancement was produced by material-led exploration and familiarisation with available textiles. In this process existing textile materials and techniques were reviewed, and applied to the design of textile metamaterials. The approach began with the exploration of an available material, which was roughly suitable for the application, which was then followed by the development of shape and function as a part of the investigation. Rather than asking, how can a textile metamaterial for frequency  $x$  be produced, it is asking, what frequency can an embroidered metamaterial produce when using conductive thread  $y$ ?

This differed to traditional material selection in that it was initiated by the availability of new materials and domain shifting of fabrication technologies, as regularly used in crafts and material-based design fields. Textiles were explored in this interdisciplinary context but within the technical design parameters of metamaterials. Seemingly

everyday designs produced by textiles designers, such as graded (e.g. shaded) surfaces, gained a new relevance when they were viewed as an electromagnetic material.

This thesis attempts to use the practice-based knowledge advancement to achieve familiarity with electromagnetic engineering methods and boundaries, and achieve new material combinations and fabrication methods that are used less in electromagnetic engineering.

To summarise:

- The work was initiated by the availability of new materials and/or new understanding of materials in the context of metamaterials. Seemingly everyday designs produced by textiles designers, such as graded surfaces, gained new relevance when viewed as an electromagnetic material.
- Reviewing elements of textile and surface design (pattern, repeat and geometric arrangement) for use in electromagnetic materials initiated the design process and delivered the technical building blocks for creating a surface. The design restrictions were led by constraints set out in materials theory, which for example defines the size, shape and arrangement of unit cells.
- Whilst producing textile metamaterials was the goal, the challenge was to identify a method with which they could be unambiguously evaluated and seen as practical alternatives for rigid and more functional metamaterials.
- Reproducibility may become an issue, as samples were produced through a manual and creative process with many iterative steps. Precise resonance frequencies are important for correct electromagnetic functionality, and altering the process of fabrication will result in changes of electromagnetic performance. However, as standard industrial manufacturing technology is available, this would be investigated in future work.
- The research process has been directed through the understanding of the function of metamaterials from a technical viewpoint. Chapter 2 describes how technical literature and access to expertise has highlighted possibilities that may have otherwise been overlooked from a design perspective. However, a designer's viewpoint has been maintained by generating original designs and manually made samples.



- The review of literature has shown that this approach is rarely used in engineering, despite providing the potential for innovative outcomes. A common reason is lack of time, as a practice-led process frequently requires more time. Moreover, work is often advanced by failure and reflection. This does not significantly differ from an engineering research process, however the description of this process does not usually form part of a thesis.
- The idea of material-based experimentation has become relevant in textile design, as electronic and smart materials enter the experimental design field. Although the materials are now commercially available, they still constitute a new field in which experimentation and testing in situ is necessary.
- There is a general lack of work related to electromagnetic textiles in textile design research. This is most likely due to the fact that functionality in electromagnetic engineering is not easily understood. Metamaterials are a research area in which the theory plays a more important role than practical fabrication, with the result that the field is led by scientists and engineers.
- The main difference to traditional textile design outcomes, which are evaluated, based on the qualitative human sensory system, is that specialist test equipment was needed to judge whether the designs were successful. Thus there was a quantitative threshold that exactly specified the criteria for a successful design.
- The research initially used standard and general measurement techniques for the first few steps, some of which are familiar to the field of e-textiles. This included measuring DC resistance with a multimeter, or using a microscope to measure dimensions that are too small for the human eye to judge. Other techniques had to be learned, such as operating a microwave network analyser, understanding the way that electromagnetic waves behave in anechoic chambers and designing for the correct frequency band. Understanding of the unknown discipline was progressed by laboratory-based experimentation up to a point where operation became intrinsic. The existence of present day electromagnetic modelling software significantly aided this understanding process.

## Chapter 4

# Material Parameter Identification

This chapter outlines the technical terminology required to define material behaviour in electromagnetic engineering. It presents the definition of properties (section 4.1) that characterises materials in terms of their response to an electromagnetic field; consisting of relative permittivity (section 4.1.1), dielectric loss (section 4.1.2), permeability (section 4.1.3), refractive index (section 4.1.4) and impedance (section 4.1.5). The following section (4.2) defines scattering parameters (S-parameters). Section 4.3 details the conversion methods used to retrieve material properties, and finally, section 4.4 describes how taking account of the electromagnetic material properties of the materials influenced design decisions and aesthetic vocabulary.

### 4.1 Material Property Overview

Electric and magnetic fields can interact with a material in two ways when passing through a sample:

- Energy can be exchanged between field and material in a lossless way,
- Energy can be absorbed by the material (usually in the form of heat) and thus be permanently lost from the field.

In microwave engineering, material behaviour is of fundamental importance, affecting the directional, transmission and reflective performance of antennas. Selecting a material appropriate for the task helps with the design of efficient and small devices.

The accuracy and repeatability required of material properties has created a demand for standardised industrially produced materials. Rigid composites, such as ‘FR-4’ (which stands for “flame retardant” grade 4) are manufactured from woven fibreglass reinforced with epoxy resins. Although they can have tolerances of 5% or more in permittivity between suppliers, they deliver a good compromise between accelerating the development process and keeping fabrication costs low, while requiring only minor changes in the design to level the tolerances. Regarding the optimisation of standardised materials, high dielectric constants and low dissipation factors are often desired parameters, with the goals of spatial diminishment, high efficiency and durability.

#### 4.1.1 Relative Permittivity

Permittivity  $\epsilon$  describes how an electric field  $E$  is affected by a dielectric material. Every material displays an electric polarisation when exposed to an electric field. The magnitude of this polarising effect determines the potential for the dielectric material to store an electric charge. A higher polarisation density describes a higher potential for electric storage and permittivity.

Relative Permittivity  $\epsilon_r$ , or the dielectric constant, describes how an electric field is affected by a dielectric material relative to the field in free space  $\epsilon_0$ . It is a dimensionless number, and the relative permittivity of a vacuum is 1.

$$\epsilon_r(x) = \frac{\epsilon(x)}{\epsilon_0} \quad (4.1)$$

Permittivity can be given as a complex number, with the real part  $\epsilon'$  resembling the storage, and the dissipation factor defined by the imaginary number  $\epsilon''$ .

$$\epsilon = \epsilon' - i\epsilon'' \quad (4.2)$$

Textile materials usually exhibit low permittivity and low dielectric losses as a result of their construction and thinness. A textile material consists of a fibrous material and air,

resulting in a material with an effective permittivity between  $\epsilon_0$  and the permittivity of the fibre material  $\epsilon_{(x)}$ . The composition is determined by fibre construction method, thickness, and uniformity of the thread. There are numerous effective medium approximations available to derive permittivity when modelling composite materials, each defined in regards to shape and geometry of inclusions.

For most materials, their permittivity varies with frequency of impinging wave, but for some specialised materials, permittivity can be controlled by external properties such as light.

#### 4.1.2 Dielectric Loss

Dielectric Loss describes the material's dissipation factor, quantifying the loss of electric energy into, for example, heat.

In general for electromagnetic devices, the loss tangent is to be kept low to ensure maximum efficiency. If the purpose is absorption, such as in electromagnetic shielding devices or microwave absorbers for anechoic chambers, then a high loss is preferable.

Dielectric losses will be described using the loss tangent  $\delta$ :

$$\tan \delta(x) = \frac{\epsilon''}{\epsilon'} \quad (4.3)$$

#### 4.1.3 Relative Permeability

Just as permittivity defines the effect a material has on the electric field, permeability  $\mu$  describes how a magnetic field is altered by a material's magnetic properties.

Relative permeability  $\mu_r$  describes how a magnetic field is affected by a material, relative to the magnetic field in free space  $\mu_0$ . It is also a dimensionless number, and the relative permeability of non-magnetic materials is 1. The relative permeability of some materials, for example ferromagnetic materials, can be significantly changed via the application of an external constant magnetic field (often applied by a magnet).

$$\mu_r(x) = \frac{\mu(x)}{\mu_0} \quad (4.4)$$

#### 4.1.4 Refractive Index

An electromagnetic wave (radio wave, light etc.) is a combination of time varying electric and magnetic field and so the refractive index  $n$  of a material describes how electromagnetic waves propagate through that material, considering both electric and magnetic field. It is defined as the ratio between the speed of light in vacuum and in the material, determined as:

$$n = \frac{c}{v} \quad (4.5)$$

where  $c = 299,792,458$  m/s is the speed of light in vacuum and  $v$  is the speed of light in the substance. For example, for visible light the refractive index of glass is around 1.5, meaning that light in glass travels at  $c / 1.5 \approx 200,000,000$  m/s.

Snell's Law of Refraction defines the relationship between the ratio of the angles of incidence and refraction for an electromagnetic wave incident at a material interface and the ratio of refractive indices between two mediums (see Figure 4.1).

$$\frac{\sin \theta_1}{\sin \theta_2} = \frac{v_1}{v_2} = \frac{n_2}{n_1} \quad (4.6)$$

with each  $\theta$  as the angle,  $v$  as the speed of light in the medium, and  $n$  as the refractive index of the medium.

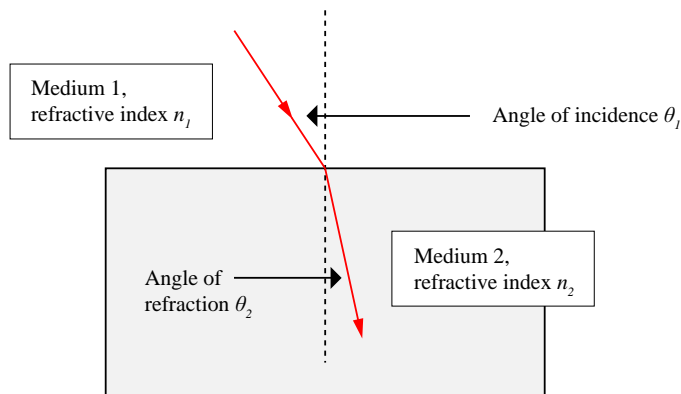


Figure 4.1: Refractive index.

To experimentally derive the refractive index from permittivity and permeability, we use the formula:

$$n = \sqrt{\epsilon_r \mu_r} \quad (4.7)$$

### 4.1.5 Impedance

Wave impedance  $Z$  is defined as the ratio of the magnitude of the electric field  $E$  to the magnitude of the magnetic field  $H$ , in a dielectric material.

$$Z = \frac{|E|}{|H|} \quad (4.8)$$

The intrinsic impedance defines the ratio of the electric and magnetic field components of an electromagnetic wave, and is given by

$$Z = \sqrt{\frac{\mu}{\epsilon}} \quad (4.9)$$

Intrinsic impedance of free-space is  $377 \Omega$ , and is zero for an electromagnetic wave incident on a metal conductive sheet, since the tangential electric field is zero.

## 4.2 Scattering Parameters

Scattering parameters (S-parameters) describe the reflection ( $S_{11}$ ,  $S_{22}$ ) and the transmission ( $S_{12}$ ,  $S_{21}$ ) occurring when an electromagnetic wave propagates through a two-port (or multi-port) network. An example of a two-port network is an electromagnetic wave normally incident on a material interface, where some of the wave will be transmitted (port-2) and some reflected (port-1).

S-parameters are noted as complex numbers containing a real part and an imaginary part representing wave behaviour. Both the magnitude and the phase (see Figure 4.2) can be extracted from the complex number.

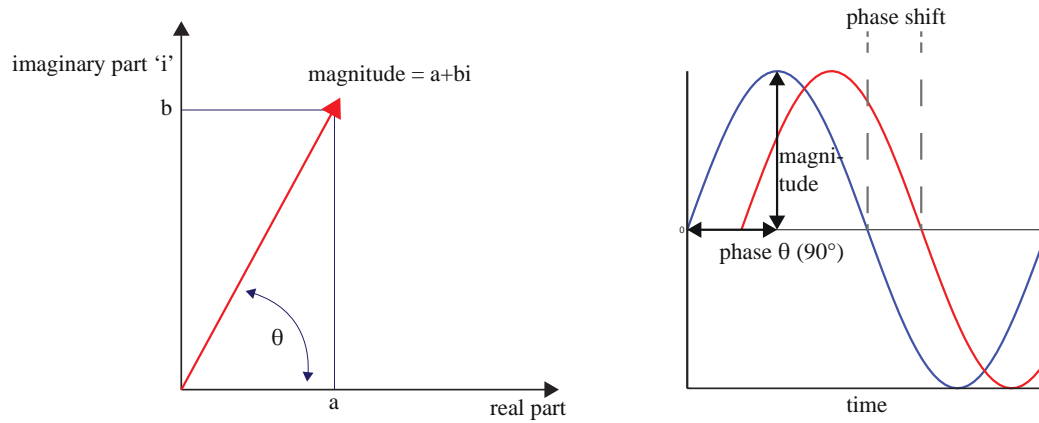


Figure 4.2 : Determining magnitude (amplitude) and phase of an electromagnetic wave.

In a two-port network, such as between two antennas, a matrix of four s-parameters fully describes transmitted and reflected propagation between the two ports, as illustrated in Figure 4.3, with a and b illustrating the power of the waves.

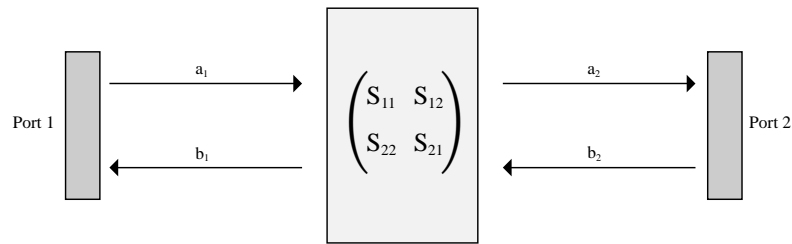


Figure 4.3: S-parameter matrix in two-port network.

The s-parameter matrix for a two-port network is defined by

$$\begin{pmatrix} b_1 \\ b_2 \end{pmatrix} = \begin{pmatrix} S_{11} & S_{12} \\ S_{21} & S_{22} \end{pmatrix} \begin{pmatrix} a_1 \\ a_2 \end{pmatrix} \quad (4.10)$$

Written in linear form as

$$\begin{aligned} b_1 &= S_{11}a_1 + S_{12}a_2 \\ b_2 &= S_{21}a_1 + S_{22}a_2 \end{aligned} \quad (4.11)$$

Each equation gives the relationship between the reflected and incident power at each of the network ports.

S-parameters measurements are carried out with a Vector Network Analyser (VNA), recording amplitude and phase signals between the two ports. The wave transmission and reflection can be plotted against either time, which delivers a spatial representation of the electromagnetic field propagation between the two antenna ports, or against frequency, which are taken over a band usually chosen according to frequency of interest or capped by the frequency range of operation of the antennas.

In a general two-port propagation process the wave suffers a number of related discontinuities. For example in a free space system with a pair of antennas and a dielectric sheet between them, a wave would be partly reflected at the antenna input port, the on-going transmitted wave partly reflected at the front face of the dielectric, then the transmitted signal would see subsequent part reflections at the dielectric air interface and at the antenna aperture. In the time domain mode of a VNA it is possible to see all interactions and place a digital window over the region of interest, which includes the thickness of the dielectric sheet as well as a small distance before and after. It is possible to derive the dielectric properties from this data.

There are four basic techniques available to measure s-parameters for the purpose of determining the dielectric properties of a material sample. Each technique has limitations regarding frequency range, substrate materials and applications (Table 4.1). The suitability of these measurement techniques are summarised in Rhode & Schwarz (2006). Description of the relevant measurement methods used will follow in section 6.4.

Table 4.1: Common material measurement techniques, including recommendations for suitability, measured parameters and retrievable properties.

Measurement Technique	Materials	Measured parameters	Dielectric properties
Transmission/Reflection line	Waveguides, Coaxial lines	$S_{11}, S_{21}$	$\epsilon, \mu$
Open-ended coaxial probe	Liquids, semi-solids	$S_{11}$	$\epsilon$
Free Space	Large flat	$S_{11}, S_{21}$	$\epsilon, \mu$
Resonant cavity Technique	Rod shaped solid materials, liquids	Frequencies, Q-factors	$\epsilon, \mu$



### **4.3 Material Parameter Retrieval**

Parameter retrieval for permittivity, permeability, dielectric loss and refractive index from experimentally derived s-parameters can be achieved using a range of mathematical approaches, depending on which parameters are required and what measurement techniques have been chosen. The conversion from measured s-parameters to material properties is sensitive to accuracy and stability of measured data, and is non-trivial. Each approach has different benefits and limitations, depending on, for example, sample dimensions, the desired dielectric properties, efficiency of conversion and certainty of the results.

#### **4.3.1 Parameter Extraction from S-parameters**

For conversion and retrieval of  $\epsilon$  and  $\mu$  of dielectric materials it is necessary to solve propagation equations for retrieving the unknown material parameters, usually employing some form of iterative process. We applied two commonly used algorithms, based on the Nicolson-Ross-Weir model and NIST Precision model, which were performed by either the commercial software package Agilent 85071E (see Appendix H) or a Matlab calculator based on previously conducted research in the Antenna and Electromagnetics Group at QMUL.

The Nicolson-Ross-Weir (NRW) model is the most popular method to determine permittivity, permeability and dielectric losses as a function of frequency from measured s-parameters (Nicolson & Ross, 1970; Weir, 1974). Its advantages are high accuracy and the ability to derive all material parameters. A disadvantage of this method is that materials with low dielectric losses and thickness larger than half the wavelength of interest can show discontinuity in their results. The algorithm and the specific challenges addressed when deriving parameters of textiles are presented in section 6.6.2.

The second method, the NIST Precision model, was developed by Baker-Jarvis et al. (1990) at the National Institute of Standards and Technology (NIST). This method applies an iterative calculation process to approximate permittivity for non-magnetic samples. The advantage of this method is the independence of the sample thickness as well as the position of the reference plane.

### **4.3.2 Parameter Extraction from Capacitance**

For measurements in the lower frequency range of 50 Hz - 5 MHz, a simple method can be employed which directly derives permittivity from capacitance. Capacitance measurements can be taken with a parallel plate capacitor, as described in section 6.4.4.

Despite not being well suited for most microwave applications, because of the low-frequency range, this technique was used to provide comparative results and aided the interdisciplinary learning process. The benefit of the parallel plate set up is its suitability for textile materials; the sample is easily accessible, while the thickness is measurable with an integrated micrometer.

### **4.3.3 Refractive Index Extraction from Transmission Phase Data**

For detection of a negative refractive index in resonant metatextiles, a different method was employed, one with less numerical ambiguity. This provided key results without a high level of numerical processing of measured data. Using this method presented a major advantage as it provided an almost instant way to separate a successful from an unsuccessful prototype during experiments.

A dip in the phase of the transmitted wave ( $S_{21}$ ) indicates the reversal of the phase velocity while retaining the propagation direction, resulting in a negative refractive index. This can be observed by comparing layers of materials in various thicknesses (Aydin, Guven, Soukoulis, & Ozbay, 2005; Aydin, Li, Sahin, & Ozbay, 2008). Whilst in a typical dielectric material the phase advances with increasing thickness, the phase decelerates in a negative refractive index metamaterial. Whether a prototype was viable could be determined immediately by observing the phase of the transmitted wave during the measurements. The retrieval of refractive index using this method is detailed in section 6.6.3.

## **4.4 Discussion**

This chapter focussed on providing definitions of a standard set of material criteria in electromagnetic engineering. Properties have been defined, which are used to evaluate material response when exposed to an electromagnetic field, and which are used to

demonstrate metamaterial characteristics in the studies presented in chapter 7 and chapter 8.

Determining electromagnetic parameters of textile materials accurately is a known challenge. This can be attributed to two factors:

- Textiles are thin, flexible and have an irregular surface. As a result, thickness and smoothness vary and are generally difficult to determine over a larger surface area.
- Textiles contain a large percentage of air. They commonly exhibit electromagnetic properties close to that of air, thus reacting strongly to environmental changes such as humidity and temperature (Bal & Kothari, 2009). As a result, the measured electromagnetic properties can vary largely depending more on these factors than the textile itself.

Both factors pose challenges for the common measurement methods described in section 6.4, as they neither provide a precise enough measurement eliminating environmental effects, nor do they take into account the intrinsic flexible and soft properties of textiles. Due to these difficulties, textiles are often replaced by other flexible non-fibrous materials such as leather or coated flexible films when soft substrates are required. This can result in narrow selections of textile substrates in electromagnetic engineering, often contradicting the reasons why textiles have been chosen in the first place. Textiles bend three-dimensionally, are subject to temperature changes, commonly wear out or degrade, and have irregular surfaces that withstand standardisation. While these qualities provide advantages for most conventional textile applications, such as the ability to drape and allow body movement, regulation of body moisture release, thermoregulation, or recyclability of mono-material fibres; electromagnetic devices need to be far more controllable and sustain the same properties in various environmental scenarios.

As a consequence of these challenges, the desired performance of textiles, such as malleability, flexibility, and drapability are often not considered in the analysis of the electromagnetic devices for which the textiles were used. This is specifically the case for simulation software. Currently electromagnetic solvers do not allow modelling the complexity of textiles, and idealised effective versions of textiles are analysed instead.

In order to approximate textile behaviour as it is intuitively applied in everyday situations, this research adopts a methodology that tolerates a less controlled material approach. Although bending, crumpling or draping has not been taken into account in the measurements; the samples have been left to move naturally without attempts to correct this behaviour using additional support structures. In cases where unambiguous results could not be achieved (for example when measuring dielectric loss of thin textiles, see section 6.6), determining acceptable limit values as thresholds allowed assessment of the outcomes. Methods, that enabled evaluating measured data with as few intermediate steps as possible, as described in section 4.3.3, led to unambiguous results.

## **Chapter 5**

# **Material as Structural Form**

In order to understand the structural characteristics of the textiles developed in the next chapters of this thesis, it is important to identify material and structural specifications as applied in electromagnetic engineering and design-led research practice. This chapter provides an overview of the terminology that describes geometrical distribution of patterns in both domains.

This chapter highlights the difference between scientific and experimental design concepts of understanding and using materials. While practice-led research utilises a practical engagement with materials and tacit knowledge is gained through this, electromagnetic engineering applies materials theory to predict materials behaviour. The chapter aims to establish the link between the technical approaches for both disciplines, potentially leading to novel functional prototypes through interdisciplinary inspiration as well as a scientifically inspired aesthetic vocabulary for textile design.

### **5.1 Material Geometry**

Three general geometric categories were identified as critical:

- Scale,
- Two-dimensional pattern,
- Three-dimensional architecture.

All three determine, and are determined by, functionality and design intention. This section briefly describes how these geometrical aspects are applied in textile design and engineering, with regard to this thesis.

### 5.1.1 Scale

The scale of a design is of interest to both textile designer and electromagnetic engineer. The designer needs awareness of scale on two levels. Firstly, cognitive and motor skills of the intended users, and secondly, an understanding of the components of a textile that cannot be detected by the naked eye, such as colour pigments or fibres. Due to the commercial availability of raw or semi-finished materials, a textile designer does not necessarily need scientific expertise of the specific construction of a single pigment or fibre. However, for some applications, and especially in view of the increased use of smart materials in textile design, the scientific knowledge of micro- and nanostructure of materials becomes more important, and allows to evaluate change of material state according to its aesthetic implications (Heinzel, 2015). Considerations of scale, at a micro- and nano-level, can be found in design literature and material inventories specifically for designers, for example shown in Figure 5.1.

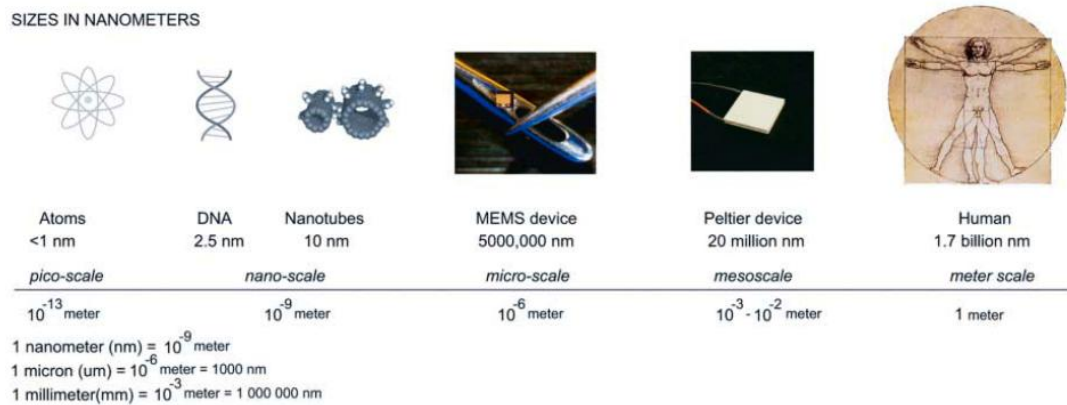


Figure 5.1: Illustration showing comparisons of sizes with matching scales (Addington & Schodek, 2005).

In electromagnetic engineering, designs target a specific wavelength or bandwidth in the electromagnetic spectrum (see Figure 5.2). As frequencies are allocated through national legislation and regulated by Ofcom in the UK (Cabinet Official Committee on UK Spectrum Strategy, 2010), target wavelengths are already pre-determined by the application. Microwaves, the focus of this work, range from 300 MHz ( $\lambda = 100$  cm) to 300 GHz ( $\lambda = 0.1$  cm), and cover a diverse range of applications. Based on research

conducted in the Antennas & Electromagnetics Group at Queen Mary University of London, and assessment of what will be achievable with textiles, Table 5.1 shows the two bandwidths in which this work is located. The main applications of these bandwidths are radar, space and satellite communications. Initial tests were also conducted to measure in S band (2.6 – 3.95 GHz), as well as at 2.4 GHz (near field communication (Bluetooth, RFID), navigation (GPS) and wireless local area networks (LAN)). However, substantial noise and interference in this popular frequency, as well as “edge effects<sup>11</sup>” produced by the gating procedure, prevented the recording of usable data.

Table 5.1: Frequency bandwidths and wavelengths relevant to this thesis (IEEE Standard 521 – 1984)

Name	Frequency bandwidth	Corresponding wavelengths	Applications
X band	8.2 – 12.4 GHz	36.58 – 24.19 mm	Military satellite communication, radar, deep space communications
C band	4 – 8 GHz	75 – 37.5 mm	Satellite communication, Wi-Fi (5GHz), weather radar

Dimensions of antennas and material structure depend on the target wavelength. Due to the relatively low permittivity of textiles, and the wavelengths under consideration, wearable antennas can be large, and problematic to place onto the body without bending. Much research has been conducted to minimise antenna size in order to support small design solutions for wearable applications (Sharma & Parini, 2013). Minimisation techniques include the use of high dielectric substrates or resonating metamaterials, where the design of the unit cell is only about one tenth of the targeted wavelength, providing the opportunity to shrink antenna designs.

---

<sup>11</sup> [http://na.support.keysight.com/materials/help/85071webhelp/85071Freespace\\_Measurement\\_Example.htm](http://na.support.keysight.com/materials/help/85071webhelp/85071Freespace_Measurement_Example.htm), accessed 12/2/2017.

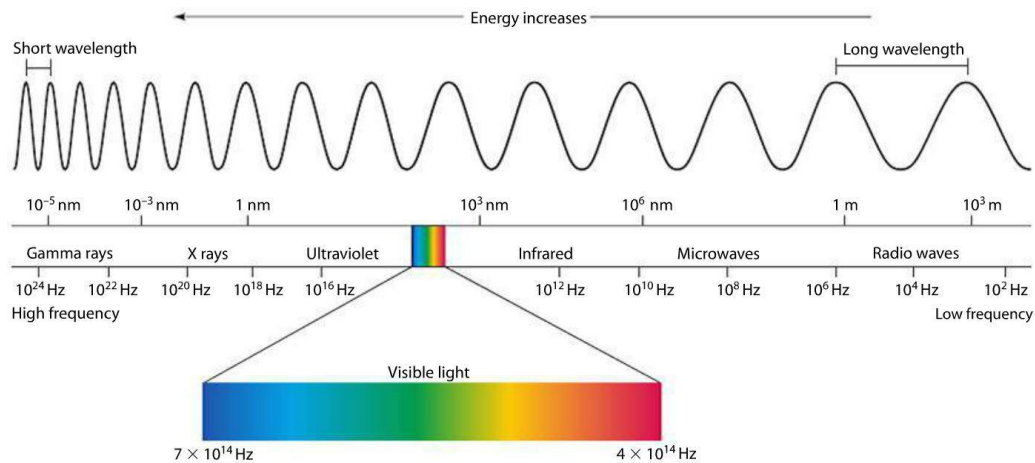


Figure 5.2: The electromagnetic spectrum. While the human eye can only perceive the small spectrum of ‘visible light’ (430–790 THz), electromagnetic devices are designed for specific frequency bands located in various parts of the spectrum.

In periodic materials (see section 5.2.4), the unit cell, which describes a single element that is repeated, needs to be smaller than the wavelength being targeted. They are considered to be homogeneous and effective materials described by global behaviour, but are heterogeneous on a small scale. The relationship between size of unit cell and wavelength applies for wave performance on the complete electromagnetic spectrum (see Figure 5.2), which reveals the challenge for designing for the visible light spectrum. Even with today’s advanced technologies to produce devices on the nano scale, precision and industrialised fabrication on the scale required is still a major challenge. Devices for microwaves are usually simpler to fabricate, as standardised mechanical processes such as milling and etching can be easily applied on solid materials in this scale. However for textiles and porous materials, the scale required for microwaves still presents a challenge. Diameters of threads and yarns are just on the threshold of a tenth of a wavelength, porous surfaces require a larger quantity of ink which results in wider lines and patterns. Mechanical fabrication issues, such as tension, result in frayed edges or round corners where sharp lines are required. The identification of these dimension and geometry limits of textile materials, as well as testing the extent to which the imperfection of form was tolerable, was one of the objectives of the studies presented in chapter 8.

### 5.1.2 Two-dimensional Surface Pattern

Two-dimensional geometric patterns are a concept relevant to both textile designers and electromagnetic engineers. In design, surface patterns are used to alter visual



expression, spanning a wide range of varieties in function and aesthetics. For example, the repetition of patterns between widths of wallpaper lengths needs to be considered. This requires the designer to be skilled in constructing repeats, and knowledgeable about the technical requirements of the manufacturing process.

In e-textiles, the application of patterns and geometric elements is mainly to facilitate electric function. Thoughtful embedding of conductive threads and electric components into a woven textile can result in patterns that also have visual appeal. Various textile design researchers have investigated the aesthetic potential through electronic function, using both their technical skills and design interest (Berzina, 2009; Veja, 2014). One example is a textile solution for the electromagnet present in loudspeakers, designed as a textile coil combined with a magnet. A simple woven example of a textile coil is shown in Figure 5.3.

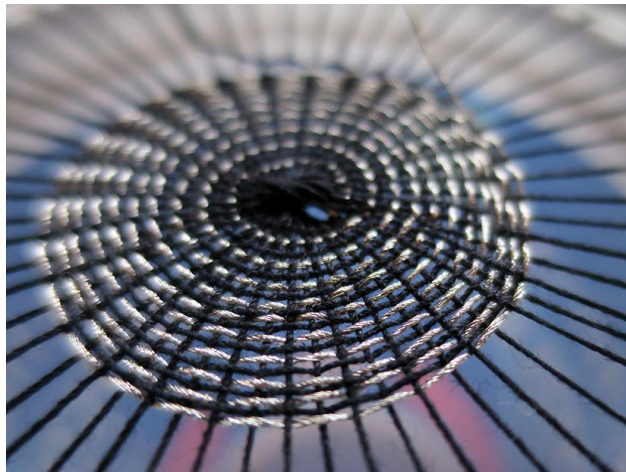


Figure 5.3: Simple woven coil for textile loudspeaker<sup>12</sup>

In the application of heat pads, e-textiles are used to manipulate visual appearance by prompting thermo-reactive dyes. Various designers have exploited this to produce dynamic colour-changing patterns, such as Robertson (2011), Worbin, (2010) or Calder (2011), seen in Figure 5.4.

---

<sup>12</sup> <http://www.kobakant.at/DIY/?p=5509> accessed 15/01/2016

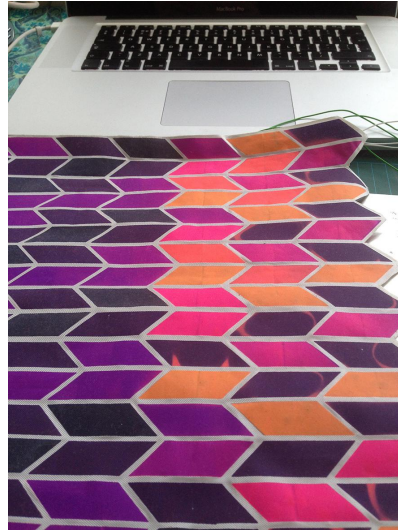


Figure 5.4: Dynamic colour pattern enabled by e-textiles and thermochromic dyes (Calder, 2014).

Although the patterns used in this thesis are simple tessellations, it is useful to point out that tools are highly adapted to designing and fabricating patterns, due to the importance of patterns in textile design. Thus, a reasonable link to electromagnetic functional patterns is established. For example, pre-programmed algorithms in digital embroidery machines provide the user with a large amount of pattern variation, which can be optimised through creative and technical experimentation, without the need to understand the mathematical relationships behind them.

In electromagnetic engineering and materials science, two-dimensional patterns define behaviour in the electric or magnetic field. The third dimension, the thickness of a conductive layer with respect to wavelength, is important. However the thickness can vary within certain thresholds without diminishing the electromagnetic functionality, as defined by the skin depth formula (Blattenberger, 2009).

### **5.1.3 Three-dimensional Architecture**

The three-dimensional architecture of threads and yarns in a textile mostly play a role in constructed textiles, such as woven and knitted structures. By modifying the position of threads within the constructed textile, different tactile and visual expressions are achieved. Whilst techniques such as screen printing are conventionally used for visual decoration, in e-textiles and especially in electromagnetic textiles, the consideration of three-dimensionality plays a significant part, as it regulates electric function.

Traditionally, considering three-dimensionality is crucial for design applications intended for use on a human scale. In fashion design the textile needs to fit around the body, and two-dimensional patterns (which here describe the blueprints on paper that form the parts of a garment) are constructed to take the curves of the human body as a template for later assembly. A similar approach is used in interior design, taking into account the different drape and configurations of various products. For Wearable Computing applications, placing circuitry on a three-dimensional model, and subsequently onto a two-dimensional pattern, helps to develop a strategy for placing electronic components onto the body. This plays a part in ‘bodystorming’, a design method that aims to understand how people interact with their physical surroundings and the tools they use (Schleicher, Jones, & Kachur, 2010).

For metamaterial related science and engineering, how the three-dimensional architecture of unit cells interact with each other defines their specific functionality. Engineering artificial materials involves, in almost all cases, the manipulation of this three-dimensional layout of material cells. Materials are not only evaluated by global performance, but behaviour is actively designed by assembling modules locally.

## **5.2 Material Performance**

Materials in electromagnetic engineering are clearly defined and chosen based on the parameter set explained in chapter 4. For controlling electromagnetic fields and designing metamaterials, it is important to describe a set of mechanical characteristics. These are not different properties, but they provide a further understanding on how both structure and material affect the electromagnetic performance in metamaterials. It should be noted that categorisations overlap, or, in some cases, have changed over time or vary with author. Most described material performances are also ubiquitous in textile design.

### **5.2.1 Effective Medium Theory**

An effective medium is defined as a composite that behaves as a homogeneous material and is evaluated based on global performance, instead of on local behaviour. In an effective medium, properties of the constituent parts are averaged to approximate

properties of the composite as a bulk material, based on the relative volume fractions of its components.

Many approximations have been developed, each with different advantages under specific conditions. In a publication from 1904, Maxwell Garnett developed a formula (Eqn. 5.1) for simple effective medium approximation based on dielectric permittivities (Garnett, 1904):

$$\left( \frac{\epsilon_{eff} - \epsilon_m}{\epsilon_{eff} + 2\epsilon_m} \right) = \delta \left( \frac{\epsilon_i - \epsilon_m}{\epsilon_i + 2\epsilon_m} \right) \quad (5.1)$$

where  $\epsilon_{eff}$  is the effective permittivity of the substrate,  $\epsilon_i$  is the effective permittivity of the inclusions and  $\epsilon_m$  is the mean permittivity of the composite;  $\delta$  is the volume fraction of the inclusions.

Effective Medium Theory has been used by Smith et al. (2005) to find a mathematical way to describe metamaterials with a negative refractive index. Here, it is stated that a material is effective when the unit elements have a maximum size of one tenth of the wavelength. The authors distinguish between symmetric and asymmetric, as well as between homogeneous and inhomogeneous materials, and suggest altered methods to retrieve the material parameters of each of them.

The limit of what can be considered to be an effective material is of major importance for this work, as the possible dimensions of textile resonators are often close to this limit. The acceptable limit of inclusion size is an on-going discussion in the open literature, with most authors stating that one tenth of wavelength is necessary (Pendry, 2000), whereas others argue that one third of the target wavelength is acceptable (Hao, 2006).

### 5.2.2 Dielectrics

Most natural materials are dielectric materials. They are electrically insulating, and thus have low electrical conductivity. Dielectrics are characterised by the way they reflect and transmit electromagnetic waves, which leads to the determination of permittivity (effect on electric field) and permeability (effect on magnetic field). Dielectrics are also dispersive, which means that their electromagnetic response changes with frequency of the field they are exposed to. In electromagnetic engineering dielectric materials are ubiquitous, providing many practical uses such as in substrates for antennas or sensors.

The precise electromagnetic properties of a material can be determined by exposing it to an electromagnetic field. In the case of visible wavelengths, an approximate guess can be made about refractive index by reviewing the opacity of a material. If a material is transparent to the eye, it has a lower refractive index, closer to that of air. If it has a high opacity, the refractive index is high. If a material has a light colour, the absorption (loss) is low. If the material has a dark colour, the absorption rate is high, dissipating the absorbed energy as heat.

Dielectric metamaterials are usually designed from permittivity indices (permeability fixed), derived from a discrete coordinate transformation process and corresponding to the virtual space map (Tang, Argyropoulos, Kallos, Song, et al., 2010). The design results in a two-dimensional or three-dimensional medium with a permittivity continuously varying across the device. However, realisation of such a design is accomplished by discretising ('pixelating') the structure into a raster. Dielectric cloaks are split into blocks of materials, often simplified to a lower resolution map to reduce material and assembling time.

### **5.2.3 Composites**

Composite materials are a combination made of individual materials. The individual materials have different physical or chemical qualities, and a synergetic effect when combined. Engineered composites often deliver mechanical benefits, making a structure lighter, or stronger, or less expensive in comparison to other materials. Composite materials are very common, for example ceramics that exhibit high permittivity and low loss. Simple binary composites are made of just two materials. By changing the ratio of the two materials (given in percentage or dimensionless volume fraction  $\phi$ ), varied permittivities are achieved.

All textiles are composite materials in their essence. They are made from fibres and air in their simplest form, defining them as binary materials. In many cases a textile that is made of at least two fibrous materials as well as air can already achieve a complex mechanical behaviour. For example a woven two-directional stretch fabric extends in one direction but not in the other direction, achieved by using different materials in warp and weft.

#### **5.2.4 Periodic Structures and Repeat Patterns**

A ‘repeat pattern’ is composed from repeated elements arranged in some form of matrix and with some form of predictability. Both metamaterial engineers and textile designers have an interest in repeat patterns, however their objectives and means of pattern compositions vary. While the former use mathematical principles to achieve a specific functionality guided by laws of physics, the latter explore symmetric formations to generate visual appeal and cultural meaning.

From a technical point of view, repeat patterns in textile design are a pragmatic solution. In their role as intermediate products, fabrics are made to be cut and sold by the metre. A textile designer must therefore be able to design a repeat without visual inconsistencies, which can be cut without significantly influencing the flow of the pattern within the fabric. The simplest form of repeat is a ‘block pattern’ which describes a pattern that repeats a unit on both horizontal and vertical lines.

The term ‘periodic material’ is a topological classification for the structural composition of materials in science and engineering. A unit cell is the basic building block, which is then repeated in all planes (isotropic materials), or in only some planes (anisotropic materials). Two-dimensional patterns in electromagnetic engineering are of significance when designing pass-band or stop-band filters using frequency selective surfaces (FSS). FSS create an interfering electromagnetic field, which is set perpendicular to the propagation direction and parallel to the repeated elements of the pattern, and which allows some frequencies to pass through and others to be reflected.

In electromagnetic engineering, three-dimensional periodic structures are important for functional and structural material development on the micro scale, such as in designing composite materials to achieve nonlinear behaviour (Shivola, 2002). These structures contribute to the unique properties of metamaterials with a negative refractive index, in which both E-field and H-field components of the electromagnetic wave oscillate. Periodicity is an essential feature of metamaterials. Only through a regularly repeated sub-wavelength structure can the desired properties be achieved.

#### **5.2.5 Resonating Surfaces**

Resonating surfaces occur when an oscillating wave creates a specific periodic amplitude distribution across a structure. Resonances are the reason for many natural

phenomena known to us in our everyday lives, such as vibration of air which leads to sounds when resonating material surfaces, or architecture which has to make sure resonant frequencies are not excited by use (e.g. London Millennium footbridge problem), or damaged by seismic waves. The basis of all resonances is vibration in its various physical forms.

Antennas often use a strong electromagnetic resonator to enhance their radiation at specific frequencies. The electromagnetically resonating elements, which form part of resonating metamaterials, are applied to achieve permittivity and permeability below 0. A single cell SRR has a pair of enclosed loops with splits in them at opposite ends. The loops are made of non-magnetic metal like copper, and have a small gap between them. The loops can be concentric or square, and gapped as needed. A magnetic flux penetrating the metal rings will induce rotating currents in the rings, which produce their own flux to enhance or oppose the incident field (depending on the resonant properties of the SRR). This field pattern is dipolar. Due to splits in the rings, the structure can support resonant wavelengths much larger than the diameter of the rings, which is not possible with closed rings. The small gaps between the rings produce large capacitance values, which lower the resonating frequency. This results in an effective surface with a negative permeability. This is combined with a periodic surface that has a negative permittivity (e.g. an array of parallel wires), and together they result in a negative refractive index.

### **5.2.6 Artificial Dielectrics**

Artificial dielectrics are a subcategory of electromagnetically resonating materials. The term “artificial dielectric” was coined by electrical engineer Winston E. Kock (1948). Being viewed as the precursor of metamaterials, they are synthetic composites consisting of evenly spaced arrays of electrically conductive material elements, mimicking the local response of natural materials on a molecular level. The compositing material blocks are dimensionally smaller than the wavelength of interest, and can thus be described macroscopically by values of permittivity and permeability. Additionally, the geometric shape of the inclusions accounts for the electromagnetic performance of the artificial dielectric, which inevitably offers only a narrow operating band.

Kock constructed lenses for microwaves by painting circular sheets of polystyrene with conductive ink, or perforating metal (see Figure 5.5). Artificial dielectrics were valuable for radar technology because they delivered lightweight and inexpensive alternatives to previously complex and heavyweight constructions (Kildishev, Cai, Chettiar, & Shalaev, 2008). Later on, artificial dielectrics led to a large body of research about frequency selective surfaces (FSS), previously mentioned above (see section 5.2.4).

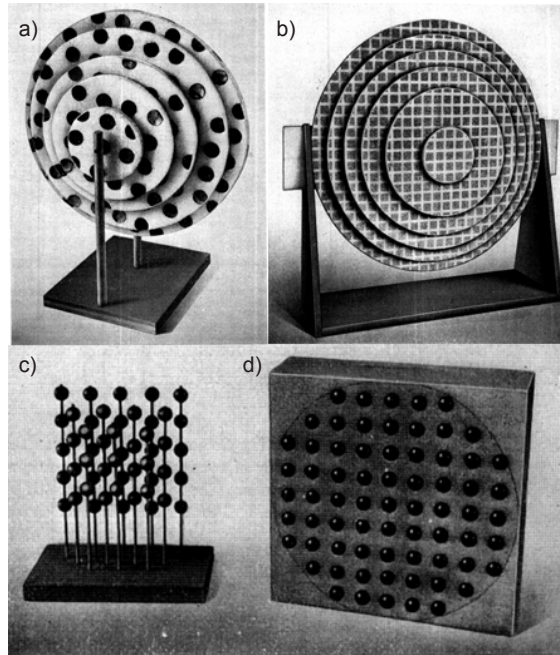


Figure 5.5: Kock's lightweight lenses. a) Copper foil disks on polystyrene, b) metal spraying on polystyrene sheets, c) conductive spheres mounted on insulated rods, d) steel balls mounted on polystyrene board.

Figure 5.6 and Figure 5.7 show two examples in which the concept of FSS has been taken further and embedded into commercial products in the fields of textile and surface design (Currey, 2013; Niembro-Martin, Barros, Eymen-Petot-Tourtollet, & Lemaître-Auger, 2015). Although for some of these products the electromagnetic functionality is questionable, they show that designers and architects are starting to express an interest in designing for, and with, functional patterns, and to propose aesthetic and practical solutions to electromagnetic shielding challenges.





Figure 5.6: Fashion designer Kunihiko Morinaga's collection 'Focus' reflects conceptually on the use of electromagnetic shielding and frequency selective bandwidth patterns (Morinaga, 2013).

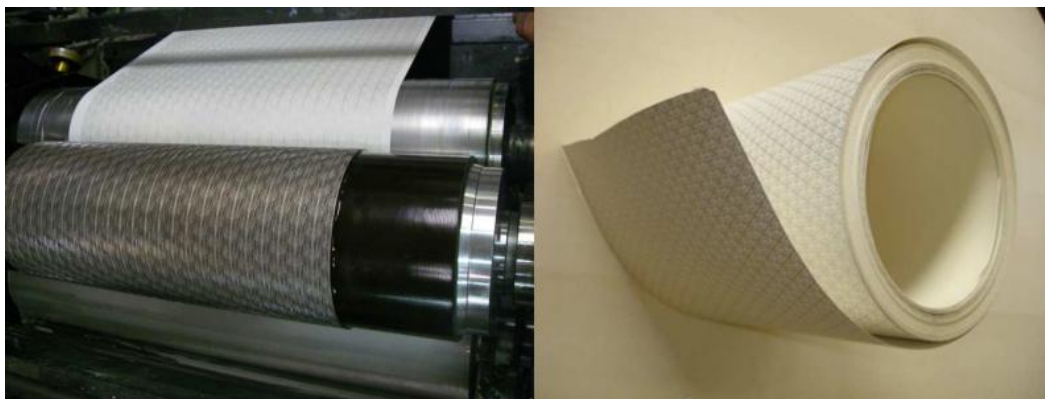


Figure 5.7: Patented FSS wallpaper, printed with silver ink to block out Wi-Fi signals (De Barros, Eymin-Petot-Tourtollet, Lemaitre-Auger, & Vuong, 2015).

### 5.2.7 Functional Directivity

Isotropic materials have uniform properties in all directions, while anisotropic materials behave differently along different axes. Orthotropic materials are a subclass of anisotropic materials, and describe unique material properties in three perpendicular axes. In electromagnetic terms, this generally means that a textile has a different permittivity and permeability when assessed from different angles. If the structure of the textile is small enough to fulfil the conditions of an effective medium, it can be treated as isotropic in two planes. Both the construction technique and the material chosen affect the directional performance of a fabric. For example, a plain weave is

woven with the same material in both warp (vertical threads) and weft (horizontal threads), ensuring the distance between threads is equal in both directions. This results in isotropic behaviour in two planes. If a different thread is used in weft than in warp, or if the warp and weft are woven in different densities, then the textile is anisotropic. An example is a two-dimensional stretch fabric, which expands in one direction but not in the other as a result of using non-stretch threads in warp and stretch threads for the weft.

Metamaterials can be constructed from both isotropic and anisotropic cells. For ground plane cloaks, isotropic dielectric unit cells are required, while free space cloaks using NIMs require anisotropic unit cells. The advantage of isotropy is that the cloak will be functional from all incident angles on the two-dimensional plane.

### **5.2.8 Graded Materials**

As a subcategory of non-periodic materials, a graded material or structure gradually changes over the volume of the material, with the result of changing mechanical or electrical properties (Miyamoto, 1996).

Graded materials are ubiquitous in both natural and engineered materials. In nature, they emerge over time as a result of adapted functionality (Maldovan & Thomas, 2009; Oxman, 2010). Material parameters, such as weight, porosity or permeability, are optimised towards specific mechanic demands, such as lightness, stability and durability.

Textile materials with gradient densities are prevalent in both textile design and textile engineering. Graded felted materials for example are used for wound dressing, providing optimal exudate passage in two stages (Scully & McCabe, 2000). In another example, a textile with a gradient electric conductivity is proposed that uses a weaving process to achieve a gradient with two types of yarn (Pittman & Kuhn, 1992). In textile design, gradients are used to create colour and three-dimensional surface effects. Mostly applied for decorative purposes in textile dyeing processes, capillary action is used to achieve colour gradients on textiles.

In the field of metamaterials, gradient materials are important when designing all-dielectric cloaks and lenses, as they are concerned with graded electromagnetic properties, in particular dielectric permittivity, permeability and dielectric losses. The

aim is to achieve surfaces that are continuous, providing an optimal functionality while being efficient in fabrication. Through digital fabrication technologies, graded materials are becoming easier to fabricate, and are of increasing interest for electromagnetic engineers as they provide new possibilities for antenna and lens designs (Ma & Cui, 2010; Tribe, Whittow, Kay, & Vardaxoglou, 2014).

### **5.3 Conclusion**

This chapter defined the terminology used to describe the geometric distribution of patterns in materials and electromagnetic engineering. Examining the definitions, it became apparent that many of the concepts are already prevalent in textile design, albeit framed with different goals in mind. Whilst it is common in material science, chemistry or physics to describe materials through structural composition, and view materials as cells of spatially aligned atoms; textile designers are concerned with the global aesthetic effect of materials on the human sensory system, such as colour, visual pattern composition and tactile sensation.

In electromagnetic engineering, materials are evaluated solely by their response or interaction with an electromagnetic field. Effective medium theory is important as it describes permittivity and permeability when the material is a bulk material.

Periodicity is increasingly considered for electromagnetic applications, as it is used to design smaller and lighter devices and open new possibilities for novel applications.

Geometry and repeated arrangements are of interest to textile designers, primarily for the purpose of creating visual effects. Thus they are designed on a larger scale, visible to the human eye. Inspiration for textile patterns is often found in geometric natural forms and their abstract pattern variations. This has led to a vast symbolic vocabulary of geometric patterns.

A textile designer considers both the composition of surfaces from components such as yarns or fibres, and the interplay of the units to form the desired effect of the finished surface. While a technological textile approach evaluates functional qualities such as strength, tensile strength and abrasion rate, a textile designer is concerned with the aesthetic and sensual quality of the fabric. Often, the microstructure of the fabric is not studied from an engineering angle, but the textile is evaluated by global response, such

as surface feel, thickness, roughness, stability and visual look. In contrast to designing structure on the macroscale, such as in architecture, textiles are often planned as an intermediate product without a fully defined end-user. This allows experimentation with structural aesthetics, and offers possibilities as to how the fabric can be applied in different products.

## **Chapter 6**

# **Materials, Fabrication Techniques and Experimental Analysis**

### **6.1 Introduction and Objectives**

During experimental work, various materials, techniques and methods were investigated to test the suitability in terms of electromagnetic functionality and textile processing. Techniques and materials were investigated for practical use and assessed for their potential electromagnetic and aesthetic qualities.

Most materials used were low-cost and commercially available, and sourced with electromagnetic functionality in mind. A broad range of procedures was explored, covering various additive and subtractive deposition techniques.

Colours, often a deciding factor for choosing materials in textile design, are defined by the material's inherent characteristic. It was assumed that colour treatments, the dyeing process for instance, would add chemicals to the fabric potentially altering its electromagnetic properties. In the case of synthetic materials, a neutral colour palette was chosen that underlined the notion of natural material colouring. Materials were carefully hand-washed before application, unless this was likely to alter them, for example felt (which shrinks and becomes dense when washed), conductive materials (washing diminishes their electric properties), and coated materials (where the coating cracks).

The principle materials investigated in section 6.2 are fabric substrates (6.2.1), conductive fabrics (6.2.2), paper and films (6.2.3), adhesive and stabiliser fabrics (6.2.4), conventional threads for machine embroidery (6.2.5), conductive threads (6.2.6), dielectric screen printing inks (6.2.7), conductive printing inks (6.2.8), resists (6.2.9) and other materials (6.2.10).

Surface design techniques are described in section 6.3, including digital embroidery (6.3.1), screen printing (6.3.2), vacuum deposition (6.3.3), inkjet printing (6.3.4), commercial ‘print and etch’ technique, (6.3.5), chemical etching (6.3.6), laser engraving (6.3.7), silver leafing (6.3.8) and pleating and thermal bonding (6.3.9).

In this chapter, sections 6.4 to 6.6 frame the technical methods for data acquisition and processing. Section 6.4 introduces the three methods commonly used for experimental data collection and discusses suitability for textiles. Section 6.5 describes the modelling technique used to acquire knowledge about electromagnetic functionality. Section 6.6 then details the algorithmic models used in the scope of this thesis to retrieve electromagnetic parameters of the tested samples. Section 6.7 summarises the outcomes of chapter 6.

## **6.2 Materials**

A list of suppliers and datasheets is provided in Appendix C.

### **6.2.1 Fabric Substrates**

The selection of substrate fabrics was determined by their tactile feel, pervasiveness in the textile industry, thermoplastic abilities and structural considerations that may impact their electromagnetic material properties.

Woven cotton and woven polyester cotton (polycotton) were obtained from Whaleys Bradford Ltd. Both fabrics were already bleached but otherwise untreated and produced industrially in large quantities, providing constant dielectric properties in different production batches. Both fabrics are commonly used in the fashion and clothing industry.

Polyester/Cotton A4079 (Optic White) has thermoplastic properties that enable semi-permanent pleating. The polyester fibres soften at about 150°C and semi-permanent

creases can be produced to fabricate three-dimensional structures. In the following chapters we will refer to this fabric as 'polycotton'.

Plain Cotton White (Optic White), also known as bleached Calico, is a low-cost plain weave cotton, common in fashion and printed textiles.

A fine non-woven wool viscose mixed fibre fabric was also obtained from Whaleys Bradford Ltd. This felt can be used for many applications, such as interlining and craft projects. With 1 mm thickness it is the thickest substrate material used in this research. It is lightweight and was chosen for drapability and ease of handling in measurement.

A range of water-repellent and water-resistant fabrics was selected as substrates to investigate their suitability for layering conductive traces. Water resistance is the result of fabric surface treatments. In the most common method the fabric is coated on one or both sides, with a resist, which can be either natural, such as latex rubber or wax, or synthetic, such as polyurethane (PU) or polyvinyl chloride (PVC). Combinations of treatments can result in the fabric being waterproofed while still breathable, which is a desirable property for sportswear.

Microfibres are made from synthetic fibres such as Polyester or Nylon. Their small structure results in water not being able to pass through them. Combinations of micro- or nanofibres and coating technology can achieve a 'lotus effect', which causes the fabric to repel water.

All waterproof and water-repellent fabrics used in this thesis were obtained from UK Fabrics online<sup>13</sup>.

- Cream Waterproof Breathable Coated Microfibre: 100% Polyester fabrics used for technical sportswear.
- Light Grey Technical Outdoor Nylon Fabric: 100% Nylon with a weight of 55g/m<sup>2</sup>. Due to the lightweight nature of this fabric, it is suitable for outdoor jackets and lightweight tents. It is coated and repels water and wind, whilst being breathable. It is also durable.

---

<sup>13</sup> <http://ukfabricsonline.com> accessed 4/10/2014

- **White Waterproof Cover Fabric:** made from 100% Polyester, is hardwearing, waterproof and water resistant, while still lightweight at 113g/m<sup>2</sup>. It is used for waterproof bags and coats.
- **Navy Blue Waterproof Coated Polycotton:** a mixed fibre composed of 65% Polyester and 35% Cotton. This fabric has a coated finish on one side and is waterproof. Due to its light weight, water resistance, breathability, windproofness, quick drying and high washing temperature of up to 90°C, it is used for many technical outdoor applications.
- **Grey Waterproof Ripstop Coated:** a thin, lightweight waterproof ripstop fabric made from 100% Nylon. It is breathable, water and windproof and dries quickly, making it suitable for outdoor applications. In the event that the fabric does get punctured, the woven square pattern keeps the fabric from tearing.
- **Air Force Blue Water Repellent Polycotton Chintz:** a mixed fibre fabric, containing 65% Polyester and 35% Cotton. As a Polycotton it is soft and moisture absorbing, as well as easy to iron due to its polyester content. This polycotton has a water repellent chintz finish and is thin and lightweight.

### **6.2.2 Conductive Fabrics**

Commercially available conductive fabrics were obtained from Less EMF, a company that specialises in electromagnetic shielding products.

- Pure copper polyester taffeta fabric is a plain woven 100% Polyester fabric, which is coated with copper on both sides. It has a thickness of 0.08 mm and provides low resistivity of 0.05 Ω/sq.
- SaniSilver™ is a cotton silver mix, made from pure cotton on one side and conductive silver on the other side. It provides low resistance of less than 1Ω/sq, and weighs 164 g/m<sup>2</sup>.

### **6.2.3 Paper and Films**

Paper is a popular choice for designers when creating electronic circuits and prototyping models in smaller scales. It is ubiquitous and available in many thicknesses, easy to manipulate in shape, flexible while dimensionally stable, and has an aesthetic



quality and tactility that is often lacking in polymer films. Designers who use electronic circuits as part of their practice apply silver and carbon inks to draw electronic connections and sensors, welcoming the familiarity of paper, pen and ink. The company Bare Conductive, one example of many recently established companies that focus on products for creative electronics, supplies carbon ink that is non-toxic and air-drying to be used on paper and other everyday materials. It is aimed at artists, designers and educators. Albeit not an entirely new product, its bespoke formula permits easy application, which enables quick prototyping. This makes it accessible to new user groups outside the electronic engineering field. Other techniques used to create circuits on paper include applying adhesive copper tape (Qi, 2012), drawing sensors and resistors with graphite pencils (Greinke, 2004) or using silver ink (Russo et al., 2011).

A variety of paper and flexible film substrates were employed for sample fabrication. These materials provided an even surface, are often less absorbent than fabrics, and are easy to fold and sculpt while providing good form stability.

Polymer films are less common in design fields for electronic circuits, however they are often included in this group due to some similar qualities, such as flexibility and fibrous structure. In electronic engineering they are of interest, because they are thin, flexible and have an even texture that prevents liquid coatings from being absorbed into the surface. When inkjet or screen print is used to coat a surface, this is referred to as thick film technology. Other methods, such as vacuum deposition, which produce a coating of just a few nanometres, are defined as thin film technology.

Paper is made from pressed cellulose pulp, fillers and additives. Both the mechanical pressing process and the composition of the ingredients determine thickness and smoothness of the paper surface. Although paper is a ubiquitous product, each type reacts differently to folding and ink applications. In this thesis, two main types of paper were used.

- A matt smooth and lightweight card obtained from Ryman Stationery. The weight is 200 g/m<sup>2</sup>, and it contains short fibres, which allows folding in all directions. It provided good form stability and an even finish.
- A technical filter paper obtained from the company Hahnemühle. The grade 2043b paper has a weight of 120 g/m<sup>2</sup>, and a thickness of 0.22 mm. It is translucent, contains short fibres and provides good foldability and form

stability. This paper was chosen for its aesthetic qualities and technical repeatability.

A film was used for ink jetting silver ink to produce NIM structures (see Appendix D). It was obtained from Mitsubishi Paper Mills Limited and was specifically advertised as suitable for circuit printing. NB-TP-3GU100 is a transparent polyester (PET) film of 170 g/m<sup>2</sup> and 135 µm thickness. It is coated on one side, and when used with Mitsubishi silver nano ink, provides fast drying, high conductivity, good adhesion and scratch resistivity. Due to the stiffness when bending the sheet the material could not be folded directly, but required grooves along the fold lines, carved manually with a scalpel.

#### **6.2.4 Adhesive ('Iron-on') and Stabiliser Fabrics**

For fusing and assembling three-dimensional structures, thermoplastic adhesive fabrics were used. These were non-woven polyester fusible interfacing fabrics with randomly aligned adhesive polyester fibres, which melted and bonded starting at about 100 C°. Heat'n Bond Lite from the company Therm-o-web proved to deliver good adherence whilst contributing little weight, material volume or dielectric losses.

#### **6.2.5 Embroidery Threads**

*Sulky* viscose thread, produced by the company Grunold, is optimised for machine embroidery and was selected as a top thread. This thread is resilient and ensures efficient production. Strength 40 is made from two plies of yarn and weighs 400 g per 10,000 m. A similar thread Classic Rayon No. 40 supplied by the company Madeira was used for some samples.

#### **6.2.6 Conductive Embroidery Threads**

Conductive threads were used as bobbin threads in embroidered circuits, due to the mechanical restrictions of the embroidery machine. A silver-plated nylon thread supplied by Statex with the quality of 234/34 4-ply was used. It is spun from four intertwined strands, has a diameter of 0.2 mm and a linear resistance of about 50 Ω/m as stated in the datasheet (see Figure C.4).

Liberator™ fibre was supplied by the company Syscom Advanced Materials. The group of Liberator™ threads combine high strength and robustness with conductivity

comparable to copper wires. A multifilament yarn made from liquid crystal polymer (LCP) is metal-cladded with copper, achieving low resistance of less than 3  $\Omega$ /m. This thread has further advantages of being resistant to abrasion, and is flexible and foldable, as well as solderable. In comparison to Statex threads, it is comparable to a strand of twisted thin copper wire with a smooth surface that does not fray.

### **6.2.7 Dielectric Printing Inks**

Commercial inks were screen printed onto various substrates to probe their suitability for textile substrates with high dielectric constants. Two readily mixed screen print inks for fabrics were obtained: AquaScreen Opaque White (AS 150) from Screen Colour Systems, and Qprint White RT from Quality Colours. The third ink (originally used for linocut) Linocut Titanium White was purchased from the arts material supplier Schmincke. All inks were chosen because they contain pigments of titanium dioxide ( $\text{TiO}_2$ ), which is known for its dielectric constant of up to 100 in rutile form. It was expected that the fabric screen print inks would have a much lower permittivity than the linocut ink because they contain a larger ratio of binders to make them suitable for textile printing, fixing and washing. Linocut ink has a high purity of pigments and a higher permittivity was expected. All three inks were water-based.

A solvent-based dielectric ink containing Barium Titanate ( $\text{BaTiO}_3$ ) pigments was obtained from the company Conductive Compounds, and was used for screen printing on fabrics and paper. While  $\text{BaTiO}_3$  shares the high permittivity of  $\text{TiO}_2$ , it has a lower dielectric loss, making it a popular choice for electromagnetic device fabrication (Bao, 2012). It should be noted that the ink was not originally intended for textile substrates and therefore less flexibility and durability was expected.

### **6.2.8 Conductive Printing Inks**

Water-based air-dry ink CuPro-Cote<sup>TM</sup> conductive paint containing 33-35  $\mu\text{m}$  copper particles was used to screen print circuit elements with a screen of 55 thread/cm (55T) mesh size. The surface resistivity as stated in the vendor's datasheet is less than 1 $\Omega$ /sq at 1 mm film thickness (see Figure C.7), however it was expected that the resistance of the printed line would significantly increase due to the absorbent and rough surfaces of the fabric and the manual printing process.

For inkjet printing circuits on film and waterproof textile, a water-based silver nanoparticle ink (NBSIJ-MU01) was used, supplied by Mitsubishi Paper Mills Limited. This silver ink contains 15% silver particles with dimensions of 20 nm and is optimised for use in home inkjet printers. The ink dries quickly to a conductive film of about 0.2  $\Omega$ /sq as stated in the datasheet and needs no further treatment.

### **6.2.9 Resists**

Liquid latex was screen printed onto various water-resistant and water-repellent fabrics to form a negative image stencil that could be peeled off once a conductive material had been applied to the fabric. Different screen meshes were tested with the aim of minimising air bubbles occurring during the printing process. Due to the viscosity and consistency of the latex, the screen printed stencils were restricted in the size of the printed patterns.

Petroleum jelly Vaseline® was screen printed onto copper fabric as a water-repellent resist for further processing with chemical etching. In order to maintain a low viscosity of the petroleum jelly, to ensure a sharp image, it was cooled to 8 °C prior to printing and was replaced after each print.

### **6.2.10 Other Materials**

A range of other materials was used, including various tapes, sprayable glues, iron-on fabrics and threads for temporary manual fixing and stitching. Teflon® and greased paper sheets were also used to protect samples when heat pressing.

## **6.3 Surface Design Techniques**

### **6.3.1 Digital Embroidery**

Embroidery is a textile technique of stitching threads onto fabrics. It traditionally provides functional reinforcement and repair of tears and worn out textiles. It is further used as a decorative embellishment technique. A combination of both applications in decorative reinforcement has been common throughout history. An example is the Japanese technique of Sashiko stitching originating in the Edo Era (1603–1867) and used until World War II, which produced protective clothing for farmers, fishermen and fire fighters (see Figure 6.1).



Figure 6.1: Sashiko fire fighter uniform, c. 1870. Reinforced and decorative embroidery.

Embroidery with conductive yarn plays an important part in the field of electronic textiles, producing conductive traces for entire soft circuits or components such as antennas and resistors in heating pads. There are several groups who specialise in embroidery technology, often collaborating with technical textiles universities. As detailed in section 2.2.1, the Wireless Communication Group at Loughborough University has designed several embroidered antennas, and analysed their performance in comparison to antennas fabricated on PCBs (Seager et al., 2008; Seager, Zhang, et al., 2013). Another example is the ElectroScience Laboratory (ESL) at Ohio State University which has a group working on textile and wearable antennas, developing a series of embroidered integrated antennas (Z. Wang, Volakis, & Kiourti, 2015). In experimental e-textile design, embroidered threads often provide stitched electrical resistance for thermally activated colour change (Robertson, Christie, Taylor, & Ibrahim, 2011).

Digital embroidery is computerised and forms part of the computer-aided-manufacturing (CAM) group of fabrication techniques. A software package is used to create the stitch pattern, which is then exported to the embroidery machine and stitched. Although it is possible to separate the stitches into colours and include programmed thread cuts into the design, embroidery is a one-thread-process, which means that it follows a continuous path and all parts of the embroidered image will be connected. In the present designs the SRR elements are small individual elements, which needed separation after the process. The designs were arranged to avoid overlays of conductive threads, and facilitate partition of the elements.

Different machines accept different types of thread depending on rigidity and thickness. Home and industrial machines use a lockstitch technique, which describes a method of intertwining a top thread with a bottom (bobbin) thread, as shown in Figure 6.2.

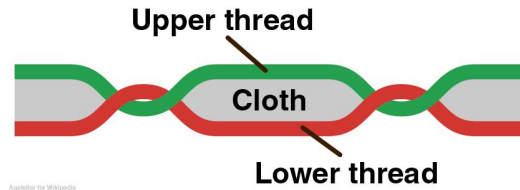


Figure 6.2: Lockstitch technique for embroidery

A Brother Innovis-1500D embroidery machine for domestic operation was used to fabricate the conductive structures. It was found that using the conductive thread as the upper thread was not feasible with this machine because the thread would break repeatedly. The top thread also passed along the main electronic circuit board in the machine body, and employing a conductive thread in the long term would have posed a risk to electrical damage of the machine. In contrast, running the conductive threads, including thin wire, as bobbin threads was possible without mechanical complications and this approach was used for all samples.

For decorative embroidery only the top thread is exposed in order to form a clear image, and the tension of the thread is adjusted so that the top thread is pulled tighter than the bobbin thread. This results in the top thread being slightly pulled on the reverse, leading to a distorted bobbin stitch image. For SRR embroidery the conductive thread was only used as the bobbin thread. It was important to maintain an accurate geometry, so that the thread tension was adjusted to achieve identical images with top and bobbin thread. The embroidery software package PE-Design<sup>14</sup> was used to programme stitch patterns; including stitch type, length and path. The design was then exported to the embroidery machine. As previously mentioned, embroidery is a linear process made from a continuous thread. To produce separated small shapes the thread must be trimmed either automatically during the embroidery process or manually after the complete design is finished. Industrial embroidery machines are capable of accurate trimming in between shapes during the embroidery process. Although the home embroidery

---

<sup>14</sup> <http://www.brother-usa.com/HomeSewing/Software/SoftwarePEDDesignNEXT.aspx> accessed 15/8/2016

machine used for these samples can perform automatic trimming, it was found that the blade wears out quickly when cutting conductive thread, producing error messages and differences in thread tension. Therefore all threads were trimmed manually with fine pliers once the embroidery was complete.

Test patterns were embroidered to gain knowledge about the practicality and challenges of various stitches using conductive thread in the digital embroidery machine. From studies conducted previously, it was known that various machines react differently, and thus the sampling process also served for familiarisation with the machine used. For example, it was found that conductive thread could only be applied as bobbin thread. Figure 6.3 shows various samples from the process to find a practical solution.

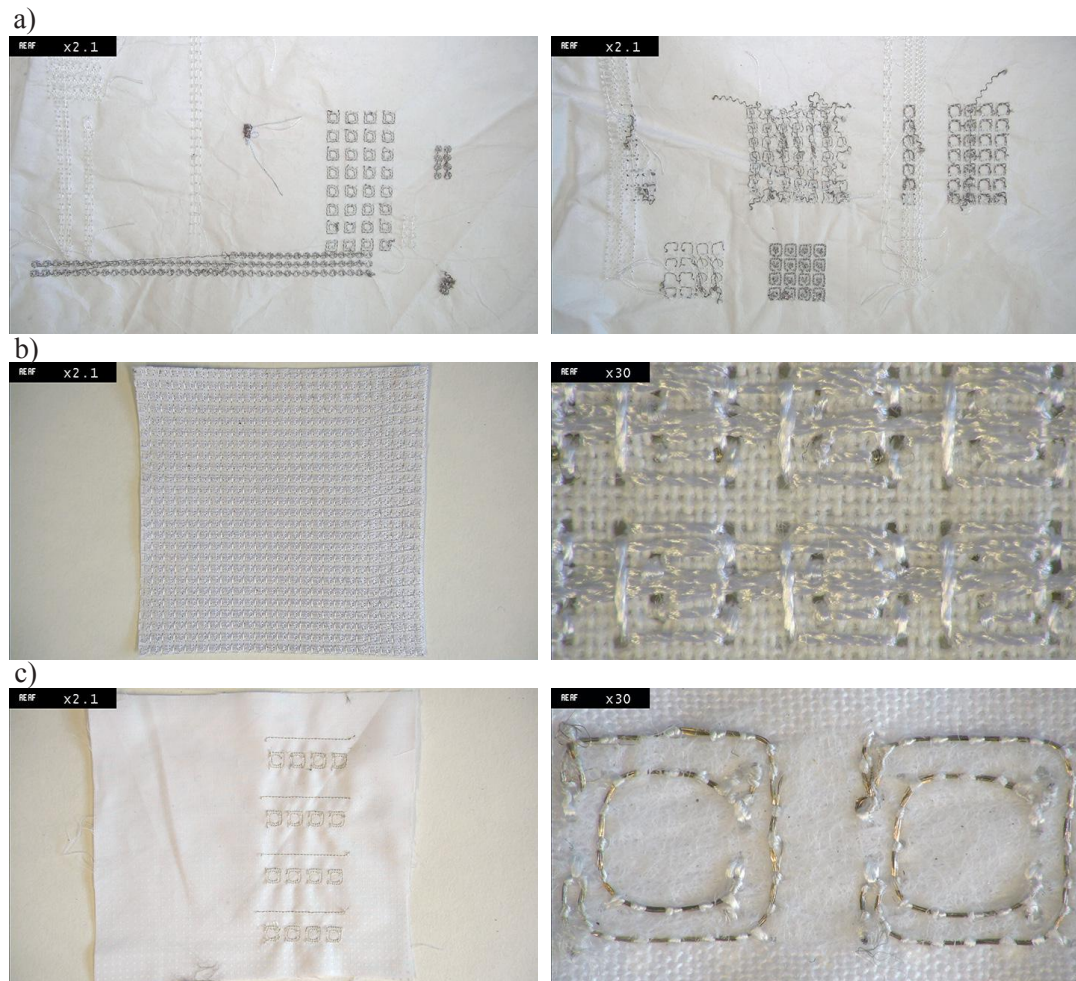


Figure 6.3: Embroidery tests with conductive threads, with complete samples on the left, and detail on the right. (a) Statex thread, tests for thread tension, embedding into surrounding thread to maintain shape geometry (b) Front of embroidery shows the overlay of threads occurring. Tests to find stitching path that allows later separation of shapes. (c) Small sample of stitched SRR with Liberator thread, after separation of shapes.

A semi-industrial embroidery machine Brother Entrepreneur® Pro PR1000e was used for stitching of non-conductive threads. An embroidery frame of 200 x 360 mm allowed the fabrication of graded patterns in one process, thus preventing the need for assembling and seams that may have caused irregularities in the graded permittivity. It was found that this embroidery machine was less suitable for the stitching of small conductive SRRs, mainly because the process of stitching was fast, which resulted in high thread tension and irregularities in the geometric form.

### **6.3.2 Screen Printing**

Screen printing is a versatile technique and established in both design and engineering disciplines. It describes the process of pressing ink through a mesh that is partially covered with a stencil, leaving areas open for the ink to pass through onto the medium. Other names for screen print are “silkscreen”, indicating the roots of this technique in 1000AD China, and subsequent use in Japan, which used a woven silk mesh as the carrier for the stencil; and “serigraphy” which aims to distinguish the industrial process of screen printing from the artistic practice using this process.

The possibility to layer low viscosity inks onto every type of flat or curved substrate has led to the technique being employed in many scenarios, ranging from ‘Do-It-Yourself’ T-Shirt printing at home to industrial screen printing of electronic nanostructures. In electronic engineering, screen print belongs to the group of “thick film” techniques, typically describing printed layers of 5–20  $\mu\text{m}$  thickness.

In design and arts education, manual screen printing is one of the main techniques taught. It is universally used in textile design for printing with a wide range of pigments, dyes and other chemicals. A main advantage is that it bridges manual and industrial production and is scalable to high production numbers when using semi-automatic or automatic equipment. The wide range of available screens, from wide meshes to high precision of a few microns, makes it possible for each discipline to choose the right tools. The masks can be produced with simple paper stencils, as well as with high precision photo-reactive emulsions to expose the required pattern. In e-textile research, screen printing is used to layer conductive and dielectric inks onto textiles. For example, researchers at Southampton University have developed a range of inks to print highly



conductive and reliable conductive structures onto textiles. Their commercial spin-off company Smart Fabric Inks<sup>15</sup> produces an “interface” layer, which smooths the surface of the textile and closes the holes of the absorbent surface, preparing it for the conductive medium, ensuring the highest conductivity possible and preventing the ink from being submerged into the textile.

In e-textile design, water-based carbon and copper inks are used for screen printing resistive heat actuators and sensor technologies. These inks and applications are typically more lenient in regards to manual processing, and less precise outcomes still exhibit the electric functionality.

For this thesis screen printing was used to place both dielectric and conductive ink onto fabrics. All samples were printed manually to facilitate adaptable experimentation. The screens used were aluminium frames enclosing stretched polyester monofilament meshes, with densities between 43T-100T (mesh count 43 - 100 per cm). Designs of SRRs were copied onto the screen using a photochemical process. First, a light sensitive emulsion was layered onto a blank screen mesh. Then, a positive image of the required design was copied onto tracing paper and attached to the screen. The screen was exposed to UV light and subsequently washed with water. The exposed areas set, while the protected areas were washed out with water. The screen now carried the stencil as a negative image of the design, and was ready for use. An advantage of this method was that it allowed the replication of complex design patterns and with sharp edges. The screen was used numerous times for printing the same design, as well as being washed and reused for new designs. For simpler design such as dielectric stripes, paper stencils were laser cut and mounted onto an empty screen. As the general aim was to layer a large bulk of ink in one print stroke, a squeegee with a soft rubber blade was used. Table 6.1 summarises the inks, substrates and desired outputs for screen printing, which will be detailed in chapter 7 and chapter 8.

---

<sup>15</sup> <http://www.fabinks.com> accessed 21/03/2015

Table 6.1: Screen printing techniques used to achieve various functionalities.

Printing materials	Screen mesh	Printed substrate	Desired output
Titanium dioxide ink	43T – 55T	Various fabrics	Increasing the dielectric constant
CuPro-Cote™	43T – 100T	Various fabrics pre-printed with Schmincke ink	Conductive print
Liquid Latex	55T	Various water-resistant and repellent fabrics	Peel-off mask
Petroleum jelly (Vaseline®)	43T-110T	LessEMF Pure Taffeta Copper fabric	Resist for chemical etching

### 6.3.3 Vacuum Deposition

Vacuum deposition is a process used to deposit atomic layers of metals onto solid surfaces. The technique belongs to the group of thin film deposition processes, typically describing thicknesses of up to a few micrometers. Thin films are used for a variety of applications, ranging from optical coatings to complex electronic components such as batteries and solar cells.

Vacuum deposition has the advantage of depositing an exact desired coat thickness in the nanometre range in the clean environment of high vacuum, producing accurate and material-efficient circuit boards for the Printed Electronics industry. This technique is not commonly used to generate circuits on fabric and absorbent materials. In this work it was tested if pure copper and conductive traces on waterproof semi-absorbent fabrics could be achieved, inspired by a technique from forensic science, in which vacuum deposited gold, zinc or silver particles enable visualisation of finger prints on fabrics (Knighting et al., 2013).

The set up at QMUL allowed samples with an area of up to 100 x 100 mm to be produced. Copper was heated in a vacuum bell jar until it vaporised at 1083 °C. The vapour expanded and coated the front surface of a sample, which was held above the

source. Figure 6.4 illustrates the set up of a typical vacuum deposition chamber. A first test onto polyester fabric resulted in high conductivity, and is shown in Figure 6.5.

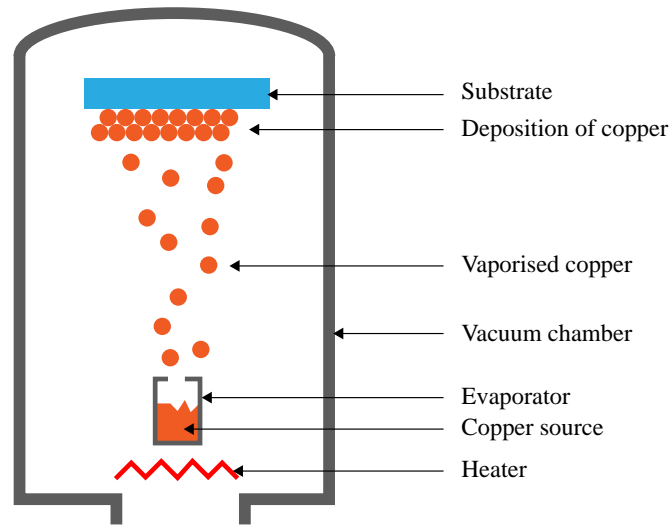


Figure 6.4: Vacuum deposition chamber

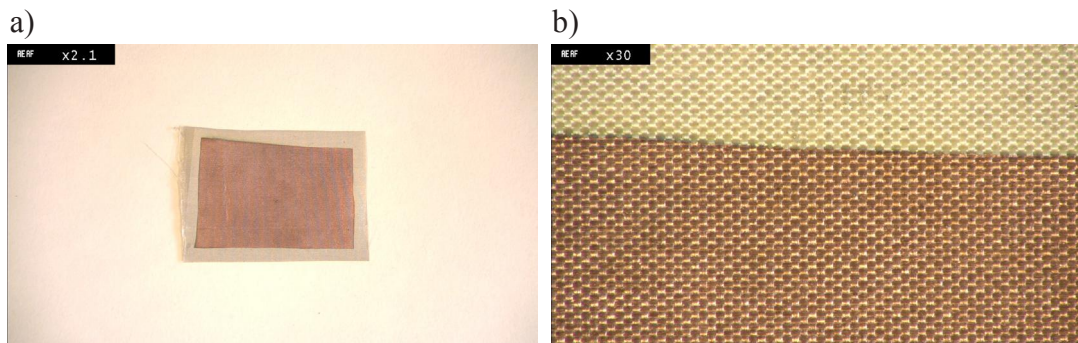


Figure 6.5: First test of vacuum deposition on polyester sample resulted in high conductivity.

(a) Sample c.8x5 cm (b) Detail

### 6.3.4 Inkjet Printing

Inkjet printing of conductive circuits appears increasingly in the literature and design community, promising simple workflows for achieving high conductivity on various paper, film and textile substrates. It belongs to a group of both manual and mechanic techniques that use silver ink containing nano-sized particles to form conductive traces and circuits. Although the technique is common in materials science and engineering, laboratories using high-priced specialist flatbed printers (for example the Dimatix piezoelectric inkjet printer), it only became cost-efficient and accessible to be adapted by designers in recent years. For example, Kawahara, Hodges, Cook, & Abowd (2013)

detail the method of using a home inkjet printer for printing circuits on various film and paper substrates. It enables designers to prototype with tools that are already familiar to them, such as inkjet printers, fountain pens and paint brushes, and which can be customised with ready-made component stickers (Hodges et al., 2014) or solderless plug-in components (Villar, Scott, Hodges, Hammil, & Miller, 2012), as seen in Figure 6.6.

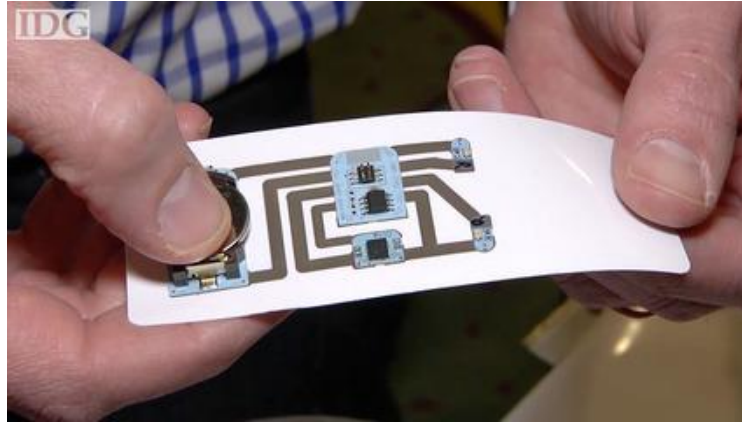


Figure 6.6: Inkjet printed silver traces with circuit stickers (Hodges et al., 2014).

Following the method of Kawahara et al. (2014) a domestic Brother DCP-197C inkjet printer was used to print conductive traces onto coated textiles and waterproof fabric. It was expected that due to the small dimensions of the silver particles (~20 nm in the ink used), any semi-porous surface would absorb the particles, resulting in an incoherent image and a disrupted trace. Tests are presented in section 8.3.3.

### **6.3.5 Off-site Fabrication: ‘Print and Etch’**

As the only samples that were fabricated by an industrial partner, this technique used a three-step process, combining an additive plating technique with a subtractive etching method. This method, developed by PEL (Printed Electronics Ltd) in conjunction with NEL Technologies produces geometrically accurate nickel traces on non-absorbent fabrics and film materials (see Figure 6.7). The fabric is sold under the trade name Neltex®.

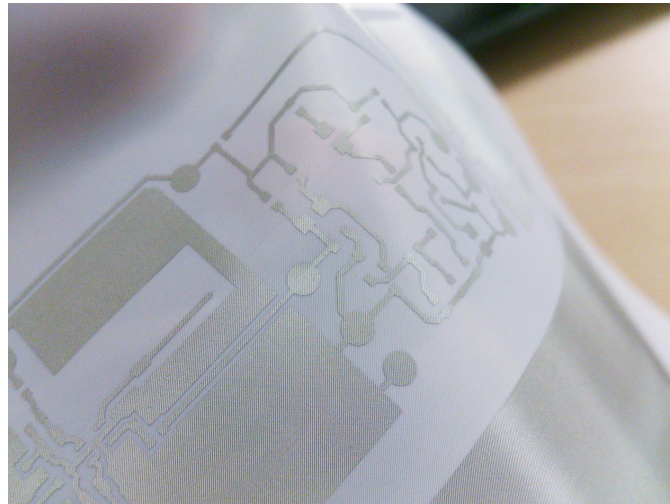


Figure 6.7: An example of Neltex® fabric by PEL.

The advantages of this technique include high abrasion resistance, low cost if nickel is used, and suitability for small circuits that are orthogonal and parallel to the threads in the weave. Conductivity depends on the woven structure, as a result of the number of crossings between warp and weft threads. The process produces an even conductive layer, providing consistent conductivity for samples of up to 500 x 450 mm or longer, and consistency between production batches.

The samples were produced with thermoplastic polycarbonate monofilaments, which were translucent and flexible. The highest conductivity was achieved with plain weave, the most basic woven pattern in which the warp (vertical threads) and the weft (horizontal threads) alternate by passing over and under each other. This pattern produced a large number of intersections between threads, resulting in many conductivity points.

### **6.3.6 Chemical Etching**

This technique of chemically etching rigid circuit boards has become prevalent within the e-textile design community for fabrication of soft circuits. This is due to its versatility and similarity to traditional crafts techniques for textiles (Tharakan, 2011).

The chemical etching process begins with applying an oil-based resist onto a conductive fabric to protect the areas from etching. This can be screen printed or drawn, similar to techniques used in wax-resist dyeing processes. The fabric is then soaked over a prolonged time in etchant chemicals, which dissolve the copper from the

unprotected parts. Afterwards the sample is rinsed in water, and the resist removed by ironing it with a sheet of absorbent paper between the sample and the iron. To achieve a conductive trace on absorbent fabrics, it was important that the fabric was covered with sufficient resist to prevent the chemical etchant infiltrating the fibres, and removing the copper from the protected parts.

In this thesis two methods for chemical etching have been explored, primarily to test if the technique is suitable to produce small width and high detail conductive traces on fabrics. A series of SRRs in increasing dimensions were fabricated as single cells to deliver a proof of concept for chemically etched metatextiles. Various sizes of SRR and wire structures were sampled, assuming resonance anywhere between 3 - 8 GHz.

The resist was applied on both sides of the fabric using a mask. For the first sample a petroleum jelly was directly applied using screen printing, with a 43T mesh size and a squeegee with a soft rubber blade. It was found that if the pattern was printed more than twice, the image would misalign due to the flexibility of the textile and the change of viscosity of the printing medium.

The sample was then soaked in a solution of one part ferric chloride and four parts water for 5-20 minutes (depending on the freshness of the solution), to remove the parts that were not covered with resist. The mixture had a dark brown colour and the fabric was dyed a darker colour as a result. An alternative solution was mixed from one part Di-Sodium Peroxodisulphate Hexahydrate and five parts water, in which the sample was soaked for 5-10 minutes. This etchant solution had the advantage that it remained clear and did not darken the fabric.

Results of these tests are detailed in section 8.3.4.

### **6.3.7 Laser Engraving**

Laser engraving textiles is a technique in which the inherent properties of textiles can be changed by applying heat controlled by a laser beam. In textile design the method is used to manipulate both natural and synthetic fabrics to achieve decorative effects. For example, Taylor & Robertson (2014) developed “Digital Lace”, a textile table runner using thermochromic ink and laser engraved optical fibres, achieving remarkable colour play. For this thesis, laser engraving was used to ‘burn off’ a layer of silver fibres to create textile circuitry, as detailed in section 8.3.5.

### **6.3.8 Silver Leafing**

The technique of applying a thin silver leaf onto a surface is derived from gilding. Gilding is a decorative technique, in which thin leaves of metal are applied to wood, leather, porcelain, paper and other materials to decorate them with a luxurious finish. Gilding has been used in crafts since the 4<sup>th</sup> century BC, and many different culturally specific techniques have been developed.

For e-textiles, gilding has been used with rare success, but in some cases has provided a simple technique to craft conductive traces on paper. Saul, Xu, & Gross (2010) suggest gold leafing as a simple means to craft circuits on paper.

Gilded materials are delicate and sensitive to touch and, while providing a beautiful handcrafted finish, production is not scalable to industrial production. In the scope of this research the technique was used in a highly experimental approach, based on aesthetic interest rather than simple and reliable production.

The pattern is screen printed onto a substrate with an adhesive and dried at room temperature. After drying the surface remains adhesive, and a layer of silver leaf is carefully brushed onto the fabric. The silver leaf remains on the adhesive parts and can be brushed away from the non-adhesive parts. Tests are shown in section 8.3.7.

### **6.3.9 Assembly: Pleating and Heat Bonding**

A pleat is a permanent or semi-permanent fold in a fabric that is either set with heat or sewn in place. The technique is used to produce three-dimensionality from flat fabric materials and is seen in many branches of industry and experimental textile design. Pleated textiles have been designed for hundreds of years, however they became increasingly popular in the mid 20<sup>th</sup> century with the rise of synthetic fabrics. The thermoplastic properties of these materials allow simple heat pressing methods to be used for creating complex folding patterns. Extending this technique with coating and bonding to achieve stiffer materials, as well as laser technology to facilitate faster and more precise generation of folds, has led to a wealth of design-led research (De Ruysser, 2009; Philpott, 2011) as well as product and textile design projects.

For this thesis, simple folds were used to design three-dimensional repeat patterns. We made use of accordion and box pleats (see Figure 6.8 (a) and (b)), both using

rectangular folds. Another type of pleat was required to produce resonant metatextiles (see chapter 8), which we termed U-fold (see Figure 6.8 (c)).

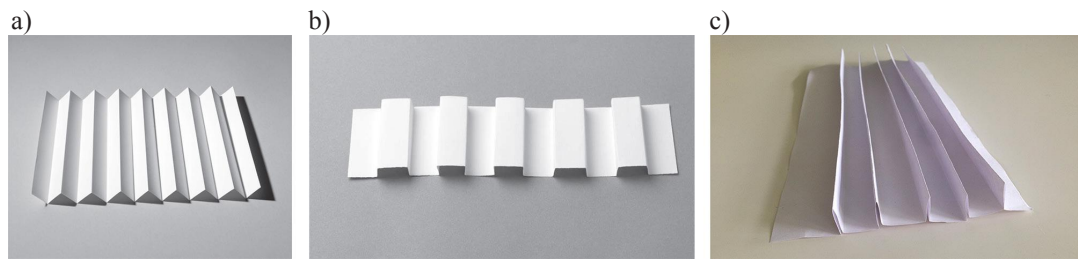


Figure 6.8: (a) Accordion pleat (b) Box pleat (c) U-fold, as used to design three-dimensional NIMs from one piece of flat textile.

Thermal bonding is a common technique used to laminate layers of textiles with the purpose of stiffening or achieving different surface effects. Thermoplastic bonding materials, as described in section 6.2.4 were initially fixed with a mini iron (Clover mini iron) and later permanently pressed with a semi-industrial heat press. Figure 6.8 shows paper demonstrator models used to illustrate the technique to collaborators.

## 6.4 Measurements of S-Parameters of Textile Samples

Determining electromagnetic parameters of textile materials accurately is problematic. Textiles are thin, porous, and inhomogeneous systems of air-fibre combinations. Additionally, the fibre itself is a complex system of dependencies, such as orientation of the fibre and surface roughness. They react strongly to environmental changes such as humidity and temperature, which impact measurement of the dielectric constant of the fibres. For instance, the influence of frequency on the dielectric properties of fibres is higher when the fibres contain more moisture. Another example is the increase of dielectric constant in conjunction with an increase in temperature (Bal & Kothari, 2009).

Three existing methods for measuring s-parameters were tested for suitability in measuring textile materials for this thesis. To simplify measurement, textiles were treated as flat, even surfaces, utilising a common reduction of textile materials found in electromagnetic engineering experiments and simulations. However, no attempt was made to further flatten, press or stabilise the form of the samples when measured. Although this method did not fully represent the complex morphology of textile



structures, it aimed to approximate how electromagnetic textiles are intuitively used in everyday situations.

#### 6.4.1 Thickness Evaluation

To assess the thickness of textiles a micrometer with a 5 mm probe was used, shown in Figure 6.9. The press foot was gently lowered onto the sample, and a reading taken. The procedure was repeated to obtain the values of thickness at five different locations. The mean value of the thickness readings was calculated, resulting in the average thickness of the sample.



Figure 6.9: For measuring thickness, a digital handheld micrometer was used. The probe has a diameter of 5 mm.

#### 6.4.2 Waveguide Measurements

A waveguide is a hollow conductive pipe used to navigate electromagnetic waves with very low wave attenuation. This is achieved by designing the dimensions of the waveguide in relation to the magnitude of the wavelength, providing total reflection from the waveguide walls and thus counteracting the inverse square law that describes the loss of power when waves propagate spherically in free space.

S-parameter retrieval using waveguide measurements is commonly used for measuring solid materials at microwave frequencies. It provides high controllability and accuracy. For the measurement of textiles, which are thin and flexible, this method only proved to be useful in some respects. Figure 6.10 illustrates the set up of a waveguide measurement system. Two waveguides, each connected to a waveguide-to-coaxial transition and connected to the ports of a Network Analyser, were joined. At the joint, a

material sample was inserted into the waveguide. The sample needed to be primed to precisely fill the cross section of the waveguide. Although the material parameters calculated from the measured s-parameters of this set up are not contingent upon the thickness of the sample, it is vital to know this value for consideration in the conversion procedure.

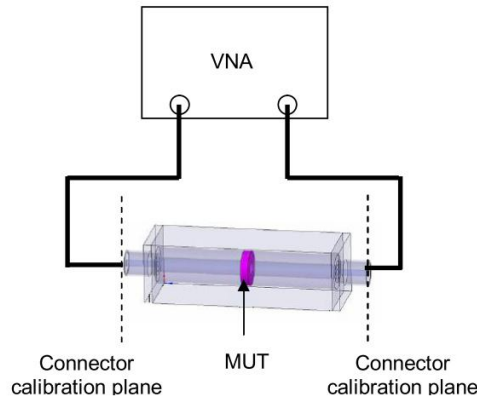


Figure 6.10: Measurement set up with waveguides. The material under test (MUT) is locked in between the two openings of the waveguides. A vector network analyse (VNA) is used to record the s-parameters.

The set up was tested with a Teflon (PTFE) sample of known permittivity 2.1 and loss tangent of less than 0.001. The thickness of the slab was 1.064 mm, and the permittivity was retrieved using Agilent Material Measurements Software, as described in section 6.6.1. Figure 6.11 shows that results for PTFE are consistent, showing little dispersion, confirming that the method is the most reliable for rigid materials in this frequency range.

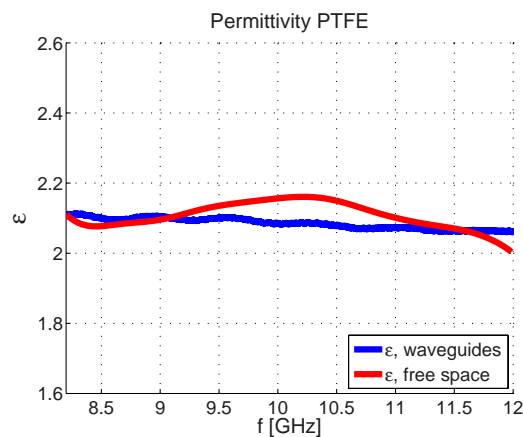


Figure 6.11: Permittivity retrieved from measured s-parameters in waveguide (blue) and free space (red) set ups.

Further waveguide measurements were done to test if the set up was suitable for measuring dielectric textiles. The challenges for measuring textiles became apparent during the mechanical set up. Textiles and related materials were difficult to insert into the waveguide while keeping them flat and in plane. If the material being tested was soft, the fabric was squeezed considerably at the edges. If a slightly larger sample was inserted and held compressed between the two waveguide openings, a gap occurred, which had to be electromagnetically shielded and considered later in parameter retrieval. Results were inconsistent and permittivity values exceeded 2.5, and it was concluded that the technique was unsuitable for measuring textiles.

### 6.4.3 Free Space

A measurement technique employing two antennas with the wave propagating through air is called the free space technique, as illustrated in Figure 6.12. It is commonly applied for flat and large samples, which cannot be cut or treated otherwise. Free space measurements allow non-destructive experiments and are especially beneficial if the sample runs through a change of matter caused by external factors, for example if the impact of temperature on a sample is investigated. Rhode & Schwartz (2006) also note the possibility to conduct measurements in hostile environments. This method seems appropriate for textiles if we can assume that the sample will be flat, and large enough to cover an area required for the measurement set up.

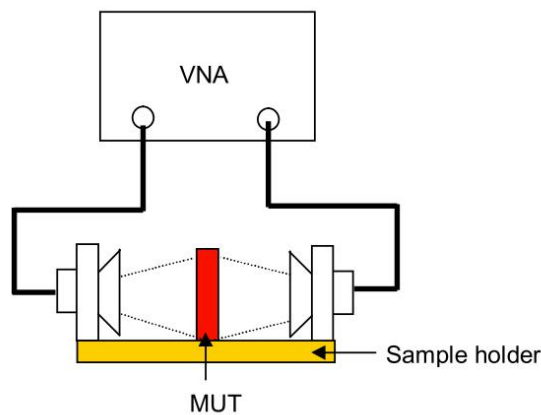


Figure 6.12: Free space measurements. The material under test (MUT) is fixed in between the two opening of the horn antennas.

Generally in free space measurements, a horn antenna is attached to the end of a waveguide, which propagates the wave into air. The propagation is far less controlled

than in waveguide measurements, and precautions need to be taken to avoid backward reflections, and ensure a maximum power exposure, as well as a plane wave front. The horn antenna needs to be far enough away from the sample to allow far field propagation (Figure 6.13), which provides a plane wave front. Far field distance, or Fraunhofer distance ( $d$ ) is calculated as;

$$d = \frac{2D^2}{\lambda} \quad (6.1)$$

The minimum size of the sample is determined by the half power beam width calculation;

$$\theta = \frac{k\lambda}{D} \quad (6.2)$$

where  $D$  is the size of the horn aperture and  $k$  is the wavenumber defined as  $2\pi/\lambda$ .

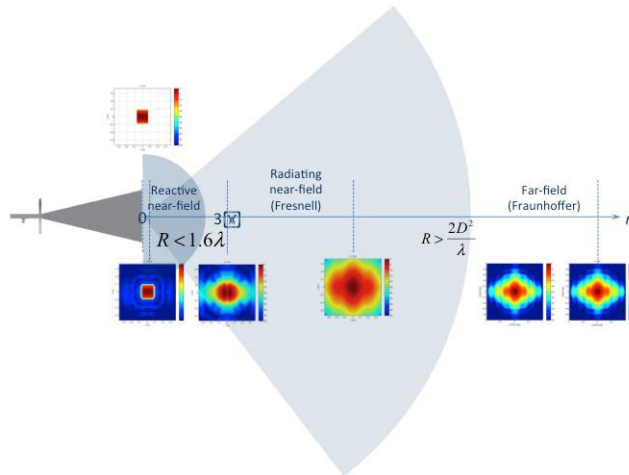


Figure 6.13: The boundary of the far field is determined by the Fraunhofer Distance, and describes the distance at which the wave front behaves like a plane wave. The radiation pattern in the far field does not change shape.

The two parameters  $D$  and  $d$  have been the main considerations for calculating the dimensions of the experimental set up that was purpose built (see Appendix E for detailed documentation). An anechoic chamber was designed for measuring textiles, permitting adaptability to a number of material and measurement scenarios. The target frequency band is X band, employing two horn antennas attached to waveguides. The horn antennas are aligned in a vertical set up with a centred circular aperture for sample

exposure. The far field distance for X band is between 350 - 530 mm. To allow the propagating wave sufficient distance to form a plane wave front, the antennas have been installed with a 760 mm distance to the sample on each side. The circular hole for sample exposure is 110 mm in diameter. To ensure that this area is fully covered, the sample should have a minimum size of 120 x 120 mm. A flexible system allows measurement of substrates in thicknesses between 1 - 25 mm. For the measurement of graded materials, a push-through mechanism has been integrated which allows samples with continuously varying permittivity in the horizontal direction to be measured at different positions. By manually pushing the sample holder in fixed intervals, a series of measurements can be taken so that a prediction of the continuously varying permittivity can be made. Figure 6.14 (a) shows the CAD drawing of the designed chamber. To benefit from gravity to maintain the samples flat and in place, it has been set up vertically. Figure 6.14 (b) shows the finished chamber.

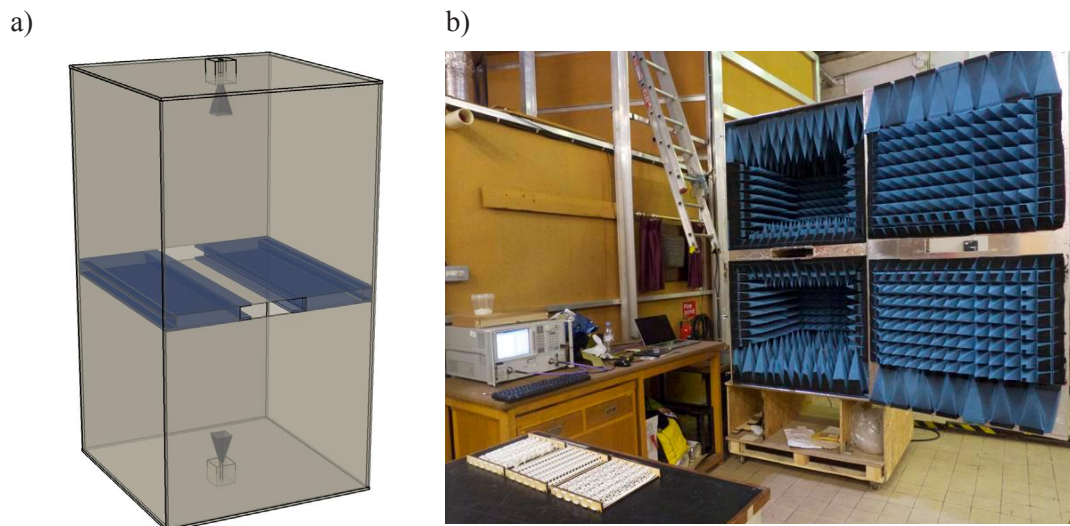


Figure 6.14: Custom-built anechoic chamber, to measure samples with graded permittivity in a free space set up. Horn antennas for either X band (8.2 – 12.4 GHz) or wideband horn antennas (c. 4 – 16 GHz) can be installed. a) Drawing and b) built chamber.

Free space measurements introduce noise through multiple reflections in the chamber, as well as back to and between the antennas. Additionally, it is known that thin samples with an expected permittivity close to air can cause multiple reflections within the sample, which again can result in difficulties distinguishing between relevant signals and noise. Using the free space set up over prolonged testing periods suggested that thorough calibration of the system was needed before each measurement sequence. It was found that in practice, there are three paths for corrections and optimisations. The

first opportunity occurred before the measurement by improving the mechanical set up, the second during measurement to achieve a smoother data flow, and the third during the numerical procedure when data is processed. Table 6.2 gives a summary of different optimisation processes at the three stages. The first stage was given the most care, and for cases where problems were identified other than mechanical ones, optimisation was applied during the second and third step.

Table 6.2: Optimisation applied before, during and after free space measurement.

Before measurement (mechanical)	Design and mechanical building execution, cable fixtures, sample holder
During measurement (instrumental)	Calibration, time gating, hourly refreshing of free space calibration
Data processing (numerical)	Further normalisation, choice of conversion method, individual adaptation of algorithm to the sample type

A two-port calibration was performed at the antenna inputs (coaxial) using a calibration kit Ecal Model N4691-60004. A further calibration was carried out using 85071E Materials Measurement Software GRL (Gated-Reflect-Line) in the software's free space option. This extended the calibration of the coaxial cables to the edges of a metal plate placed at the same location, which were ideally of the same thickness as the sample. This method diminished errors from diffracted waves within the anechoic chamber. Additionally, its outcomes could be directly compared to results collected in electromagnetic simulation set ups, facilitating unambiguous data collection.

To further reduce the effect of backwards reflections of the propagated wave, a technique was applied that places a gate around a digital time window, filtering only the transmission and reflection occurring at the sample. This requires conversion of the frequency-based signal into a time-based signal (pseudo time domain achieved by a frequency sweep and then Fourier transform to provide the time domain view). It was found that when using the Agilent software, gating eliminated noise and produced a smoother result for permittivity and loss tangents. The effects of gating the signal have further been found useful for understanding the path of the wave, and how it is affected by multiple reflections.

The chamber is tested with an FR-4 slab of 1.518 mm thickness to verify the operational reliability and calibration technique. The results as presented in Figure 6.15 have been retrieved using the NIST method described in the next section.

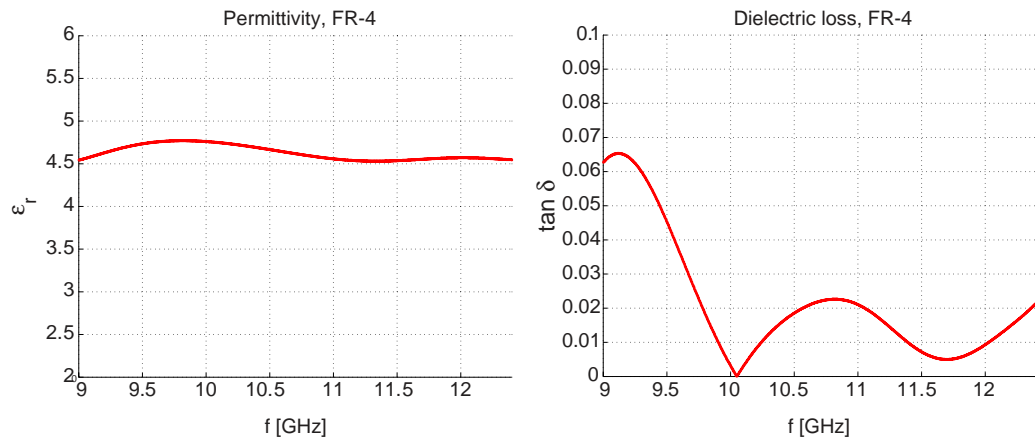


Figure 6.15: FR-4 measurement results from measurement in the free space chamber. Agilent Materials Software was used for retrieval, applying the NIST algorithm. While permittivity results are smooth and comply with values given in the data sheet ( $\epsilon = 4.8$  at 1 MHz), dielectric losses are inconsistent.

Permittivity was around 4.5 for FR-4 at 11 GHz, which was constant with a permittivity of 4.8 at 1 MHz, as given in the datasheet. Both permittivity and loss tangent results are more accurate and robust when s-parameters are measured in a waveguide set up. While the permittivity retrieved from free space measurements was comparable to the waveguide results, the loss tangent retrieved from free space measurements showed insufficient agreement. This was most likely due to the noise that occurs in free space measurements, which becomes more important when low permittivity materials are measured. However within the scope of this research, it was important to determine that materials have a dielectric loss tangent below 0.1, which has been determined as a critical threshold through simulations. With consideration of published results regarding dielectric losses of materials, similar to the ones used in this thesis, it was concluded that presented results deliver sufficient proof that materials are below the threshold.

To verify the suitability of the method for the measurement of textile and paper materials, samples of polycotton, card and felt were measured. Results retrieved with NIST method are shown in Figure 6.16.

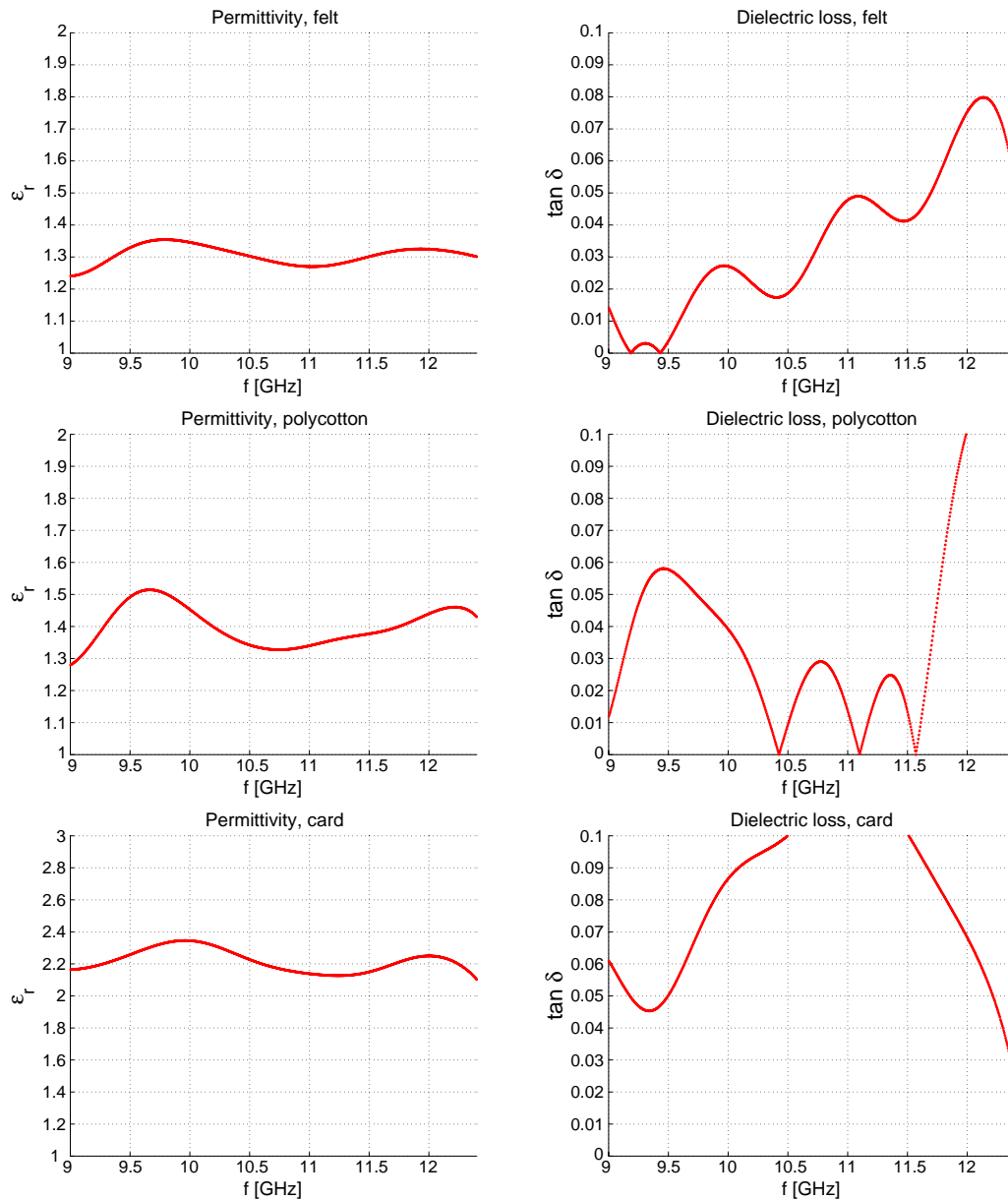


Figure 6.16: Measurements of viscose felt, polycotton and card in the free space chamber. Retrieval of permittivity and dielectric losses show that, while permittivity results are sufficiently smooth, inconsistencies in dielectric loss results become less reliable with thinner materials.

In Figure 6.16 the relative permittivity and dielectric loss tangent of the textile being measured are plotted against X band frequency range. Permittivity results for fabric materials are below 2 as expected, permittivity of card is approximately 2.2. Divergence from a linear rise can be attributed to the difficulty of measuring thin and low loss materials in free space set-ups. Dielectric losses of felt and polycotton are below 0.1 as expected. Dielectric loss of card peaks between 10.5 and 11.5 GHz, which can be attributed to the higher density of the material compared to the textiles. As there



is no published data for comparison available, the results will be compared to results taken with other measurement techniques in the following two sections and conclusion drawn in the discussion in section 6.4.5.

#### 6.4.4 Parallel Plate Capacitance

The dielectric constant can be derived directly from capacitance measurements taken with a parallel plate set up, as shown in Figure 6.17. The test set up Agilent 16451B (Figure 6.18) is usually used for solid thin film dielectrics and measures a frequency range of 50 Hz - 5 MHz.

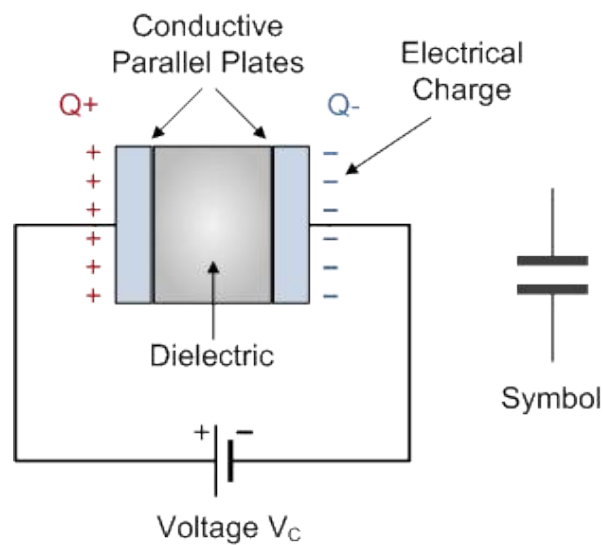


Figure 6.17: A typical parallel plate capacitor configuration.

Despite not being suitable for most microwave applications because of its low frequency range, this method can provide results for a comparable study with free space measurements, as many dielectrics have minimal frequency dispersion for permittivity and permeability. The benefit of the Parallel Plate set up is its suitability for textile probes. The sample is accessible, while the space between upper and lower plate is variable to measure samples of various thicknesses. The Agilent 16451B is connected to an Agilent 4294A Impedance Analyser with which measurements can be recorded.

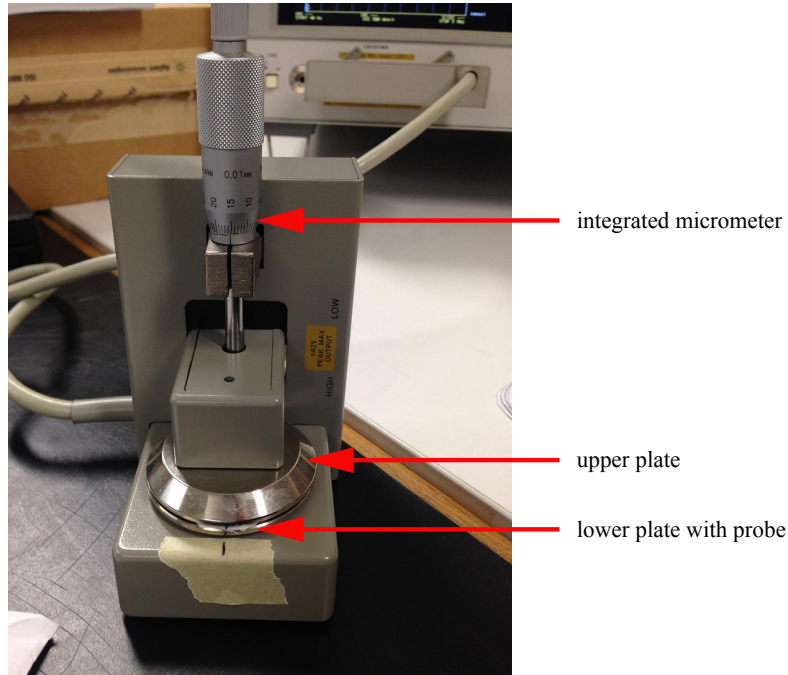


Figure 6.18: Test fixture Agilent 16451B.

From capacitance, permittivity can be calculated using

$$\begin{aligned}\epsilon &= \frac{t}{A} C_p \\ \epsilon &= \epsilon_0 \epsilon_r\end{aligned}\tag{6.3}$$

Where  $C_p$  is the capacitance value [F],  $t$  is the thickness of the material [m] and  $A$  the area of electrode [ $\text{m}^2$ ].

Thus, the relative permittivity can be obtained by using the following equation.

$$\begin{aligned}\epsilon_r &= \frac{t \times C_p}{A \times \epsilon_0} \\ \epsilon_r &= \frac{t \times C_p}{\pi \times \left(\frac{d}{2}\right)^2 \times \epsilon_0}\end{aligned}\tag{6.4}$$

Where  $d$  is the diameter of the electrode [m]. The dielectric loss  $\delta$  can be obtained directly through measurement.

We have tested the set up with a slab of FR-4 with a known permittivity of 4.3 and a loss tangent of less than 0.01. The thickness was measured with a micrometer at five

points of the sample and averaged to 1.518 mm. The parallel plate electrode has a diameter of 38 mm (Electrode-A). Results for permittivity and dielectric loss are shown in Figure 6.19, indicating the expected permittivity of around 4.3. The dielectric loss correctly is less than 0.006.

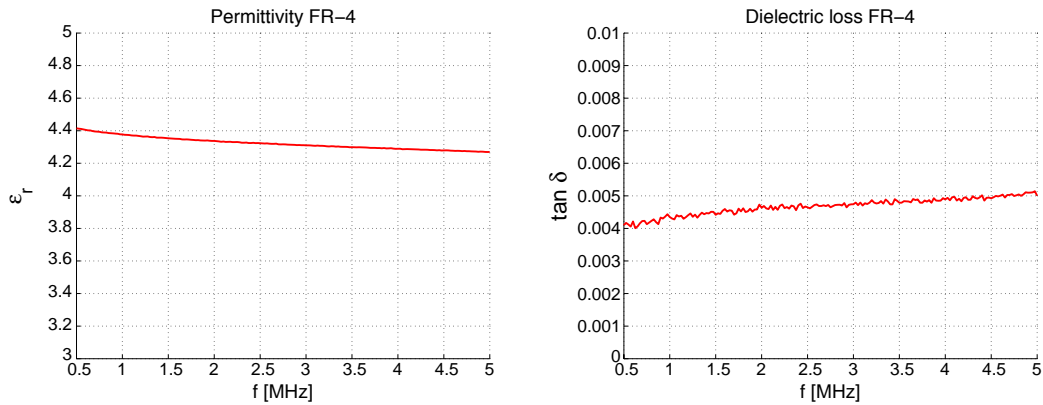


Figure 6.19: FR-4 results, Parallel Plate capacitance method, 50Hz – 5MHz.

To verify the suitability of this method for textile and paper materials, we have also tested this method with an untreated polycotton. Figure 6.20 shows that there is a reasonable agreement between the results of polycotton measured in the parallel plate set up and the free space setup. The plot of the dielectric loss also shows a low loss tangent of around 0.02, which provides further confirmation that thin textile materials are suitable as substrates.

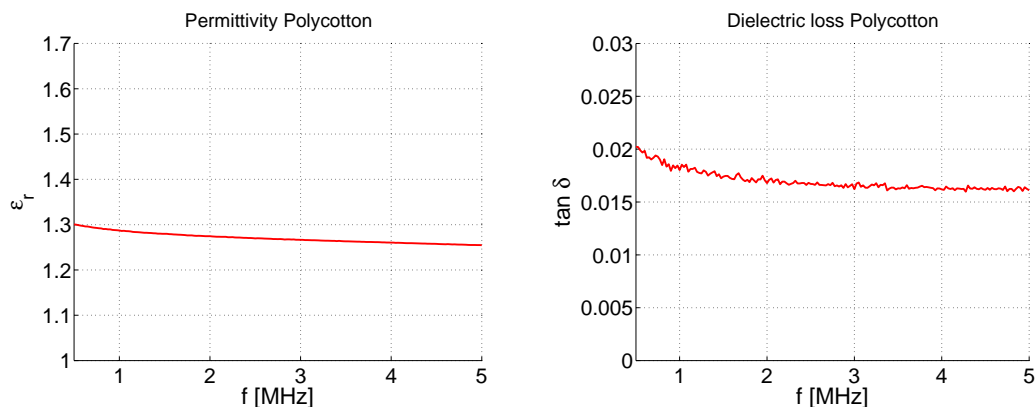


Figure 6.20: Polycotton results, Parallel Plate capacitance method, 50Hz – 5MHz.

#### 6.4.5 Discussion

Three common methods for material parameter measurements were explored; using a rigid FR-4 and PTFE material with known properties, compared to polycotton, felt and

card. While FR-4 and PTFE measurements were correct and consistent with all methods, the results for the flexible and textile materials varied. This can be attributed to known challenges when measuring low loss and thin materials.

Mechanical challenges in measuring textiles are known and have been addressed in numerous publications (Bal & Kothari, 2010). It should also be noted that for this thesis we had no access to specialist equipment for technical textiles, such as a gauge meter or surface roughness evaluation instruments, and thus a more approximate method was required. In the context of this knowledge, this thesis relied on on-going critical observation of particular data sets. This method stands in contrast to applied scientific data collection, in which statistical tools lead to reliably predictable outcomes in the future.

Parallel Plate measurements generally result in higher than expected permittivity. Based on observation, we concluded that thickness measurements are a particular challenge here, as the set-up of the parallel plates applies force to the fabric, which may not give the same results as its uncompressed state. Thus air is excluded from the measurement, which results in higher permittivities. This means that the results, while not being incorrect, had to be adjusted for permittivity in the uncompressed state including added air. There is a difficulty that arises with this. The thicker and softer a textile is, the more it is compressible.

With thin materials, the thickness is difficult to determine. For this thesis, an approximation approach was chosen, in which materials were measured compressed with a micrometer, or using an optical microscope to evaluate thickness in an uncompressed state.

In free space set up, the results for textiles and card were lower and closer to values indicated in open literature. However, the challenge of fluctuating results emerged. Through experimentation we found that this can be attributed to several steps within the property retrieval process, including measurement set up, materials chosen and data conversion. While results were accurate for most thick and rigid materials, thin and low-loss materials resulted in measurement variation due to difficulties that arise with digital time gating, multiple reflections and interfering frequencies within the anechoic chamber.

Using the Agilent materials analysis software posed a particular challenge. Although this tool was essential to produce results within a short timeframe, the software package only allowed limited access to the data flow. This made it difficult to follow the path of data processing and error identification. An example of this was the large decrease in permittivity at the lowest and highest frequencies, which led to unusable results in these bands. Free space measurements were used in this work due to the mechanical suitability for accommodating large flat samples. Fluctuations within the frequency range of one measurement were tolerated and interpreted as optimised linear values. Where necessary, free space measurements were always backed by Parallel Plate results, which in general provided smoother and reliable results.

Despite the advantage of waveguide measurements as the most contained form of measurement and thus the least susceptible to interference, the mechanical difficulties of inserting textile and other flexible materials into the waveguide led us to deem this method as unsuitable for textiles.

## **6.5 Numerical Modelling**

A requirement for conducting interdisciplinary research is the availability of methods and tools that enable the researcher to advance in a non-familiar discipline. This can be achieved through collaboration, where different stakeholders contribute their knowledge (Kimbell & Street, 2009), or the provision of technical tools which allow the researcher to explore the unfamiliar field and achieve outcomes without the need to fully understand the detail of the process. The latter is common in design and increasingly common in engineering. Software packages designed and customised for specific purposes allow the researcher to apply mathematical and scientific principles as simulations. In design, software packages like Adobe Creative Suite, allow designers to simulate certain visual aspects without the need to physically prototype using materials. This thesis benefited from software tools such as the electromagnetic 3D simulator ‘CST’ and the software package supplied by Agilent.

### **6.5.1 Unit Cells, Periodic Structures and Perfect Boundary Conditions in CST**

The commercial software Computer Simulation Technology (CST) for electromagnetic design and analysis has been used for all simulations. The electromagnetic analysis was

achieved by a finite element frequency domain solver (CST) method, relying on subdividing the physical 3D model into a discretised mesh (see Figure 6.22), and optional optimisation techniques depending on the boundary conditions of the modelled structure. Following the custom of most Computer-aided Design (CAD) software packages, it is geometry-based with the capability to assign material properties, which are taken into account when solving Maxwell's equations for the discretised model.

In many electromagnetic engineering development processes simulation software is used to first design and optimise a design and then only be fabricated afterwards, with the aim to match both as much as possible. Given the complexity of modelling textiles, which the standard electromagnetic simulation software is not designed for, as well as the lack of detailed knowledge about the properties of the used materials, the design process in this research was more iterative and exchanging between model and experiment. Simulations were used to devise a general idea of electromagnetic design, with the thought of textile techniques in mind. The models were then altered based on experience of practical prototyping.

Overall it was found that modelling did not provide an accurate way to predict textile metamaterial behaviour, specifically in the case of resonating surfaces. However it was useful to determine approximate design geometries, as well as beneficial for understanding how an electromagnetic field interacts with a material.

Two methods of simulations were implemented. One was using waveguide ports, which simulates a physical three-dimensional structure. This method was taking into account the sample, the surrounding space, dimensions between ports and materials, and used a realistic dispersion of the electromagnetic wave. Considering the relatively large problem of the devices looked at, this method quickly led to model sizes, which were impractical to simulate with provided computer memory power. For these cases, only simplified simulations of effective materials were carried out.

For the analysis of periodic materials a 'unit cell' simulation technique was used. In this set up, the boundaries are assumed as open-ended and the array is assigned as double-periodic cells. Floquet ports are set at defined distances off the structure. The wavefront in the unit cell structure is planar, and thus the distance can be set as an arbitrary number without consideration of Fraunhofer Distance. For parameter retrieval, the wavefront is shifted to the edge of the sample, as shown in Figure 6.21 (a). This

provides a phase offset that is consistent with experimental data as the shift of phase towards the edge of the sample is equal to a calibration in the measurement set up.

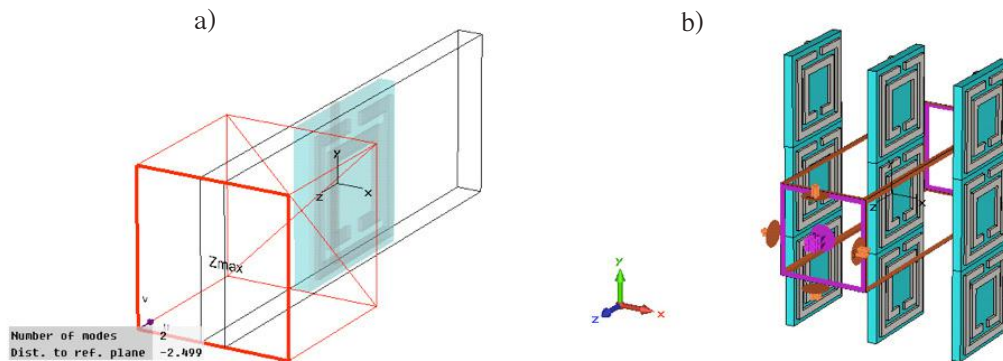


Figure 6.21: A typical set up a unit cell with a shifted phase offset. Material is repeated in Y and Z direction. (a) Propagation direction is X, electric field (E-field) is Y direction and magnetic field (H-field) in Z direction. (b) The infinite array is set up in x and y direction.

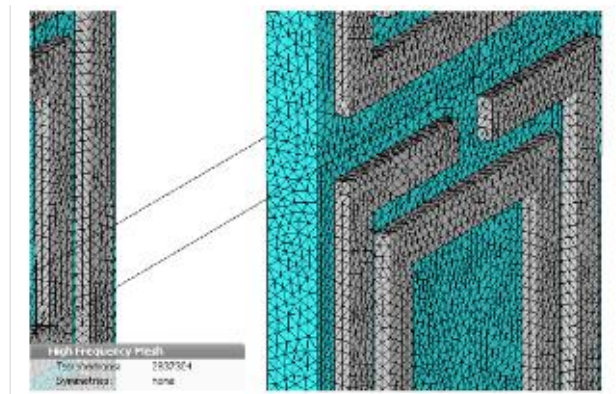


Figure 6.22: Partitioning into tetrahedrons for meshing.

A full set of s-parameters was extracted after the simulation was run and imported to Matlab environment to perform the parameter retrieval described in section 6.6.2.

## 6.6 Material Parameter Retrieval

### 6.6.1 Agilent 85071E Material Measurement Software

This software package is built to enable fast data processing and yield results for material measurements and property retrieval. The software is installed on the Agilent vector network analyser (VNA) and allows fast processing of s-parameter measurement

data. It provides eight common algorithms to process the measurements, each made for different purpose and measurement set up. The software package allowed the researcher to conduct measurements and yield results without the requirement to fully conduct the numerical processing. This method has disadvantages, as intermediate results are not provided and error analysis is impeded. Additionally, the software package has programming flaws that can lead to inaccurate results when used by an inexperienced engineer. Throughout the research, contact with Agilent has been maintained to identify best measuring methods and clarify questions.

The Agilent software package was used for free space and waveguide measurements. The free space process includes a calibration that allows to minimise the distance of measurement to the thickness of a metal plate inserted in between the two antennas. The applied algorithm then uses the thickness of the measured sample in relation to the thickness of the metal plate by performing a numerical phase shift.

Three algorithms for parameter retrieval were applied in this software package. The first and most common is the Nicolson-Ross-Weir algorithm, which retrieves both permittivity and permeability of materials. The second is the NIST method, retrieving permittivity only, the third is the Fast Transmission' technique which uses transmission data only to retrieve permittivity of materials.

### 6.6.2 Nicolson-Ross-Weir Algorithm

Used as techniques both in the Agilent software package and as a Matlab algorithm provided by fellow researchers at Queen Mary University of London (QMUL), the Nicolson-Ross-Weir procedure is the most standard technique to retrieve complex material parameters (Nicolson & Ross, 1970; Weir, 1974). Measured s-parameters of material are converted to refracted index (n) as follows:

$$n = \frac{1}{kd} \cos^{-1} \left[ \frac{1}{2S_{21}} (1 - S_{11}^2 + S_{21}^2) \right] \quad (6.5)$$

where  $S_{11}$  and  $S_{21}$  are the complex reflection and transmission coefficients,  $k$  is the wavenumber, and  $d$  the thickness of the measured sample. In the scope of this research, the method was used for simulated results and dielectric textiles; however, the conversion requires a high level of measurement precision for sample placement, thickness and stability, which is challenging to achieve with large textile structures.



### 6.6.3 Refractive Index Retrieval with Transmission Phase Results

A dip in the phase of the transmitted wave ( $S_{21}$ ) indicates the reversal of the phase velocity while retaining the propagation direction, indicative of a negative refractive index. This phenomenon has been termed "backwards phase" and is commonly used to describe NIM behaviour. It can be experimentally observed by comparing layers of materials in multiple thicknesses (Aydin et al., 2005). While in a conventional dielectric material the phase advances with increasing thickness, in a negative refractive index metamaterial, the phase declines. With this approach only the real part of the refractive index can be retrieved. For this reason the method is not useful for most antenna applications as the loss of a material impacts the antenna performance. However for this research, the method proved to be valuable as it provides a simple and robust method to verify the existence of a negative refractive index from experimental data.

For the measurement preparation, the cables were calibrated up to the antennas using a calibration device. Then the chamber was measured without inserted sample and the transmission phase normalised. The material was then inserted and measurements data taken from the transmission phase. The refractive index was retrieved as follows:

$$n = \frac{\Delta\theta}{\Delta L} \cdot \frac{c}{\omega} \quad (6.6)$$

where  $\Delta\theta$  is the phase difference in degrees,  $\Delta L$  the width of the additional layer,  $c$  is speed of light and  $\omega$  the angular wavelength.

## 6.7 Summary

This chapter provided an overview about materials and measurement techniques used in this thesis. It framed hardware and software-related methods for data acquisition and processing, laying out the specific requirements when working with textile metamaterials. Some initial measurements with standard materials such as PTFE and FR-4, as well as polycotton were conducted to test general suitability.

The purpose of this chapter was to prepare a 'kit' of textile and electromagnetic materials, techniques and evaluation methods. The studies presented in the following two chapters will investigate in detail the limits to applying these to textile dielectric

and resonating metamaterials, as well as assess if standard methods for measurement and retrieval of electromagnetic properties are applicable to textiles.

## **Chapter 7**

# **Dielectric Textiles**

### **7.1 Introduction and Objectives**

This chapter presents a series of experiments, in which properties of textiles and paper were manipulated to produce flexible dielectric maps for microwave applications; using digital embroidery, screen print and laser cutouts. These experiments were motivated by textile design approaches using patterning and surface manipulation techniques. While the primary aim in textile design would normally be to accomplish an aesthetic style or an effect on human senses, we investigated how these techniques could serve electromagnetic functionality of metamaterials, and be utilised to compose visually interesting, all-dielectric metatextiles.

To recap, all-dielectric metamaterials are composed of intricate arrays of permittivity cells, which form a complete anisotropic structure. They are used for ground plane cloaks (section 2.1.4), and are made of high-resolution maps of small material blocks, enabling smooth guidance of an electromagnetic wave through cells of varying permittivity. However, due to the fabrication challenge of producing finely graded structures, alternative forms of construction have been proposed. One such solution is lowering the resolution of the permittivity map (Bao et al., 2011; Kallos et al., 2009).

This chapter investigates the possibility of replacing rigid all-dielectric metamaterials with flexible and soft anisotropic textiles that are constructed in a single fabrication process. The goal was to design two-dimensional and three-dimensional flexible

structures that have a permittivity gradient. The structures proposed form the basis of flexible metamaterial devices, providing binary and graded surfaces to build seamless all-dielectric ground plane cloaks.

The permittivity map for a ground plane cloak developed at QMUL (Bao, 2012), shown in Figure 7.1 was used as a guideline for the required range of permittivities. Bao's cloak was tested for the bandwidth 7-12 GHz, approximately corresponding with X band frequency range. The height of the material blocks was 10.16 mm, which was equivalent to the height of the respective waveguide aperture. Permittivities ranged from 1-2, as shown in Figure 7.1 (a). This high-resolution map was quantised to a permittivity map of just four values, as shown in Figure 7.1 (b); these are 1.02, 1.17, 1.30 and 1.46. 1.02 was neglected and replaced by air. The fabricated cloak is shown in Figure 7.1 (c).

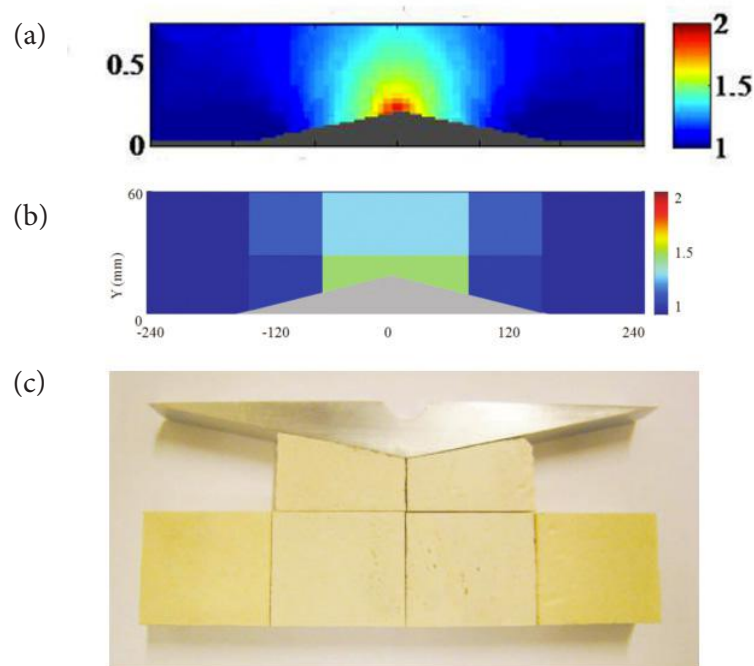


Figure 7.1: All-dielectric cloak by Bao (2012). (a) High resolution map of permittivity blocks (b) Lower resolution map (c) Fabricated cloak from BaTiO<sub>3</sub> blocks.

Instead of following this approach, and using a low-resolution map to simplify fabrication, we propose to produce finely graded dielectric materials within one fabrication process, using textile techniques.

To summarise, the objectives of the studies presented in this chapter are to:

- Identify suitable textile techniques to achieve permittivity ranges between approximately 1 and 2 that can be fabricated as graded textiles in one fabrication process;
- Use techniques common in textile design, and question if they have the potential to produce visually interesting all-dielectric metatextiles;
- Perform electromagnetic analysis of flat textiles with graded permittivity;
- Explore how the technique of pleating could be used to design three-dimensional all-dielectric graded textiles.

## 7.2 Manipulating Dielectric Properties of Textiles

There are two ways to increase the effective permittivity of a textile. Firstly, the volume fraction  $\phi$  of the constituent component materials can be varied by adding air to the composite. Secondly, a high permittivity coating can be added to a low permittivity textile substrate, replacing air pockets in the fabric with the coating material. In both cases, the thickness of the textiles has to remain the same. Figure 7.2 illustrates both alternatives with an example of a woven fabric. The base fabric is a simple (plain) weave shown on the right, with a cross section shown on the left. Changing the volume fraction of the woven material is achieved by weaving a closer structure, as shown in Figure 7.2 (b) compared to (a). By adding a coating material, the air gaps between the threads are filled, as seen in Figure 7.2 (c).

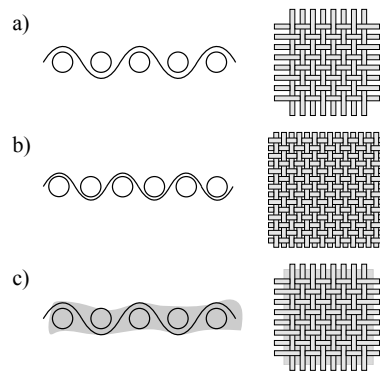


Figure 7.2: Manipulation of permittivity of woven textile. (a) 75% fibre, 25% air (b) 88.8% fibre, 11.1% air (c) 75% fibre soaked with ink, 25% ink.

To design a printed textile with graded permittivity, a pattern with increasing element size needs to be applied to the substrate. The size of the largest element should be within the boundaries of effective medium considerations. Figure 7.3 shows two ways of designing these. In Figure 7.3 (a), the same unit element was repeated, with increasing distance between the elements. In Figure 7.3 (b), a one-directional scaling factor was introduced, increasing the element size in one direction, but maintaining the size in the perpendicular angle. The increase of permittivity is defined by the changing volume fraction  $\phi$  of the two substances.

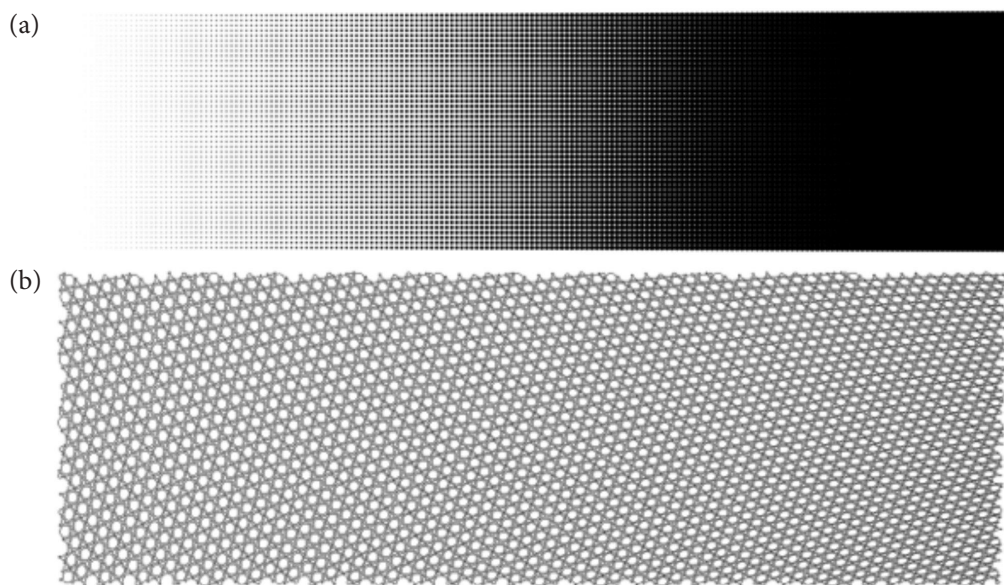


Figure 7.3: Two ways of designing graded patterns. (a) Dot matrix with varying unit size.  
(b) Pattern with one-directional scaling factor.

The method for applying a gradient was chosen based on the suitability of the respective textile technique. For laser cutouts and screen printing, this meant increasing the space around the element whilst maintaining the element size. This technique was not viable for embroidery, as embroidery uses a continuous thread linking all elements and making separation impossible. Therefore, in this case, a scaling factor was used to achieve stitching of graded structures.

### 7.3 Study 1: Embroidered Dielectric Textiles

Three samples were made to explore digital embroidery as a technique to produce graded all-dielectric textile structures. In the first study, a two-dimensional sample was embroidered and analysed using the free space method. In a second and third study, two samples were constructed to explore pleating as a technique for the formation of three-dimensional textiles with variable height. Both samples were first measured in their two-dimensional shape, with free space and parallel plate capacitor methods. They were subsequently pleated, in order to explore the possibility of creating three-dimensional all-dielectric graded textiles.

#### 7.3.1 Two-dimensional Embroidered Textiles with Graded Permittivity

##### **Sample 1: two-dimensional embroidered sample with gradually increasing line-density**

A sample gradually varying in density was embroidered with a Brother PR1000e embroidery machine. The viscose felt substrate provided an experimentally determined dielectric constant of 1.27 at 11 GHz. The pattern was stitched with No. 40 Sulky thread as top thread, and polyester as bobbin thread. The sample was embroidered with a line pattern, with a stitch length of 3 mm parallel to the E-field. The gradient was linear, varying from 1 to 7 lines/mm over a sample length of 360 mm. Figure 7.4 shows the design as a vector graph, with the dots indicating the interlocking of top and bobbin thread.

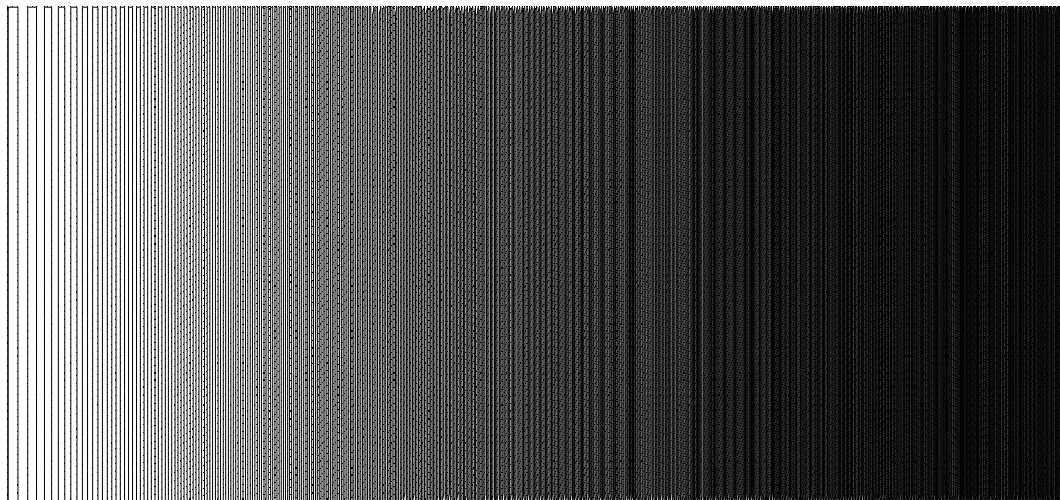


Figure 7.4: Sample 1 with a length of 360 mm. Complete design as a vector graphic.

Measurements were taken in the free space chamber in the frequency range 9-12 GHz. Permittivity and dielectric loss were retrieved using the NIST algorithm in the Agilent Materials Software (section 6.6.1). 34 measurements in intervals of 10 mm were taken over the length of the sample, using the push through mechanism of the chamber. Sample thickness was 1.5 mm, corresponding to the thickness measured at the thickest end of the pattern, which was kept constant for the complete length of the sample.

Experimental results of permittivity are plotted against frequency in Figure 7.5. Permittivity was found to vary between 1.2 and 1.8 across the 360 mm sample length, representing a permittivity increase of 0.002 per mm. Whilst dielectric loss  $\tan \delta$ , shown in Figure 7.5 (b), increases with increasing density of embroidery, it stays below 0.1 overall. Figure 7.5 (c) shows the results of permittivity at 11 GHz plotted against stitch density, demonstrating the increase over the length of the sample.

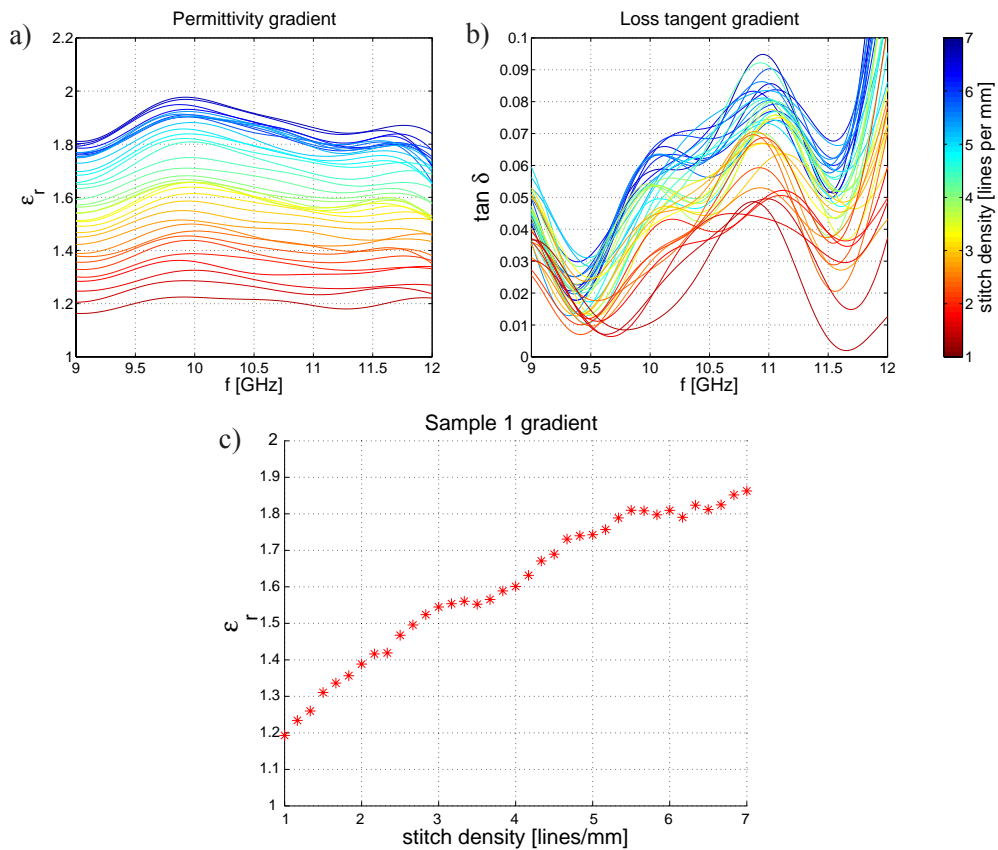


Figure 7.5: Results of Sample 1: dielectric two-dimensional embroidery with increasing line density. (a) Permittivity range measured, with red line showing least dense end, and blue line showing most dense end of the sample. (b) Loss tangent measured, with red line showing least dense end, and blue line showing most dense end of the sample. (c) Permittivity range measured at 11 GHz. Permittivity gradients over length of the sample, experimental results.



This first study shows that detailed two-dimensional permittivity gradients can be achieved with an embroidered sample, providing a path for graded permittivity maps while maintaining a sufficiently low dielectric loss. This technique delivers low-cost and customised production, while having the advantage that the structure can be fabricated in one process without further assembling. Two-dimensional graded textiles are potentially beneficial for innovative metamaterials and antennas, as well as inspire new application scenarios, based on the use of textiles in everyday life.

### **7.3.2 Three-dimensional Embroidered Textiles with Graded Permittivity**

This section explores the potential of using textile techniques to produce graded three-dimensional permittivity maps.

To recap, in textile and fashion design, two-dimensional textile surfaces are frequently manipulated by pleating, to achieve controlled voluminous and soft structures. Pleated textiles are used to mould garments around the body in decorative ways, but also have functional aspects, for example to allow freedom of movement. This section investigates if embroidered textiles can be further processed with pleating, to achieve graded three-dimensional permittivity maps. Two studies aim to explore the upper threshold of permittivity, and the relation between textile density and permittivity gradient. Two samples were produced for the study. Their electromagnetic properties were measured at five sections over the length of the sample to identify the increase of permittivity with increasing stitch density.

Both samples were measured in two-dimensional states. The challenge of the analysis of graded three-dimensional textile samples lies in the measurement set up. For free space analysis, a sample requires minimum dimensions of 120 mm in both E-field and H-field directions. For an X band ground plane cloak, the height of the sample must be 10.16 mm (Bao et al., 2011). When folded, the gradient of the produced samples occurs over a much smaller distance than 120 mm, making it impractical to fabricate a graded textile with a sufficient length to be analysed. Therefore, it was decided to produce five samples with constant permittivities to act as non-graded representatives for five regions of the graded textile. These five representative samples were measured in one layer and two layers in a capacitor (50 Hz – 5 MHz) and free space (9 – 12 GHz) set up. Results of single and double layer measurements were averaged to level errors in thickness measurements and fabrication differences.

**Sample 2: three-dimensional embroidered sample with gradually increasing density**

A textile gradually varying in density was embroidered. The polycotton substrate provided an experimentally determined dielectric constant of 1.3. The pattern was stitched using a Brother PR1000e embroidery machine with No. 40 Sulky yarn as top thread, and 100% polyester thread as the bobbin thread. Optimal stitch type, design and dimensions of embroidery were found through iterative sampling. The final design, as depicted in Figure 7.6 consisted of blocks 5 mm wide and 160 mm long. Blocks densities varied from 1 line/mm to 6.8 lines/mm, and were stitched with a fill stitch parallel to the gradient. Between two blocks a gap of 0.3 mm was inserted to facilitate easy and precise pleating. The sample was made from 58 blocks, resulting in an overall length of 353.60 mm. The design was stitched at a speed of 1000 spm and a stitch length of 2.5 mm.

Figure 7.7 shows the five regionally representative disks fabricated for analysis, with the complete sample in states of tight and loose fold shown in Figure 7.8. Two layers of tiles for each density were stitched for free space, and five layers of disks for each density were stitched for parallel plate measurements. The densities were 1 line/mm, 2.3 lines/mm, 3.8 lines/mm, 5.3 lines/mm and 6.8 lines/mm.

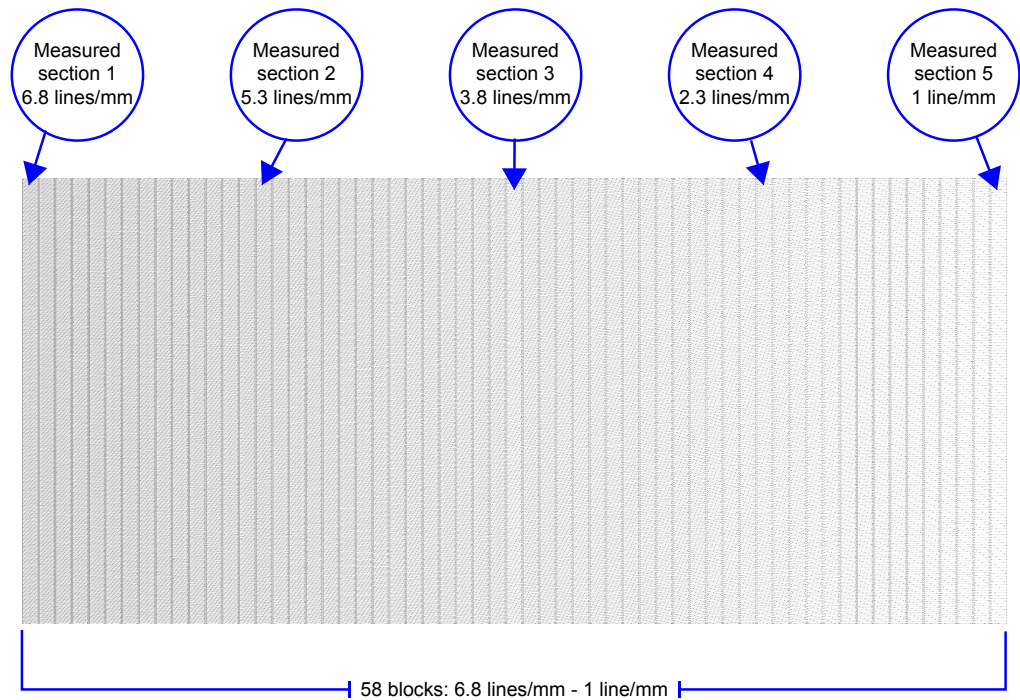


Figure 7.6: Illustration of Sample 2 as a vector graphic. Circles show the five regions, which were stitched separately for electromagnetic analysis (Figure 7.7)

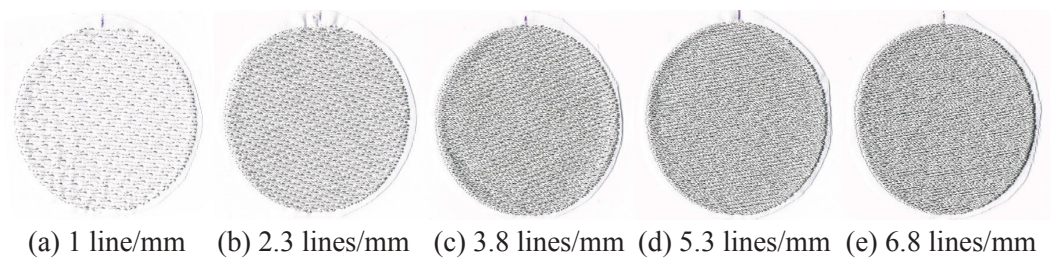


Figure 7.7: Sample 2: Five stitched disks that represent five regions of the graded sample. Disks were used for capacity measurements in the parallel plate set up. Five larger tiles (120 x 120mm) with the same stitch densities, not shown in the figure, were used for free space measurements.

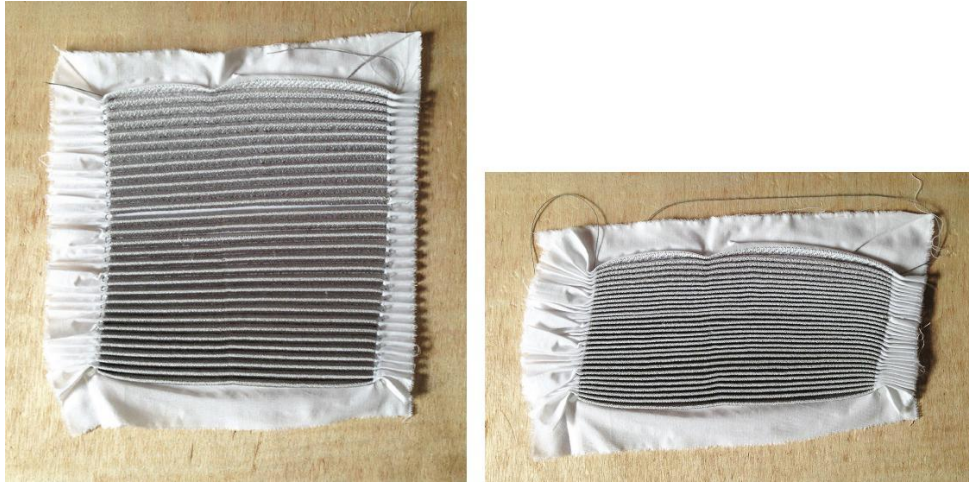


Figure 7.8: Embroidered Sample 2. (a) Loosely folded ( $\sim 45^\circ$ ). (b) Tightly folded ( $\sim 170^\circ$ ).

The embroidered disks were measured using the Parallel Plate Capacitance method over the frequency band of 50 Hz – 5 MHz. For 9 – 12 GHz the free space method was applied using the NIST conversion method available for parameter retrieval in Agilent’s Materials Software.

To generate repeatable data, we implemented the following measures:

- Each density disk was embroidered five times and measured independently. Results were averaged subsequently to level fabrication differences.
- Disks were measured in stacks of increasing number of disks. Results were subsequently averaged to compensate for errors in thickness measurements and fabrication differences.

We then assessed the range of permittivity and dielectric loss achieved over the length of the sample.

Results for Sample 2 are shown in Figure 7.9. For 9 – 12 GHz a permittivity range of 1.2 – 1.6 was achieved (Figure 7.9 (c)). Dielectric losses varied, but stayed below 0.1 (Figure 7.9 (d)). For 50 Hz – 5 MHz a permittivity range of 1.05 – 1.6 was achieved Figure 7.9 (a), indicating that more dispersion occurs in lower stitch densities. Dielectric loss tangents (Figure 7.9 (b)) were low and constant at around 0.016.

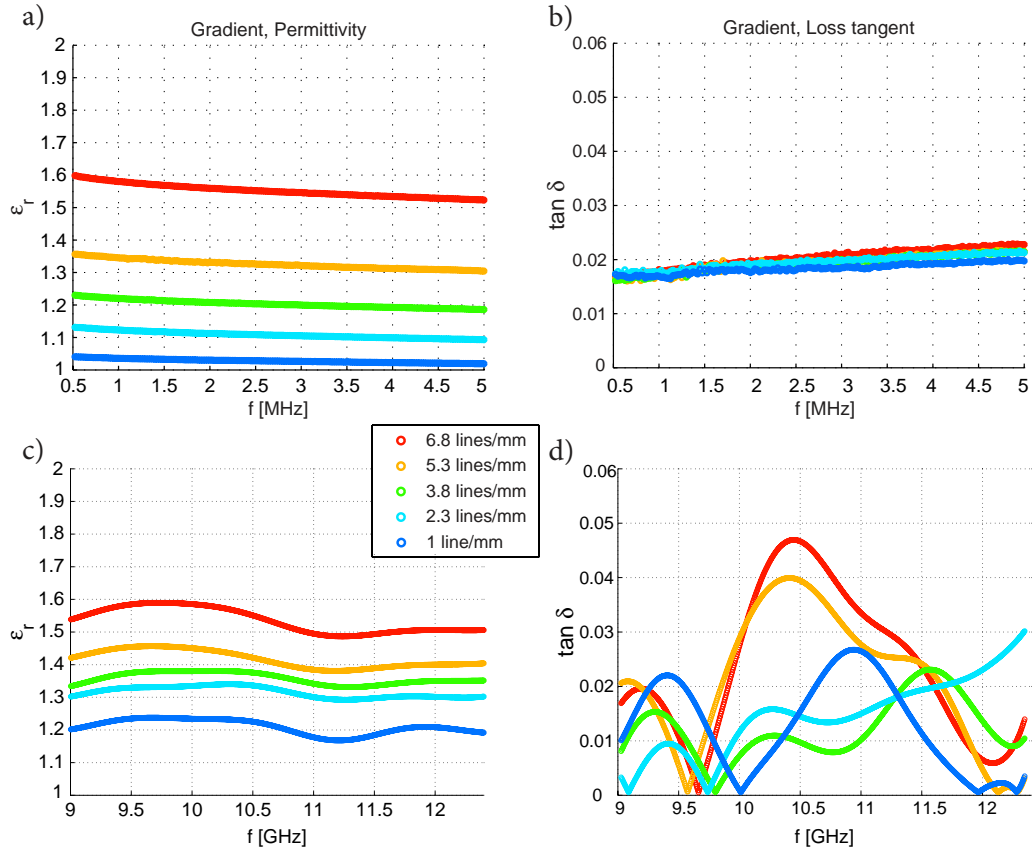


Figure 7.9: (a)-(b) Parallel plate measurements for disks of Sample 2. (c)-(d) Free space measurements for tiles of Sample 2.

Figure 7.10 shows stitch densities plotted against permittivity and dielectric loss, demonstrating the gradients achieved over the length of the sample. The gradient at 1 MHz (red line) covered a broader range of permittivity values, and differences between stitch lines had a larger impact on permittivity. At 9 GHz, the permittivity gradient was less dramatic. Dielectric loss tangents at both 1 MHz and 9 GHz were below 0.04.

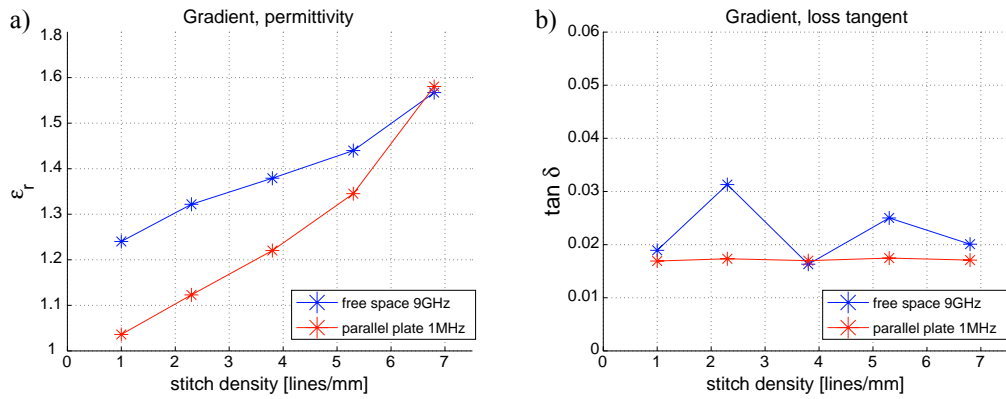


Figure 7.10: Gradient Sample 2. (a) Permittivity gradient and (b) dielectric loss, plotted against stitch density.

The samples illustrate how accordion pleats can be used to shape complex three-dimensional textile forms. The block design facilitated straightforward folding of the sample enabled by the small gaps, which created clear folds at required locations and helped to maintain a constant height.

Pulling threads sewn into the centre of the folds ('smocking') were used to compress the textile and create complex draped curves and corrugated structures. Figure 7.11 shows a series of variations in which the frequency of folds were varied, or extreme tension on the outer sides led to the structure expanding upwards. These simple manipulations of textiles, which are not so easily achieved with rigid materials, can be utilised to create intricate gradients for all-dielectric three-dimensional metatextiles.

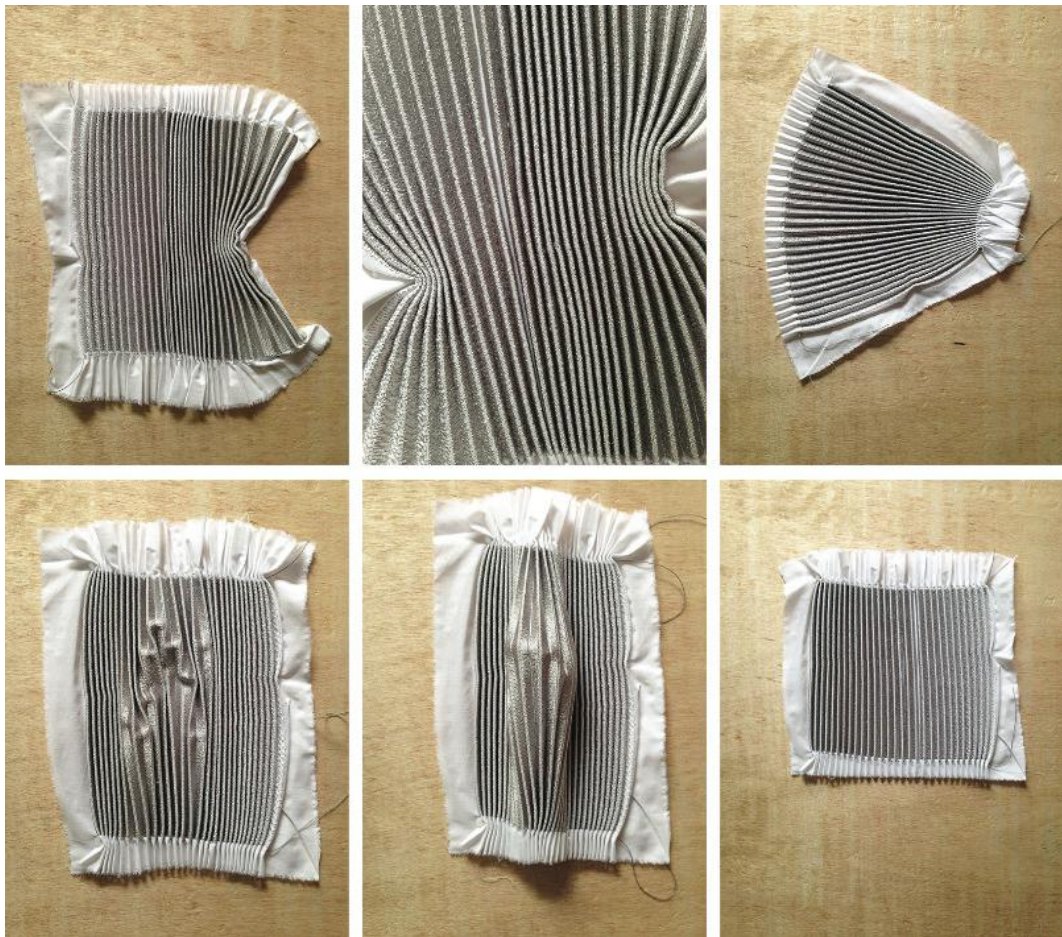


Figure 7.11: Shape experimentation utilising 'smocking', Sample 2

**Sample 3: three-dimensional cross-element embroidered sample with gradually increasing density**

A textile gradually varying in density with a decorative cross-pattern was embroidered. The single cell of the repeat pattern was 5 mm long and 5 mm wide, and thus fell into the effective material threshold for 9 GHz (33.3 mm). The polycotton substrate provided an experimentally determined dielectric constant of  $\sim 1.22$  (8 GHz). The pattern was stitched with No. 40 Sulky rayon yarn as top thread, and polyester bobbin thread. Optimal stitch type, design and dimensions of embroidery were again found through iterative sampling. The final design, as shown in Figure 7.12, was stitched as a continuous surface. Densities varied from 1 line/mm to 5 lines/mm, and were filled with a decorative stitch. The overall length was 350 mm and the design was stitched at a speed of 1000 spm.

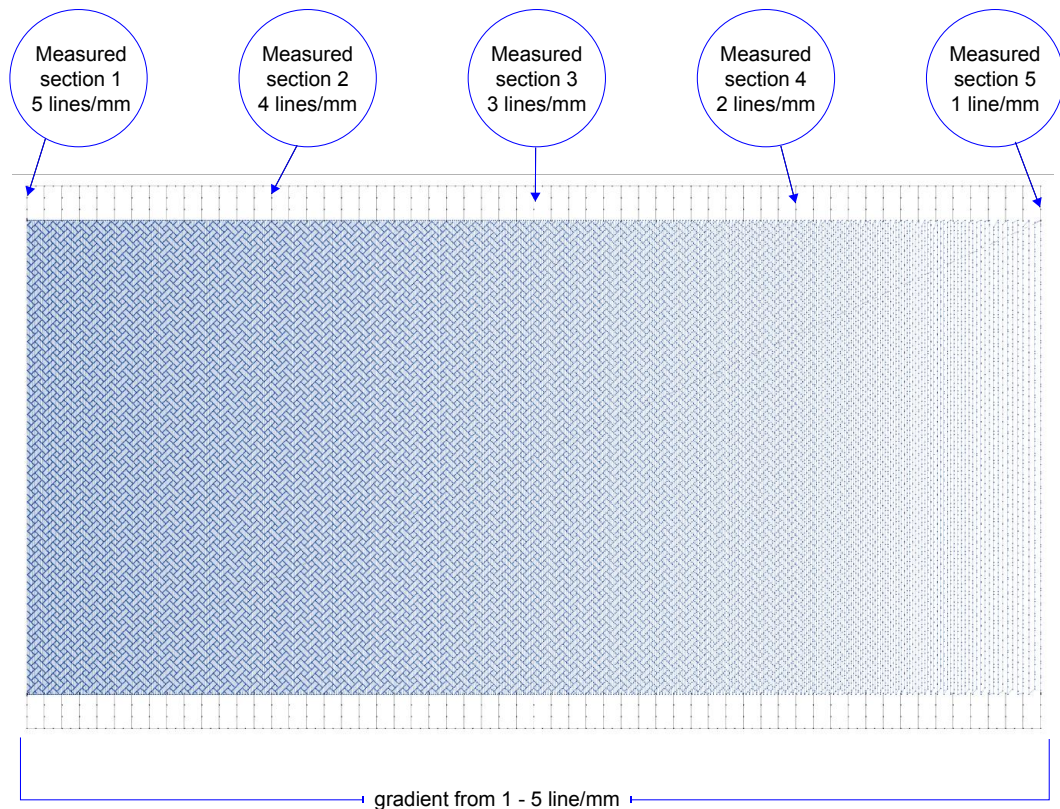


Figure 7.12: Sample 3: Illustration of embroidery with locations of five sections (see Figure 7.13) which were measured as disks and tiles.

Figure 7.13 shows the five regionally representative samples fabricated for analysis in free space and parallel plate set-ups. Two tiles for each density were stitched for free space, and five disks for each density were stitched for parallel plate measurements. The densities are 1 line/mm, 2 lines/mm, 3 lines/mm, 4 lines/mm and 5 lines/mm.

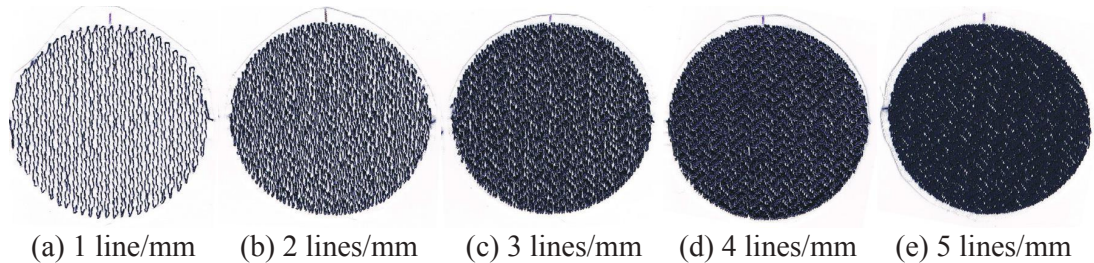


Figure 7.13: Sample 3: Five stitched disks that represent five regions of the graded sample. Disks were used for capacity measurements in parallel plate set up. Two larger tiles (120 x 120mm) with the same stitch densities, not shown in the figure, were used for free space measurements.

The embroidered disks were measured with the free space set up over the frequency band of 9 – 12 GHz and the range of permittivity and dielectric loss achieved over the length of Sample 3 was then assessed.

Results for Sample 3 are shown in Figure 7.14. For 9 – 12 GHz a permittivity range of 1.2 – 1.6 was achieved (Figure 7.14 (c)). Dielectric losses vary but stay below 0.1 (Figure 7.14 (d)). For 50 Hz – 5 MHz a permittivity range of 1.05 – 1.8 was achieved (see Figure 7.14 (a)), indicating that in lower stitch densities more dispersion occurs. Dielectric loss tangents (Figure 7.14 (b)) are low and constant around 0.016.



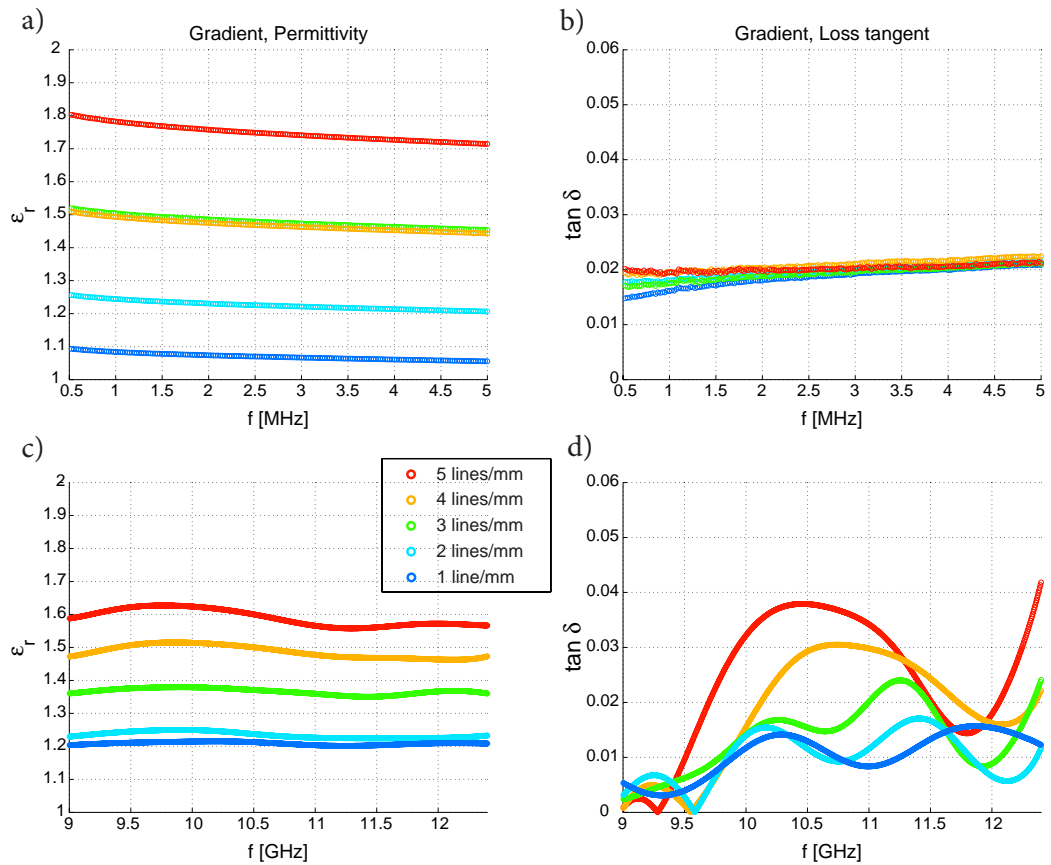


Figure 7.14: Results of Sample 3 (a-b) Parallel plate measurements for disks (c-d) Free space measurements for tiles.

Figure 7.15 shows stitch densities, plotted against permittivity and dielectric loss, demonstrating the gradients achieved over the length of the sample. The gradient at 1 MHz (red line) covers a broader range of permittivity values ranging from 1.1 to 1.8 (Figure 7.15 (a)). The permittivity increase is similar measured at 9 GHz, however with a narrower range of 1.2 to 1.6. The samples displayed a linear increase in permittivity with stitch density using both methods of measurement. The dielectric loss measured at 1 MHz declines from 0.020 to 0.015 over the length of the sample, whilst the loss tangent measured at 9 GHz does not vary linearly with stitch density, and varies between 0.005 and 0.040.

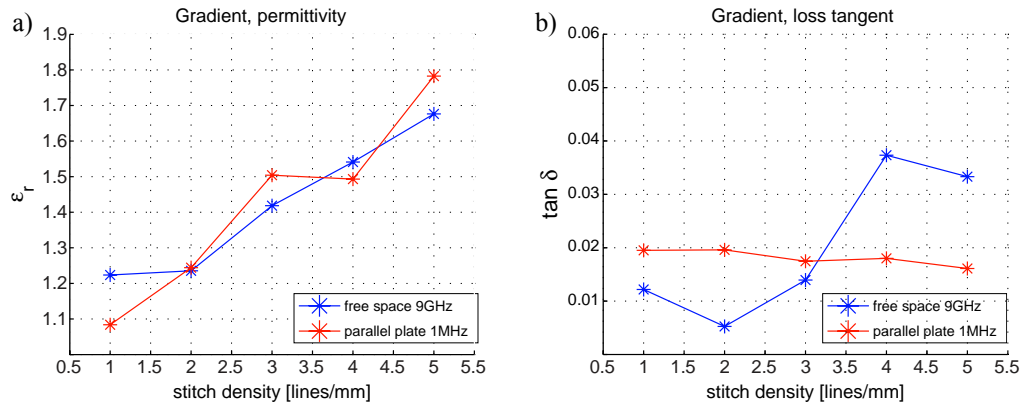


Figure 7.15: Results for embroidered Sample 3 (a) Graded permittivity and (b) dielectric loss tangent

To investigate whether pleated fabrics could be formed into three-dimensional dielectric graded maps, the two embroidered samples were folded into accordion folds of approximately 5.1 mm in width (half the height of an X band waveguide), guided by a ruler that was stitched alongside the design (Figure 7.16). The structure was tightened with four pulling threads and placed in an unclosed heat press for three minutes at 180°, to settle the pleats.



Figure 7.16: Smocking process of Sample 3.

The pulling threads were then tightened and loosened to vary the frequency of folds, achieving various shapes (Figure 7.17).

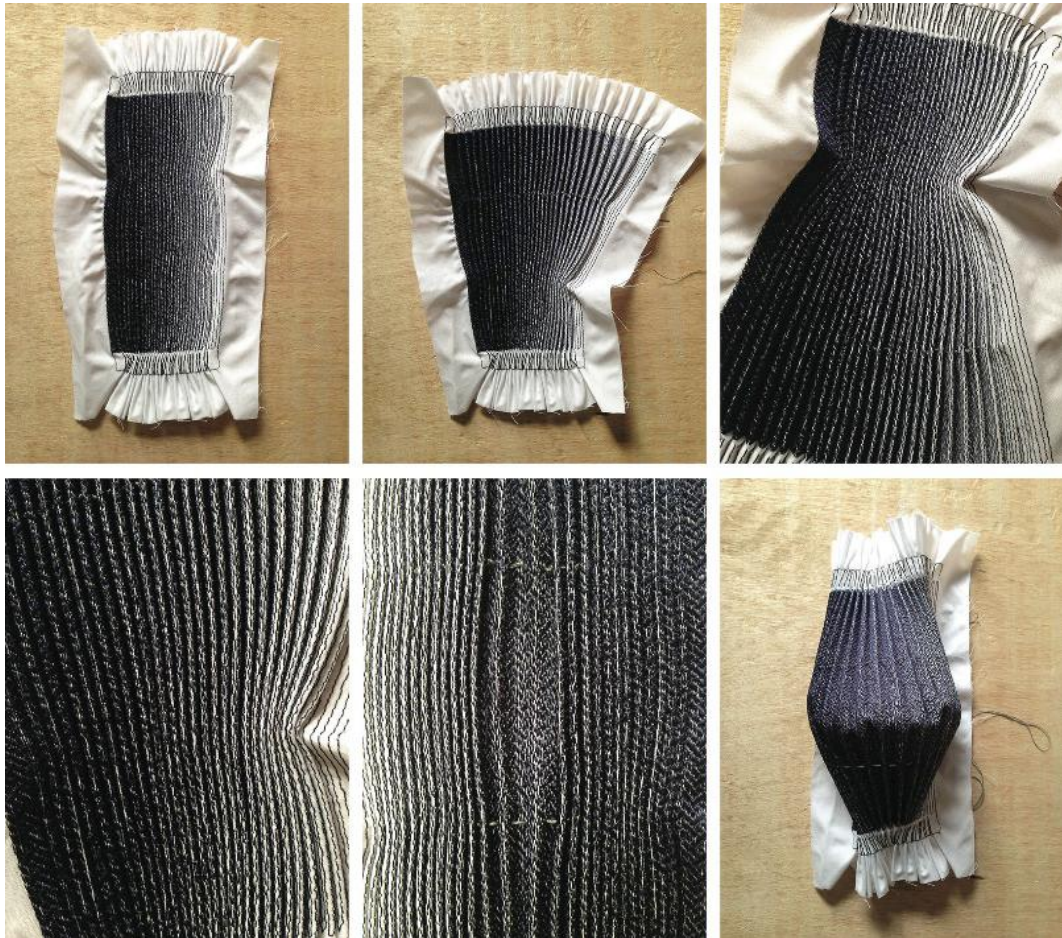


Figure 7.17: Shape experimentation, Sample 3

For a textile ground plane cloak, a carefully composed map consisting of different stitch densities and tensions would need to be planned. Whilst we were not able to achieve a complete cloak, we have demonstrated the potential for textiles to be used in this way, and hope that this will inspire engineers to experiment with this method.

Known challenges, when working with textiles in electromagnetic engineering (detailed in section 2.2.1), were noted. For example, whilst electromagnetic analysis demonstrated approximate property values, retrieving unambiguous data was difficult. Textiles are thin and have low dielectric loss, resulting in significant changes of material parameters when they are exposed to environmental and mechanical alterations. For this thesis, we averaged results from repeated measurements. However, if consistent accuracy was required, the textile would need to be fabricated with industrial equipment and kept under controlled conditions. A solution may be to fabricate the material with a heat or UV light sensitive resin that is then baked to give a

final rigid structure. In addition, our results suggest that, even when unit cells were kept well within the effective medium threshold, some samples still showed anisotropic properties.

## 7.4 Study 2: Screen Printed Dielectric Textile

The second study explored the use of manual screen printing to fabricate all-dielectric graded permittivity maps. This study consisted of permittivity and dielectric loss analysis of a two-dimensional graded sample, printed with TiO<sub>2</sub> lino ink.

### 7.4.1 Two-dimensional Screen Printed Textile with Graded Permittivity

A cotton substrate was screen printed with a matrix of dots, which varied in diameter, as shown in Figure 7.18. The dots remain at the same distance apart, so that the proportion of surface area covered with ink increases gradually. The printing medium was TiO<sub>2</sub>-based lino ink and the sample had an overall length of 560 mm.

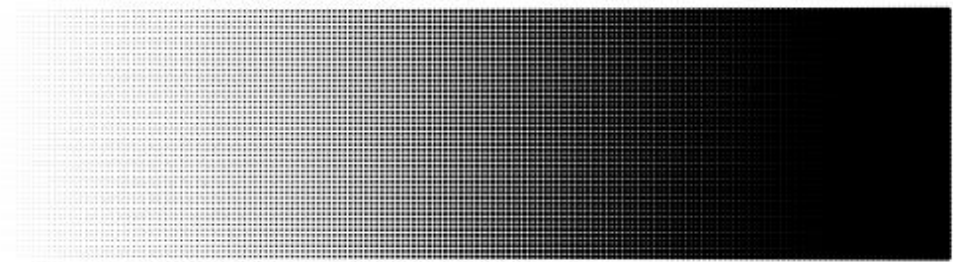


Figure 7.18: Screen printed dot matrix over a sample length of 560 mm. Dot diameters vary between 0.1 - 5.0 mm

Measurements were taken in free space, with eight measurements taken over the whole length of the sample. Previous waveguide measurements had shown that the cotton substrate printed with TiO<sub>2</sub>-based ink achieved a permittivity of up to 2.5. The overall thickness of the substrate was not changed by more than 0.1 mm, because the ink filled the spaces between the woven threads, replacing the air medium with ink medium. A simple model was constructed to simulate the structure. A single dot on cotton substrate was modelled as a unit cell in CST software to obtain an estimate of permittivity to compare to the experimental results. The cotton substrate was modelled as an effective

medium with a permittivity of 1.3 and a thickness of  $d = 0.319$  mm. An illustration of the model is shown in Figure 7.19.

The print was represented as a dot, which has a thickness of  $0.419$  mm ( $d + 0.1$  mm). A permittivity of  $3.78$  was assigned, determined through an iterative process, matching the threshold of permittivity of the simulated composite with the experimental results. The overall thickness of the unit cell increased to  $0.419$  mm, which included a layer of air. The complete model was made of a three-part composite: substrate, printing medium and air.

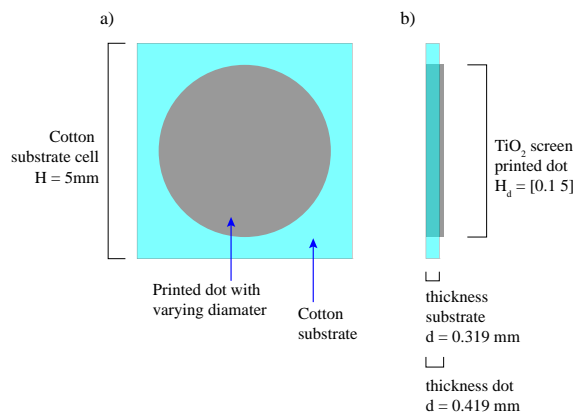


Figure 7.19: The unit cell modelled using CST to obtain a predicted permittivity for a matrix of screen printed dots. (a) Front view and (d) side view with dimensions.

Experimental and simulated results are shown in Figure 7.20, with simulated results plotted in blue, and experimental results plotted in red. Both indicate a permittivity range between approximately 1.6 and 3.7.

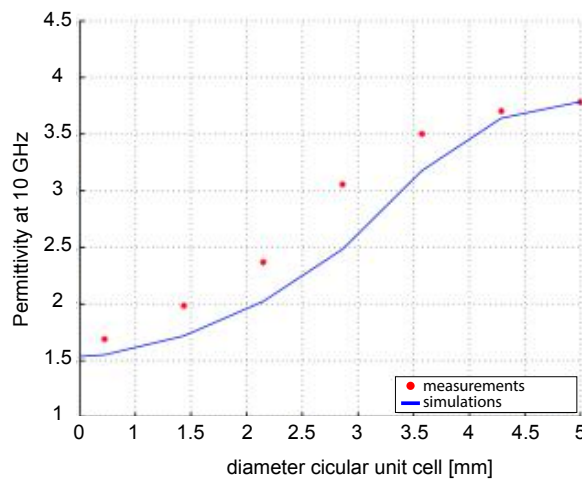


Figure 7.20: Permittivity range for screen printed Sample 1. Permittivity gradient for diameter dot change. Measured (red) and simulated (blue) results.

Permittivities of the experimental and simulated material showed a reasonable match, with a small increase between dots of diameter 0.5 – 1.5 mm, and a larger increase between 1.5 – 4.5 mm. The permittivity stabilised when dot diameter was 4.5 mm, in both experimented and simulated results.

## **7.5 Study 3: Patterned Paper Cut-outs**

In the third study, permittivity and dielectric loss ranges were examined for samples of paper with symmetric and asymmetric cutout patterns. In this study it will be explored, whether or not complex decorative patterns can be used to achieve dielectric materials suitable for metatextile applications.

### **7.5.1 Two-dimensional Symmetric and Randomised Patterns**

Symmetric patterns are used to produce visual balance and effects in traditional textile design. Patterns can vary from simple square block lattices, to complex repeated patterns using rotated, reflected and multiple dropped elements (Schattschneider, 1978). Resonating metamaterials use one-directional repeated block patterns, in which multiple elements are repeated in horizontal and vertical lines, corresponding to Speiser's first group of symmetries (Speiser, 1927). Non-resonant metamaterials however, can use randomised patterns as long as the overall dielectric properties are measurable and constant, requiring it to be isotropic in two planes (within one block of the permittivity map). This suggests that the design of dielectric metamaterials can utilise either randomised or aligned block patterns, allowing a more flexible design choice, than is possible for resonating metamaterials. Using laser cut is a way to vary the volume fraction of air and paper fibres, without adding another material.

It was necessary to maintain an overall small pattern with elements of dimensions of less than 1/6 of the measured wavelength, to ensure that bulk material properties could be determined. Two versions of the same pattern were created. The first was a direct adaption of a regular symmetric pattern, taken from "Grid Index" (Nicolai, 2009). The second was an irregular adaptation of this pattern, based on hand drawings incorporating irregular elements arising from the manual process.

The patterns were laser cut from A4 sized 200 g/m<sup>2</sup> card, and screen printed twice with BaTiO<sub>3</sub> using a wet-on-wet process, with a 43T screen and a soft blade squeegee. The

prints were then dried at room temperature and fixed at 130° for 90 seconds. The complete designs are shown in Figure 7.21, with white areas representing air, and black areas representing card. The final prototypes were 130 mm wide and 170 mm long. Details of both patterns are shown in Figure 7.22.

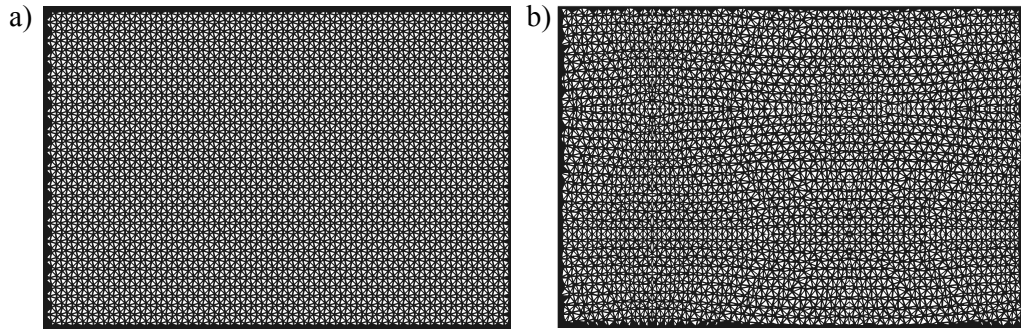


Figure 7.21: Laser cut card, screen printed with BaTiO<sub>3</sub> ink. One pattern was created as two versions, a symmetric pattern with equal repeats and a manual adaptation using a hand drawn version of the pattern. (a) symmetric (b) asymmetric.

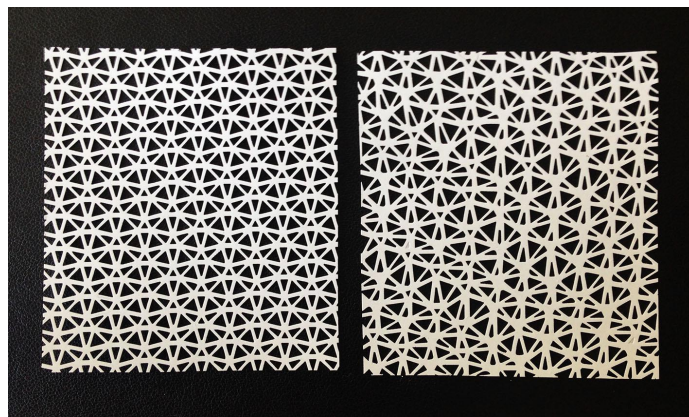


Figure 7.22: Tiles of BaTiO<sub>3</sub> screen printed and cut out card. Each tile is 5.5 cm wide and 6 cm high.

The two samples were measured using the free space method over a frequency band of 9 – 12.4 GHz. Permittivity and loss tangent were retrieved using the NIST conversion technique.

The following measurements were taken:

1. Isotropy measurement: Sample measured at arbitrary angles to investigate if isotropy in two planes had been achieved.
2. Consistency over length: Sample measured at random positions along the length to assess if permittivity was constant over the entire area of the sample.

The results of the isotropy measurements are shown in Figure 7.23 (a) and (b) for the symmetric pattern, and Figure 7.23 (c) and (d) for the asymmetric pattern. The sample was measured in five different positions, which was done by rotating the sample at random angles in the chamber.

The symmetric pattern has an overall lower permittivity of between 2.20 - 2.25 at 11 GHz, compared to 2.25 - 2.35 for the asymmetric pattern. This difference was expected, as it is the result of the hand drawn pattern having a less controlled overall volume fraction. The results also show that the margin of permittivity in the symmetric sample is lower (0.05 at 11 GHz) than in that of the asymmetric sample (0.10 GHz at 11 GHz). This suggests that isotropy in permittivity is more difficult to achieve for asymmetric samples, than isotropy in symmetric samples. Although the aim of this study was to extend the variety of visual aesthetics, it could also be an important consideration for other more common engineered randomised structures, such as foam materials.

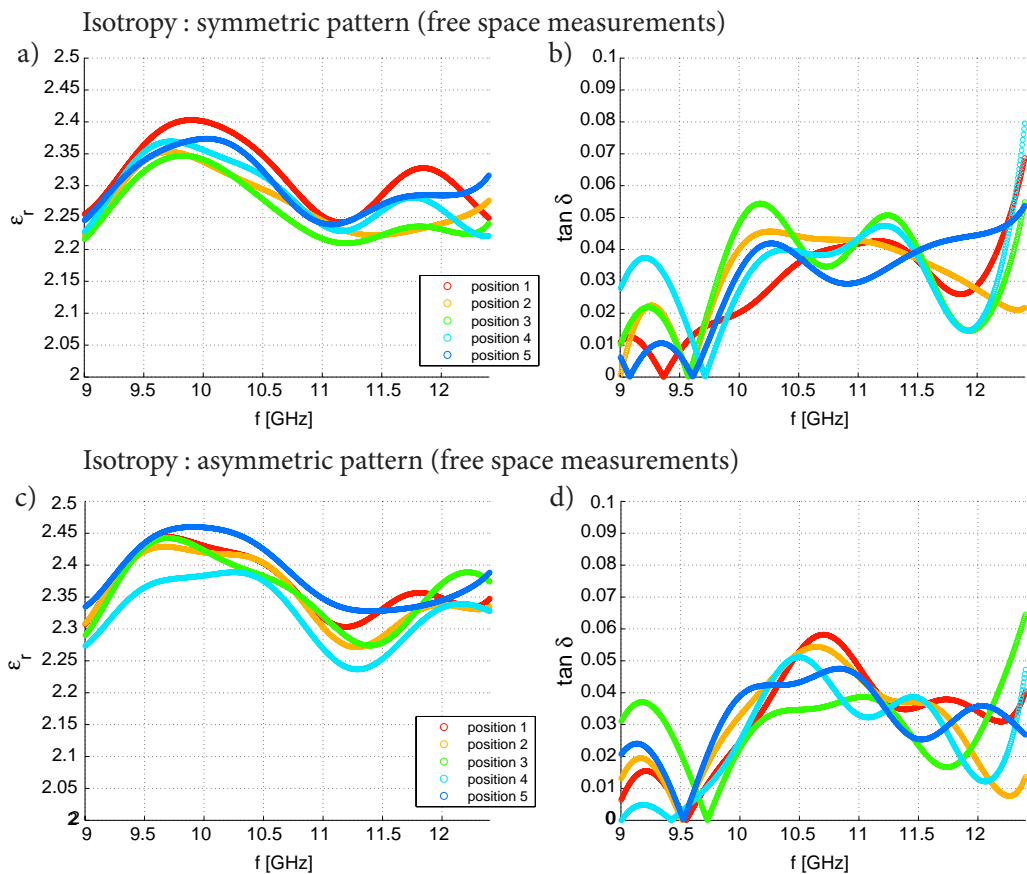


Figure 7.23: Results of permittivity and dielectric losses for measurements of directional change (isotropy) of the sample, to investigate the possibility to design asymmetric isotropic samples. (a) Symmetric pattern permittivity and (b) dielectric losses. (c) Asymmetric pattern permittivity and (d) dielectric losses.



The samples were then measured keeping the angle constant, but at three different positions over the length of the sample. The aim was to investigate whether asymmetric patterns provide constant permittivity over the length of the sample, and so could be used as a replacement for symmetric patterns. Results for the permittivity and dielectric losses are shown in Figure 7.24. It can be seen that permittivity of both symmetric and asymmetric pattern have a similar profile, while the range of permittivity differs. For example, the permittivity at 10.5 GHz for the asymmetric pattern is 2.38 - 2.42, but slightly higher for the symmetric pattern 2.30 - 2.37.

The average permittivity of the symmetric sample is lower than for the asymmetric pattern, indicating that the proportion of air in the symmetric pattern is higher overall. A target average unit cell size is difficult to achieve using a manual hand drawing process.

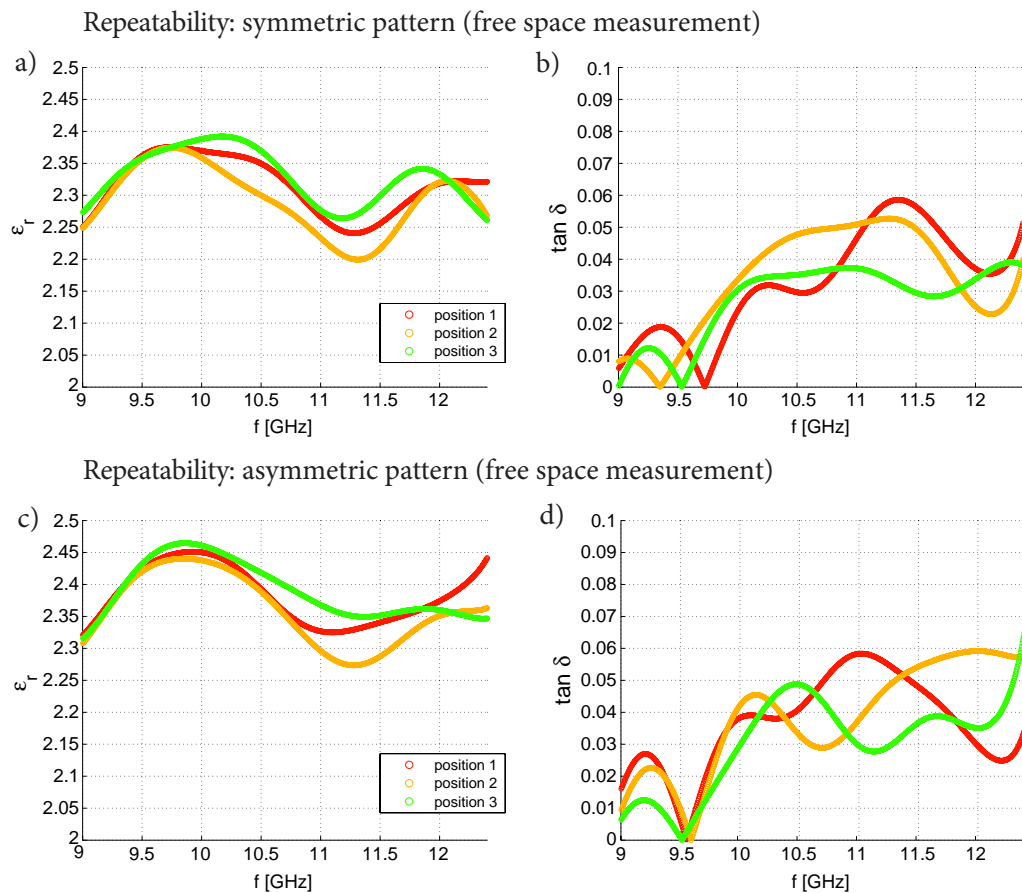


Figure 7.24: Results ‘consistency over length’ measurements at three different locations on the sample, to indicate whether the asymmetric pattern could be used as an alternative for the symmetric pattern. (a) Symmetric pattern permittivity and (b) dielectric losses. (c) Asymmetric pattern permittivity and (d) dielectric losses.

An advantage of using this technique to fabricate dielectric materials is the high permittivity and low dielectric losses, which were achieved overall. The cut out patterns achieve a lightweight and visually interesting structure, whilst the printed BaTiO<sub>3</sub> ink delivers high permittivity while maintaining low dielectric loss.

This study has briefly explored the possibility of using handdrawn and cutout patterns for dielectric materials, using screen printed commercially available BaTiO<sub>3</sub> ink. As the ink is not flexible, further tests would need to be conducted to study its usefulness for textile substrates. However, permittivities of around 2.3 were achieved for very thin, and typically low-permittivity (when uncoated), substrates, such as paper and card. Randomised patterns could be utilised in the design of anisotropic structures, as permittivity difference at various locations of the sample was similar to that of the symmetric patterns.

## 7.6 Conclusion

This chapter explored embroidery, screen printing and laser cutting for the fabrication of all-dielectric anisotropic textiles and card, with the aim of investigating their potential to be used for microwave metamaterial devices. Three studies were conducted.

### **Embroidered dielectric structures with graded permittivity:**

The first explored two-dimensional and three-dimensional embroidered and graded textiles. For the first two-dimensional textile, permittivities of 1.2-1.8 and dielectric losses of less than 0.1 were achieved. This demonstrated that replacement of the rigid structures, presented in Bao (2012), is feasible, if a number of textiles would be stacked to achieve the required height.

For a second and third embroidered sample, the structures were pleated to investigate whether this traditional textile technique could offer an alternative to stacking layers. Two structures were folded and shaped using a pleating technique with smocked pulling threads to tighten and loosen the pleats. The samples were measured in their unfolded state, using a parallel plate capacitor (1 - 5 MHz) and free space set up (9 - 12 GHz).

Permittivity ranges of 1.20 - 1.60 (free space) and 1.05 - 1.60 (parallel plate capacitor) were achieved for Sample 2, which was stitched with a line pattern in fill stitch. Sample 3 was stitched with a decorative cross pattern, and achieved permittivity of 1.2 - 1.6 (free space) and 1.05 - 1.8 (parallel plate capacitor). The resulting dielectric losses of both samples were sufficiently low at around 0.02.

Additionally, to explore possible three-dimensional forms, the samples were pleated and manipulated into different shapes, then documented as photographs.

Throughout the process of the work, the two main observed challenges of embroidered structures would need investigation:

- Folding adds a considerable amount of air to the structure, which needs to be considered when designing towards a specific permittivity.
- Embroidery added an amount of material to the substrate, and the increased thickness of the materials posed a challenge for measurement. Thickness was measured at the densest area of the sample, and was kept constant for the complete sample. Although this provided a workaround for the prototypes presented in the study, it could cause challenges when repeating the fabrication with another embroidery machine or thread, as small changes in the fabrication technique could lead to changes in the thickness.

#### **Screen printed graded textile:**

For the second study, screen printing  $\text{TiO}_2$  ink onto a textile substrate in a graded dot pattern resulted in permittivity ranging between 1.6 – 3.7. A simple unit cell model simulated in CST was used to explore if complex textiles structures could be simulated as simple effective material blocks. A reasonable match between experimental and simulated results was achieved. The study also provided a useful addition for samples presented in chapter 8, as the  $\text{TiO}_2$  (“Schmincke”) ink was a good low-cost printing material when higher permittivity of substrate textiles was required.

#### **Laser cutouts and screen printed card:**

In the third study, symmetric and asymmetric patterns were explored that would allow more flexibility for the designer in the patterning process. Two samples were laser cut, and subsequently screen printed with  $\text{BaTiO}_3$  ink. Even though some elements were

smaller and different in shape than others over the whole measured surface, the cutouts were distributed so as to achieve an even permittivity overall, even when the larger sample was shifted to a different position or angle. It was found that taking the measurements at various locations over the length of the sample resulted in similar ranges of permittivity for symmetric and asymmetric patterns. However, isotropy was not achieved with the hand drawn pattern. Overall, permittivity of at least 2.3 was achieved in X band frequencies. The binary patterns (such as card and air) have the advantage of being lightweight and simple to design, and demonstrate potential for the fabrication of cloaking materials. Separating the higher dielectric material from the simple card base material also provides low-cost and adaptable designs.

Table 7.1: Summary of techniques applied in chapter 7, stating success and challenges encountered when prototyping and analysing samples.

Technique	Advantages	Disadvantages
Embroidery	<ul style="list-style-type: none"> <li>• Fabrication of gradient in single process</li> <li>• Pleats can be easily achieved by adding small gaps into the structure</li> <li>• Scaleable as industrial equipment is standard in textile industry</li> <li>• Quick pattern adaptability as it is part of the group of CAM techniques</li> </ul>	<ul style="list-style-type: none"> <li>• Thickness increases with increasing density</li> <li>• Large industrial machine would be needed to prototype three-dimensional embroidery large enough for electromagnetic analysis.</li> </ul>
Screen printing	<ul style="list-style-type: none"> <li>• Fabrication of gradient in single process</li> <li>• High flexibility can be maintained by separating the printed shapes (dots)</li> <li>• Scaleable as industrial equipment is standard in textile industry</li> <li>• Low-cost</li> </ul>	<ul style="list-style-type: none"> <li>• Very small difference in thickness requires specialist equipment to measure thickness accurately</li> <li>• Pattern cannot be adapted easily, as screen needs new stencil and exposure for every new pattern</li> </ul>
Laser cut-outs with subsequent screen printing	<ul style="list-style-type: none"> <li>• Quick pattern adaptability as it is part of the group of CAM techniques</li> <li>• Innovative customisable technique</li> <li>• Applicable for textiles</li> </ul>	<ul style="list-style-type: none"> <li>• Two-stages process</li> <li>• Slow fabrication</li> <li>• High cost for both laser cutting and BaTiO<sub>3</sub> ink</li> </ul>

## Chapter 8

# Negative Refractive Index Textiles

### 8.1 Introduction and Objectives

To recap, in section 2.1.3, we described negative refractive index metamaterials (NIM) as engineered metallo-dielectric composites designed to bend electromagnetic waves at a ‘negative’ angle. NIMs were a significant discovery, both as a theoretical model (Veselago, 1968) and as a practical realisation (Smith, Padilla, Vier, Shelby, et al., 2000), and played a main role in the development of the field of Transformation Optics, enabling the first design of a free space invisibility cloak at microwave frequencies (Pendry et al., 2006). Previous NIMs have been realised on circuit boards and other rigid materials, and later assembled into three-dimensional matrices. Only a small number of publications discuss simulation or fabrication of metatextiles with a refractive index lower than 1 (Burgnies et al., 2015; Ghebrebrhan et al., 2014; Tao et al., 2010).

This chapter presents experiments in which the conductive properties of textiles and paper have been manipulated with the aim of constructing pleated metatextiles that exhibit a negative refractive index in the microwave region. While standard printed-circuit-board (PCB) fabrication techniques enable straightforward realisation of the small conductive structures required as rigid circuit boards, textile materials pose limitations to the size achievable, conductivity, substrate permittivity, substrate dielectric loss and thickness of prototypes. In addition, assembled three-dimensional

textiles are not permanently fixed, and irregularities and angular variations occur. As this disrupts the overall uniformity of the matrix, a lower response in the resonating frequencies is predicted.

Using Smith's unit cell design as a starting point (Smith, Vier, Koschny, et al., 2005), dimensions and material properties have been adjusted according to the characteristics of the various textile materials and fabrication techniques. A textile unit cell was developed for simulation in CST, with changes made iteratively, following knowledge gained through practical experimentation.

The fabrication techniques explored were embroidery, screen printing, laser engraving, vacuum deposition, inkjet printing, chemical etching and silver leafing. This chapter includes the outcomes of initial experiments, in which techniques designed to produce conductive traces on textiles were tested, and subsequent studies in which the most promising samples were developed further into measurable prototypes.

To summarise, the objectives of the studies presented in chapter 8 were to:

- Design a textile-based unit cell to be used for the fabrication of conductive and dielectric elements as a two-dimensional surface, which allows subsequent folding and assembling into anisotropic three-dimensional structures.
- Identify suitable manual and semi-automatic e-textile techniques to fabricate small conductive SRR structures, using a variety of textile and paper substrates.
- Analyse the electromagnetic behaviour of the prototypes fabricated for evidence of a negative refractive index, using methods appropriate to textile samples.

A complete index of samples that were fabricated for chapter 8 is included in Appendix D.

## **8.2 Textile Unit Cell**

Figure 8.1 illustrates the SRR and wire design that the studies presented in this chapter were based on (Smith, Vier, & Koschny, 2005). Smith's original unit cell was designed to achieve a negative refractive index at a frequency between 9 - 12 GHz. The

dimensions of the cell are 2.5 mm in all planes. The SRR and wire are located on opposite sides of the cell, with a substrate thickness of 0.250 mm and copper thickness of 0.017 mm. The cell has a dielectric constant of 4.4 and a loss tangent of 0.02. The width of the outer ring of the SRR is 2.20 mm, and the width of the inner ring is 1.50 mm. Both rings have a line width of 0.20 mm with a gap of 0.30 mm between them. The width of the wire is 0.14 mm. Simulations of the unit cell using CST and subsequent parameter extraction using the NRW technique confirmed Smith's results. The typical dip in the phase part of the transmitted wave ( $S_{21}$ ), indicating a reversal of the phase velocity, can be clearly seen in Figure 8.2. The structure has a negative refractive index at around 9 - 10 GHz, as shown in Figure 8.3. However due to the high loss (imaginary part of refractive index) the usable range of negative refractive index lays in a narrow band around 10 GHz. Although the resonating frequency will change for textile prototypes, the material parameters will have a similar profile, and the plot is used for comparison for results developed in this thesis.

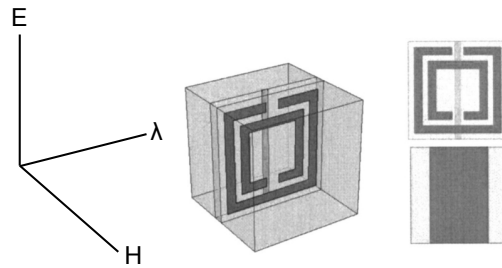


Figure 8.1: NIM unit cell as presented by Smith, Vier, & Koschny (2005). The cell has been used as starting point and guide for NIM designs presented in this chapter. The cell is designed for X band frequencies, with an overall cell dimension of 2.50 mm.

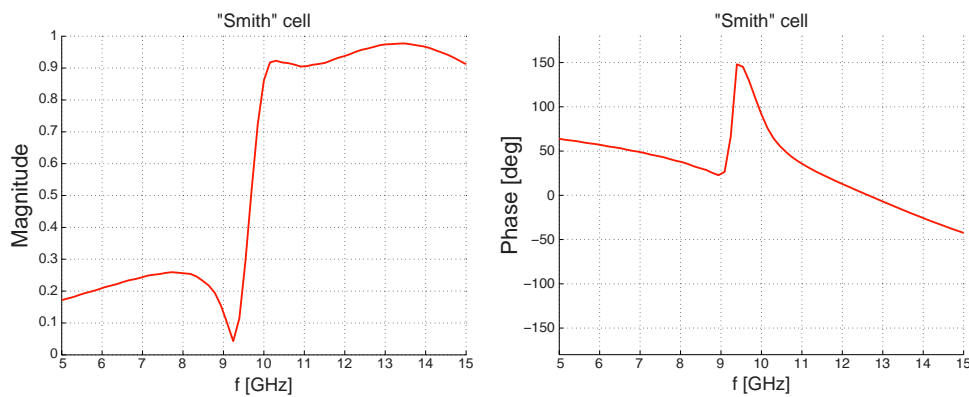


Figure 8.2: Simulations confirming  $S_{21}$  magnitude and phase of the original 'Smith cell'. Note the slope of phase in the transmitted wave, which is an indicator of the presence of a negative refractive index at that frequency band.

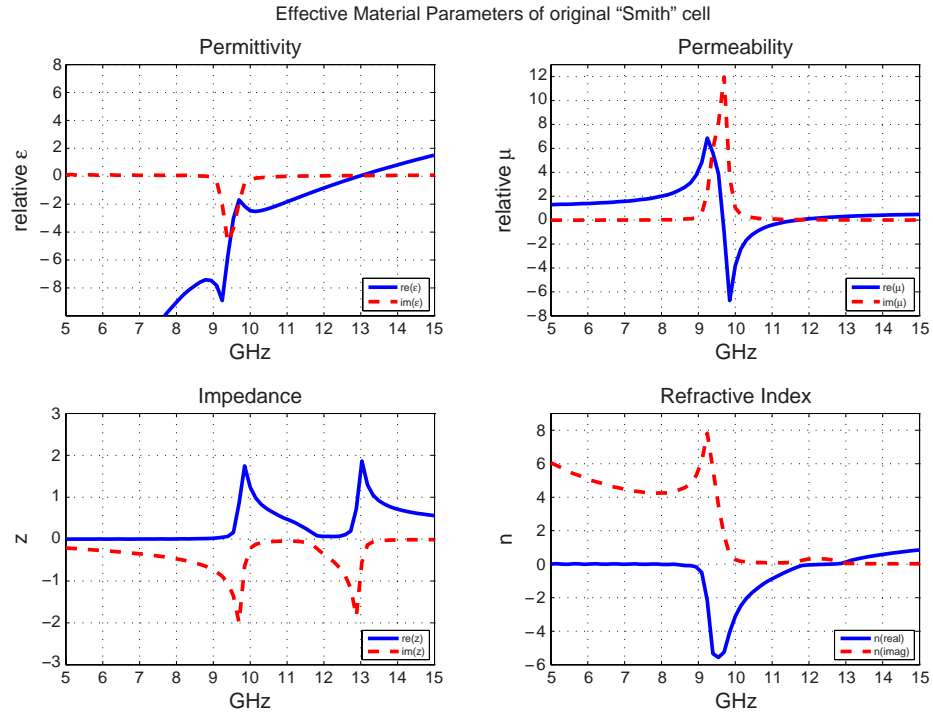


Figure 8.3: Material parameters from the original simulated ‘Smith cell’, retrieved using the NRW method. The non-physical nature of the negative imaginary permittivity is referred to in Smith's paper and is an artefact of the imprecise nature of the parameter extraction process.

Starting from the original ‘Smith cell’, a design was developed, which was inspired by textile fabrication techniques. The SRR and wire pattern were applied to a flat textile surface (Figure 8.4 (a)), and subsequently folded into a three-dimensional structure. The conductive parts were applied to one side of the textile, and dielectric ink to the other side, resulting in a higher permittivity of the substrate inside the crease between the SRR and the wire. The dimensions of the simulated cubic textile cell shown in Figure 8.4 (b) are 2.50 mm. The SRR and wire are located on opposite sides, with a substrate thickness of 0.20 mm. The substrate had a dielectric constant of 1.3 and a loss tangent of 0.01. The strip of high dielectric ink in the fold had a permittivity of 2.5. The outer ring length of the SRR was 2.20 mm and the inner ring 1.50 mm. Both rings had a line width of 0.20 mm with a gap of 1.00 mm. The width of the wire was 0.14 mm. Copper traces had a thickness of 0.05 mm and a conductance of 100,000 S/m.



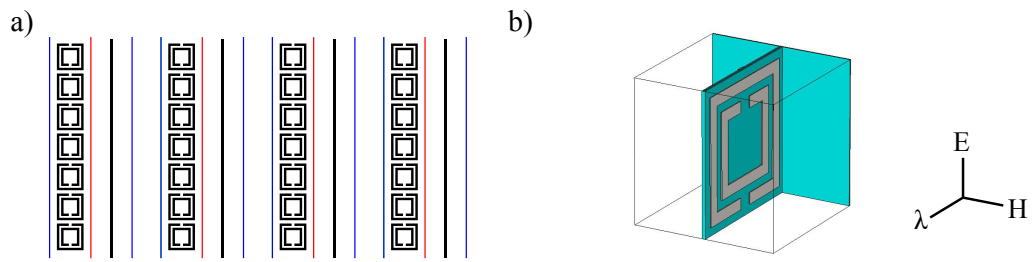


Figure 8.4: ‘Smith cell’ adapted to textile fabrication. (a) SRR, wire and high dielectric substrate are applied to a flat textile, prepared for pleating in mountain folds (red) and valley folds (blue). (b) Pleated unit cell as simulated in CST.

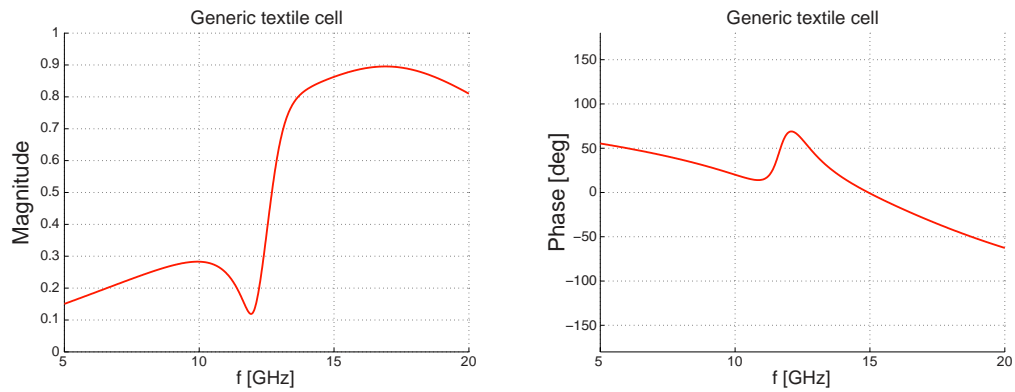


Figure 8.5: Simulations showing  $S_{21}$  magnitude (left) and phase (right) of the transmitted wave for a generic textile unit cell. Note the slope in phase, which is an indicator of the presence of a negative refractive index at that frequency band.

The cell matrix was simulated as a unit cell arrangement in CST, and material parameters retrieved using the NRW method. Figure 8.6 shows the results. Permittivity is negative below 14 GHz, and a negative permeability is reached between approximately 12 and 14.5 GHz. This leads to a usable negative refractive index band between 12 and 14.5 GHz.

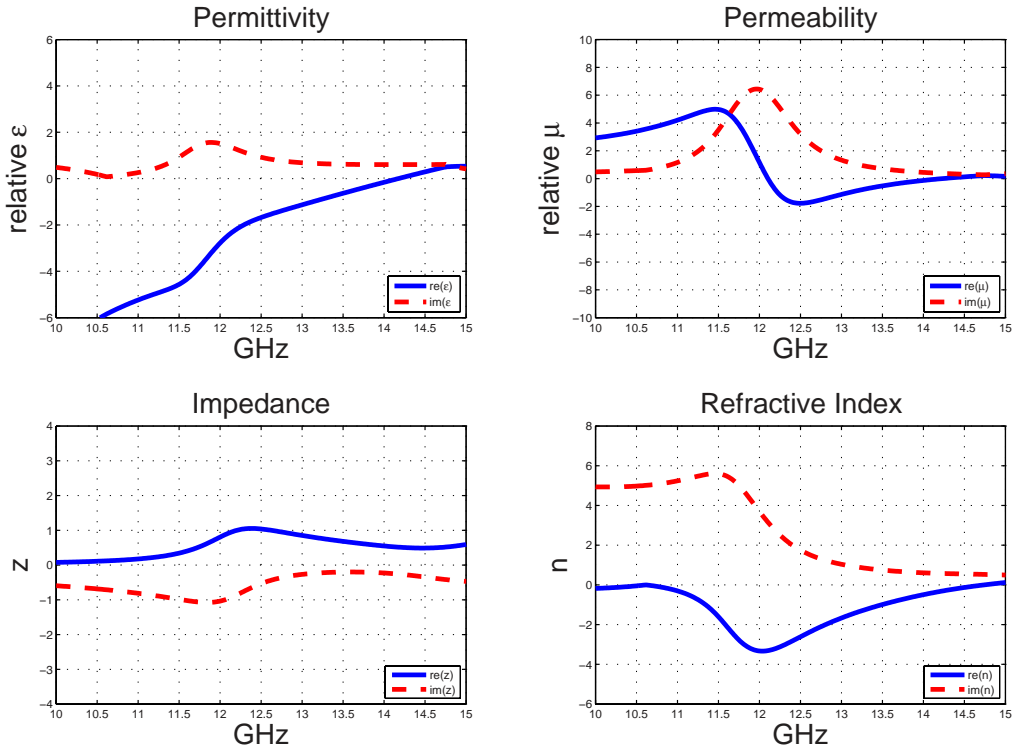


Figure 8.6: Material parameters from simulated pleated textile unit cell. Retrieval using the NRW method.

The results display a similar progression profile, compared to the results of the ‘Smith cell’ (Figure 8.3). However, it is noted that the negative phase velocity is less pronounced, resulting in a smaller negative refractive index. This is caused by a higher electrical resistance of the metal parts, which is a prevalent practical disadvantage of conductive textiles. Based on initial measurements of dielectric inks presented in chapter 6, it was also expected that  $\text{TiO}_2$ -coated textiles would have a higher dielectric loss, contributing to higher absorption of transmitted power and making them less efficient. Taking these factors into consideration, the band of negative refractive index was found between approximately 12 - 12.5 GHz.

Overall, the resonating frequency band in the textile cell was about 2 GHz lower compared to resonance band of the Smith cell, as a result of the lower permittivity and thinness of the substrate.

Throughout the following studies using various fabrication techniques, the model of the textile unit cell was adapted, taking into account the characteristics given by the respective materials and geometries used.

### **8.3 Study 1: Applying Resonator Arrays to Textile Substrates**

As outlined previously, the e-textile industry and design community use both additive and subtractive techniques to create conductive traces on textiles. Some procedures are based on PCB technologies, such as chemical etching, and are adapted to the requirements of textile materials. Others use textile-specific equipment and techniques, such as digital embroidery and weaving, and rely on the availability of new conductive textile materials.

Applying small and disconnected elements with low resistance onto textile materials still poses a significant challenge. Techniques that are effective on non-absorbent and smooth surfaces often fail when directly applied to textiles or semi-absorbent papers. Textile materials with higher conductivity on the other hand, often display lower flexibility and crack when bent; contradicting the reasons why textiles were chosen in the first place.

In this thesis, experimental practice-led exploration played an important role in the prototyping process. We therefore focused primarily on techniques that were accessible and familiar to e-textile designers, and used commercially available consumables. This had the advantage that structures were low-cost both in terms of materials and equipment. The disadvantage was the limited availability of highly conductive textile materials and application techniques, which generally resulted in a less pronounced electromagnetic resonance. However, in all cases, the production process had the potential to be scaled up to industrial production, as the automated processes and machinery required already exist in the textile industry. It can be assumed that industrial techniques would generally allow higher precision and repeatability, and therefore improve electromagnetic function.

In regards to the interdisciplinary nature of this thesis, the work was also motivated by the author's previous work in the field of e-textiles. With an emphasis on the craft-based making of conductive textiles, this thesis deals with the problem of using 'low-tech' techniques to fabricate state-of-the-art metatextiles. Consequently, some simple procedures were adopted that are commonly found in e-textile design, but unconventional in engineering disciplines, allowing rapid production of samples and iterations. With regard to fabrication, there are differences between manually and industrially produced outcomes. Whilst the former often results in individual solutions

through creative decision-making by the designer, informed by their particular experience; the latter offers the advantage of producing textiles with constant properties on a larger scale.

Problems associated with the measurement of conductivity and thickness of textiles are outlined in section 6.4.1. The processes adopted as a result were as follows:

- Electrical resistance was assessed with a handheld digital multimeter, with the two probes placed onto the two points next to the gap of the outer split ring. Whilst this technique did not take into account the bulk conductivity or sheet resistance, it was found to be sufficient for the purpose of comparison. An advantage was that measurements could be taken instantly. Complex equipment and measurement set-ups were not needed.
- Substrate thickness was measured with a handheld digital micrometer.
- Some textiles were fabricated using manual techniques, such as screen printing. Others were made with domestic machinery, such as the Brother Innov-is 1500d embroidery machine.
- The author's background and interest lies in handmade and bespoke e-textiles, with an emphasis on the making aspect. For each of the techniques presented, there exists an industrial version of fabrication, such as automated processes for screen printing, or large scale and robust machine embroidery. Hence it is possible to scale up production of the prototypes discussed in this section.

### **8.3.1 Screen Printing**

A series of fabric and paper samples were produced to investigate conductivity and form stability of small screen printed copper SRR structures. Geometry was limited by the copper particle size of the chosen ink CoPro-Cute™, which determined a screen mesh size of 55T (threads/cm) or lower. The width of the outer SRR was modified to 7 mm, and the inner SRR to 4.8 mm. The SRR array was printed with copper ink onto cotton fabric, which had already been coated, using screen printing with TiO<sub>2</sub> lino ink.

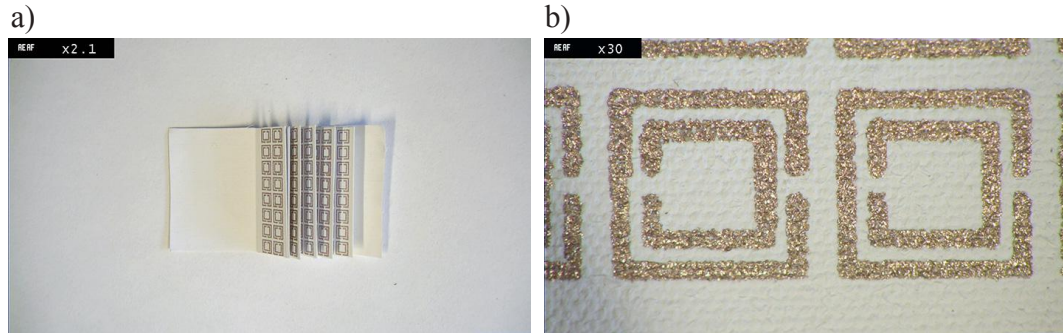


Figure 8.7: Manually screen printed SRRs on  $\text{TiO}_2$  coated cotton textile. (a) Small assembled structure (b) Detail.

The design was printed with a soft rubber blade squeegee. Two layers of conductive ink were printed in a wet-on-wet technique. The screen was washed after each print to avoid a build up of copper particles clogging up the screen over time. The sample is seen in Figure 8.7, with Figure 8.7 (a) after folding and assembling, and Figure 8.7 (b) showing a detail. Geometrically accurate printed structures were achieved, with only minor fraying of the outlines of the copper lines. Consistent printing results were obtained from repeated sets of prints. However, electrical resistance, as measured at the two furthest points of the outer SRR, was inconsistent with no less than  $70 \Omega$ , and a few SRRs being non-conductive. This occurred in areas where the ink coating was thinner, resulting in a low number of connections between copper particles. Whilst the results were inconsistent, some samples showed potential to work on refining the technique. Thus, in view of the geometrical accuracy, repeatability and conductivity achieved on the more successful samples, screen printing was chosen as a technique for further exploration through sample production and electromagnetic analysis, presented in section 8.4.2.

### 8.3.2 Vacuum Deposition

Having successfully applied copper to textiles with a thickness sufficient to produce conductive surfaces using vacuum deposition in previous tests (section 6.3.3), this test focused on finding a low-cost mask option to produce the SRR and wire design. Four waterproof or water-repellent fabrics were sampled, and electric resistances assessed with a multimeter.

The unit cell size was identical to the one used previously for screen printing, with dimensions of 7.12 mm for the outer SRR, and 4.86 mm for the inner SRR, with a gap size of 1.00 mm.

A negative image of the design was screen printed with liquid latex onto the substrates, to mask the areas that were required to be non-conductive. The screen mesh size was 55T, and the image was printed once and air-dried. The samples were then placed into the vacuum bell and deposited with a copper layer of 500 nm thickness, at a deposition rate of 1.2 nm/s. As shown in Figure 8.8 (a), the copper was distributed over the complete sample, covering both the mask and open fabric. In the next step, the latex mask was carefully removed (Figure 8.8 (b) and (c)). Of the four samples, two masks were successfully removed. On microfiber and polycotton chintz (Figure 8.9 (a) - (d)), the latex was absorbed into the surface, leading to a non-removable bond. On the polyester and the nylon fabric, the mask was removable and left accurate SRR geometries (Figure 8.9 (e) - (h)). The measured resistance for the polyester sample was high overall at 1 M $\Omega$  for the outer SRR. The copper traces on nylon fabric exhibited low resistance, similar to that of pure copper. However, due to the thinness of the coating and the thread topology, a consistent connection was not achieved.

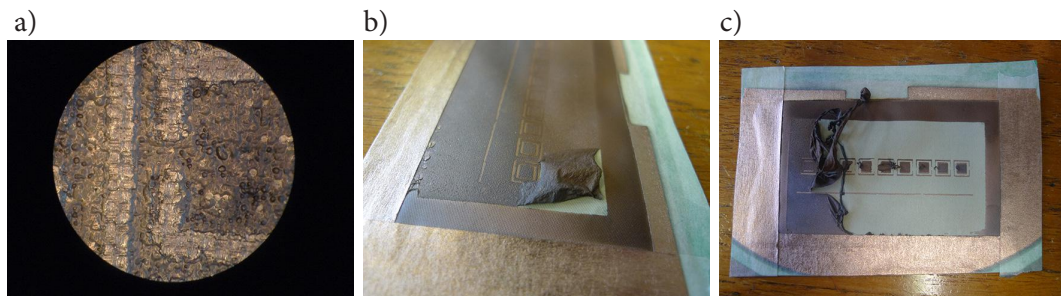


Figure 8.8: Steps of vacuum deposition process. (a) Copper laid onto both mask and textile surface after deposition. (b) and (c) Careful removal of latex mask.

It was concluded that vacuum deposition on textiles was impractical due to the absorption of nano-sized copper particles into the porous textile surface, resulting in fewer connections between particles. Higher conductivity could be achieved by coating with a thicker layer of copper, as was done in the initial tests shown in section 6.3.3. However, as exposure time increased, the copper particles would leak below the mask and resulting in diffuse SRR images.

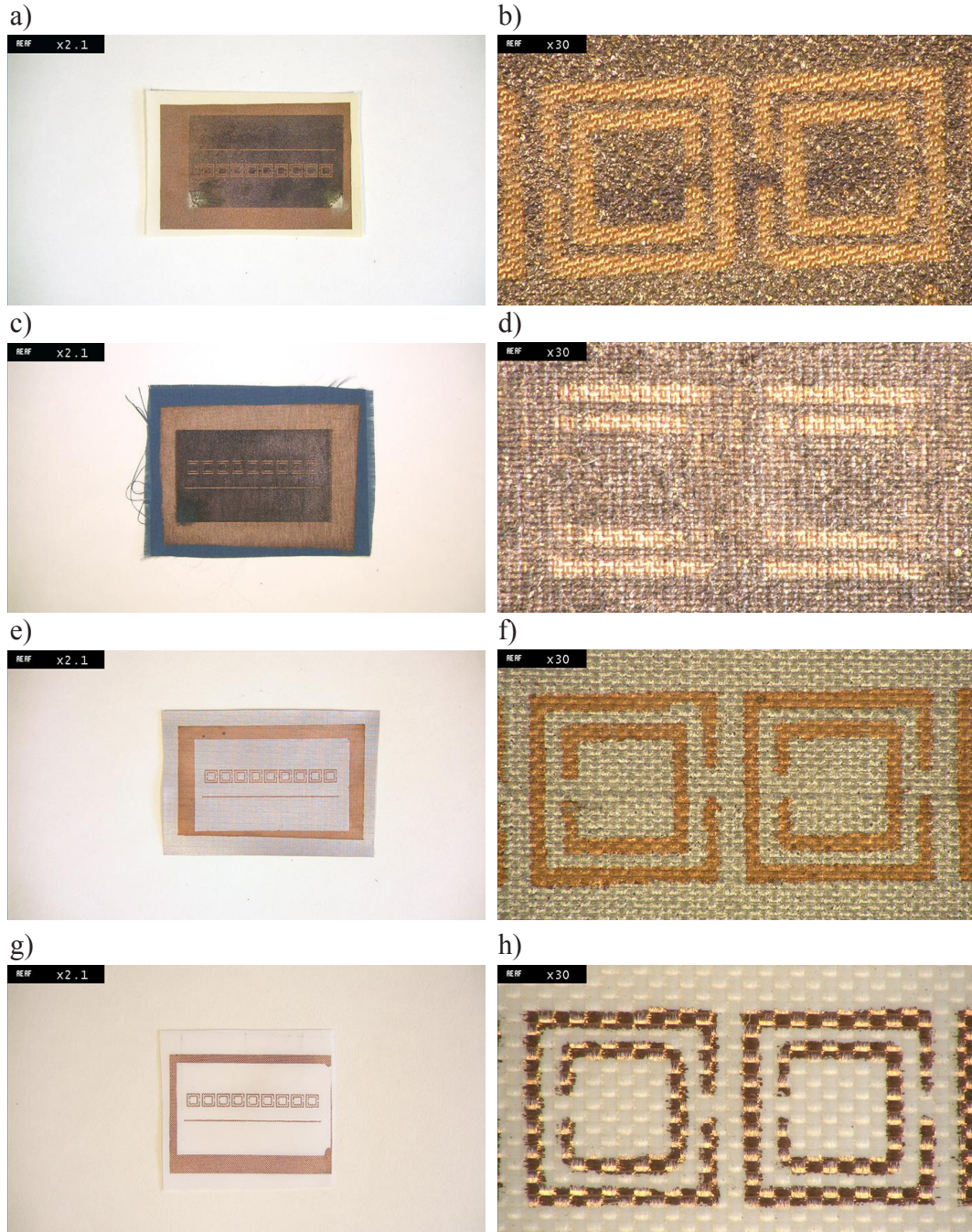


Figure 8.9: Four samples produced on waterproof or water-repellent fabrics using a latex mask, which varied in their geometric accuracy. (a)-(b) Microfibre: mask bonded with substrate and was non-removable (c)-(d) Polycotton Chintz: mask bonded with substrate and was non-removable (e)-(f) 100% Polyester: Mask was easily removable and SRR geometry was accurate. Resistance for outer SRR: 1 M $\Omega$  (g)-(h) 100% Nylon: Mask was easily removable and SRR geometry was accurate. Resistance for outer SRR: similar to copper but inconsistent with broken traces.

### 8.3.3 Ink-jet Printed Silver Ink with Nanoparticles

Silver nanoparticle ink was printed onto cotton substrate, using a piezoelectric inkjet Printer (Dimatix Materials Printer). Substrates were previously screen printed with TiO<sub>2</sub> ink. The silver ink was passed through a 0.45 µm filter into a 10 pl cartridge and printed according to recommendations of the ink supplier. The printed sample is shown in Figure 8.10. The print was subsequently sintered at 150° for 60 seconds with a hot air gun.

No conductive connections were achieved, concluding that this printing method is not yet reliable enough and lacks a standardisation technique for producing conductive traces on semi-absorbent or absorbent substrates. Furthermore, low-cost products that smooth the surface of a textile to prepare for inkjet printing with nano-particle ink are not yet available for inkjet printers. Unlike the vacuum deposition technique, where the thickness of the conductive layer could be increased, this was not possible for ink-jet printing, as multi-pass printing led to blurring of the printed image.

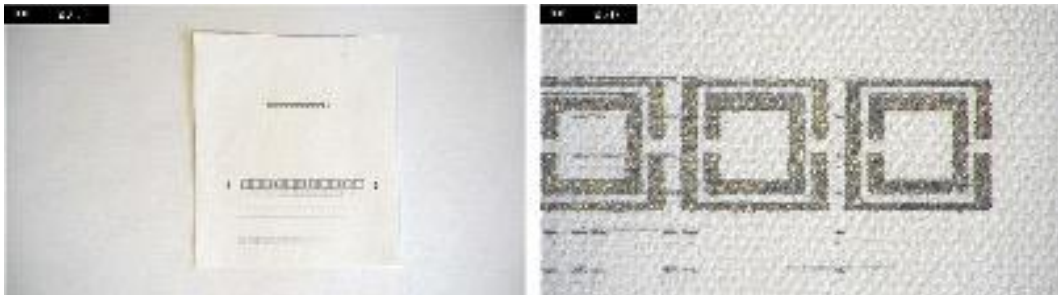


Figure 8.10: Inkjet printed silver ink onto TiO<sub>2</sub>-coated cotton. Although care was taken to achieve a smooth and non-absorbent substrate surface, no conductive traces were achieved.

In view of simpler and low-cost inkjet technologies recently becoming available to designers, we used a conventional inkjet printer (section 6.3.4) to test if the structures could be printed onto waterproof textiles. To feed the fabric through the printer rolls, it was loosely fixed onto a sheet of paper to stabilise it. Although the print looked promising (see Figure 8.11), the fabric absorbed the silver particles and the print was not measurably conductive. In comparison, the silver ink printed on Polyester film achieved lower resistances of about 5Ω for an SRR of 3.8 mm width, demonstrating the advantage of films (see Appendix D.1 for sample photo), but moving us away from the processing advantages of textiles.



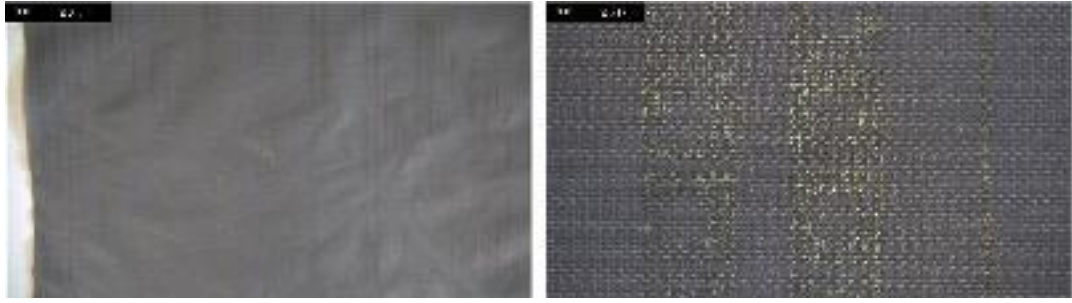


Figure 8.11: Sample of waterproof fabric inkjet printed with nano-particle silver ink.

### 8.3.4 Chemical Etching

After initial tests ruled out the possibility of producing small conductive structures on conductive fabrics with manual screen printing and direct chemical etching (see Appendix D), in this experiment non-absorbent copper tape was bonded to the fabric substrate before the etching process. Two small and one large sample were produced. For the first and second samples, a strip of copper tape was bonded with iron-on fabric onto porous cotton fabrics. A mask was applied by screen printing petroleum jelly onto the tape. Then, the samples were etched for ten minutes in a bath of one part Ferric Chloride and four parts of water, and carefully rinsed afterwards.

Details of the textile can be seen in Figure 8.12, showing clearly etched designs. While some SRRs were eroded by the etchant, overall the geometries were precise. Conductivity of the copper was equal to conductivity of the copper tape. One disadvantage of the technique was the residue of the iron-on fabric, with which the copper tape and fabric were bonded, leaving an adhesive layer on the fabric in the places where the copper had been etched.

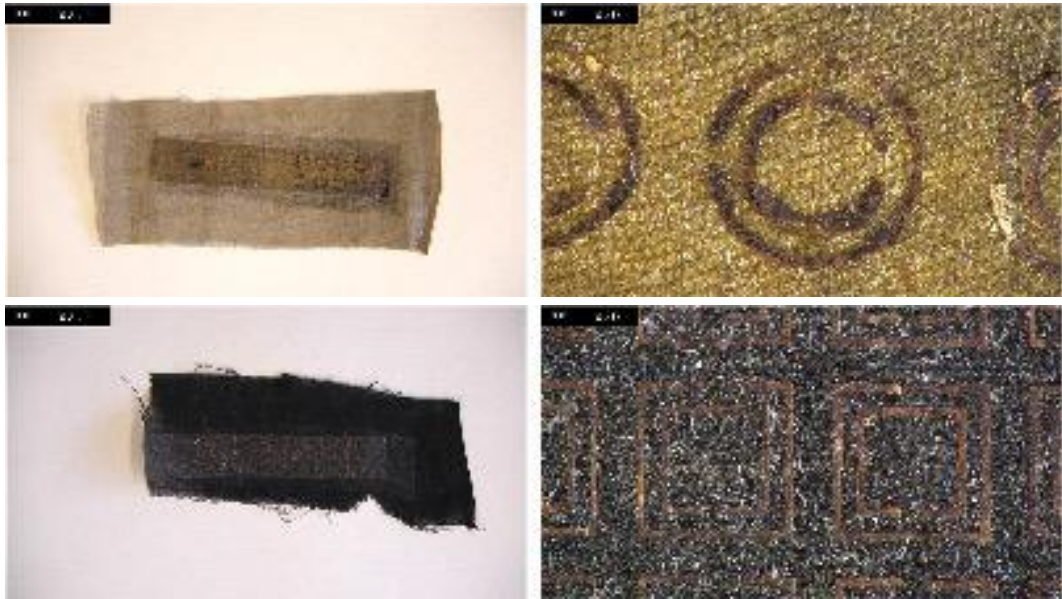


Figure 8.12: Copper tape bonded onto cotton fabrics. Complete samples (left), details (right). Mask applied with screen printed petroleum jelly. Chemical etching results in clear geometries and high conductance, but bonding fabric results in adhesive residue.

To test the impact of etchant and adhesive on a larger surface, another sample was fabricated with overall dimensions of 200 x 300 mm, as shown in Figure 8.13. It was more difficult to achieve an evenly etched image at this scale, and some parts of the design were etched off. It was also found that the adhesive residue made further processing of the fabric (e.g. pleating) impractical.

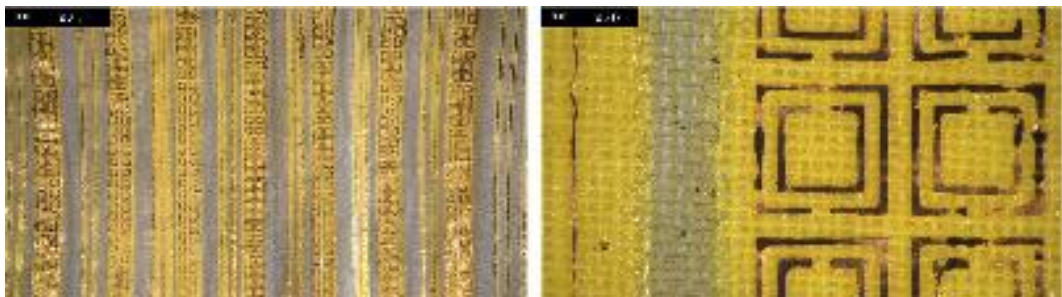


Figure 8.13: Testing chemical etching on a larger sample resulted in uneven design. Adhesive residues hindered pleating. Large sample (left), detail (right).

In summary, as seen with other techniques, manual chemical etching of fabrics was successful for small samples, for which the process was quick, controllable and repeatable. Conductivity on these samples was comparable to the conductivity of copper, but there were problems with quality, due to the adhesive residue, which presented minor issues. However, when scaling samples up to larger size, the results

were inconsistent making chemical etching impractical for the production of measurable samples of materials with a negative refractive index in microwave frequencies.

### **8.3.5 Laser Engraving**

Laser engraving was used to engrave the surface of a silver-coated cotton knitted fabric (section 6.3.7). A careful adjustment of the laser power (1.3%), speed (8.3%) and laser pulse resolution (300 ppi) resulted in the silver layer being burnt, whilst the base cotton layer was maintained. Although the laser offered a high resolution of up to 1000 ppi, the size of the unit cell was restricted by the thread count and surface of the fabric. Through experimentation, it was found that dimensions used previously for the unit cell were achievable. The outer SRR was 7.12 mm, and the inner SRR was 4.86 mm, with a gap size of 1 mm. The wire was 0.73 mm wide.

When successful, this method delivered a sharp image with highly accurate boundaries and low resistance of about  $11\Omega$  for the outer SRR. However, the success of the results varied for different sample sizes, as well as throughout the production of a series of samples. Whilst the first two samples resulted in a conductive structure with accurate boundaries to the non-conductive part of the structure (the ‘burnt’ part, see Figure 8.14 (a) and (b)), these results were only partially repeatable. Firstly, this can be explained by the lack of flatness of the fabric, resulting in a less coherent result for larger samples. Secondly, the point where the laser meets the textile is important, as it will have a higher impact on ‘thread up’ parts than on ‘thread down’ parts. A further disadvantage was that the lasering process was long, as a slow speed of the laser was needed to achieve accurate and conductive geometries. Aesthetically, these samples were interesting, as they presented a unique process for producing e-textiles that avoided the typical ‘metallic’ appearance of conductive textiles.

When applying the correct laser settings, the SRR and wire arrays on the small samples were geometrically precise and had a high conductivity. Encouraged by this result and the unique visual characteristics, this technique was chosen for further investigation as presented in section 8.4.3.

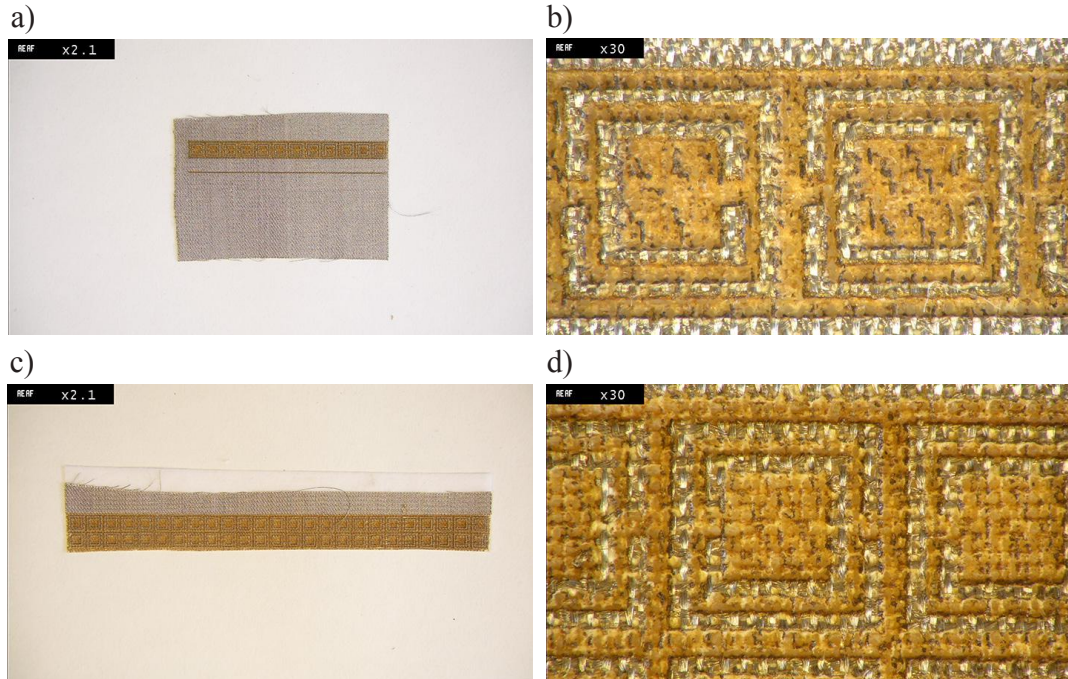


Figure 8.14: Two small samples of laser engraved silver cotton fabric. (a) First sample and (b) detail. (c) Two rows of SRRs and (d) detail.

### 8.3.6 Digital Embroidery

A series of samples were stitched using a digital embroidery machine, the Brother Innov-is 1500d, in order to gain knowledge about the practicability and challenges of various stitches, when using conductive thread. From studies conducted prior to this thesis, it is also known that various machines require different workflows when working with conductive threads, and the sampling process also enabled familiarisation with this particular machine. It was found that conductive thread could only be applied as bobbin thread (section 6.2.6). As the bobbin thread is usually only a support thread hidden on the back of the fabric and is not meant to be seen, the default higher thread tension had to be lowered to -2 accordingly, to maintain geometrical accuracy. Figure 8.15 shows an extract of the sampling process, with further samples included in Appendix D. Two types of conductive threads were used successfully in this thesis as shown in Figure 8.15 (c) - (f). The measured resistance of the outer SRR using Liberator® thread (Figure 8.15 (c) - (d)) was below  $1\Omega$ , and  $45\Omega$  for the Statex thread (Figure 8.15 (e) - (f)). The substrates had no impact on success of geometry and electrical resistance of the embroidery, making it a versatile technique adaptable to many design scenarios. It was found that a compromise had to be made between conductivity and the feel of the thread. The softer and more ‘sewing thread-like’ a

thread felt, the less conductive it was. The more conductive it was, the stiffer and more wire-like the thread was.

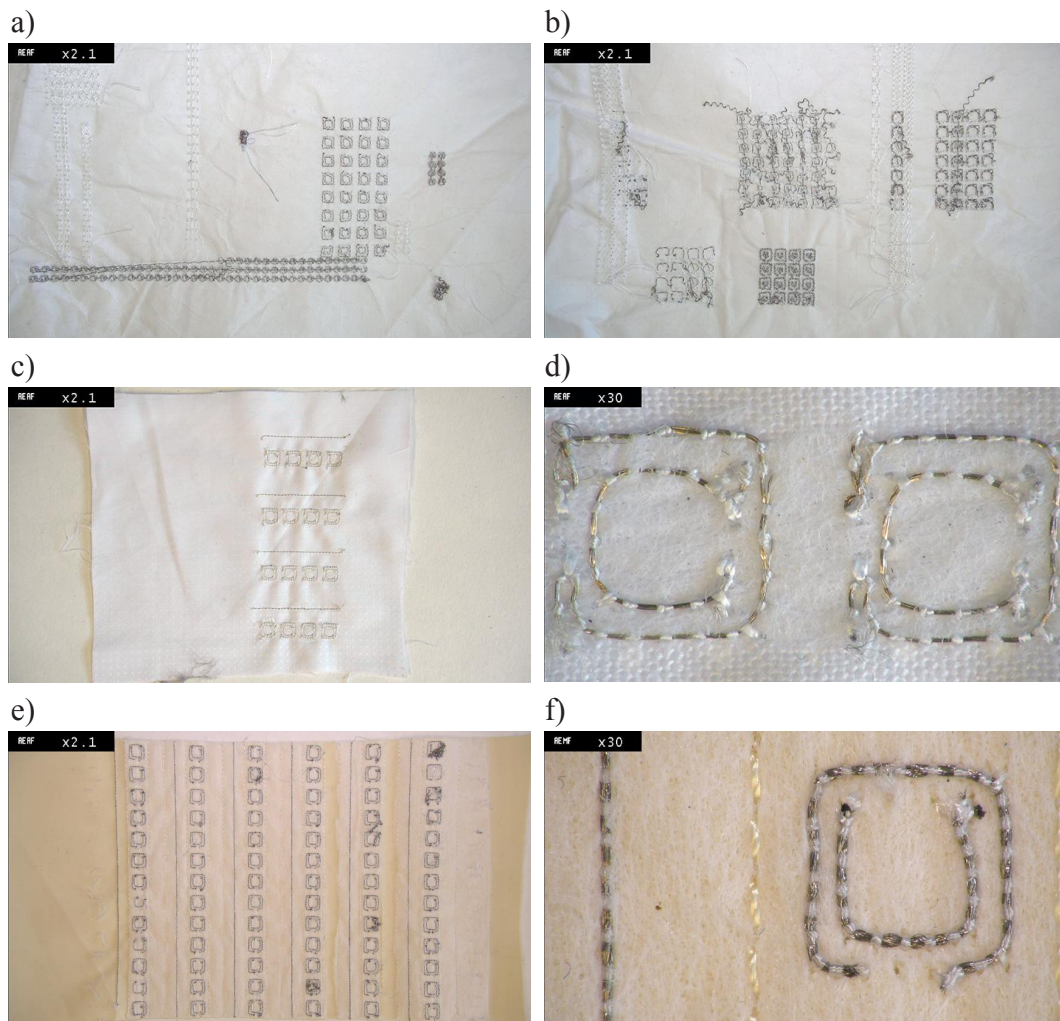
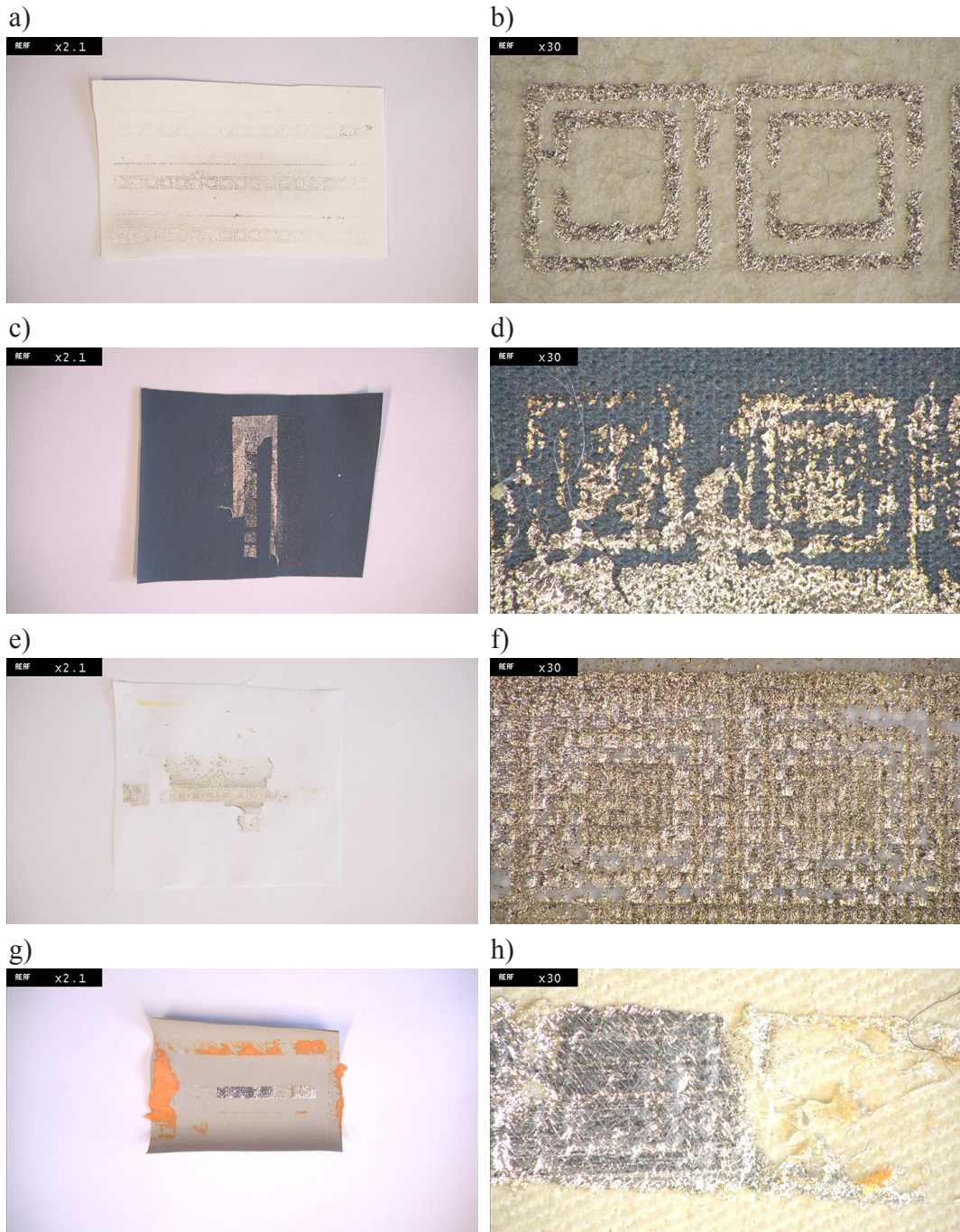


Figure 8.15: Examples of embroidered SRR and wire designs. (a)-(b) Form finding process and testing of dimensions achievable with the embroidery machine. (c)-(d) Liberator thread, using lower top thread tension (e)-(f) Statex thread, which delivered more accurate corners, however the gap size was difficult to maintain evenly.

### 8.3.7 Silver Leafing

The SRR and wire geometry was screen printed with water-based adhesive onto one paper and four water-repellent and water-resistant textiles. Unit cell dimensions were the same as for the previous screen printed structure (section 8.3.1). After air-drying, the print remained adhesive. A silver leaf was then carefully deposited using a paintbrush, and the excess silver brushed off. Of the five samples, only the paper (Figure 8.16 (a) – (b)) adopted a clear geometry with low resistance of about  $10 \Omega$  for

the outer SRR. It was not possible to fully remove the silver leaf from three textiles (Figure 8.16 (c) – (h)). Although the technique was partially successful on the fourth fabric (Figure 8.16 (i) – (j)), the process was inconsistent resulting in only a few SRRs being geometrically accurate and conductive. It was concluded that the silver leaf was too thin to provide consistent conductivity and the technique was impractical for the production of measurable samples.



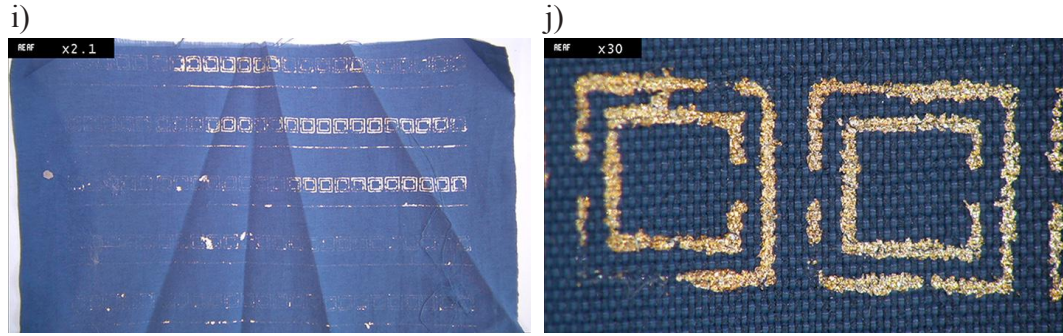


Figure 8.16: Samples of silver leafing (a)-(b) Hahnemühle filter paper (c)-(d) Polycotton Chintz fabric (e)-(f) Polyester (g)-(h) Polyester microfiber (i)-(j) Polycotton

### 8.3.8 Summary

This section presented the results of initial material exploration with the aim of identifying suitable substrate materials and techniques to produce small conductive SRR arrays. Processes were mostly manual or semi-automatic, based on the premise of this thesis to use techniques, which are low-cost and accessible to designers. Of the six techniques studied, three were selected for further investigations, namely screen printing, digital embroidery and laser engraving. Whilst manual screen printing is a long-established manual technique in textile design, it also has the advantage that it can easily be scaled towards industrial production, both in terms of machinery available and the dimensions of printed textiles. Laser engraving, as used in this study, constitutes an experimental method. Results may be less repeatable and less predictable. However, due to the uniqueness of the appearance and promising results on a small scale, this will be further explored in the next study. Digital embroidery was the most promising technique in regards to functionality. It is expected that scaling up with industrial fabrication processes would be possible, using commercial threads with constant and reliable conductivity. Although embroidery is typically a process using a continuous thread, it was possible to separate the SRR shapes manually. Depending on the thread cutting mechanism, fully industrial embroidery machines would be able to cut threads automatically without distorting the image or damaging the machine.

## **8.4 Study 2: Pleated Prototypes to Study Single-layer Transmission Behaviour**

Based on conductivity results and experience in fabrication gained in the first study, in this second study, a series of fully assembled single layer SRR and wire arrays were prototyped using screen print, embroidery and laser engraving. The samples were then measured in the free space set up, and the frequency versus transmission magnitude and phase results compared to simulated structures.

Whilst it was possible to calculate material parameters from the simulated s-parameters using the NRW technique, the experimentally retrieved data presented challenges that resulted in ambiguous material parameters. This was caused by the imprecision of the textile structure, including varying thickness and position within the measurement set up. In addition, results from the NRW technique require mathematical adjustment when used for NIMs (Chen et al., 2004). High accuracy in retrieved s-parameters is also a requirement. As this precision is not possible when working with textile materials, our analysis in this study focuses on detection of the ‘dip’ in the transmitted phase, which is typical for the frequency range in which a negative refractive index occurs. Based on the generic textile unit cell used in these studies, the simulated geometry was adjusted to textile materials and fabrication technique. We then applied approximations in both geometry and material properties to represent the configuration of the textile unit cell.

### **8.4.1 Milled FR-4 Circuit Boards for Comparative Analysis**

For comparison of results of textile prototypes, a traditional PCB array was simulated and measured. The unit cell, modelled in CST, is shown in Figure 8.17. A milled circuit board prototype was fabricated in-house on a LPKF S103 PCB milling machine for the purpose of comparison. The 1.6 mm thick FR-4 board had a permittivity of 4.4, and dielectric loss tangent of 0.01. The unit cell size was 4.885 mm in E-field and H-field direction, and 7.885 mm in the direction of propagation. The outer SRR was 4.290 mm, and the inner SRR was 2.925 mm, with a gap size of 0.445 mm. The gap between the two SRRs was 0.292 mm. The wire was 0.30 mm wide. A matrix was assembled from strips that totalled 28 cells in the E-field direction, and 20 cells in the H-field direction (see Figure 8.18). The results were accurate, however small variations in the geometry occurred due to the forceful impact of the milling head.



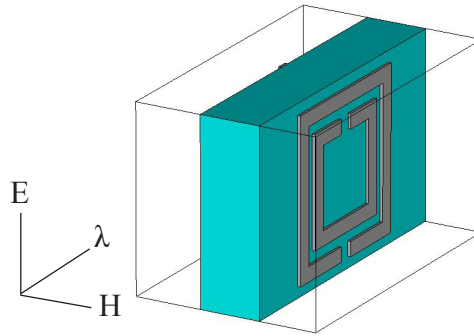


Figure 8.17: Study 2: Unit cell for PCB milling

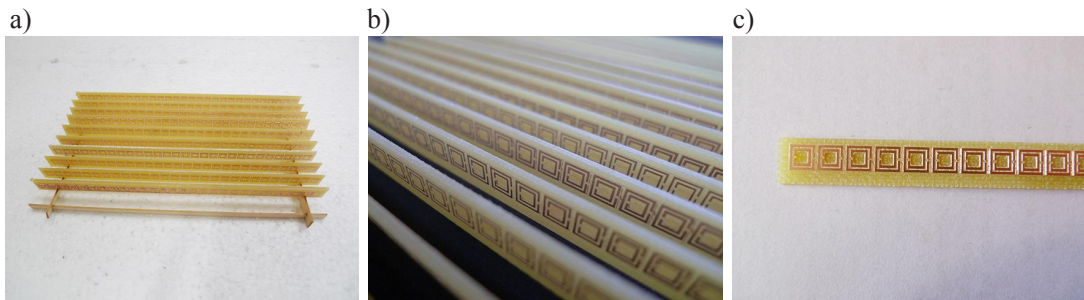


Figure 8.18: Milled geometry on strips of FR-4 (a) PCB strips on notched cardboard (b) Assembly detail (c) PCB strip detail.

The prototype was measured in the free space set up in the frequency range of 2-20 GHz. Figure 8.19 shows transmitted ( $S_{21}$ ) magnitude in dB (a), and phase in degrees (b) of both simulation (red) and measurement (blue). Both simulated and measured structure showed a strong resonance. This was expected, considering the high conductivity and geometric accuracy of the individual circuit elements, and the consistent permittivity and low losses of the dielectric FR-4 board.

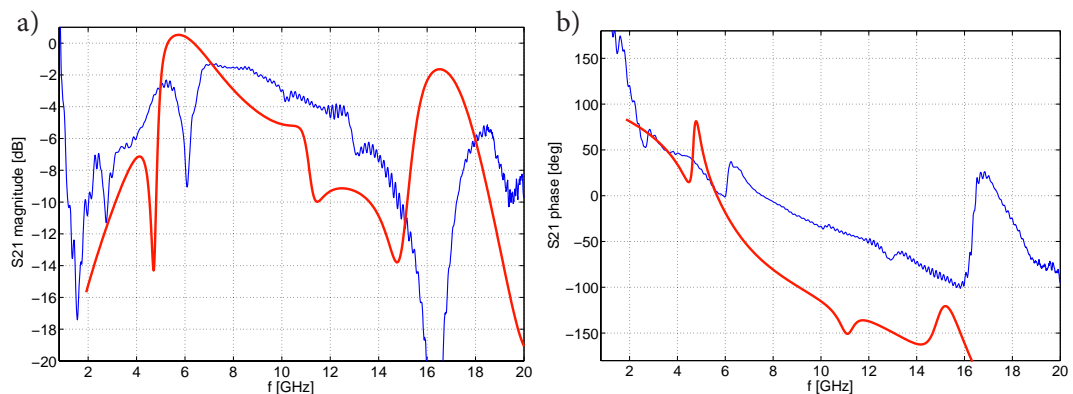


Figure 8.19: (a)  $S_{21}$  magnitude and (b)  $S_{21}$  phase of the simulated cell (red line) and measured sample (blue line) for a milled circuit board.

The dip in phase of  $S_{21}$  at 6.3 GHz of the measured structure indicates a reversed phase velocity, and hence a small negative refractive index over a narrow bandwidth. The resonating frequency band of the simulated structure is about 1.5 GHz lower than the one of the sample, which may be the result of imprecision in the periodic arrangement. Also simulation is periodic in both horizontal and vertical direction, while measurement is only periodic in horizontal direction. It can be assumed that, as a result of the larger thickness and high permittivity of the substrate, this and other small inconsistencies in the array of strips have an impact on the resonating frequency band: whilst for textile structures, in which the substrate has the characteristics close to that of air, the impact is less important.

#### **8.4.2 Screen Printed and Pleated Paper and Fabric**

Three screen printed samples were fabricated, of which two used paper and one used fabric as substrates. For comparison, the textile unit cell model was adapted to the dimensions possible with screen printing and the used materials, which were found through the practical sampling process.

The screen printed SRR and wire geometry was limited by the copper particle size of the chosen ink and the mesh size of the screen. Accordingly, the modelled unit cell size was modified to 7.33 mm in E-field direction, 6.3 mm in H-field direction, and 11.83 mm in the direction of the propagation. The outer SRR was 6.47 mm, and the inner SRR was 4.41 mm, with a gap size of 1 mm. The wire was 0.64 mm wide. All copper traces were modelled with 0.05 mm thickness. The model of the unit cell is shown in Figure 8.20.

The base substrates for the prototypes were technical filter paper, card (section 6.2.3) and polycotton (section 6.2.1).  $\text{TiO}_2$  lino ink was printed first using a screen mesh size of 43T. Copper ink was then printed in one stroke using a soft blade squeegee and a screen with a mesh of 55T. The samples were then folded and the pleats fixed with iron-on fabric. All samples are shown in Figure 8.21, with a perspective view of the white card sample shown in Figure 8.22.

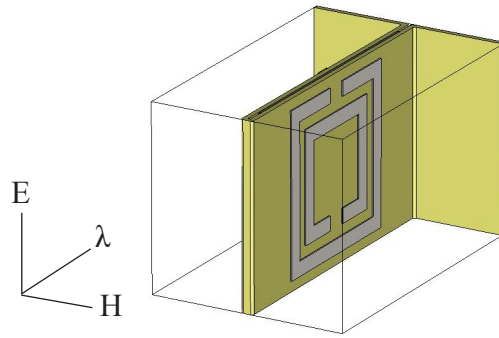


Figure 8.20: Unit cell for screen print.

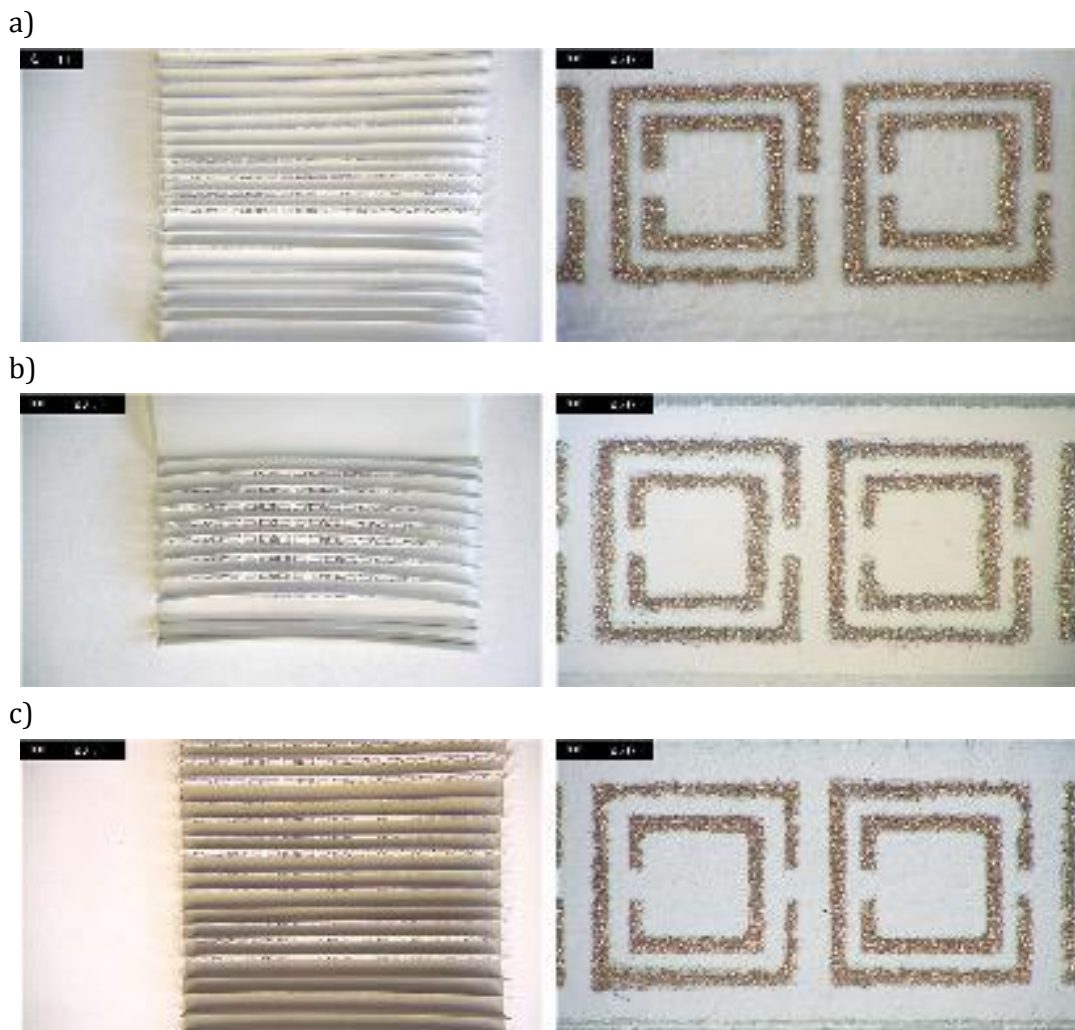


Figure 8.21: Three prototypes of screen printed papers and fabric, assembled in three-dimensional architectures. (a) Technical filter paper (b) White card (c) Polycotton.

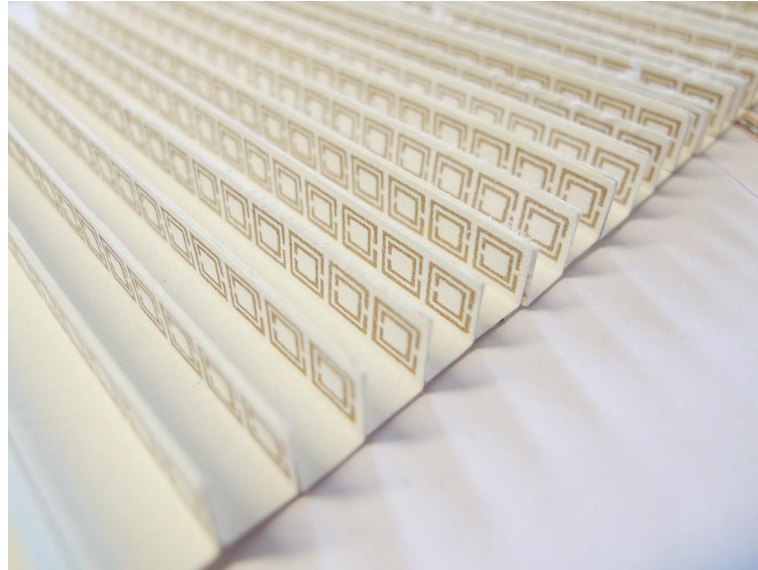


Figure 8.22: Assembled sample of screen printed white card

All samples were measured in the free space set up, in the frequency range of 3 - 12 GHz. The results, as shown in Figure 8.23, differed significantly from the simulated results. Transmission results indicate low resonance, which was attributed to low conductivity of the circuit elements resulting from thin and uneven ink application. A small dip is seen in the phase data for the polycotton and white card samples at around 4 GHz, however it is not explicit enough to indicate a negative refractive index.

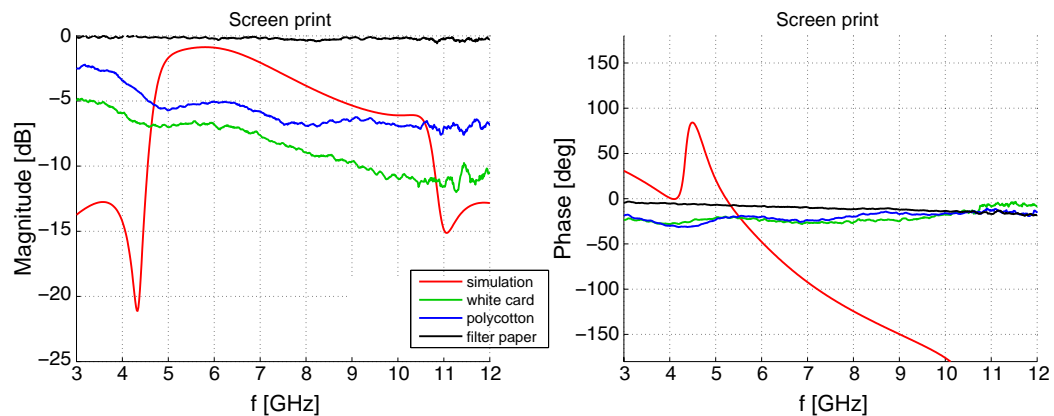


Figure 8.23: Magnitude and phase of S21 for screen printed samples, simulation (red) and measurements of the white card (green line), polycotton (blue line) and filter paper (black line).

It was concluded that the disadvantages of screen printing three-dimensional negative refractive index metatextiles were significant. Firstly, electrical resistance measurements confirmed that conductivity was low. Secondly, screen printing of

copper ink in a manual process was inconsistent, due to the ink drying quickly when printed on larger areas.

It should be noted that these disadvantages were the result of using the technique in a manual set up. Whilst screen printing is successfully used in industrial set ups to construct highly conductive traces on textiles (such as by the company ‘fabinks’), the lack of affordable water-based copper inks on the commercial market makes it difficult for e-textile designers to use the technique. As this thesis is concerned with exploring techniques that are accessible and low in cost, screen printing was not pursued further.

### 8.4.3 Laser Engraved and Pleated Cotton

A laser cutter was used to engrave the surface of a silver-coated cotton knitted fabric (section 8.3.5). The modelled textile unit cell size was modified to 7.33 mm in E-field direction, 6.3 mm in H-field direction, and 11.83 mm in the direction of the propagation. The outer SRR was 6.47 mm, and the inner SRR was 4.41 mm, with a gap size of 1.00 mm. The wire was 0.64 mm wide. All copper traces were again modelled with 0.05 mm thickness. The model is shown in Figure 8.24.

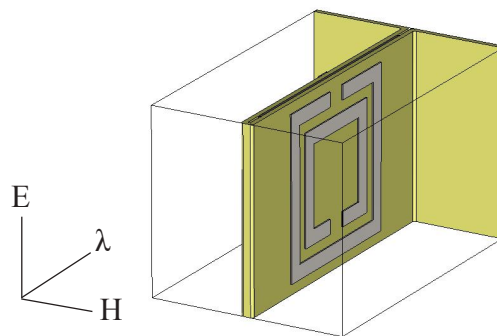


Figure 8.24: Unit cell for laser engraving.



Figure 8.25: Laser-engraved silver cotton. Assembled prototype (left), detail (right).

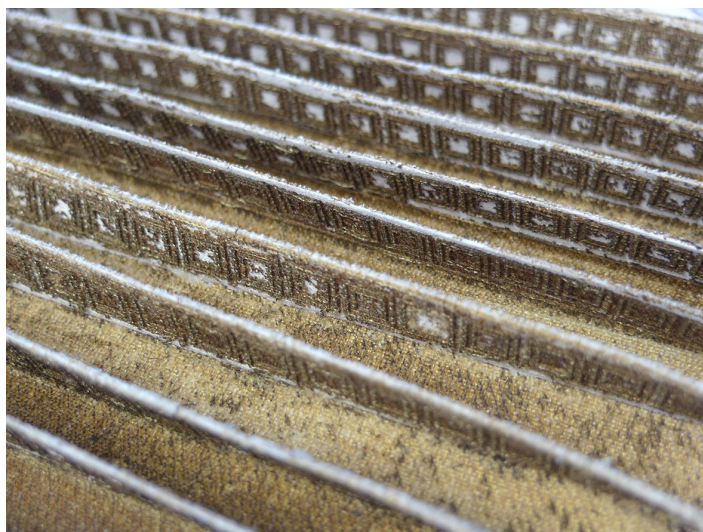


Figure 8.26: Perspective view of assembled and pleated sample of laser engraved silver cotton.

To fabricate the sample, the pattern was first laser engraved onto the fabric. As can be seen in Figure 8.25, the engraved surface was less uniform than what was achieved in the previous study on small samples. However, the resistance measured and geometrical accuracy were consistent across the complete surface. Strips of  $\text{TiO}_2$  lino ink were subsequently printed onto a fine cotton mesh and laminated onto the back of the areas of the engraved sample. Then, the textile was folded and fixed with iron-on fabric. This technique resulted in a distinct, crafted appearance less common for technical textiles. However, it was observed that for larger samples it was difficult to achieve an evenly burnt layer, resulting in metallic residues around the circuit elements.

The sample was then measured in the free space anechoic chamber in the frequency band of 8 - 12 GHz. The measurements of the laser engraved sample differed significantly from the simulated results, as seen in Figure 8.27. Transmission results indicated a small resonance and dip in the phase. It was concluded that although promising on a small-scale, the technique was unreliable for larger surfaces.

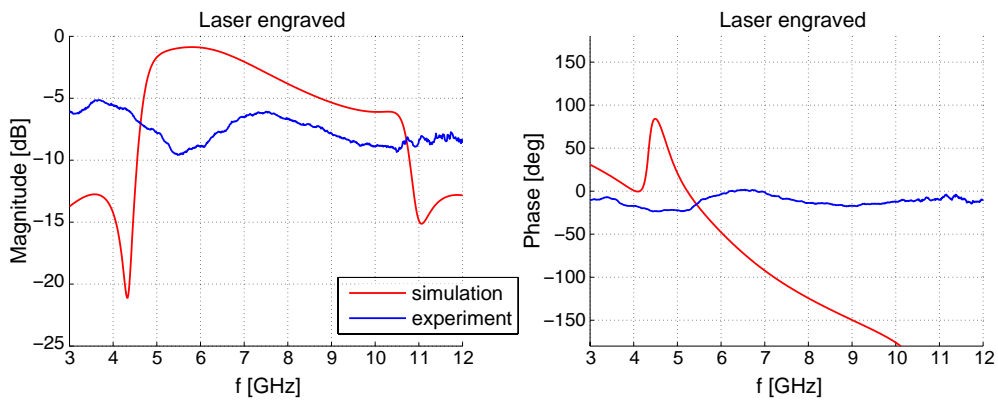


Figure 8.27: Magnitude and phase of  $S_{21}$  for laser-engraved sample, simulation (red) and measurements (blue).

#### 8.4.4 Embroidered and Pleated Cotton

One embroidered prototype was fabricated and analysed. The conductive geometry for the embroidered design was restricted by thread thickness and tension caused by the stitching process. In the model, the copper traces were replaced by cylinders resembling threads of 0.16 mm thickness, which were sunk into the polycotton substrate by 0.04 mm to resemble an embroidered thread. The design was scaled to a cubic unit cell size of 9 mm. The outer SRR was 6.72 mm, and the inner SRR was 4.72 mm. The gap in both rings was 1.00 mm wide. The wire was replaced by one line of thread with the thickness of 0.16 mm. The 0.20 mm thick substrate was modelled with a permittivity of 1.3 and dielectric loss tangent of 0.01. The higher dielectric in the fold had a thickness of 0.20 mm, permittivity of 2.5 and a dielectric loss tangent of 0.1. The unit cell is shown in Figure 8.28.

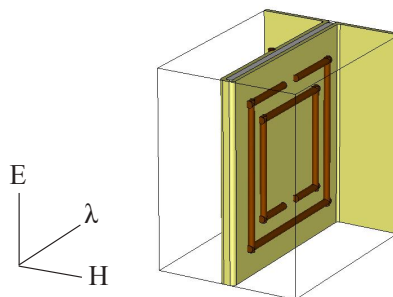


Figure 8.28: Embroidery unit cell as modeled in CST.

Two small structures were embroidered on the Innov-is embroidery machine, using Statex thread 234/34 4-ply as bobbin thread, and Rayon as a top thread. The stitch

length was 1 mm. The samples were embroidered onto two different substrates; a soft cotton structure and a medium weight polycotton structure, both shown in Figure 8.29.

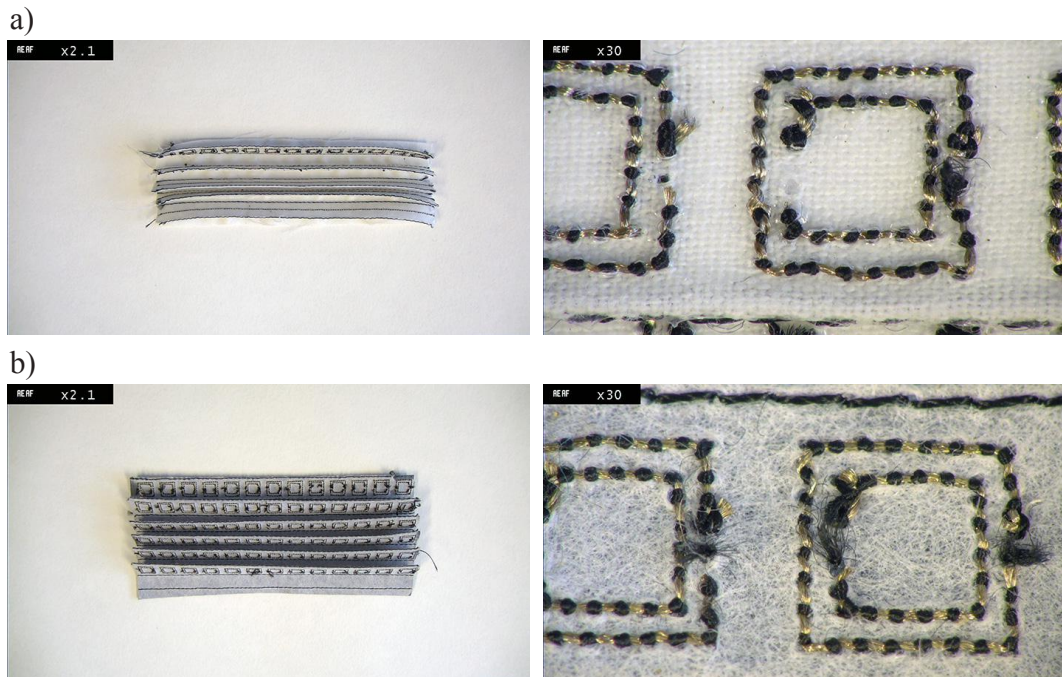


Figure 8.29: Samples embroidered with Statex thread. Assembled prototype (left) and detail (right). (a) Cotton (b) Polycotton

For the measurement, the two structures were loosely assembled into one prototype, in order to create a sample large enough to allow an initial measurement.  $S_{21}$  measurements were taken over a frequency range of 3 – 12 GHz, with results plotted in Figure 8.30.

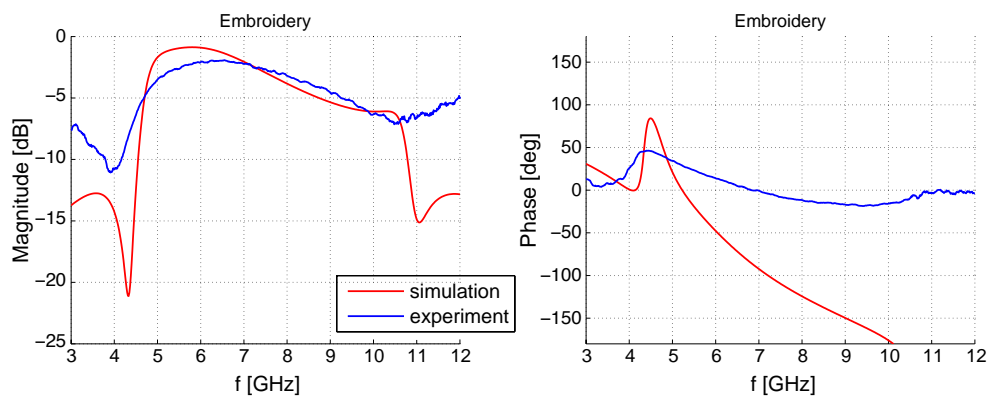


Figure 8.30: Magnitude and phase of  $S_{21}$  for the embroidered sample. Simulation results are shown in red, measurement results shown in blue. For the latter a sample was loosely assembled from two smaller samples, to obtain an area large enough to fill the illumination area in the measurement set up.



Despite geometric inaccuracy and relatively low conductivity of the silver plated thread, transmission measurements show that the embroidered sample resonates between 4 - 5 GHz. The measurement also showed that the textile was more lossy than was predicted by the simulated cells, hence a less pronounced dip in the transmission phase.

A drawback of the technique was the cumbersome removal of connections between the SRRs, due to the fact that the design was stitched from one thread. However, it is known that more advanced embroidery machines are able to trim threads in between small elements.

Although the resonance was not as strong as suggested by the simulation, it was concluded that a negative refractive index at about 4.7 GHz was plausible for this sample. Thus, a further study with embroidered samples was pursued and will be presented in section 8.5.2.

#### **8.4.5 Summary**

Three three-dimensional textile prototypes fabricated with screen print, laser engraving and digital embroidery, were analysed in free space measurements. A PCB prototype was designed and milled, in order to investigate resonating behaviour in general. In order of importance, the success of the samples was evaluated in terms of electromagnetic response, fabrication feasibility, and visual appearance. At this point it was not possible to unambiguously retrieve a refractive index with experimental data. Therefore, this study focused on the detection of a 'dip' in the transmitted phase results, in order to determine if further pursuit of the fabrication method was technically justifiable. Based on the results, embroidery was chosen for further investigation in the third study presented in the next section.

In regard to the fabrication of three-dimensional resonant metatextiles, it was observed that all geometrical and material criteria had an impact on the electromagnetic performance of the textile. Some were critical, such as a sufficient conductance of the circuit parts, and a clear geometric separation of the two split rings. Others were more acceptable, such as non-perpendicular alignment of the unit cells, a variation of the permittivity of the dielectric substrate, and a dielectric loss tangent of up to 0.1.

## 8.5 Study 3: Negative Refractive Index Textiles

In this study, several samples of textile prototypes were fabricated and analysed in bandwidths between 3.5-12 GHz in the free space set up. Based on the results from embroidered structures, three layers were produced. In addition, the ‘print and etch’ technique, developed by PEL Ltd. (section 6.3.5), was used to produce multiple layers of designs for two different frequencies. For comparison, a second PCB prototype was fabricated using chemical etching in an industrial facility. To deliver evidence for the presence of a negative refractive index, phase shift in transmitted data was studied, and negative phase velocity was calculated as detailed in section 6.6.3.

### 8.5.1 Printed Circuit Boards for Comparative Analysis

A multi-layer PCB prototype, constructed from individual SRR and wire strips, was produced for comparative analysis. A chemical etching process was used to avoid the mechanical impact of the milling head, and the strips were manufactured in an industrial facility. Figure 8.31 shows the complete strips (a) and a detail (b). The geometry and conductivity of SRRs and wires on a strip was consistent, and consistent throughout the production batch.

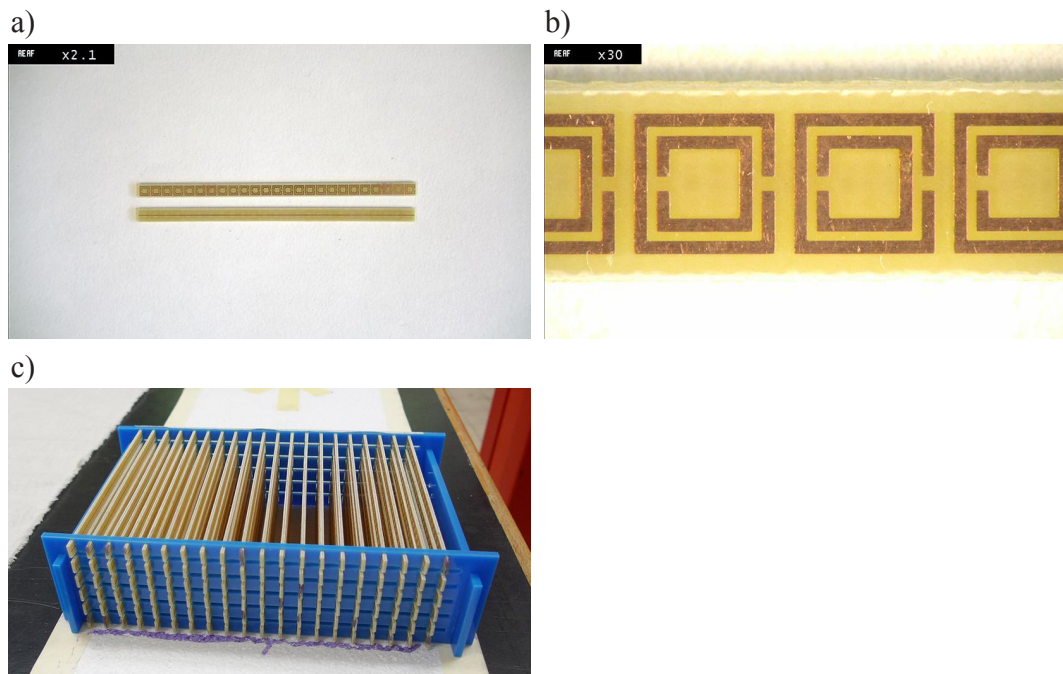


Figure 8.31: Study 3: Etched PCB strips (a) Front of PCB with SRR array (b) Detail of SRR (c) Assembled structure with six layers.

Approximating the frequency ranges that were achievable with textile structures, the cell design was adapted to 7.609 mm in propagation direction, and 4.725 mm in both E-field and H-field direction. The outer SRR was 4.150 mm and the inner SRR was 2.830 mm, both with a gap of 0.436 mm. The gap between the SRRs was adapted to 0.283 mm. The wire on the back of the PCB was 0.300 mm wide. The design was produced as strips of 134.780 mm length. The FR-4 board was 1.600 mm thick and had a permittivity of 4.4 and dielectric loss tangent of 0.001. The copper on both sides was 0.0347 mm thick. To assemble the structure, two acrylic holders held the strips, as shown in Figure 8.31 (c).

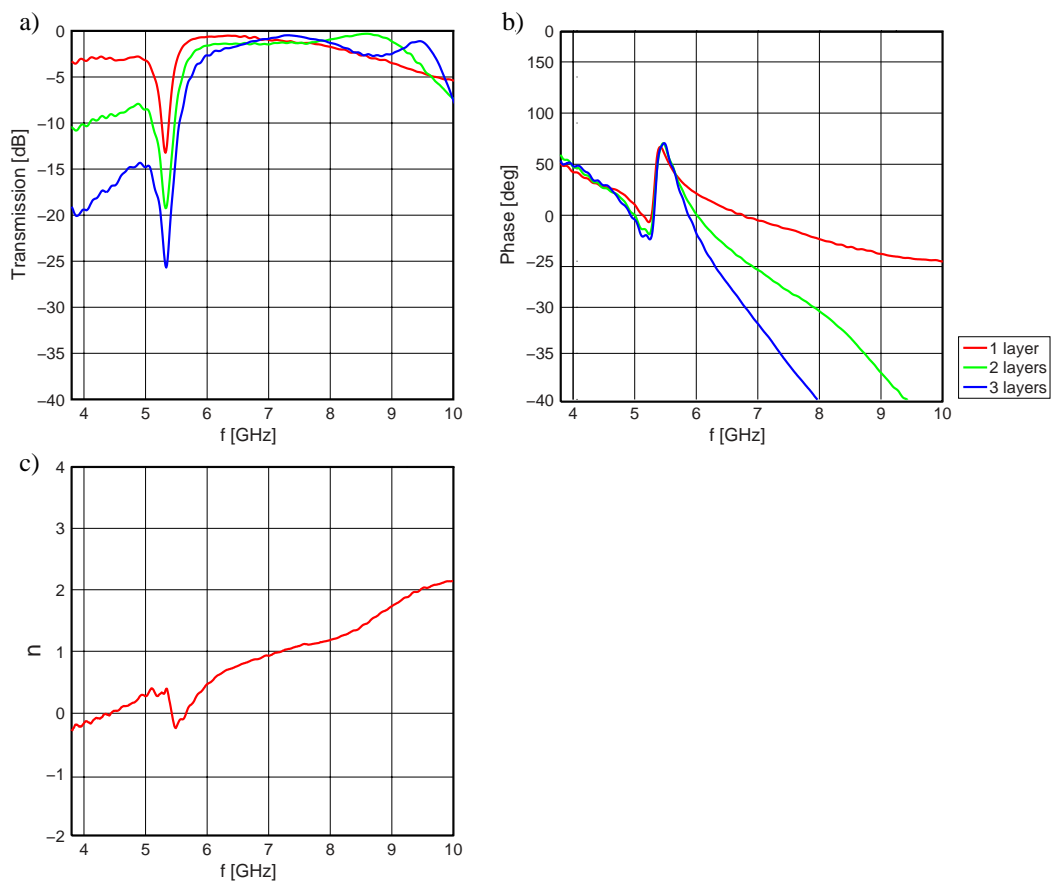


Figure 8.32: Three layers of PCB SRR/wire designs. Transmission results (a) magnitude (b) phase (c) retrieved refractive index of three layers.

The strips were measured in the free space anechoic chamber, and transmission  $s$ -parameters recorded for a single, double, and triple layer. Measured transmission results are shown in Figure 8.32 (a) and (b), with retrieved refractive index in (c). A negative refractive index was achieved at frequency band 5.4-5.7 GHz, with the lowest figure of -0.26 at 5.5 GHz. Accordingly, a reversed phase shift can be seen in plot b in

the same frequency band. Below 4.3 GHz the refractive index again falls below 0, however as there is no power transmitted in that region this can be disregarded.

### 8.5.2 Embroidered Cotton and Polyester Fabric

The SRR and wire design was embroidered onto a polycotton fabric substrate with the digital embroidery machine Innov-is 1500D. Liberator® 40 thread was used as a bobbin thread and Madeira No. 40 as the top thread. The circuit elements were stitched in one fabrication process and separated manually after finishing the embroidery. A running stitch (of 1.5 mm stitch length) was applied with thread tension of 2. Using the same process as in previous samples, strips of screen printed TiO<sub>2</sub> lino ink were fused onto the back of the substrates, in order to increase the dielectric constant of the structure in the folds and bond the folds after pleating.

The complete pleated structure was found to bend in a convex shape over the width of the sample, causing inconsistent angles of the SRRs. To counterbalance this, the sides of the pleats were stitched onto the base fabric on the opposite side, resulting in a more consistent pleat angle. The finished prototype is shown in Figure 8.33, of which three layers were produced, required to study the phase shift.

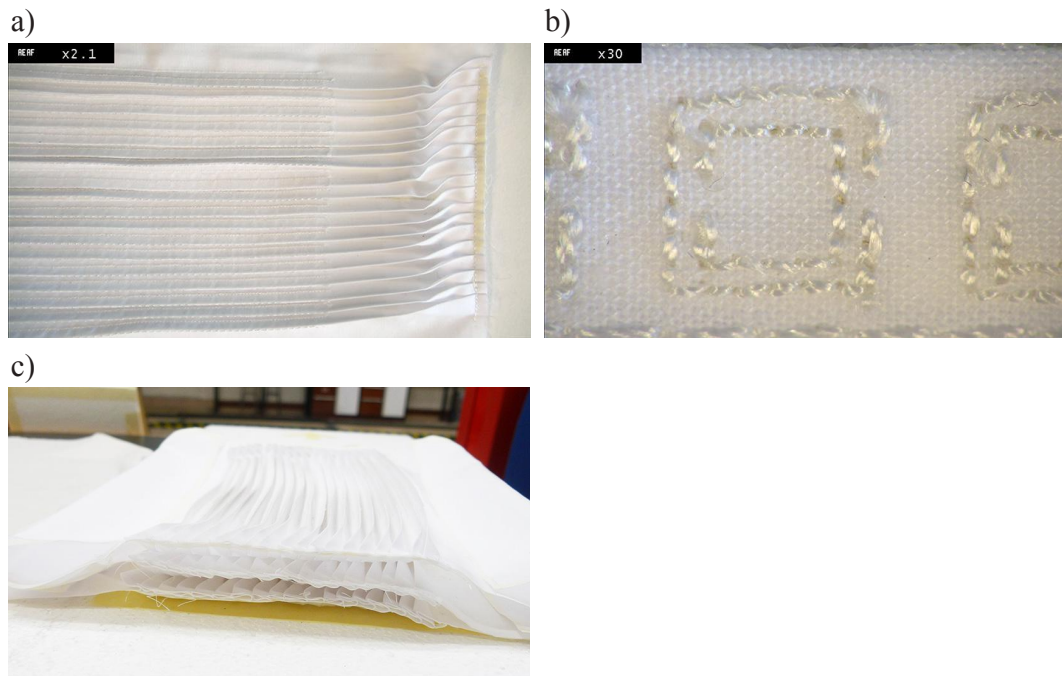


Figure 8.33: Embroidered samples (a) One layer (b) Detail of non-conductive top thread stitch. (c) Stacked three-layer prototype.

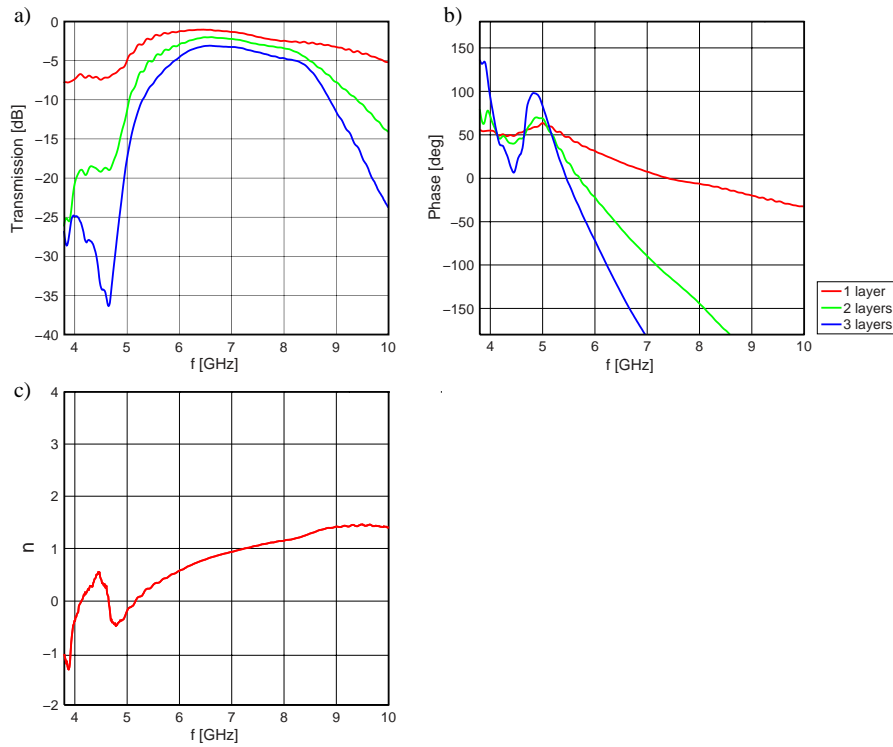


Figure 8.34: Three layers of embroidered designs. Transmission results (a) magnitude (b) phase (c) retrieved refractive index of three layers.

The samples were measured in the free space anechoic chamber, and transmission  $s$ -parameters recorded for the single, double, and triple layer. Transmission results are shown in Figure 8.34 (a) and (b), and the retrieved refractive index in c. A negative phase shift was achieved in the band of 4.7-5.1 GHz, with a clear increase of resonance, when measuring a rising number of layers. The lowest value of refractive index of -0.4 is shown at 4.9 GHz. Both narrow bandwidth (0.4 GHz) and high absorption ( $\sim 87\%$ ) behaviour corresponds to NIM behaviour described in the literature. Whilst there is another bandwidth at lower frequencies, which displays backwards phase (below 4.2 GHz), no power ( $< 3\%$ ) is transmitted, and thus this bandwidth can be disregarded. In comparison to the etched PCB prototype, it can be observed that loss of power is larger, which can be attributed to the less accurate geometry and lossy  $\text{TiO}_2$ -printed substrate.

### 8.5.3 Printed and Plated Polycarbonate Woven Fabric (Neltex®)

Two prototypes of different dimensions were fabricated off-site using the ‘print and etch’ process described in section 6.3.5. The reliability of this technique and the ability to produce smaller conductive structures resulted in two SRR/wire designs for approximate negative refractive indices at 7 GHz and 9 GHz. The modelled unit cell of

the larger design (Figure 8.35) was modified to 4.211 mm in E-field direction, 5.786 mm in H-field direction, and 6.174 mm in the direction of the propagation. The outer SRR was 3.719 mm, and the inner SRR was 2.54 mm, with a gap size of 0.39 mm. The gap between the SRRs was 0.25 mm. The wire was 0.24 mm wide.

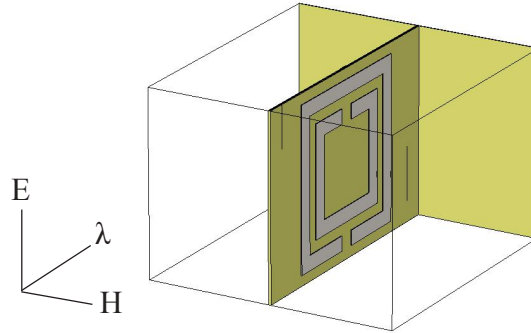


Figure 8.35: Unit cell design for larger SRR/wire structure, designed for ‘print and etch’ fabrication technique.

In the smaller design (Figure 8.36) the unit cell was modelled as 3.345 mm in E-field direction, 4.81 mm in H-field direction, and 4.893 mm in the direction of the propagation, the outer SRR was 2.945 mm, the inner SRR was 2.008 mm, with a gap size of 0.391 mm. The gap between the SRRs was 0.402 mm. The wire was 0.187 mm wide.

All nickel traces were modelled with 0.021 mm thickness, taking into consideration that the nickel coating looks similar on both sides of the fabric, suggesting that the trace continues inside the fabric by filling the gaps between the woven threads.

After printing and etching, the flat sheets were manually pleated and the folds ironed with TiO<sub>2</sub> printed strips sandwiched in the folds. As the woven substrate was quickly affected by heat, care needed to be taken to use low enough temperatures to not deform the fabric but high enough to bond the iron-on fabric. Temperatures between 90 - 100° were found to be acceptable.

Both prototypes were placed in the free space chamber and transmitted magnitude and phase data of up to four layers for each prototype recorded. Results are shown in Figure 8.38 for the larger design, and Figure 8.40 for the smaller design. For reference, the phase results for four layers of a conventional wood material have been added to the phase plots, indicating that with increasing thickness the phase shifts uniformly into one direction over the whole frequency band. For the metatextile prototype however, a

small bandwidth of negative phase shift can be observed, before the phase shift then changes again to a positive value. Another bandwidth of negative phase shift is seen on the lower ends of the frequency bands. This matches with statements given in the literature, however this can be ignored because there is no transmission occurring in these frequency bands.

Refractive index was calculated through phase difference between layers 2 and 3. Results are shown in Figure 8.39 and Figure 8.41. Both prototypes achieved a small negative refractive index over a small bandwidth between 7.45 - 7.60 GHz and 9.40 - 9.70 GHz. Both frequency responses deviated from the simulation by about 0.4 GHz. It was also noted that the resonance was less pronounced than in the embroidered prototypes.

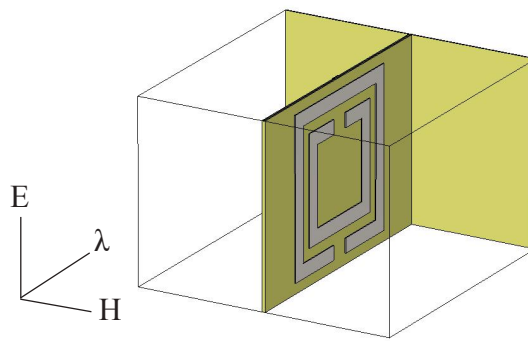


Figure 8.36: Unit cell design for smaller SRR and wire structure, aimed for 'print and etch' fabrication technique.

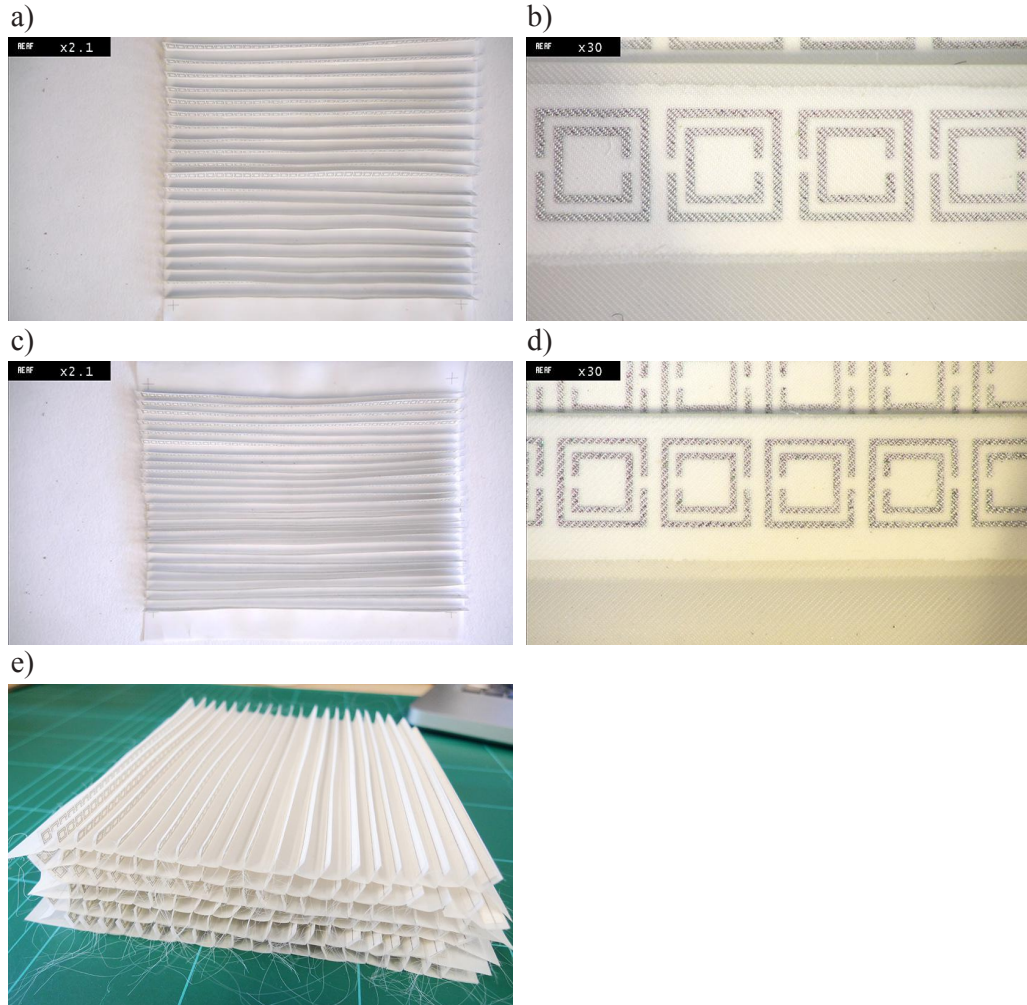


Figure 8.37: Prototypes 'print and etch'. The circuits were produced by PEL on polycarbonate woven textile. Two sizes were designed, of which one was designed for negative refractive index at (a) - (b) 7 GHz and one for (c) - (d) 9 GHz. (e) Assembled and stacked samples. Irregularities in the frequencies of folds are the result of the handmade pleating and assembling process. The aim was to achieve precise arrays, some irregularities were tolerated as part of textile behaviour.

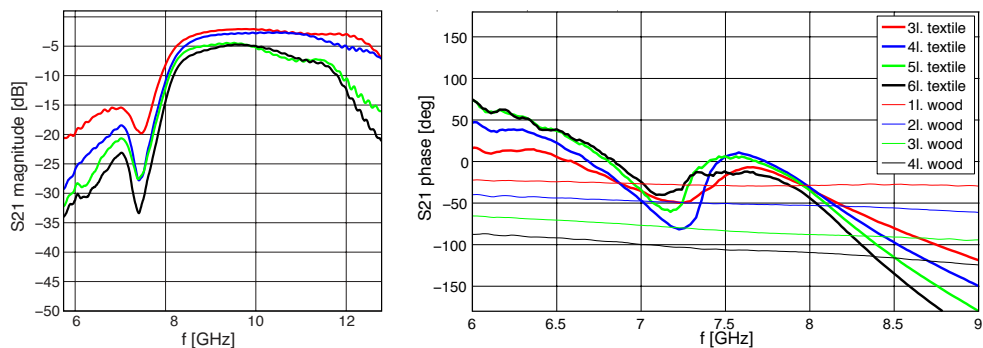


Figure 8.38: Results for 'print and etch' prototype 1, larger design. The flat designs were fabricated by PEL Ltd. And subsequently printed with TiO<sub>2</sub> ink, pleated and assembled.



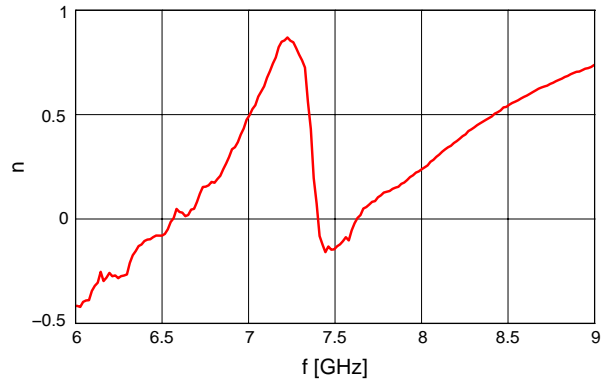


Figure 8.39: PEL 'print and etch' prototype with larger design. Measured result was retrieved by calculating the refractive index from the negative phase shift.

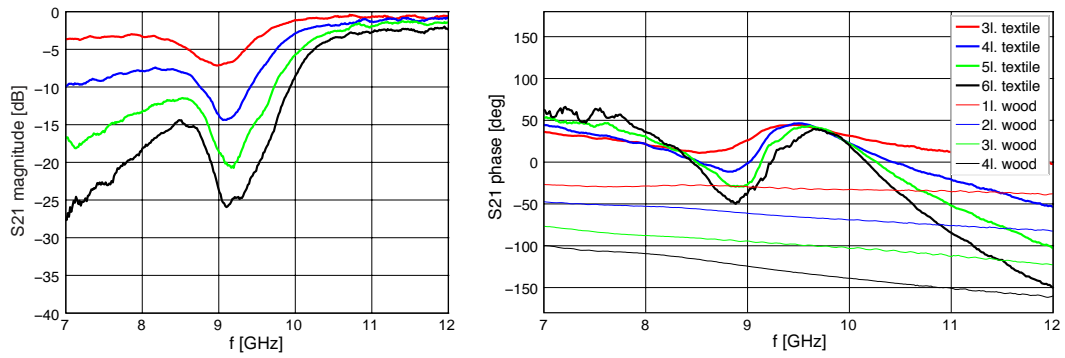


Figure 8.40: Results for 'print and etch' prototype 2, smaller design. The flat designs were fabricated by PEL and subsequently printed with  $\text{TiO}_2$  ink, pleated and assembled. The measured results show a deviation of 0.4 GHz to the simulated results, and the resonance is weaker than the simulations.

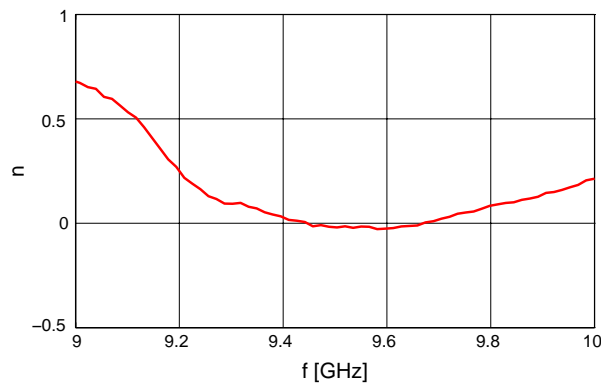


Figure 8.41: PEL 'print and etch' prototype with smaller design. Measured result was retrieved by calculating the refractive index from the negative phase shift.

### 8.5.4 Summary

This section presented the results of the investigation of fabrication techniques for textile NIM metamaterials. Three textile SRR and wire structures were constructed on flat substrates, of which one was made in-house on a domestic embroidery machine and the other two industrially fabricated by PEL Ltd. using the ‘print and etch’ technique. Both were subsequently assembled into three-dimensional pleated structures, with strips of TiO<sub>2</sub> printed lino ink embedded into the folds to achieve a higher permittivity between the SRR and the wire. For comparison, a PCB FR-4 prototype was etched in an industrial facility. A negative refractive index was demonstrated in all samples, which was calculated from the negative phase shift between multiple layers of the samples. Results are summarised in Table 8.1. It was observed that resonances in textile prototypes were less pronounced than in the PCB structures, resulting in lower negative refractive indices in comparison to simulated structures, as well as higher power losses. This was the case in particular for the ‘print and etch’ prototype.

Table 8.1: Summary Results Study 3: Negative Refractive Index Textiles

Prototype	Frequency range of negative refractive index	Lowest value of Refractive index
Etched FR-4 (PCB)	5.50 – 5.70 GHz	-0.30
Digital embroidery, Liberator thread on polycotton	4.70 – 5.10 GHz	-0.50
Print and etch, large design	7.45 – 7.60 GHz	-0.20
Print and etch, small design	9.45 – 9.70 GHz	-0.05

## 8.6 Conclusion

Figure 8.42 summarises the three studies presented in chapter 8. In the first study, seven techniques were explored for their suitability to produce small, separate and conductive SRR and wire shapes on textile substrates. The most successful techniques were used to produce one-layer samples in the second study, which were then measured, in order to determine if a negative refractive index was plausible. In the last study, the two most successful techniques were used to produce multiple layers of samples, and negative refractive indices were verified.

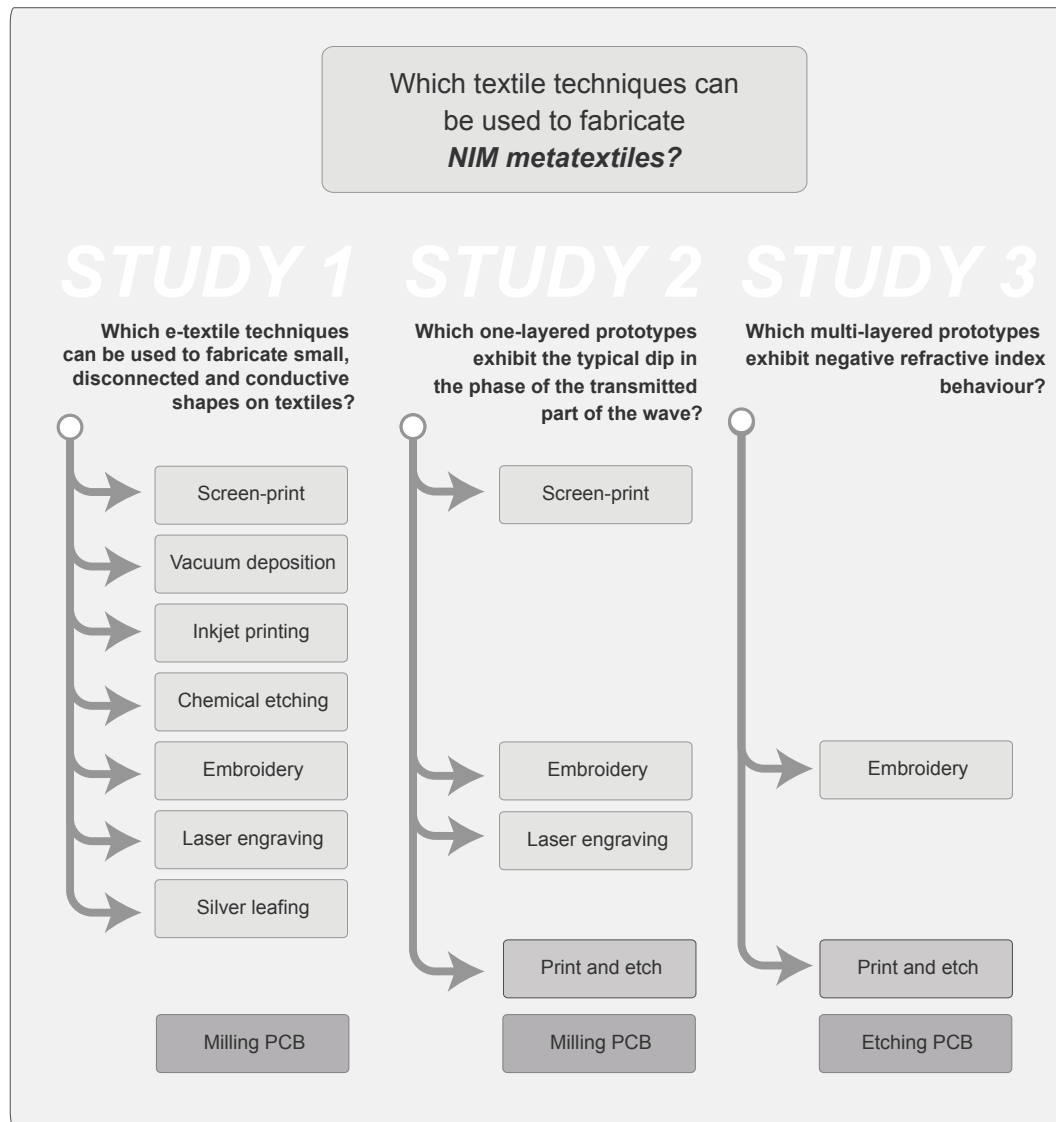


Figure 8.42: Three studies were presented in chapter 8. In the first study (left column), seven textile techniques were tested. The three most successful samples were then used to produce single-layer samples in the second study (centre column), compared to an industrially produced sample (print and etch). In the third study (right column), three samples were constructed in multiple layers (two ‘print and etch’ structures with different dimensions, and one embroidered structure) and negative refractive indices verified. PCB structures were designed for comparison in each study.

Throughout the studies, it was apparent that both sample potential and sample flaws were closely related to the technique used for sample fabrication. The following list states observations collated during the process, each of which brings up new questions and avenues that would need further investigation:

- Small samples have a higher success rate than large samples;
- Some techniques which were unsuccessful would be feasible if applied with industrial machinery;
- Accurate geometry of the SRRs were not the deciding factor for success or failure;
- Electrical conductance of the SRRs and wires were of high importance (confirmed in simulations);
- Some techniques provided high accuracy but low conductivity (chemical etching, screen print). Others had higher conductivity (embroidery), but their geometry was difficult to control;
- For embroidery, the machine should be adapted to facilitate greater strength to aid geometric stability, as well as have an automatic thread cutter that is able to cut conductive thread and avoid resulting tensions;
- The pleats should be fabricated with precise regular folds, to obtain uniform spaces between strips of SRR and wires, providing an improved 'response' by the entity of the cells. It appeared that this was the deciding factor for the overall strength of response. The more irregular the single cells were, the less they responded as a unit;
- 'Print and etch' samples had a weaker response than the embroidered samples, which was unexpected. Print and etch single cells are geometrically accurate and more conductive, therefore it was expected that they would show the best results of all of the textiles.

Many techniques were not suitable for a second study, due to the large differences observed when producing small and large samples. These were material and technique-specific, as summarised in Table 8.2.

Table 8.2: Summary of techniques applied in chapter 8, including success and challenges encountered when prototyping small and large samples.

Technique	Small sample	Large sample
Screen printing	Geometry accurate, resistance low.	Geometry accurate, resistance high. No resonating response in Study 2.
Vacuum deposition	Geometry accurate on some waterproof fabrics. Resistance varies for substrates, but minimum of 120Ω achieved using polyester.	Not applicable as maximum possible sample size is 80 x 80 mm.
Ink-jet printing	n/a	Geometry accurate on both waterproof fabric and PES films. No conductance on fabric, low resistances on films.
Chemical etching	Chemical etching of copper tape bonded with cotton fabrics successful in both geometry and conductivity. Adhesive residue from bonding fabric was a problem.	Geometry difficult to control over larger surface, only about 40% of SRRs were successful. Adhesive residue from bonding fabric made impractical to fabricate a three-dimensional prototype.
Laser engraving	Geometry accurate and highly conductive. Success rate about 80%.	Larger samples were inaccurate over the complete surface. Fragile when assembled. Only weak response in Study 2.
Digital embroidery	Geometry not accurate but sufficient. Conductivity depends on the thread used (down to 1Ω/300mm with Liberator thread).	Geometry not accurate but sufficient. Conductivity depends on the thread used (down to 1Ω/300mm with Liberator thread). Successful in Study 2 and 3.
Silver leafing	Geometry inaccurate and non-conductive.	None
Print and etch (PEL)	None	Geometry accurate and sufficiently conductive. Successful in Study 2 and 3.

## **Chapter 9**

# **Conclusions and Future Work**

### **9.1 Overview**

The idea for this thesis was formed during conversations between the author and electromagnetic engineers from the Antennas and Electromagnetics Group at QMUL. Based on common interests found in the topic of structural materials, the research questions were developed as follows:

1. How can advanced electromagnetic metamaterials for microwave operation be fabricated with textile materials and textile design techniques?
2. Can a practice-led textile design approach provide more options for material selection in metamaterials research?

Metamaterials are part of a relatively new yet already large research field in electromagnetic engineering, physics, and materials engineering. They are used to construct practical engineering solutions for devices designed with Transformation Optics; a design tool used to shape electromagnetic field propagation by manipulating properties of materials.

In the first phase of metamaterial research, physicists developed theories for guiding electromagnetic waves. They proposed the use of highly complex and anisotropic materials to achieve perfect functionality. In the search for more practical engineering solutions, simpler designs were then developed by engineers to ensure that fabrication

costs and efforts were kept low. The third phase covered new materials and fabrication for metamaterials, utilising new technologies to enable the production of complex structures. The findings of this thesis contribute to the last phase.

This work was based on an interdisciplinary approach, using an experimental textile design method, taking advantage of techniques that are prominent in textile and e-textile design. The overall aim was to discover if more options could be provided for the fabrication of metamaterials for engineers.

The thesis adopts the structural aspects of metamaterials as a source of inspiration, using design methods to fabricate textile metamaterials. Initially, the research goal was to produce a textile antenna using a metamaterial as a base. As the work developed, a deeper understanding of metamaterials and multifaceted applications were achieved. Thus, it was decided that producing a specific antenna was less relevant than a detailed understanding of new ways to manufacture textile metamaterials, and their electromagnetic evaluation using standard methods.

Textile metamaterials can be part of larger Wearable Technology systems, and have potential for interior design applications, for example, wallpaper, curtains and carpets. Their electromagnetic functionality could be concealed or highlighted to add an aesthetic benefit to pre-existing technologies.

In summary, the technical aims of this research were to:

- Identify suitable ‘one-process’ fabrication techniques to create textiles with graded permittivity;
- Explore the suitability of standard electromagnetic methods to measure and analyse the behaviour of textile materials;
- Explore a range of e-textile design methods to produce textiles with a negative refractive index.

## **9.2 Research Findings**

For this thesis, two types of metamaterials were investigated. One was constructed from all-dielectric materials, and the other from a resonating conductive structure. Both were

explored with a range of textile fabrication technologies. In addition, fabrication techniques that are traditionally used for films or paper materials were adapted and tested for textile use.

### **9.2.1 All-dielectric Graded Materials**

The all-dielectric samples, presented in detail in chapter 7, were produced using standard textile techniques, digital embroidery, screen printing and laser cutting.

Embroidery and screen printing were used to produce two-dimensional samples with graded permittivity. Embroidered samples achieved permittivity ranging from 1.2 to 1.8 (Study 1, Sample 1, section 7.3.1), and 1.2 to 1.6 (Study 1, Sample 2, section 7.3.1). A screen printed sample achieved a permittivity gradient of between 1.6 and 3.7 (Study 2, section 7.4.1). Regular and irregular laser cut samples were also produced (section 7.5.1) to see if more pattern choices could be found. These experiments showed that BaTiO<sub>3</sub> screen printed cut-out paper samples had a measured permittivity of about 2.3.

All samples had dielectric loss tangents lower than 0.1 (section 7.3 - 7.5), which was set as a threshold to guarantee suitability for cloaking devices.

Embroidery was found to be the technique most susceptible to inaccuracies, as dense stitching changed the thickness and stiffness of the base textile significantly. The folds needed to be kept clear of embroidery thread, which allow for easy and precise folding. The structure was supported by smocking, which is a technique using a loosely stitched thread perpendicular to the fold, to tighten and loosen the fabric. Three-dimensional form was explored using a simple accordion pleat and smocking line.

Screen printing was found to be an accessible and low-cost technique for producing dielectric structures, with the addition of TiO<sub>2</sub> ink, originally used for linocut in visual arts prints as a good dielectric base. Additionally, as shown in chapter 7, the ink increased the permittivity of substrate fabrics, which were then used for negative refractive index textiles. TiO<sub>2</sub> ink has a high dielectric loss, which rises sharply with increasing frequency. However, the quick-drying and versatile physical properties of the ink far outweighed this disadvantage, given that the measured frequency of these experiments was relatively low (3 - 12 GHz). In the experiments dielectric losses of less than 0.1 were measured.



In section 7.5, two card samples were presented. These were screen printed with BaTiO<sub>3</sub> ink, and subsequently laser cut, one with a regular pattern, and one with an irregular pattern. The samples were larger than the illumination area of the measurement set up (120 x 120 mm), and measurements at different parts of the sample were taken. The results were compared to investigate if the samples had a consistent permittivity when measured at different positions.

The results showed that the irregular pattern had a higher anisotropy than the regular pattern, when rotated and measured at different angles. When measured at the same angle, but at different positions of the length of the sample, the regular pattern had more differences in permittivity.

Although not explored in detail in this thesis, the experiment showed that materials with random or irregular patterns (such as foam) could be used for metamaterial fabrication. In regard to the application that the metamaterial is designed for, further benefits, such as aesthetic style or light weight of the cut out material, could be exploited.

By varying the sample patterns the different permittivities can be targeted; an advantage when producing high-resolution gradients. These fabrication methods showed that producing complex gradients are of equal effort and cost to producing less complex ones. This offers a wide choice for designing metamaterials. Previous research proposed different methods, which aimed to simplify fabrication by lowering the resolution of gradient maps to only a few material blocks (Bao, 2012).

Textiles are sensitive to mechanical and environmental changes, which presented challenges. Measurements were less precise in comparison to that of rigid and standardised materials, and also varied over time.

In summary, the following aspects need to be considered when using textiles as dielectrics:

- Textiles are susceptible to humidity, which can significantly change their electromagnetic properties.
- Mechanical properties such as flexibility and air permeability, which are usually seen as advantages of fabrics, can result in ambiguous measurement results.

- Inconsistencies occur as a result of manual fabrication processes.
- The free space measurement technique used in this work is known to be less precise when used with thin, low permittivity and low loss materials, a common characteristic of textiles.

### **9.2.2 Negative Refractive Index Textile Metamaterials**

In three studies, a range of e-textile materials and fabrication techniques were explored to test their suitability for fabricating NIM metatextiles. For one embroidered and two ‘printed and etched’ prototypes, negative refractive indices were achieved at around 4.9 GHz (section 8.5.2), 7.5 GHz and 9.5 GHz (section 8.5.3). Fabricating the material as a single two-dimensional surface with subsequent screen printing and eventual pleating into a three-dimensional shape was proposed. Previously, single cells or strips, and external support structures were assembled individually (section 2.1.3), a complex and expensive process.

First, a folded unit cell design was modelled that emulated the folded textiles. The simulation was also used to explore the suitability of different materials to be used in various techniques. Although effective material properties were applied to the computer-modelled cells, alterations had to be made to mirror the respective fabrication technique. For example, in the case of embroidery, the SRRs and wires were replaced by conductive rods, which were semi-inserted into the textile substrate. Subsequent resonating frequencies provided a good match to experimental results. However, it was found that the efficiency results were irregular and did not match the experiments, most likely due to imprecise measurement of electrical resistance of the e-textile materials.

There are existing methods to more accurately measure conductivity in textiles, which vary based on material type and require specialist equipment. For future work, more accurate material specifications would be required to investigate whether a better match between simulation and experiment can be achieved.

### **9.2.3 Measurement and Analysis**

An anechoic chamber was designed and built that facilitated free space measurements between 4 - 16 GHz (section 6.4.3). A mechanism was developed that allowed assessment of graded materials by measuring them in intervals. To calculate

permittivity and dielectric losses of the samples, standard algorithms were run in a commercial software package provided by Agilent.

It was found that accuracy in retrieval of material parameters was not always consistent. The following measures were taken, when measurements could not be improved mechanically:

- A loss tangent threshold of 0.1 was set. This figure was found through computer simulations, which showed that if a loss was larger than 0.1, the sample was unsuccessful in transporting energy. If the dielectric losses were below this threshold, the technique and material were used for further studies.
- Material thickness was measured five times, and an average taken. Due to the varying textile thickness being difficult to measure, retrieval of accurate permittivity data was problematic.

The work presented in chapter 8 gave a first look into how textiles can be used for Transformation Optics devices that make use of textile NIMs. More precise fabrication techniques would need to be explored and computational tools developed, in order to optimise the structure and maximise the consistency between the models and the textile prototypes. Using the commercial software tool CST provided some information but it was found that on a smaller scale the details of textile materials could not be modelled with sufficient detail.

### **9.3 Design Methodology and Interdisciplinary Contribution**

An iterative material-based approach was proposed for this work. Three stages of design were used to identify how textile materials and fabrication techniques could serve the functionality of metamaterials. The process started with an in-depth exploration of a material, after which the design that determined process, shape and function was developed.

This method differs from traditional engineering methods such as materials selection (Ashby, 1999), which are usually goal-orientated processes, in that materials were tested before the application was defined. Other engineering methods, such as “kit-of-

parts” (Howe et al., 1999) were used, but needed to be adapted to suit the procedures in this work.

This approach is related to practice-led research methods in that it uses practical processes to map out the boundaries of a given material and process. In the case of this thesis, it also provided the author with a way to explore the unfamiliar discipline.

The advantage was the originality that could be applied to designing and assembling the samples. Technical crafting skills played a major part, as well as domain shifting, which enabled the transfer of textile making knowledge into the field of metamaterials. The main disadvantage of this method was the time it took to gather findings and achieve positive results.

## **9.4 Future Work**

### **9.4.1 Optimisation of Textiles**

In order to minimise the structural challenges and inconsistencies that were encountered during the fabrication of samples, in the future, two main routes should be investigated:

- Reinforcement
- Industrial fabrication processes

If the textiles do not need to remain flexible, they can be reinforced. This could be done either with a carrying structure, or permanently fixed with a sprayable resin or encased in low-density foam. When the textiles are required to be flexible and maintain their appearance, a different fabrication approach is recommended. First, the manual process could be changed to an industrial one, and for example, a more precise and robust embroidery machine could be used, one which could handle automatic thread cutting of conductive threads, or automatic needle change when the needle starts to wear out. Additionally, there are already techniques available that only apply the conductive thread to the surface, which is then kept in place by a non-conductive second thread, similar to sequence embroidery. This was already partially achieved by adjusting the thread tension and pairing a thick conductive thread with a thin viscose thread to hold it

in place, but greater precision could be possible by using an industrial machine and a sequence foot (M. Metzler<sup>16</sup>, personal communication, 22nd January, 2015).

Even in an industrial facility, folding a three-dimensional structure with very small pleats would be difficult; it would be challenging to produce pleats with the exact level of precision required to avoid displacement of the SRR and wire within the unit cell. A plausible future solution for this could be nano-folding, suggested previously by Nogi, Komoda, Otsuka, & Sukanuma (2013). Another solution would be to use technologies that allow the fabrication of the conductive structure and folding mechanism in parallel, such as 3D printing with two materials, or laser etching metallised nano-fabrics.

#### **9.4.2 Accessible Computational Tools**

To date, applying Transformation Optics requires knowledge of the complex numerical processes involved, and there are no computational tools available to model metamaterials in such a way. Current modelling software, such as CST, is not accessible enough to be used by those outside of the field of engineering due to its high cost and specific application area. As a result, solely scientists and engineers study metamaterials. To allow designers to enter the field and explore design opportunities of metamaterials, accessible computational tools need to be developed.

A simulation tool that considers material and fabrication techniques could help make more efficient metatextiles. In current electromagnetic modelling software, the emphasis is put on a static form of the model. In order to explore characteristics specific to textiles (modularity, sensitivity to environmental changes and flexibility), a dynamic modelling technique would more realistically mimic the behaviour of textiles in both fabrication process and use.

Translation into the modelling process needs to adopt material behaviour familiar to the textile designer when working with textiles. This includes, folding three-dimensional structures, which results in compression in the folds, soaking of fibres with ink when printed and overall flexibility of surfaces or shape-memory effects of pleated textiles.

---

<sup>16</sup> Michael Metzler, ZSK Embroidery Machines GmbH

### **9.4.3 Design Scenarios**

Soft and thin textile metamaterials offer a number of applications, highlighted briefly throughout the thesis. At public demonstrations, trade fairs, meet ups, workshops, and arts and science events, the potential and implications of this work were discussed. It was found that, due to the novelty and technical expertise required in this field, illustrations and artistic impressions were a good way to initiate discussions across research areas. This helped to start a dialogue between designers, engineers and scientists, with the wider aim of exploring design scenarios for metamaterials.

The following paragraphs introduce experimental design ideas using metatextiles, which are separated into short term (now – 10 years), mid term (10 – 20 years) and long term (20 years and more) future scenarios.

#### **Microwave applications (now-10 years)**

Analysis of the results of the samples presented here show that textile metamaterials can be applied in microwave applications, such as textile antennas, and that metamaterial cells with dimensions satisfying the effective medium theory (section 5.2.1), can be achieved using currently available fabrication technologies.

Metatextiles are feasible for use with mobile phones and Wi-Fi signals at the frequencies of 2.4 GHz and 5 GHz, for which the cubic unit cell dimensions need to be 12 mm or less. For textile antennas in this region, metatextiles could improve on existing antenna designs by being smaller and more directional.

Textile metamaterials could also be used as an interesting alternative for distributing Wi-Fi fields in smart home applications, making use of textile surfaces and objects that are created in interior design. For example, in most architectural spaces a number of routers are required to distribute signals. An alternative solution could be to utilise metatextile floor and wall coverings to passively distribute the fields, meaning no energy would be required. They could also be used as absorbers rather than reflectors, diminishing the effects of disturbance in indoor spaces. Metatextiles could serve as selective shielding materials in wearable systems, disrupting signal flow in some places whilst maintaining it in others.

In regard to the negative refractive index achieved with ‘print and etch’ samples in the lower parts of the X band frequency band, metatextiles could find use in satellite

communications radar applications. This could again be in the form of wearable textile antennas embedded into clothing, or outdoor gear such as tents. The advantage of textile antennas in these products would be foldability and light weight. With some improvements in manufacturing the 12/14 GHz VSAT satellite communication band could exploit metatextiles to produce portable deployable high gain antennas for such applications as ‘anywhere in the world’ news gathering, and may even be viable for the latest micro-VSAT 20/30 GHz systems.

### **Terahertz applications (10 – 20 years)**

Many possibilities for metatextile applications are imaginable in the Terahertz region. For example, bio sensing (~0.1-1.5 THz) is located in this bandwidth. For these wavelengths, the unit cell dimension of metamaterials needs to be less than 1 mm. In regard to the fabrication techniques used in this thesis, the ‘print and etch’ technique has potential for some of these applications.

As shown already by Tao et al. (2010), bio-compatible silk film and gold materials are an interesting material combination for bio-sensing applications. Using silk threads and fabrics instead of film could provide additional benefits, such as more flexibility, stretchability or lighter weight. This could offer a number of possibilities for implanted designs and possibly help detect abnormalities in the body as a diagnosis tool.

### **Visible light (20 years and more)**

There are a number of exciting possibilities for textile metamaterials in the visible spectrum (430 - 790 THz). The dimensions of a unit cell for a metatextile in this range would need to be 80 nm or less. At this size, the fabrication clearly becomes a challenge. Nano-coatings and nano-sized threads for textiles are already available for technical research and even commercial applications, but the arrangement of the nano-particles in their application is mostly disordered. To ensure the geometric alignment of SRR and wire required, the textile substrate and conductive elements would need to be fabricated simultaneously. A folding mechanism for nano-structures has already been proposed in the literature (Nogi et al., 2013), and it can be assumed that fabrication of three-dimensional aligned nano-structures would be an option for textiles in the future.

Whilst a wearable invisibility cloak is yet to be invented, textile metamaterials could be used as a ‘projector’ to guide images around bodies, creating interesting dichroic colour

effects. This would not result in the concealment of the body per se, but could create intriguing colour effects and optical illusions, to be exploited by certain industries, such as fashion design or film media.

Another application of wearable textile metamaterials in the visual spectrum could be their use for data transmission in Li-Fi (Light Fidelity) operation. Li-Fi devices are a promising technology for wireless communication, however signals are not able to penetrate walls or architectural structures. Transformation Optics could be an interesting option to solve issues of signal guiding, and create a demand for optical metamaterials in smart home and interior applications.

## **9.5 Closing Remark**

This thesis provides an insight into the design and fabrication of metatextiles from a textile design practitioner's point of view. The work was a unique opportunity to interweave experimental textile design and electromagnetic engineering, exploiting the potential created by an interest in structured materials present in both fields.

Some alternatives for fabrication of flexible and textile metamaterials were presented, and it is hoped that this will inspire electromagnetic engineers, physicists and materials engineers to make use of textile techniques in their work.

As the functionality and potential of metamaterials have not yet been fully researched, many opportunities for designers to realise their futuristic design scenarios lie ahead.



## References

- Addington, M., & Schodek, D. (2005). *Smart Materials and New Technologies - For architecture and design professions*. Oxford: Elsevier.
- Albers, A. (2001). *Anni Albers: Selected Writings on Design*. Middletown: Wesleyan University Press.
- Alù, A., & Engheta, N. (2009). Cloaking a sensor. *Physical Review Letters*, *102*(23), 1–4.
- Ashby, M. F. (1999). *Materials Selection in Mechanical Design* (2nd editio). Oxford: Butterworth-Heinemann Ltd.
- Ashby, M. F. (2010). New Materials - The Potential for Innovation. In *Materials and Design: The Art and Science of Material Selection in Product Design* (pp. 159–170). Oxford: Elsevier.
- Averitt, R. D. (2013). *Introduction to metamaterials*. Retrieved from <http://physics.bu.edu/~redner/482/13/averitt-slides.pdf>
- Aydin, K., Guven, K., Soukoulis, C. M., & Ozbay, E. (2005). Observation of negative refraction and negative phase velocity in left-handed metamaterials. *Applied Physics Letters*, *86*(12), 124102.
- Aydin, K., Li, Z., Hudlička, M., Tretyakov, S. a, & Ozbay, E. (2007). Transmission characteristics of bianisotropic metamaterials based on omega shaped metallic inclusions. *New Journal of Physics*, *9*(9), 326–326.
- Aydin, K., Li, Z., Sahin, L., & Ozbay, E. (2008). Negative phase advance in polarization independent, multi-layer negative-index metamaterials. *Optics Express*, *16*(12), 8835–44.
- Babu, S. (2014). *Architected Objects through Selective Laser Sintering* (Doctoral thesis, University College London, London, UK)
- Bai, Q., & Langley, R. (2012). Crumpling of PIFA Textile Antenna. In *IEEE Transactions on Antennas and Propagation* (Vol. 60, pp. 63–70).
- Baker-Jarvis, J., Vanzura, E., & Kissick, W. A. (1990). Improved Technique for Determining Complex Permittivity with the Transmission/Reflection Method.

- IEEE Transactions on Microwave Theory and Techniques*, 38(8), 1096–1103.
- Bal, K., & Kothari, V. (2009). Measurement of dielectric properties of textile materials and their applications. *Indian Journal of Fibre and Textile Research*, 34(June), 191–199.
- Bal, K., & Kothari, V. (2010). Permittivity of woven fabrics: A comparison of dielectric formulas for air-fiber mixture. *IEEE Transactions on Dielectrics and Electrical Insulation*, 17(3), 881–889.
- Bao, D. (2012). *Design and Applications of Optical Transformation Devices* (Doctoral thesis, Queen Mary University of London, London, UK).
- Bao, D., Rajab, K. Z., Hao, Y., Kallos, E., Tang, W., Argyropoulos, C., ... Yang, S. (2011). All-dielectric invisibility cloaks made of BaTiO<sub>3</sub>-loaded polyurethane foam. *New Journal of Physics*, 13(10), 103023.
- Baurley, S. (2004). Interactive and experiential design in smart textile products and applications. In *Personal and Ubiquitous Computing* (Vol. 8, pp. 274–281).
- Berzina, Z. (2009). e\_static shadows. Retrieved March 15th, 2013 from <http://www.zaneberzina.com/e-staticshadows.htm>
- Billings, L. (2013). Exotic optics: Metamaterial world. *Nature, News Feature*, 500(7461).
- Blattenberger, K. (2009). Skin Depth. Retrieved March 13, 2016, from <http://www.rfcafe.com/references/electrical/skin-depth.htm>
- Bloom, D. M., Park, M., & Hill, M. (1985). U.S. Patent No. 4,527,166. Washington, DC: U.S. Patent and Trademark Office.
- Burgnies, L., Lheurette, É., & Lippens, D. (2015). Textile inspired flexible metamaterial with negative refractive index. *Journal of Applied Physics*, 117(14), 144506.
- Burkinshaw, S. M. (2015). *Physico-chemical Aspects of Textile Coloration*. New Jersey: John Wiley & Sons.
- Bye, E. K. (2010). A Direction for Clothing and Textile Design Research. *Clothing and Textiles Research Journal*, 205–217.

- Cabinet Official Committee on UK Spectrum Strategy. (2010). *UK Frequency Allocation Table*.
- Calder, L. (2011). *A Mixed Methods Study into the Measurement of the Effects of Monochromatic Optical Pattern on Perceived Female Form* (Doctoral thesis, Heriot-Watt University, Edinburgh, UK).
- Charles, J. A. (1997). *Selection and use of engineering materials*. (3rd editio). Oxford: Butterworth Heinemann.
- Chauraya, A., Zhang, S., Whittow, W., Acti, T., Seager, R., Dias, T., & Vardaxoglou, Y. C. (2012). Addressing the challenges of fabricating microwave antennas using conductive threads. *Proceedings of 6th European Conference on Antennas and Propagation, EuCAP 2012*, 1365–1367.
- Chen, X., Grzegorzczak, T., Wu, B.-I., Pacheco, J., & Kong, J. (2004). Robust method to retrieve the constitutive effective parameters of metamaterials. *Physical Review E*, 70(1), 16608.
- Coelho, M., Hall, L., Berzowska, J., & Maes, P. (2009). Pulp-based computing: a framework for building computers out of paper. *CHI '09 Extended Abstracts on Human Factors in Computing Systems*, 3527–3528.
- Cork, C. R. (2015). *Conductive fibres for electronic textiles. Electronic Textiles: Smart Fabrics and Wearable Technology* (1st Editio). Sawston, Cambridge: Woodhead Publishing.
- Cummer, S. A., Rahm, M., & Schurig, D. (2008). Material parameters and vector scaling in transformation acoustics. *New Journal of Physics*, 10(115025), 1–12.
- Cummer, S. A., & Schurig, D. (2007). One path to acoustic cloaking. *New Journal of Physics*, 2630(7), 1–8.
- Currey, M. (2013, June). Surface Invasion. Retrieved April 12, 2015, from <http://www.metropolismag.com/June-2013/Surface-Invasion/>
- De Barros, F., Eymin-Petot-Tourtollet, G., Lemaitre-Auger, P., & Vuong, T.-P. (2015). U.S. Patent No. US 9065180 B2. Washington, DC: U.S. Patent and Trademark Office.
- De Ruysser, T. (2009). *Wearable Metal Origami? The Design and Manufacture of Metallised Folding Textiles*. (Doctoral thesis, Royal College of Art, London, UK)

- Dias, T., & Rathnayake, A. (2015). Integration of micro-electronics with yarns for smart textiles. In *Electronic Textiles* (pp. 109–116). Elsevier Ltd.
- Dias, T., Zhang, S., Acti, T., Seager, R., Vardaxoglou, Y., Whittow, W., & Chauraya, A. (2013). Effect of the fabrication parameters on the performance of embroidered antennas. *IET Microwaves, Antennas & Propagation*, 7(14), 1174–1181.
- Dolling, G., Enkrich, C., Wegener, M., Soukoulis, C. M., & Linden, S. (2006). Low-loss negative-index metamaterial at telecommunication wavelengths. *Optics Letters*, 31(12), 1800–1802.
- Dong, Y., & Itohdan, T. (2012). Promising Future of Metamaterials. *IEEE Microwave Magazine*, (March), 39–56.
- Edison, T. A. (1880). Electric Lamp. U.S. Patent No. 223.898. U.S.: United States Patent Office.
- Engheta, N., & Ziolkowski, R. W. (2006). *Metamaterials: Physics and Engineering Explorations*. Wiley-IEEE Press.
- Ertas, A., & Jones, J. C. (1993). *The Engineering Design Process*. New York, USA: John Wiley & Sons.
- Esen, M., Ilhan, I., Karaaslan, M., Unal, E., Dincer, F., & Sabah, C. (2014). Electromagnetic absorbance properties of a textile material coated using filtered arc-physical vapor deposition method. *Journal of Industrial Textiles*.
- Fonseca, D. S., Seager, R., & Flint, J. A. (2015). Textile-to-rigid microstrip transition using permanent magnets. *Electronic Letters*, 51(9), 709–710.
- Frayling, C. (1993). Research in Art and Design. *Royal College of Art Research Papers* (Vol. 1).
- Freestone, I., Meeks, N., Sax, M., & Higgitt, C. (2007). The Lycurgus cup—a roman nanotechnology. *Gold Bulletin*, 270–277.
- Fridman, M., Farsi, A., Okawachi, Y., & Gaeta, A. L. (2012). Demonstration of temporal cloaking. *Nature*, 481(7379), 62–5.
- Garnett, J. C. M. (1904). Colours in Metal Glasses and in Metallic Films. *Philosophical Transactions of the Royal Society A: Mathematical, Physical and Engineering Sciences*, 203(359–371), 385–420.

- Geesin, F. (1995). *The chemical and structural manipulation of fabrics and fibres through stiffening techniques with specific emphasis on electrodeposition : the resulting materials have applications in fine art, fashion and the applied arts* (Doctoral thesis, Royal College of Art, London, UK).
- Ghebrehghan, M., Aranda, F. J., Ziegler, D. P., Carlson, J. B., Perry, J., Archambault, D. M., ... Kimball, B. R. (2014). Tunable millimeter and sub-millimeter spectral response of textile metamaterial via resonant states. *Optics Express*, 22(3), 2853–9.
- Greinke, B. (2004). Monoline. Retrieved August 20, 2014, from <http://beritgreinke.com/test/>
- Hao, Y. (2006). From electromagnetic bandgap to left-handed metamaterials: Modelling and applications. *Journal of Zhejiang University SCIENCE A*, 7(1), 34–40.
- Heinzel, T. (2015). Synthetic Beuys: on Nano-Materials and the Aesthetics of Imperceptibility. *Artnodes*, (15).
- Hertleer, C., Tronquo, a., Rogier, H., & Van Langenhove, L. (2008). The Use of Textile Materials to Design Wearable Microstrip Patch Antennas. *Textile Research Journal*, 78(8), 651–658.
- Hertleer, C., Van Laere, a., Rogier, H., & Van Langenhove, L. (2009). Influence of Relative Humidity on Textile Antenna Performance. *Textile Research Journal*, 80(2), 177–183.
- Hodges, S., Villar, N., Chen, N., Chugh, T., Qi, J., Nowacka, D., & Kawahara, Y. (2014). Circuit Stickers: Peel-and-stick Construction of Interactive Electronic Prototypes. *Proceedings of the 32Nd Annual ACM Conference on Human Factors in Computing Systems*, 1743–1746.
- Howe, A., Ishii, I., & Yoshida, T. (1999). Kit-of-parts: A review of object-oriented construction techniques. *IAARC/IFAC/IEEE. International Symposium*, 165–171.
- Husain, M. D., Kennon, R., & Dias, T. (2014). Design and fabrication of Temperature Sensing Fabric. *Journal of Industrial Textiles*, 44(3), 398–417.
- Jiang, W. X., & Cui, T. J. (2011). Radar illusion via metamaterials. *Physical Review E*, 83(2), 26601.

- Joshi, J. G., Pattnaik, S. S., & Devi, S. (2012). Metamaterial Embedded Wearable Rectangular Microstrip Patch Antenna. *International Journal of Antennas and Propagation*, 2012, 1–9.
- Joshi, J. G., Pattnaik, S. S., & Devi, S. (2013). Geo-textile based metamaterial loaded wearable microstrip patch antenna. *International Journal of Microwave and Optical Technology*, 8(1), 25–34.
- Kallos, E., Argyropoulos, C., & Hao, Y. (2009). Ground-plane quasicloaking for free space. *Physical Review A*, 79(6), 63825.
- Kawahara, Y., Hodges, S., Cook, B. S., & Abowd, G. D. (2013). Instant Inkjet Circuits : Lab-based Inkjet Printing to Support Rapid Prototyping of UbiComp Devices. In *UbiComp '13*.
- Kawahara, Y., Hodges, S., Gong, N.-W., Olberding, S., & Steimle, J. (2014). Building Functional Prototypes Using Conductive Inkjet Printing. In *IEEE Pervasive Computing* (Vol. 13, pp. 30–38).
- Kennedy, T. F., Fink, P. W., Chu, A. W., Champagne, N. J., Lin, G. Y., & Khayat, M. a. (2009). Body-Worn E-Textile Antennas: The Good, the Low-Mass, and the Conformal. *IEEE Transactions on Antennas and Propagation*, 57(4), 910–918.
- Kildishev, a V, Cai, W., Chettiar, U. K., & Shalaev, V. M. (2008). Transformation optics: approaching broadband electromagnetic cloaking. *New Journal of Physics*, 10(11), 115029.
- Kimbell, L., & Street, P. (2009). Beyond design thinking: Design-as-practice and designs-in-practice. *CRESC Conference, Manchester*, (May), 1–15.
- Klemm, M., Locher, I., & Troster, G. (2004). A novel circularly polarized textile antenna for wearable applications. In *7th European Conference on Wireless Technology* (pp. 285–288). IEEE.
- Knighting, S., Fraser, J., Sturrock, K., Deacon, P., Bleay, S., & Bremner, D. H. (2013). Visualisation of fingermarks and grab impressions on dark fabrics using silver vacuum metal deposition. *Science and Justice*, 53(3), 309–314.
- Kock, W. E. (1948). Metallic Delay Lenses. *Bell System Technical Journal*, 58–82.
- Kolko, J. (2010). Abductive Thinking and Sensemaking: The Drivers of Design Synthesis. *Design Issues*, 26(1), 15–28.

- Komolafe, A. O., Torah, R. N., Yang, K., Tudor, J., & Beeby, S. (2015). Durability of Screen Printed Electrical Interconnections on Woven Textiles. In *Electronic Components & Technology Conference* (pp. 1142–1147).
- Lamontagne, V. (2012). Wearable Technologies: From Performativity to Materiality. *Studies in Material Thinking*, 7.
- Leclerc, V., & Berzowska, J. (n.d.). No Title. Retrieved December 6<sup>th</sup>, 2014 from <http://xslabs.net/accouphene/>
- Lee, S., Kim, S., Kim, T.-T., Kim, Y., Choi, M., Lee, S. H., ... Min, B. (2012). Reversibly Stretchable and Tunable Terahertz Metamaterials with Wrinkled Layouts. *Advanced Materials*, 24, 3491–3497.
- Leonhardt, U. (2006). Optical conformal mapping. *Science (New York, N.Y.)*, 312(5781), 1777–80.
- Lheurette, É., Houzet, G., Carbonell, J., Zhang, F., Vanbésien, O., & Lippens, D. (2008). Omega-type balanced composite negative refractive index materials. *IEEE Transactions on Antennas and Propagation*, 56(11), 3462–3469.
- Li, J., & Pendry, J. B. (2008). Hiding under the Carpet: A New Strategy for Cloaking. *Physical Review Letters*, 101(20), 1–4.
- Li, Y., Torah, R., Beeby, S., & Tudor, J. (2012). Inkjet printed flexible antenna on textile for wearable applications. *2012 Textile Institute World Conference*.
- Liu, R., Ji, C., Mock, J. J., Chin, J. Y., Cui, T. J., & Smith, D. R. (2009). Broadband ground-plane cloak. *Science (New York, N.Y.)*, 323(5912), 366–9.
- Locher, I., Klemm, M., & Kirstein, T. (2006). Design and characterization of purely textile patch antennas. *IEEE Transactions on Advanced Packaging*, 29(4), 777–788.
- Locher, I., & Troster, G. (2007). Screen-printed Textile Transmission Lines. *Textile Research Journal*, 77(11), 837–842.
- Ma, H. F., & Cui, T. J. (2010). Three-dimensional broadband and broad-angle transformation-optics lens. *Nature Communications*, 1(8), 124.
- Maldovan, M., & Thomas, E. L. (2009). *Periodic Materials and Interference Lithography*. CHAP, Wiley-VCH Verlag GmbH & Co. KGaA.

- McCall, M. W., Favaro, A., Kinsler, P., & Boardman, A. (2011). A spacetime cloak, or a history editor. *Journal of Optics*, *13*(2), 029501–029501.
- Mitchell-Thomas, R. C., McManus, T. M., Quevedo-Teruel, O., Horsley, S. A. R., & Hao, Y. (2013). Perfect surface wave cloaks. *Physical Review Letters*, *111*(21), 1–5.
- Miyamoto, Y. (1996). *Functionally Graded Materials*. Engelska: Elsevier.
- Morinaga, K. (2013). Radio frequency shielding fashion to help you focus. Retrieved March 2, 2015, from <http://www.spoon-tamago.com/2014/04/28/radio-frequency-shielding-fashion-to-help-you-focus/>
- Mossé, A., Gauthier, D., & Kofod, G. (2012). Towards Interconnectivity: Appropriation of Responsive Minimum Energy Structures in an Architectural Context. *Studies in Material Thinking*, *7*.
- Nicolai, C. (2009). *Grid Index*. Berlin: Gestalten Verlag.
- Nicolson, A., & Ross, G. F. (1970). Measurement of the intrinsic properties of materials by time-domain techniques. *IEEE Transactions on Instrumentation and Measurement*, *IM-19*(8), 377–382.
- Niembro-Martin, A., Barros, F. De, Eymin-Petot-Tourtollot, G., & Lemaître-Auger, P. (2015). Metapaper : a Frequency Selective Surface Wallpaper for the attenuation of Wi-Fi signals. In *Proceedings of the 45th European Microwave Conference* (pp. 466–469).
- Nogi, M., Komoda, N., Otsuka, K., & Suganuma, K. (2013). Foldable nanopaper antennas for origami electronics. *Nanoscale*, *5*(10), 4395–9.
- Oxman, N. (2010). *Material-based Design Computation* (Doctoral thesis, Massachusetts Institute of Technology, Cambridge, U.S.)
- Paul, G., Torah, R., Yang, K., Beeby, S., & Tudor, J. (2014). An investigation into the durability of screen-printed conductive tracks on textiles. *Measurement Science and Technology*, *25*(2), 25006.
- Pendry, J. B. (2000). Negative refraction makes a perfect lens. *Physical Review Letters*, *85*(18), 3966–9.
- Pendry, J. B., Holden, A. J., Robbins, D. J., & Stewart, W. J. (1999). Magnetism from



- conductors and enhanced nonlinear phenomena. *IEEE Transactions on Microwave Theory and Techniques*, 47(11), 2075–2084.
- Pendry, J. B., Schurig, D., & Smith, D. R. (2006). Controlling electromagnetic fields. *Science (New York, N.Y.)*, 312(5781), 1780–2.
- Perner-Wilson, H. (2011). *A Kit - of - No - Parts A Kit - of - No - Parts* (Master's thesis, Massachusetts Institute of Technology, Cambridge, U.S.).
- Perner-Wilson, H. (2014). Igne Oyasi motor. Retrieved June 23<sup>rd</sup> 2015 from <http://etextile-summercamp.org/2014/movement-of-fabric-and-coils/>
- Philpott, R. (2011). *Structural Textiles : Adaptable Form and Surface in Three Dimensions* (Doctoral thesis, Royal College of Art, London, UK).
- Philpott, R. (2013). Engineering Opportunities for Originality and Invention: The importance of playful making as developmental method in practice-led design research. *Studies in Material Thinking*, 9.
- Pittman, E. H., & Kuhn, H. H. (1992). U.S. Patent No. US 5102727 A. Washington, DC: U.S. Patent and Trademark Office.
- Prabir, I., Leader, K. P., Calvert, P. D., Warner, S. B., Umd, D. K., Ajayan, P. M., ... Umd, Y. (2007). Textile Based Carbon Nanostructured Flexible Antenna. Retrieved June 5, 2014, from <http://davidlu.net/M06-MD01-07.pdf?G=736&ln=jp>
- Qi, J. (2012). *The fine art of electronics : paper-based circuits for creative expression* (Master's thesis, Massachusetts Institute of Technology, Cambridge, U.S.).
- Ramsgard Thomsen, M., & Tamke, M. (2009). Narratives of Making: thinking practice led research in architecture. In *Communicating (by) Design* (pp. 1–8).
- Rathnayake, A., & Dias, T. (2015). Yarns with Embedded Electronics. *UbiComp '15 / ISWC '15 - Adjunct Proceedings of the 2015 ACM International Joint Conference on Pervasive and Ubiquitous Computing and the 2015 ACM International Symposium on Wearable Computers*, 385–388.
- Rhode & Schwarz. (2006). Measurement of dielectric material properties. Retrieved July 23, 2014, from [http://www2.rohde-schwarz.com/file\\_18207/RAC-0607-0019\\_1\\_5E.pdf](http://www2.rohde-schwarz.com/file_18207/RAC-0607-0019_1_5E.pdf)
- Robertson, S. (2011). An Investigation of the Design Potential of Thermochromic

Textiles used with Electronic Heat-Profiling Circuitry (Doctoral thesis, Heriot-Watt University, Edinburgh, UK).

- Robertson, S., Christie, R., Taylor, S., & Ibrahim, W. (2011). Virtual colour : additive colour mixing on textiles with liquid crystal dye systems. In *Proceedings of Ambience11*.
- Russo, A., Ahn, B. Y., Adams, J. J., Duoss, E. B., Bernhard, J. T., & Lewis, J. A. (2011). Pen-on-paper flexible electronics. *Advanced Materials*, 23(30), 3426–3430.
- Rust, P. C., Mottram, P. J., & Till, P. J. (2007). Practice-Led Research in Art, Design and Architecture. Retrieved April 15<sup>th</sup> 2014 from [http://arts.brighton.ac.uk/\\_\\_data/assets/pdf\\_file/0018/43065/Practice-Led\\_Review\\_Nov07.pdf](http://arts.brighton.ac.uk/__data/assets/pdf_file/0018/43065/Practice-Led_Review_Nov07.pdf)
- Salonen, P., Keskilammi, M., & Sydanheimo, L. (2001). A low-cost 2.45 GHz Photonic Bandgap Patch Antenna for Wearable Systems. In *ICAP International Conference on Antennas and Propagation*.
- Salonen, P., & Rahmat-Samii, Y. (2006). Wearable Antennas: Advances in Design, Characterization, and Application. In *Antennas and Propagation for Body Centric Communications*.
- Salonen, P., Sydanheimo, L., Keskilammi, M., & Kivikoski, M. (1999). A small planar inverted-F antenna for wearable applications. In *The Third International Symposium on Wearable Computers, 1999*. (pp. 95–100). IEEE.
- Satomi, M., & Perner-Wilson, H. (n.d.). Kobakant. Retrieved July 24, 2013, from <http://www.kobakant.at/DIY/>
- Saul, G., Xu, C., & Gross, M. D. (2010). Interactive paper devices: end-user design & fabrication. *Proceedings of the Fourth International Conference on Tangible, Embedded, and Embodied Interaction*, 205–212.
- Schattschneider, D. (1978). The Plane Symmetry Groups : Their Recognition and Notation. *The American Mathematical Monthly*, 85(6), 439–450.
- Schleicher, D., Jones, P., & Kachur, O. (2010). Bodystorming as embodied designing. *Interactions*, 17(6), 47.

- Schurig, D., Mock, J. J., Justice, B. J., Cummer, S., Pendry, J. B., Starr, F., & Smith, D. R. (2006). Metamaterial electromagnetic cloak at microwave frequencies. *Science (New York, N.Y.)*, *314*(5801), 977–80.
- Scrivener, S. (2000). Reflection in and on action and practice in creative-production doctoral projects in art and design. *Working Papers in Art and Design 1*.
- Scully, D. C., & McCabe, C. (2000). U.S. Patent No. US 6077526 A. Washington, DC: U.S. Patent and Trademark Office.
- Seager, R., Bowman, J., Philpott, R., Chauraya, A., Broughton, M., & Nimkulrat, N. (2013). Fabric based frequency selective surfaces using weaving and screen printing. *Electronics Letters*, *49*(13), 1507–1509.
- Seager, R., Chauraya, A., & Vardaxoglou, J. C. (2008). Fabric Antennas Integrated with Metamaterials. In *Metamaterials* (Vol. 1, pp. 533–535).
- Seager, R., Whittow, W., Vardaxoglou, Y., Chauraya, A., & Zhang, S. (2013). Flexible radio frequency connectors for textile electronics. *Electronics Letters*, *49*(22), 1371–1373.
- Seager, R., Zhang, S., & Chauraya, A. (2013). Effect of the fabrication parameters on the performance of embroidered antennas. *IET Microwaves, Antennas & Propagation* (p. 1174-1181)
- Sennett, R. (2008). *The Craftsman*. London: Penguin Group.
- Shalaev, V. M., Cai, W., Chettiar, U. K., Yuan, H.-K., Sarychev, A. K., Drachev, V. P., & Kildishev, A. V. (2005). Negative index of refraction in optical metamaterials. *Optics Letters*, *30*(24), 3356–3358.
- Sharma, M., & Parini, C. G. (2013). A Miniature Wideband Antenna for Wearable Systems. In *2013 Loughborough Antennas and Propagation Conference (LAPC)* (pp. 619–623).
- Shelby, R. a, Smith, D. R., & Schultz, S. (2001). Experimental verification of a negative index of refraction. *Science (New York, N.Y.)*, *292*(5514), 77–9.
- Shivola, A. (2002). Electromagnetic Emergence in Metamaterials. In *Advances in Electromagnetics of Complex Media and Metamaterials* (pp. 3–17). Springer Netherlands.

- Simon, H. A. (1997). *The Sciences of the Artificial* (3rd Editio). Cambridge MA: MIT Press.
- Simovski, C. R., & Sauviac, B. (2003). Toward creating isotropic microwave composites with negative refraction. *Radio Science*, 39, 1–23.
- Smith, D. R., Padilla, W. J., Vier, D. C., Nemat-Nasser, S. C., & Schultz, S. (2000). Composite medium with simultaneously negative permeability and permittivity. *Physical Review Letters*, 84(18), 4184–7.
- Smith, D. R., Padilla, W., Vier, D. C., Shelby, R., Nemat-Nasser, S., Kroll, N., & Schultz, S. (2000). Left-Handed Metamaterials. In *NATO-ASI, Photonic Crystals and Light Localization* (pp. 1–21).
- Smith, D. R., & Schultz, S. (2002). Determination of effective permittivity and permeability of metamaterials from reflection and transmission coefficients. *Physical Review B*, 65(19), 195104.
- Smith, D. R., Vier, D. C. D., Koschny, T., & Soukoulis, C. M. (2005). Electromagnetic parameter retrieval from inhomogeneous metamaterials. *Physical Review E*, 71(3), 36617.
- Smith, D. R., Vier, D., & Koschny, T. (2005). Electromagnetic parameter retrieval from inhomogeneous metamaterials. *Physical Review E*, 1–11.
- Speiser, A. (1927). *Die Theorie der Gruppen von endlicher Ordnung – mit Anwendungen auf algebraische Zahlen und Gleichungen sowie auf die Kristallographie* (2nd Edn.). Berlin: Springer.
- Tanaka, M. (2003). Wearable microstrip antenna. In *IEEE Antennas and Propagation Society International Symposium* (Vol. 2, pp. 704–707).
- Tang, W., Argyropoulos, C., Kallos, E., & Hao, Y. (2010). Discrete transformation electromagnetics and its applications in antenna design. In *International Workshop on Antenna Technology (iWAT)* (Vol. 1, pp. 1–4).
- Tang, W., Argyropoulos, C., Kallos, E., Song, W., & Hao, Y. (2010). Discrete coordinate transformation for designing all-dielectric flat antennas. *IEEE Transactions on Antennas and Propagation*, 58(12), 3795–3804.
- Tang, W., Hao, Y., & Mittra, R. (2012). Design of a Carpet Cloak to Conceal an Antenna Located Underneath. *IEEE Transactions on Antennas and Propagation*,

60(9), 4444–4449.

- Tao, H., Amsden, J. J., Strikwerda, A. C., Fan, K., Kaplan, D. L., Zhang, X., Omenetto, F. G. (2010). Metamaterial silk composites at terahertz frequencies. *Advanced Materials (Deerfield Beach, Fla.)*, 22(32), 3527–31.
- Taylor, S., & Robertson, S. (2014). Digital lace: a collision of responsive technologies. In *Proceedings of the 2014 International Symposium for Wearable Technology (ISWC)* (pp. 93–97).
- Tharakan, M. (2011). NeoCraft: Exploring Smart Textiles in the Light of Traditional Textile Crafts. In *Proceedings of Ambience 11*.
- Torrent, D., & Sánchez-Dehesa, J. (2008). Acoustic cloaking in two dimensions: a feasible approach. *New Journal of Physics*, 63015(10).
- Tribe, J., Whittow, W. G., Kay, R. W., & Vardaxoglou, J. C. (2014). Additively manufactured heterogeneous substrates for three-dimensional control of local permittivity. *Electronics Letters*, 50(10), 745–746.
- Tsioris, K., Tao, H., Liu, M., Hopwood, J. A., Kaplan, D. L., Averitt, R. D., & Omenetto, F. G. (2011). Rapid transfer-based micro patterning and dry etching of silk microstructures. *Advanced Materials*, 72(2), 181–204.
- Ung, B. (2009). Metamaterials: a metareview. Retrieved November 6, 2014, from [https://www.researchgate.net/profile/Bora\\_Ung/publication/228706251\\_Metamaterials\\_a\\_metareview/links/0c96053ab831cc8bf9000000.pdf](https://www.researchgate.net/profile/Bora_Ung/publication/228706251_Metamaterials_a_metareview/links/0c96053ab831cc8bf9000000.pdf)
- Urzhumov, Y., Landy, N., Driscoll, T., Basov, D., & Smith, D. R. (2013). Thin low-loss dielectric coatings for free-space cloaking. *Optics Letters*, 38(10), 1606.
- Valentine, J., Zhang, S., Zentgraf, T., Ulin-Avila, E., Genov, D. a, Bartal, G., & Zhang, X. (2008). Three-dimensional optical metamaterial with a negative refractive index. *Nature*, 455(7211), 376–9.
- Veja, P. (2014). *An investigation of integrated woven electronic textiles (e-textiles) via design led processes* (Doctoral thesis, Brunel University London, UK).
- Veselago, V. G. (1968). The electrodynamics of substances with simultaneously negative values of  $\epsilon$  and  $\mu$ . *Physics-Uspekhi*, 10(4).
- Villar, N., Scott, J., Hodges, S., Hammil, K., & Miller, C. (2012). . NET gadgeteer: a

- platform for custom devices. In *Pervasive Computing* (pp. 216–233).
- Walser, R. M. (2001). Electromagnetic Metamaterials. In *Proceedings of SPIE Vol. 4467* (Vol. 4467, pp. 1–15).
- Wang, Z., Volakis, J. L., & Kiourti, A. (2015). Embroidered antennas for communication systems. In *Electronic Textiles* (1st Editio, pp. 201–237). Amsterdam: Elsevier Ltd.
- Wang, Z., Zhang, L., Bayram, Y., & Volakis, J. L. (2011). Multilayer printing of embroidered RF circuits on polymer composites. In *2011 IEEE International Symposium on Antennas and Propagation (APSURSI)* (pp. 278–281). IEEE.
- Weir, W. B. (1974). Automatic measurement of complex dielectric constant and permeability at microwave frequencies. In *Proceedings of the IEEE* (Vol. 62, pp. 33–36).
- Weiser, M. (1991). The Computer for the 21st Century. *Scientific American*, 94–104.
- Whittow, W. G., Chauraya, A., Vardaxoglou, J. C., Li, Y., Torah, R., Yang, K., ... Tudor, J. (2014). Inkjet-printed microstrip patch antennas realized on textile for wearable applications. *IEEE Antennas and Wireless Propagation Letters*, 13, 71–74.
- Worbin, L. (2010). *Designing Dynamic Textile Patterns* (Doctoral thesis, Chalmers University of Technology, Gothenburg, Sweden).
- Yan, S., Vandenbosch, G. a. E., & Soh, P. J. (2014). Wearable dual-band composite right/left-handed waveguide textile antenna for WLAN applications. *Electronics Letters*, 50(6), 424–426.
- Yang, K., Freeman, C., Torah, R., Beeby, S., & Tudor, J. (2014). Screen printed fabric electrode array for wearable functional electrical stimulation. *Sensors and Actuators, A: Physical*, 213, 108–115.
- Zhang, S., & Chauraya, A. (2013). Repeatability of embroidered patch antennas. In *Antennas and Propagation Conference (LAPC)* (pp. 140–144).
- Zhang, S., Chauraya, A., Whittow, W., Seager, R., Acti, T., Dias, T., & Vardaxoglou, Y. (2012). Embroidered wearable antennas using conductive threads with different stitch spacings. In *LAPC 2012 - 2012 Loughborough Antennas and Propagation Conference* (pp. 6–9).

- Zhang, S., Fan, W., Malloy, K. J., Brueck, S. R. J., Panoiu, N. C., & Osgood, R. M. (2006). Demonstration of metal-dielectric negative-index metamaterials with improved performance at optical frequencies. *Journal of the Optical Society of America B*, 23(3), 434--438.
- Zhang, S., Fan, W., Malloy, K. J., Brueck, S. R., Panoiu, N. C., & Osgood, R. M. (2005). Near-infrared double negative metamaterials. *Optics Express*, 13(13), 4922--4930.
- Zhang, S., Fan, W., Panoiu, N. C., Malloy, K. J., Osgood, R. M., & Brueck, S. R. J. (2005). Experimental Demonstration of Near-Infrared Negative-Index Metamaterials. *Physical Review Letters*, 95(13), 137404.
- Zhang, S., Seager, R., Chauraya, A., Whittow, W. G., & Vardaxoglou, J. C. (2014). Textile Manufacturing Techniques in RF Devices. *Loughborough Antennas & Propagation Conference (LAPC)*, (November), 10--11.
- Zhang, S., Seager, R., Chauraya, A., Whittow, W., & Vardaxoglou, Y. C. (2014). Non-uniform meshed embroidered patch antennas. In *2014 USNC-URSI Radio Science Meeting (Joint with AP-S Symposium)*.

# Appendix A

## A.1 Publications

The following conference publications have been made in relation to the work contained in this thesis;

- Greinke, B., Candotti, M., Alomainy, A., & Parini, C. (2013). Parameters Extraction of Three-Dimensional Structures for Graded Textile Cloaking Materials. In *Loughborough Antennas & Propagation Conference (LAPC)* (pp. 7–10). Loughborough, UK.
- Greinke, B., Alomainy, A., & Parini, C. G. (2014). Towards Meta-textiles with a Negative Refractive Index. In *Proceedings of Ambience'14 & 10i3m*. Tampere, Finland.
- Greinke, B., Alomainy, A., & Parini, C. G. (2014). Meta-textiles: An experimental “material-preferential” approach for prototyping electromagnetic periodic textile surfaces. In *Proceedings of Transition: Re-thinking Textiles and Surfaces*. Huddersfield, UK.

Supplementary Poster Presentations and Demonstrations:

- The IET Transformation Optics Seminar, London, UK, 26<sup>th</sup> October 2012
- Digital Fashion Conference, London College of Fashion, 13<sup>th</sup> – 15<sup>th</sup> May 2013
- Innovate UK 2014, London, UK, 5<sup>th</sup> – 6<sup>th</sup> November 2014 (see Figure A.1)
- Wearable Technology 2015, London, UK, 10<sup>th</sup> – 11<sup>th</sup> March 2015

Invited talks

- *Making Holes in Space with Textiles*, 18<sup>th</sup> June 2015, Nottingham Trent University.



- *Materials reborn?*, Saatchi Gallery, London. Organised by the Crafts Council UK in response to the author being shortlisted for Materials Innovation Fellowship 2015 (Arts Foundation).

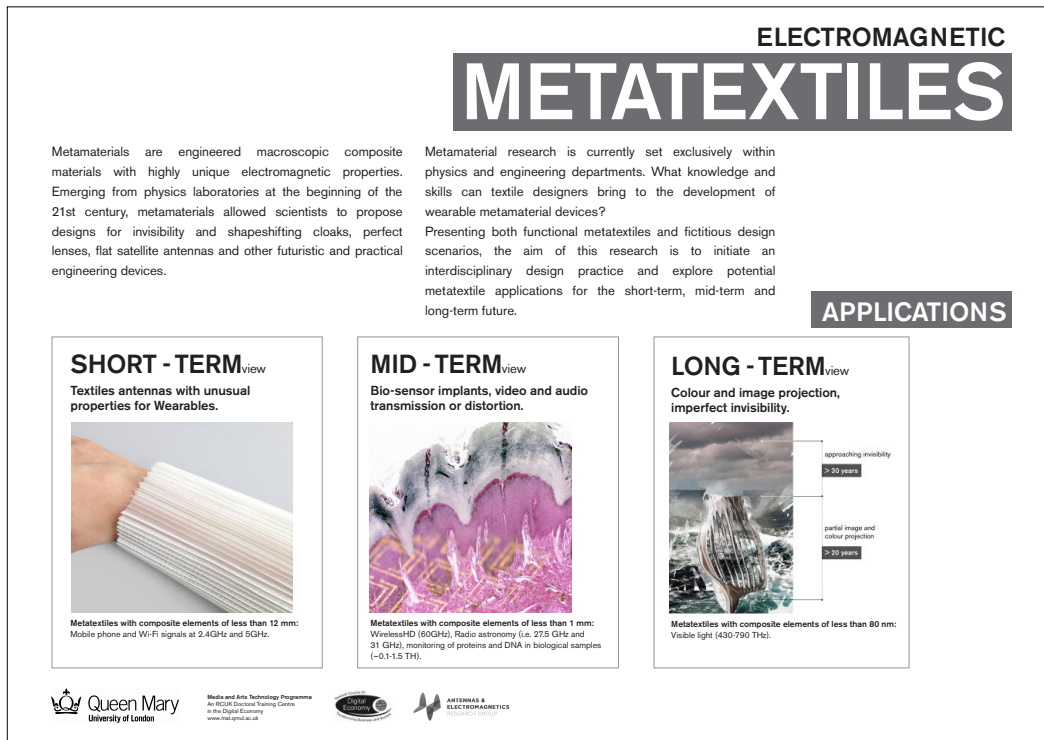


Figure A.1: Poster design for INNOVATE UK annual conference 2014

## A.2 Workshops and Outreach

The author held a range of workshop and outreach activities in the wider field of e-textiles. Although these were not specifically based in the field of electromagnetic textiles, knowledge of materials was transferred and aided the progress of experiments conducted in this work.

- “Thermochromics and Sound”, at Central Saint Martins College of Art and Design (CSM), London, 2012.
- “Paper Orchestra”, ESRC Festival of Social Science, V&A, London, 2012.
- “Sound and Textiles”, School of Art Berlin-Weißensee. Berlin, 2012.

- “CHROME live”, KHiB, Bergen, in collaboration with Bergen Center for Electronic Arts. Bergen, 2012.
- “Paper Orchestra”, ESRC Festival of Social Science, V&A, London, 2012.
- “Soft Circuitry: Bolton at Home”, Bolton, 2013
- “Chameleon Textiles: Thermochromic Inks and Soft Circuitry”, Central Saint Martins College of Art and Design (CSM), London, 2014.
- “Teaching e-textiles and Arduino programming for beginners and intermediate experience”, Codasign Ltd., London, July 2014 – December 2015.

# Appendix B

## B.1 Definitions of Metamaterials

Table B.1: Definitions of term ‘metamaterials’ found in literature

Quote	References
Metamaterials are defined as macroscopic composites having a man-made, three dimensional, periodic cellular architecture designed to produce an optimised combination, not available in nature, of two or more responses to a specific excitation.	(Walser, 2001)
A new class of electromagnetic materials is currently under study: metamaterials, which owe their properties to subwavelength details of structure rather than to their chemical composition, can be designed to have properties difficult or impossible to find in nature	(Pendry et al., 2006)
...New concepts in synthesis and novel fabrication techniques have allowed the construction of structures and composite materials that mimic known material responses or that qualitatively have new, physically realizable response functions that do not occur or may not be readily available in nature. These metamaterials can in principle be synthesized by embedding various constituents/inclusions with novel geometric shapes and forms in some host media.	(Engheta & Ziolkowski, 2006)
... a composite material whose microstructure is artificially designed such that the emerging effective macroscopic response of the structure to a given excitation is not readily encountered in nature.	(Ung, 2009)
The essential property in metamaterials is their unusual and desired qualities that appear due to their particular design and structure. These advantageous properties are not straightforward linear functions of the constituents from which the metamaterial is built up. A sample of metamaterial is more than a sum of its parts, analogously to the taste of ice-cream, which is not a direct sum of the flavors of ice and cream.	(Shivola, 2009)
I think it's a mistake to define metamaterials in terms of properties not found in nature, simply because it's really hard to create things that don't exist in nature. Instead, I think the value of metamaterials is that we can design materials so precisely, we can extend their properties beyond what nature provides easily. I think this might be a better definition.	David Smith <a href="http://www.space.com/28660-forging-metamaterials-for-invisibility-cloaks-and-nanostructures.html">http://www.space.com/28660-forging-metamaterials-for-invisibility-cloaks-and-nanostructures.html</a>
No unique definition for metamaterials can be written down.	(Shivola, 2009)

**Excerpt from interview, conducted by Alan Brown, Kavli Foundation in February 2015<sup>17</sup>**

Interviewees were:

1. **Julia Greer**, professor of Materials Science and Mechanics and board member of the Kavli Nanoscience Institute at California Institute of Technology.
2. **David Smith**, chair of the Department of Electrical and Computer Engineering and director of the Center of Metamaterials and Integrated Plasmonics at Duke University. Smith demonstrated the first optical metamaterials in 2000, and went on to use metamaterials to create an invisibility cloak.
3. **Xiang Zhang**, professor of Mechanical Engineering and member of the Kavli Energy NanoSciences Institute, at the University of California, Berkeley. He is also director of the Materials Sciences Division of the U.S. Department of Energy's Lawrence Berkeley National Laboratory. After developing the first perfect optical lens and pioneering new ways of building nanoscale devices, he developed an acoustic cloak device.

The Kavli Foundation: Some people define metamaterials as materials with structures that do not exist in nature. Is this definition adequate? Does it really capture what makes metamaterials unique?

**Julia Greer:** I don't think so. People have been struggling because there really isn't a good definition. The three of us on this roundtable clearly highlight this: Xiang knows metamaterials that can mask sound, David knows about metamaterials that can manipulate light, and I know metamaterials that have mechanical properties. The very fact that we have to specify the type of metamaterial tells you that any definition is not as simple as saying it's just something that doesn't exist in nature. Many things don't exist in nature.

My spin on it is that metamaterials are materials whose properties deviate from what would be expected from the same atoms if they were repeated in a normal atomic structure. In that case, we might expect its properties to be one thing. But in these so-called artificial grids of atoms, or lattices, that we've created, those properties are different.

**Xiang Zhang:** If you look at the Greek definition of "meta," it means something that goes beyond ordinary. It's important to distinguish between metamaterials and their properties. Metamaterials are indeed built from nature materials. However, they can have properties, such as negative refraction index, that do not exist in nature, and that certainly differ from the parent materials.

Yet this unusual behavior is not limited to just optical or acoustic or structural properties. It could be any property. Their range of properties is very broad.

**David Smith:** I think it's a mistake to define metamaterials in terms of properties not found in nature, simply because it's really hard to create things that don't exist in nature. Instead, I think the value of metamaterials is that we can design materials so precisely, we can extend their properties beyond what nature provides easily. I think this might be a better definition.

A good example is transformation optics, where we change the material's structure to control the wavelengths with which it will interact. These precise, controlled structures enable us to create material properties on demand. There are a lot of ways to accomplish this, but the goal is to obtain precisely the properties you want by creating structures that were either impossible or difficult to achieve before.

---

<sup>17</sup> <http://www.space.com/28660-forging-metamaterials-for-invisibility-cloaks-and-nanostructures.html#sthash.J3WAIh5l.dpuf> accessed 2/4/2016

**J.G.:** May I just add one more thing? I think that the "meta" part emerges when we get into the nanoscale realm. This is when the dimensions within the structure approach the dimensions of whatever energy is exciting it. In photonic metamaterials, for example, the structures are comparable in size to the wavelength of light they interact with. In my mechanical metamaterials, the repeating structures approach the scales of the links that hold the materials together. Whenever the lattice's critical features are small enough to interact with whatever excites it, that's when you start seeing these very interesting effects.

TKF: So are metamaterials all about size?

**J.G.:** It's not only size. For us, it's very much the combination of size, the material, and the material's geometry, its structure. What makes metamaterials unique is that these aspects are not independent of one another anymore.

For example, metamaterials have unique properties because they interact with forces at the nanoscale in ways that we can only explain by using quantum mechanics. If we scaled those structures up to a meter or a kilometer, they would no longer exhibit the same properties. At that size, we could describe their properties using conventional structural engineering and material science.

In a metamaterial, the material, structure, and properties are coupled together in ways that produce unexpected results. Size is a huge component of this, but only because it's linked with material composition and structure.

TKF: Does everyone agree? Must metamaterials be small enough to interact with the waves and energy around them?

**D.S.:** We're really talking about two different regimes. Some of the first work on metamaterials started after we began modifying photonic crystals, which are the optical analogs of semiconductors. The spacing of elements on photonic is typically on the order of the wavelength you want to work with.

In metamaterials, there is another, smaller regime. Roger Walser, who coined the term "metamaterials," thought we could structure magnetic materials in new ways to handle heat better and improve other properties. His idea was to make elements much smaller than the excitations we were trying to manage.

When our group talks about metamaterials, we generally mean elements that are much, much smaller than the wavelengths we want to work with.

**X.Z.:** That is true in our group, as well. Historically, metamaterials referred to materials with repeating periodic building blocks called "unit cells" that were smaller than the wavelength of electromagnetic, acoustic, or other waves we wanted to manipulate. That is still the case for Dave and me. In a sense, we are creating mixtures. But instead of getting properties that reflect the amount of materials we combine randomly, the properties of metamaterials can be very different from simply averaging the properties of the starting materials.

**J.G.:** That's a really good point. There's also another distinction between metamaterials. One type interacts with some type of wave. The wave passes through it, but doesn't damage the metamaterial in any way. Then there are structural metamaterials, where some type of force deforms the material or changes its properties. From a distance, the material looks like any other homogeneous material, but then it exhibits properties that you would never anticipate.

[...]

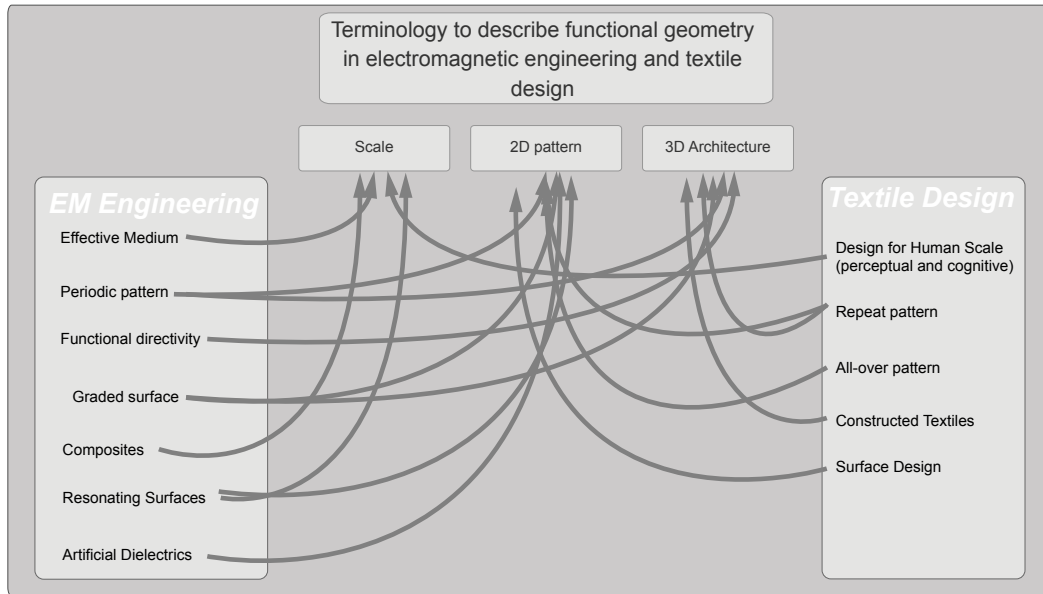


Figure B.1: Geometry of material arrangement in electromagnetic engineering and textile design.

# Appendix C

## C.1 Material Resources

Table C.1: List of material resources

Material	Description	Vendor Details	Section
Polyester/Cotton A4079 (Optic White)	Fabric substrate	Whaleys (Bradford) LTD. Harris Court Great Horton Bradford BD7 4EQ <a href="http://www.whaleys-bradford.ltd.uk/polyester-cotton-a4079-optic-white-see-note-13">http://www.whaleys-bradford.ltd.uk/polyester-cotton-a4079-optic-white-see-note-13</a>	7.3.2, 8.3.1, 8.3.3, 8.3.6, 8.4.2, 8.4.4, 8.5.2
Plain Cotton White (Optic White)	Fabric substrate	Whaleys (Bradford) LTD. Harris Court Great Horton Bradford BD7 4EQ <a href="http://www.whaleys-bradford.ltd.uk/plain-cotton-white-33040">http://www.whaleys-bradford.ltd.uk/plain-cotton-white-33040</a>	7.4.1
Non-woven wool viscose mixed fibre fabric	Fabric substrate	Whaleys (Bradford) LTD. Harris Court Great Horton Bradford BD7 4EQ <a href="http://www.whaleys-bradford.ltd.uk/wool-viscose-felt-white">http://www.whaleys-bradford.ltd.uk/wool-viscose-felt-white</a>	7.3.1
Cream Waterproof Breathable Coated Microfibre	Fabric substrate	UK Fabrics online <a href="http://ukfabricsonline.com">http://ukfabricsonline.com</a>	8.3.2, 8.3.7
Light Grey Technical Outdoor Nylon Fabric	Fabric substrate	UK Fabrics online <a href="http://ukfabricsonline.com">http://ukfabricsonline.com</a>	8.3.2, 8.3.3, 8.3.7

<b>Material</b>	<b>Description</b>	<b>Vendor Details</b>	<b>Section</b>
White Waterproof Cover Fabric	Fabric substrate	UK Fabrics online <a href="http://ukfabricsonline.com">http://ukfabricsonline.com</a>	8.3.2, 8.3.7
Navy Blue Waterproof Coated Polycotton	Fabric substrate	UK Fabrics online <a href="http://ukfabricsonline.com">http://ukfabricsonline.com</a>	8.3.2, 8.3.7
Grey Waterproof Ripstop Coated	Fabric substrate	UK Fabrics online <a href="http://ukfabricsonline.com">http://ukfabricsonline.com</a>	8.3.2, 8.3.7
Air Force Blue Water Repellent Polycotton Chintz	Fabric substrate	UK Fabrics online <a href="http://ukfabricsonline.com">http://ukfabricsonline.com</a>	8.3.2, 8.3.7
Pure copper polyester taffeta  (For datasheet see Figure C.1)	Conductive fabrics	Less EMF Inc. 776B Watervliet Shaker Rd Latham NY 12110 USA <a href="http://www.lessemf.com/fabric4.html">http://www.lessemf.com/fabric4.html</a> - 1212 <a href="http://www.lessemf.com/1212.pdf">http://www.lessemf.com/1212.pdf</a>	Initial tests, see D.1
SaniSilverTM  (For datasheet see Figure C.2)	Conductive fabrics	Less EMF Inc. 776B Watervliet Shaker Rd Latham NY 12110 USA <a href="http://www.lessemf.com/fabric2.html">http://www.lessemf.com/fabric2.html</a> - 1229	8.3.5, 8.4.3
Matt smooth and lightweight card	Paper and films	Ryman Ltd Ryman House Savoy Rd Crewe Cheshire CW1 6NA <a href="http://www.ryman.co.uk/ryman-card-a4-200gsm-100-sheets">http://www.ryman.co.uk/ryman-card-a4-200gsm-100-sheets</a>	7.5.1



<b>Material</b>	<b>Description</b>	<b>Vendor Details</b>	<b>Section</b>
2043b paper	Paper and films	Hahnemühle UK Suite 5, St. Mary's Court Carelton Forehoe Norwich NR9 4AL <a href="http://www.hahnemuehle.com/en/filtration/lab-filtration/filter-paper/specialty-papers/chromatography.html">http://www.hahnemuehle.com/en/filtration/lab-filtration/filter-paper/specialty-papers/chromatography.html</a>	Initial tests, see D.1
NB-TP-3GU100  (For datasheet see Figure C.3)	Paper and films	Mitsubishi HiTec Paper Europe GmbH Werk Flensburg Husumer Str. 12 24941 Flensburg <a href="http://www.kmpm.com/agnanoen/agnano_ink.html">http://www.kmpm.com/agnanoen/agnano_ink.html</a>	Initial tests, see D.1
Heat'n Bond Lite	Adhesive and stabiliser fabrics	Therm'o Web Online 770 Glenn Avenue Wheeling, IL 60090 US <a href="http://www.thermowebonline.com/p/he atnbond-ez-print-lite-•-8-5x11">http://www.thermowebonline.com/p/he atnbond-ez-print-lite-•-8-5x11</a>	All pleated samples
Sulky	Embroidery threads	Gunold GmbH Oberburger Str. 125 63811 Stockstadt (Deutschland) <a href="http://www.gunold.de/Produkte/Obergarne/103">http://www.gunold.de/Produkte/Obergarne/103</a>	7.3.2
Classic Rayon No. 40	Embroidery threads	Madeira 12 Hallikeld Close Barker Business Park Melmerby Ripon North Yorkshire HG4 5GZ <a href="http://en.madeira.de/threads/classic-rayon-viscose/en-classic-no-40/">http://en.madeira.de/threads/classic-rayon-viscose/en-classic-no-40/</a>	8.5.2

<b>Material</b>	<b>Description</b>	<b>Vendor Details</b>	<b>Section</b>
234/34 4-ply  (For datasheet see Figure C.4)	Conductive embroidery threads	Statex Produktions & Vertriebs GmbH Kleiner Ort 11 28357 Bremen <a href="http://statex.de/index.php/en/fibres-and-yarns/item/153-shieldex@-garne">http://statex.de/index.php/en/fibres-and-yarns/item/153-shieldex@-garne</a>	8.3.6, 8.4.4,
Liberator™  (For datasheet see Figure C.5)	Conductive embroidery threads	Syscom Advanced Materials 1305 Kinnear Rd Columbus OH 43212 US <a href="http://www.metalcladfibers.com/liberator/">http://www.metalcladfibers.com/liberator/</a>	8.4.4 8.5.2
AquaScreen Opaque White (AS 150)	Dielectric printing inks	Screen Colour Systems Unit C, 19 Deer Park Road, South Wimbledon, SW19 3UX <a href="http://www.screencoloursystems.co.uk/atextile3.html">http://www.screencoloursystems.co.uk/atextile3.html</a> - AB100	Initial tests, see D.1
Qprint White RT	Dielectric printing inks	Quality Colours (London) Ltd 4c Juno Way LONDON SE14 <a href="http://static.premiersite.co.uk/1564/docs/4159820_1.pdf">http://static.premiersite.co.uk/1564/docs/4159820_1.pdf</a>	Initial tests, see D.1
Linocut Titanium White	Dielectric printing inks	H. Schmincke & Co.-GmbH & Co.KG Otto-Hahn-Straße 2 D-40699 Erkrath <a href="http://www.schmincke.de/produkte/linoldruckfarben.html?L=1">http://www.schmincke.de/produkte/linoldruckfarben.html?L=1</a>	7.4.1, 8.4.2, 8.4.3, 8.4.4, 8.5.2, 8.5.3, some initial samples shown in D.1
BT-101  (For datasheet see Figure C.6)	Dielectric printing inks	Conductive Compounds, Inc. 17 Hampshire Drive Unit 8 Hudson, NH 03051 <a href="http://www.conductivecompounds.com">http://www.conductivecompounds.com</a>	7.5.1

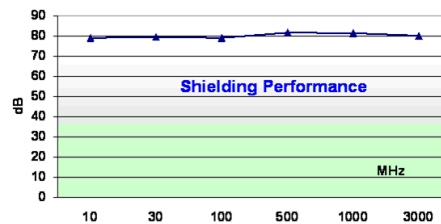
<b>Material</b>	<b>Description</b>	<b>Vendor Details</b>	<b>Section</b>
CuPro-Cote™  (For datasheet see Figure C.7)	Conductive printing inks	Less EMF Inc. 776B Watervliet Shaker Rd Latham NY 12110 US <a href="http://www.lessemf.com">http://www.lessemf.com</a>	8.3.1, 8.4.2
NBSIJ-MU01  (For datasheet see Figure C.8)	Conductive printing inks	Mitsubishi HiTec Paper Europe GmbH Werk Flensburg Husumer Str. 12 24941 Flensburg <a href="http://www.k-mpm.com/agnanoen/agnano_ink.html">http://www.k-mpm.com/agnanoen/agnano_ink.html</a>	Initial tests, see D.1

## C.2 Datasheets

### **PURE COPPER POLYESTER TAFFETA FABRIC** (Compare to Flectron®)



Shiny, smooth fabric with pure copper. Light weight and flexible. Easy to cut and sew like ordinary fabric. Better color stability due to tarnish resistant finish. High conductivity and shielding performance. Use it for drapes, wall covering, garments, pouches and more. Great price too!



Width: 1080 mm (42.5 inch)  
Thickness: 0.08mm (3 mil)  
Weight: 80 g/m<sup>2</sup> (about 35% Copper)  
Surface Resistivity: 0.05 Ohm/sq.

#### **Pure Copper Polyester Taffeta Fabric (Cat. #1212)**

*Available from:*  
*Less EMF Inc*  
*+1-518-608-6479*  
[www.lessemf.com](http://www.lessemf.com)

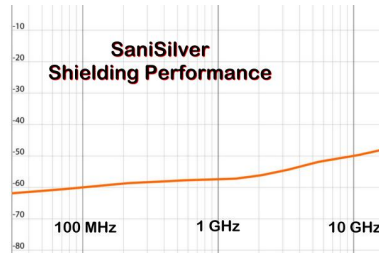
Figure C.1: Pure Copper Polyester Taffeta Fabric (LessEMF)

## SaniSilver™

*One-sided Pure Cotton, other is Conductive Silver*

Like soft? Like the idea of cotton against your skin? SaniSilver is a reversible fabric- one side is highly conductive (<1 Ohm per sq) pure Silver, the other side is pure cotton (~100 Ohm/sq). Nice to touch. About 55 dB shielding for common RF frequencies, and groundable.

Great for drapes, bedding, grounding and clothing. Use multiple layers to increase shielding! Easy to cut and sew. Use it facing either way. One side is gray/silver, the other side is light tan. Weight: 164g/m<sup>2</sup>. 59 inch wide



### **Washing Instructions:**

- 1) Softly wash by hand, with neutral detergent such as TexCare (Don't use any strongly alkaline detergent such as washing powder).\*\*
- 2) Water temperature below 40°C.
- 3) No bleach, do not use detergent with bleach ingredients.
- 4) Hang dry. Do not wring, do not hang in blazing sun for a long time, and pick up promptly from the water to dry.
- 5) Do not dry clean.

\*\* Poor water quality will damage Silver. In particular Sulphur, high Fluoride, and low pH will react strongly with Silver and destroy conductivity and shielding performance.

Test your tap water on a small fabric swatch before washing your fabric or garment:

- 1- soak a small fabric swatch in tap water for 1 hour.
- 2- look for color change in the water or swatch, especially blackening.
- 3- air dry the swatch and check for conductivity (by touching an Ohm meter to 2 points on the fabric)

If color change or loss of conductivity occurs, DO NOT use tap water to wash/rinse your fabric, use distilled or deionized, reverse osmosis water.

*Washing will eventually degrade Silver coating and shielding performance. Discoloration over time is normal. Fabric will conduct electricity. Keep away from electrical sockets and bare wires.*

### ***Available from:***

Less EMF Inc. "The EMF Safety SuperStore"  
776B Watervliet Shaker Rd Latham NY 12110-2209 USA  
[www.lessemf.com](http://www.lessemf.com)

Figure C.2: Datasheet SaniSilver™ Fabric (LessEMF)



**Mitsubishi Nano Benefit Series  
NB-TP-3GU100**

- Product:** NB-TP-3GU100 is single side coated transparency PET film that is used for inkjet printing of water-based silver nanoparticle ink.
- Benefits:** Quick drying and immediate conductivity.  
Good resistivity against bent and scratch.  
Good adhesion of the pattern.  
Photographic images can be printed with conductive patterns.

Physical properties	Result	Unit	Standard
Basic weight	175 ± 10	g/m <sup>2</sup>	ISO 536
Paper thickness	135 ± 12	μm	JIS P-8118
Tensile strength MD	1400 ± 300	Kgf/cm <sup>2</sup>	ISO527
Yield strength MD	1400 ± 300	Kgf/cm <sup>2</sup>	ISO527
Ultimate elongation MD	120 ± 20	%	ISO527
Young's modulus MD	3400 ± 500	MPa	ISO527
Coefficient of friction kinetic	0.55±0.20	-	ISO8295
The adhesion of silver patterns	0-1	Grade	JIS K 5600-5-6 (with reference ink)
Shrinkage MD	<0.5	%	30 min. at 125°C
TD	<0.5		

Available

Format	Size
Sheet	T.B.D.
Roll	17" x 100' (3" core diameter)

The above mentioned data represents recommended value. Changes in the product design due to technical further developments will not be announced in advance.

Version: Dec. 2011

Figure C.3: Datasheet NB-TP-3GU100 PET film (Mitsubishi)

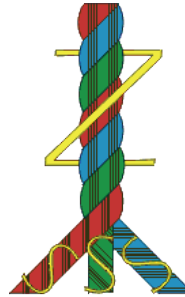


# Technical Data Sheet

PN# 20012123535HCB

## Shieldex® Conductive Twisted Yarn Silver Plated Nylon 66 Yarn 235/34 dtex 4-ply

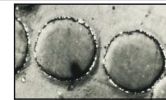
- **Purpose:** anti-microbial applications for garments, smart textiles, and sewing thread
- **Description:** 99% pure Silver plated Nylon yarn 1160/132 dtex
- **Liner Resistance:** < 50Ω/M
- **Yield:** 6,400 M/Kg
- **Tenacity:** Average 37 cN/tex
- **Elongation:** abt. 27%
- **Denier:** 520/68f (S 500 400 tpm Z)
- **Melt Point (F):** 492



### Package Properties

**Core Type:** 3 Deg-30 Min Cone 9"  
**Core Material:** Pressed Paper or plastic  
**Product ID Color:** Gray  
**Package Weight:** 0.1 LB Nominal  
**Package Weight Control:** +/- .1 lb. within single case

Cross section views of nylon fiber showing silver deposits



### Accreditations:

**RoHS:** Compliant  
**Reach:** Compliant  
**Acc. ISO 9001:2000**



*A Woman's Owned Small Business*

**VTT/Shieldex Trading USA**  
4502 Rt-31 Palmyra, NY, 14522

**Phone:** 315-597-1674  
**Fax:** 315-597-6687  
**Email:** whoge@rochester.rr.com  
**www.shieldextrading.net**

Statex Productions & Vertriebs GmbH  
Kleiner Ort 11 28357 Bremen Germany  
Tel: +49 421 275047/8, Fax: +49 421 273643  
info@statex.de

  
© 2012 VTT  
Rev 1.20.12

Figure C.4: Datasheet Silver coated thread 234/34 4-ply (Statex)

**Liberator™** fiber is one of **Syscom Advanced Materials'** novel conductive metal-clad fibers. By pairing a light-weight, flexible, and high-strength **Vectran®** fiber core with a conductive metal outer layer, **Liberator™** fiber gives freedom to design and manufacture outside the constraints of traditional wires. Designed to have excellent thermal stability, strength, and cut resistance, **Liberator™** fiber is optimized for use as a shielding braid, bare wire, or coated with insulation material.

### LIBERATOR™ 40

Fiber	Kururay Vectran®
Structure	Liquid Crystal Polymer (LCP)
Filament count	40
Outer Metallization Layers Available	Copper/Nickel/Silver
Yarn Diameter*	0.0070 in
Flat Width**	0.0219 in
% Metal by Weight	82.10%
Weight	0.0849 lbs/1,000 ft
Weight	0.0385 g/ft
DC Resistance	~1 Ω/ft
Breaking Load	11.42 lbs
Tensile Strength	3.0 GPa
Operating Temperature	Up to 200 °C
Melting point	350 °C

\* Ideal close-packed calculated diameter

\*\* Width of material as it lays in a braiding configuration

The data presented here is provided only as a guide and is based on internal and/or external testing of samples of standard production runs of **Liberator™** Fiber. Please contact Syscom Advanced Materials for additional property data or customization options.

### PROPERTIES

- 72% lighter in weight than 30 AWG (stranded 40/46 Type C) copper wire
- Superior coverage results in up to 90% total weight savings in aerospace applications
- 5 times greater break strength than 30 AWG (stranded 40/46) copper wire
- Can be soldered or crimped
- Compatible with metal wire braiding equipment
- Supplied twisted or untwisted on braider bobbins
  - 1.7 twists/inch (TPI): Braiding Applications
  - 4.5 twists/inch (TPI): Sewing Applications

**Liberator™** metal clad fiber has excellent thermal stability, strength, cut resistance, and tailored electrical conductivity. **Liberator™** fiber utilizes **Vectran®** fiber and is available in 40 and 80 filaments metalized with nickel, copper or silver cladding.

1305 Kinnear Rd.  
Columbus, OH 43212  
614.487.3626  
[www.metalcladfibers.com](http://www.metalcladfibers.com)

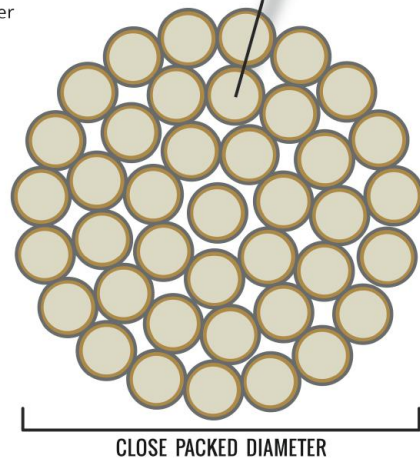
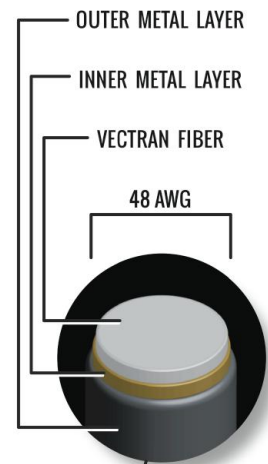


Figure C.5: Datasheet Liberator 40 (Syscom Advanced Materials)



TECHNICAL DATA SHEET

**BT-101 BARIUM TITANATE DIELECTRIC**  
*a capacitive dielectric*

BT-101 is suitable for use as a **capacitance layer between phosphor and back electrodes on EL lamps**

**DESCRIPTION**

- Provides excellent electrical insulation while maintaining a high dielectric constant to optimize the performance of EL lamps
- Suitable for screen print applications, and is designed to provide an optimal balance between long open time on screens and fast drying in conventional ovens
- Offers outstanding moisture resistance when dried completely
- Suitable for use on polyester films and ITO substrates
- Compatible with our conductive materials for EL electrodes

**TYPICAL PROPERTIES**

Appearance	Thick white ink
% Solids	67% ± 2%
Viscosity: Brookfield DV III SC4-14 spindle @ 25°C, Shear 2	10,000 cps +/- 10%
Hegman Gauge	<10 µm
Drying Conditions	90 seconds to 6 minutes at 130°C (depending upon air flow)

**PHYSICAL PROPERTIES AFTER CURE**

Voltage Breakdown (VAC, 25µm, 25°C) Ref ASTM D149-97a	> 500 volts
Dielectric Constant (Approximate, 25°C) Ref ASTM D-150	35 to 40
Volume Resistivity Ref ASTM D-257	> 1 x 10 <sup>14</sup> Ω-cm

Figure C.6: Datasheet BT-101 (Conductive Compounds)

# CuPro-Cote™

## Water-Based High-Conductivity Shielding Coating



This is a sprayable, brushable, or rollable conductive metallic coating using a specially formulated, **tarnish resistant copper** as the conductive agent for superior performance in electric field and RF shielding. Developed initially as an RFI/EMI shield for plastic electronic equipment housings, it can be applied directly onto acrylic, ABS and structural foams, as well as solvent sensitive materials such as polycarbonate and polystyrene. Can also be applied to other non-porous surfaces including primed wallboard, wood and clean metals after priming. Can be applied by sprayer, brush or roller just like ordinary latex paint! Thin with water. Good surface resistivity of 5 ohm/sq at 1 mil dry film thickness. Attenuation: more than 75 dB from 1 MHz to 1 GHz. Covers 670 ft<sup>2</sup> per gallon per mil thickness if application is 100% efficient (typically 400 ft<sup>2</sup> per gallon when applied by roller). Can be used indoors or out, but you must topcoat with a weather protective paint if the material will be exposed to the elements. Color = Glitter Copper, but you can paint over with ordinary latex paint to achieve desired aesthetics. VOC: 1.0 ± 0.1 lbs/gallon (120.0 ± 12 grams/liter), has some ammonia smell (use good ventilation), but uses a water base.

*Important note about conductive paint and the National Electric Code:*

The is nothing in the NEC which prohibits painting your walls with conductive paint. However, because this product does NOT carry a UL listing, some electrical inspectors, by virtue of being the "Authority Having Jurisdiction" can require the homeowner to hire an electrical engineer to certify that the product is safe to connect to the electrical ground. They can also require that a licensed electrician perform the ground connection. If your application requires an electrical inspection AFTER installation, you should check with your local inspector BEFORE you proceed to avoid any surprises.

Supplied in 4 sizes.

Cat. #292-5G ... 5 Gallon      Cat. #292-G ... gallon      Cat. #292-Q... quart      Cat. #292-4...4 oz

Available Exclusively from:

**Less EMF Inc.**

776B Watervliet Shaker Rd Latham NY 12110-2209 USA +1 (518) 608-6479

### Specifications

<b>SYSTEM:</b>	one component, air dry, water base
<b>SOLIDS:</b>	47 ±3% by weight
<b>PARTICLE SIZE:</b>	33-38 microns
<b>VOC:</b>	1 ± 0.1 lb per gallon as packed
<b>THINNER:</b>	reduce to desired viscosity with water (approx 4:1) for spray application, no dilution for brush/roller application
<b>PRIMER:</b>	use standard latex primer on any absorbent or metallic surface, do not use primer OVER CuPro-Cote
<b>APPLICATION METHOD:</b>	standard air gun with pressure pot with agitation to keep copper in suspension, brush, or roller. <b>MIX WELL BEFORE AND DURING USE!</b>
<b>DRYING TIME:</b>	air dry, OR flash off for 5 minutes at room temp then dry for ½ hour at 160°F
<b>ADHESION:</b>	excellent to most plastic surfaces
<b>HUMIDITY RESISTANCE:</b>	no change in resistivity or attenuation when tested in accordance with MIL-STD-202 Method 106 - 40 cycles: MIL-STD-810 Method 507 Procedure 5 - 48 hours cycling: meets UL specification 746-C
<b>SURFACE RESISTIVITY:</b>	<5 Ω/sq at 1 mil dry film thickness
<b>ATTENUATION:</b>	more than 75 dB from 1 MHz to 1 GHz
<b>COVERAGE:</b>	670 ft <sup>2</sup> /gallon per mil at 100% efficiency
<b>STORAGE LIFE:</b>	6 months from date of shipment in unopened container. Older material should be checked for surface resistivity before using. Protect from freezing.

**Application notes:** Clean-up is simple with warm soapy water. Dry coating is soluble in basic solution. To improve abrasion resistance, paint over with ordinary latex paint after completely dry, in any desired color. For outdoor applications, you must paint over with exterior grade latex paint. Use ordinary latex primer when indicated.

Proper grounding improves shielding effectiveness. One simple way to ground the paint is to coat a suitable area and allow to dry, then attach a properly grounded metalized tape with conductive adhesive in an inconspicuous area such as along a corner of the room or enclosure. Then simply paint right over the conductive tape, making good paint contact between the painted surface and conductive tape. Thicker application does not necessarily provide better performance as copper particles may settle during drying.

Figure C.7: Datasheet CuPro-Cote™ (LessEMF)

**Mitsubishi Nano Benefit Series  
NBSIJ-MU01 (Silver Nano Particle Ink)**

**Product:** NBSIJ-MU01 is the waterborne silver nanoparticle ink for inkjet printing.

**Benefits:** Optimized for Mitsubishi Nano Benefit Series Special Media.

Suitable for major inkjet heads.

Physical properties	Result	Unit	Standard
Silver concentration	15	wt%	-
Viscosity	2.30 ± 0.50	mPa · s	JIS K 7117-2 at 25°C
Surface Tension	32.0 ± 2.0	mN/m	Wilhelmy plate method
Density	1.200 ± 0.020	g/mL	JIS B 7525
Pattern Conductivity	0.1-0.2	Ohm/sq.	apply 20-30mL/m <sup>2</sup> for our media
Stability	6	month	store at 0-8 degC

Inkjet Printing on Mitsubishi Nano Benefit Series Special Media

- Please filter the ink with proper syringe filters (5.0 microns pore size recommended) prior to use for better jetting performance.
- Conductivity of patterns depends on humidity of printing environment. 20 degC and >40%RH is recommended. If color of patterns does not change from silver into gold-like color after printing, printing environment may be too dry.



- If color of patterns is dark metallic like below, this is the sign of ink overflowing and the conductivity of pattern may become poor.



Ink Storage Information

- Please store the ink in a refrigerator (0 to 8 degC). Excessive exposure to light and high temperature environment (>50 degC) should be avoided. Shaking is recommended prior to use.

The above mentioned data represents recommended value. Changes in the product design due to technical further developments will not be announced in advance.

Version: Jun. 2012

Figure C.8: Datasheet Silver Nano Particle Ink (Mitsubishi)

# Appendix D

## D.1 Index of Samples

Table D.1: Index of produced samples that utilise conductive materials.

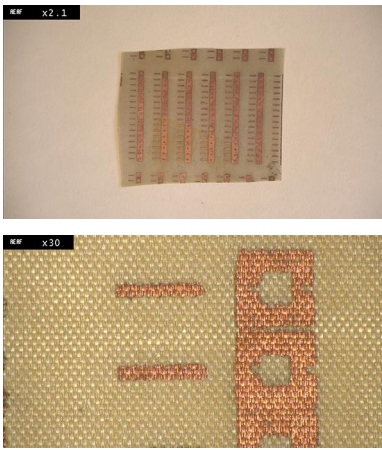
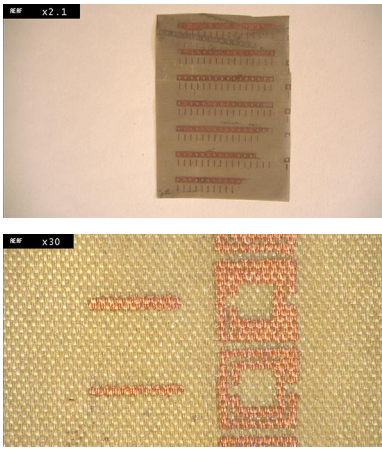
Photo	Main Technique	Intended Use	Notes
 <p>Pure copper polyester taffeta (for datasheet see Figure C.1)</p>	Chemical etching of copper fabric. Mask screen printed with petroleum jelly.	NIMs	Several strokes of printing were applied to achieve a thick layer of resist. The SRR structure was too blurred after etching.
 <p>Pure copper polyester taffeta (for datasheet see Figure C.1)</p>	Chemical etching of copper fabric. Mask screen printed with petroleum jelly.	NIMs	One stroke of printing was applied to achieve a clear image. The SRR structure was not sufficiently conductive after etching.

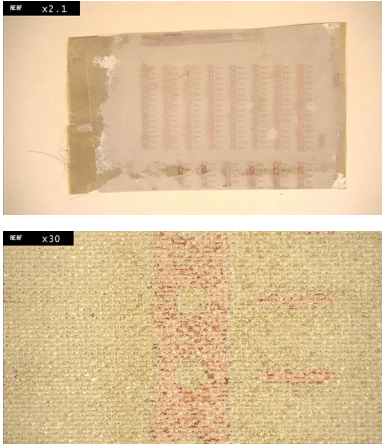
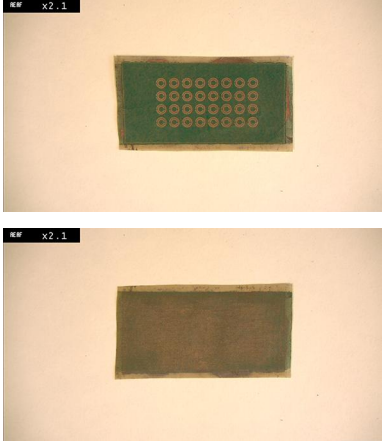
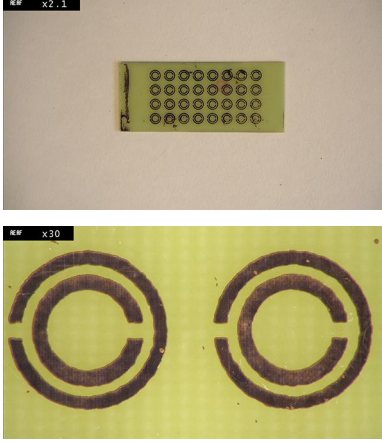
Photo	Main Technique	Intended Use	Notes
 <p data-bbox="316 775 678 837">Pure copper polyester taffeta (for datasheet see Figure C.1)</p>	<p data-bbox="715 315 879 468">Screen printing TiO<sub>2</sub> ink onto etched copper fabric.</p>	<p data-bbox="901 315 970 344">NIMs</p>	<p data-bbox="1085 315 1321 499">One layer of printing TiO<sub>2</sub> ink onto the sample did not sufficiently or evenly covers the textile surface.</p>
 <p data-bbox="316 1346 678 1408">Pure copper polyester taffeta (for datasheet see Figure C.1)</p>	<p data-bbox="715 887 874 1160">Copper fabric coated on single side with photo-sensitive emulsion, commonly used for PCBs.</p>	<p data-bbox="901 887 970 916">NIMs</p>	<p data-bbox="1085 887 1353 1070">The photosensitive emulsion did not penetrate the fabric. Fabric was etched from both sides, with no clear image being etched.</p>
 <p data-bbox="316 1917 598 1946">FR-4, single-sided copper</p>	<p data-bbox="715 1458 879 1760">Copper coated FR-4 PCB coated on single side with photo-sensitive emulsion, commonly used for PCBs.</p>	<p data-bbox="901 1458 970 1487">NIMs</p>	<p data-bbox="1085 1458 1345 1610">Test of FR-4 for comparison with textile samples. Clear image resulted from etching process.</p>

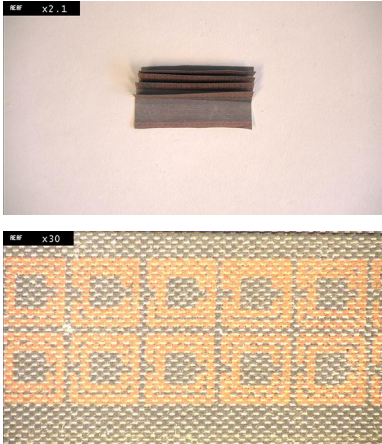
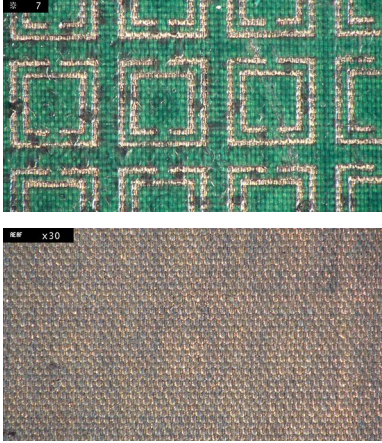
Photo	Main Technique	Intended Use	Notes
 <p data-bbox="316 779 678 835">Pure copper polyester taffeta (for datasheet see Figure C.1)</p>	<p data-bbox="715 320 874 533">Chemical etching of copper fabric. Mask screen printed with petroleum jelly.</p>	<p data-bbox="900 320 970 342">NIMs</p>	<p data-bbox="1082 320 1345 622">Two strokes of printing were applied to achieve a thicker layer of resist. The SRR structure was slightly blurred after etching. Sample was used to test folding mechanism. The folds were fixed with iron-on fabric.</p>
 <p data-bbox="316 1350 678 1406">Pure copper polyester taffeta (for datasheet see Figure C.1)</p>	<p data-bbox="715 891 874 1160">Copper fabric coated on single side with photo-sensitive emulsion, commonly used for PCBs.</p>	<p data-bbox="900 891 970 913">NIMs</p>	<p data-bbox="1082 891 1305 981">The photosensitive emulsion did not penetrate the fabric.</p>

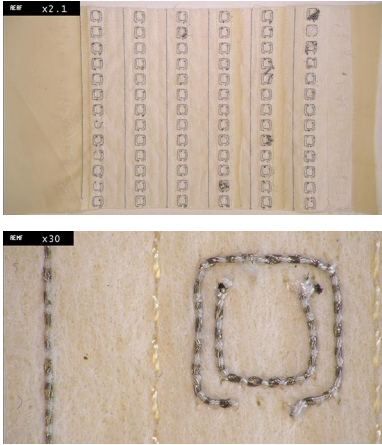
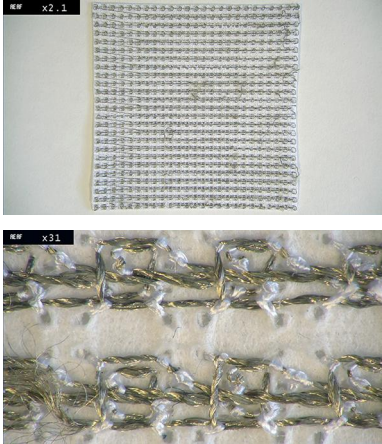
Photo	Main Technique	Intended Use	Notes
 <p data-bbox="316 775 679 913">Statex silver thread 234/34 4-ply on Cream Waterproof Breathable Coated Microfibre (For datasheet see Figure C.4)</p>	Embroidery with Brother Innovis-1500D machine	NIMs	Embroidery worked well due to the smooth surface of the fabric. Folding was unsuccessful, as fabric did not pleat permanently.
 <p data-bbox="316 1404 671 1512">Statex silver thread 234/34 4-ply on Viscose Felt (For datasheet see Figure C.4)</p>	Embroidery with Brother Innovis-1500D machine	NIMs	Testing of small structures (outer SRR 5mm), with double rings. Not possible to structure the embroidery in a way that overlaps could be cut off afterwards. Thread tension resulted in inconsistent SRR geometry.

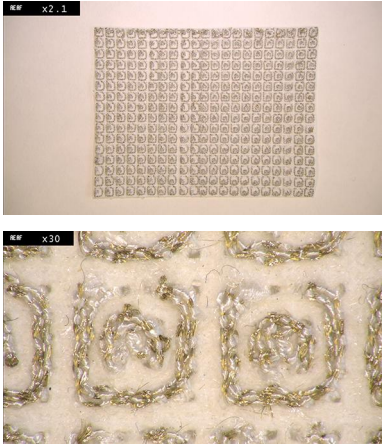
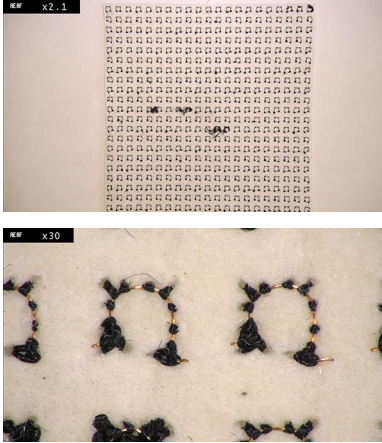
Photo	Main Technique	Intended Use	Notes
 <p data-bbox="316 775 671 882">Statex silver thread 234/34 4-ply on Viscose Felt (For datasheet see Figure C.4)</p>	<p data-bbox="715 315 863 465">Embroidery with Brother Innovis- 1500D machine</p>	<p data-bbox="898 315 970 342">NIMs</p>	<p data-bbox="1082 315 1353 775">Sample produced to test if double-stitched SRRs would maintain their form (outer SRR c. 8mm), with double rings. While the outer SRR maintained shape, the inner SRRs were too small and formed a closed conductive ring structure. Over the sample, outer and inner SRRs did not match as tension shortened the sample.</p>
 <p data-bbox="316 1375 544 1402">Wire on Viscose Felt</p>	<p data-bbox="715 916 863 1066">Embroidery with Brother Innovis- 1500D machine</p>	<p data-bbox="898 916 970 943">NIMs</p>	<p data-bbox="1082 916 1353 1249">Embroidery test with thin wire (outer SRR c.5mm). While the form was maintained, it was not possible to achieve narrower gaps between SRRs due to tension caused by the wire. Gaps were too large to render the sample useful.</p>



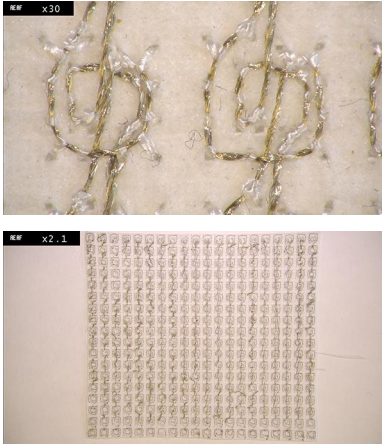
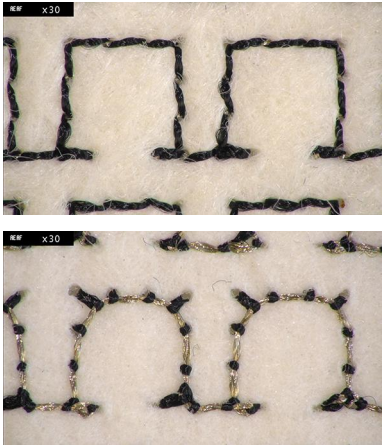
Photo	Main Technique	Intended Use	Notes
 <p data-bbox="316 775 671 882">Statex silver thread 234/34 4-ply on Viscose Felt (For datasheet see Figure C.4)</p>	<p data-bbox="715 320 863 472">Embroidery with Brother Innovis- 1500D machine</p>	<p data-bbox="900 320 970 349">NIMs</p>	<p data-bbox="1082 320 1342 443">Testing the direction of stitching, to facilitate later separation of elements.</p>
 <p data-bbox="316 1373 671 1480">Statex silver thread 234/34 4-ply on Viscose Felt (For datasheet see Figure C.4)</p>	<p data-bbox="715 920 863 1072">Embroidery with Brother Innovis- 1500D machine</p>	<p data-bbox="900 920 970 949">NIMs</p>	<p data-bbox="1082 920 1342 1285">Testing thread tension. Image on top shows the front side, using Madeira No. 40 Rayon thread. Bottom thread is Statex silver thread. SRR size is c.9mm. Shape geometry is not as sharp as on the front, however tension is equal over complete sample.</p>

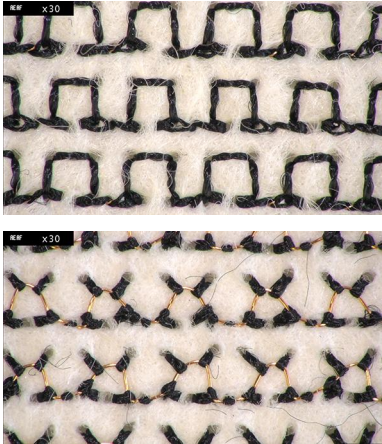
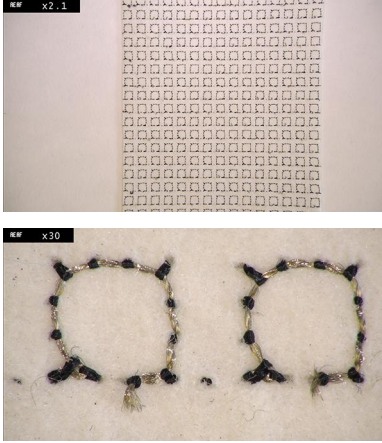
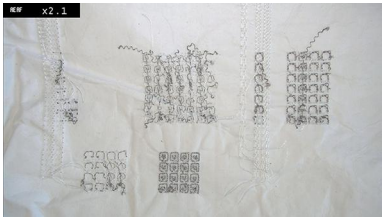
Photo	Main Technique	Intended Use	Notes
 <p data-bbox="316 775 547 801">Wire on Viscose Felt</p>	<p data-bbox="719 315 863 465">Embroidery with Brother Innovis-1500D machine</p>	<p data-bbox="904 315 970 342">NIMs</p>	<p data-bbox="1086 315 1353 680">Testing thread tension. First image on top shows the front, using Madeira No. 40 Rayon thread. Bottom thread is thin copper wire. SRR size is c.6mm. Shape geometry is not as sharp as on the reverse, and wire not sufficiently fixed when elements are separated.</p>
 <p data-bbox="316 1346 671 1406">Statex silver thread 234/34 4-ply on Viscose Felt</p> <p data-bbox="316 1424 651 1451">(For datasheet see Figure C.4)</p>	<p data-bbox="719 887 863 1037">Embroidery with Brother Innovis-1500D machine</p>	<p data-bbox="904 887 970 913">NIMs</p>	<p data-bbox="1086 887 1310 976">Embroidery worked well, single ring was large with c.9mm.</p>
 <p data-bbox="316 1718 671 1778">Statex silver thread 234/34 4-ply on Polycotton</p> <p data-bbox="316 1796 651 1823">(For datasheet see Figure C.4)</p>	<p data-bbox="719 1482 863 1632">Embroidery with Brother Innovis-1500D machine</p>	<p data-bbox="904 1482 970 1509">NIMs</p>	<p data-bbox="1086 1482 1302 1603">Various tests to investigate possible sizes, shapes and formations.</p>

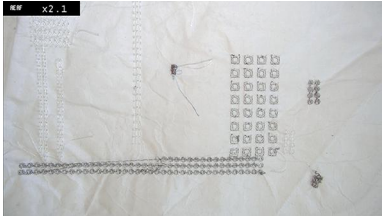
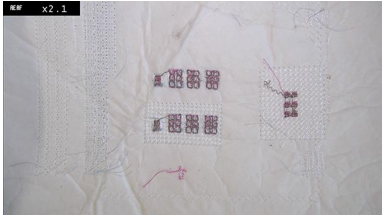
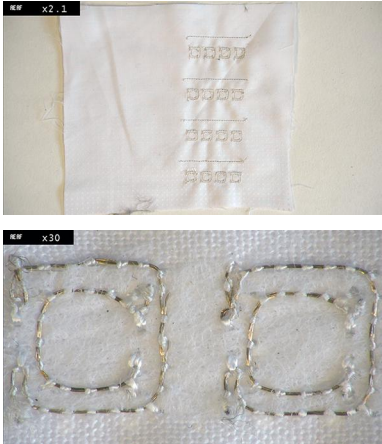
Photo	Main Technique	Intended Use	Notes
 <p>Statex silver thread 234/34 4-ply on Polycotton (For datasheet see Figure C.4)</p>	Embroidery with Brother Innovis-1500D machine	NIMs	Various tests to investigate possible sizes, shapes and formations.
 <p>Statex silver thread 234/34 4-ply on Polycotton (For datasheet see Figure C.4)</p>	Embroidery with Brother Innovis-1500D machine	NIMs	Testing if a double-ring shape could be separated by non-conductive thread. Resulted in very dense embroidery and overlapping of conductive and non-conductive threads.
 <p>Liberator™ thread on polycotton (for datasheet see Figure C.5).</p>	Embroidery with Brother Innovis-1500D machine	NIMs	First successfully embroidered sample using Liberator thread. Outer SRR c.9mm.

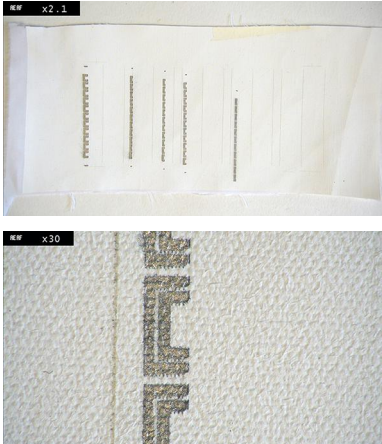

Photo	Main Technique	Intended Use	Notes
 <p data-bbox="316 775 687 864">Silver nano fluid inkjet printed on cotton, which was previously screen printed with TiO<sub>2</sub> ink</p>	<p data-bbox="715 315 863 465">Inkjet nano-silver with Dimatix Materials Printer DMP</p>	<p data-bbox="901 315 970 342">NIMs</p>	<p data-bbox="1085 315 1326 465">The nano ink was absorbed by the substrate, resulting in both a blurred image and non-conductivity.</p>
 <p data-bbox="316 1357 687 1447">Silver nano fluid inkjet printed on cotton, which was previously screen printed with TiO<sub>2</sub> ink</p>	<p data-bbox="715 898 863 1048">Inkjet nano-silver with Dimatix Materials Printer DMP</p>	<p data-bbox="901 898 970 925">NIMs</p>	<p data-bbox="1085 898 1353 1025">More production resulted in sharper images. No conductivity was achieved.</p>

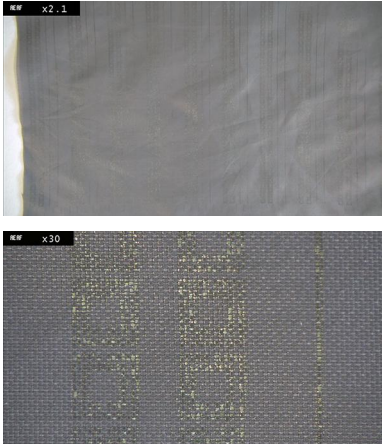
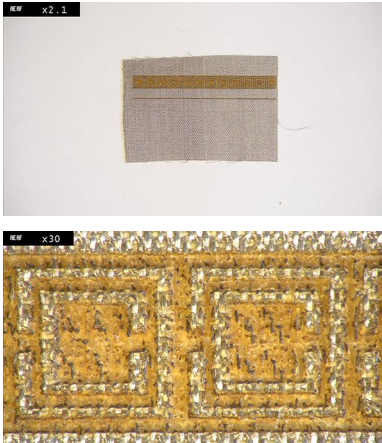
Photo	Main Technique	Intended Use	Notes
 <p data-bbox="316 775 699 864">Silver nano fluid inkjet printed on Light Grey Technical Outdoor Nylon Fabric.</p>	<p data-bbox="715 315 879 472">Inkjet nano-silver with Brother domestic printer.</p>	<p data-bbox="901 315 975 349">NIMs</p>	<p data-bbox="1085 315 1355 439">The print resulted in a sharp image, however no conductivity was measured.</p>
 <p data-bbox="316 1357 699 1424">Laser engraved SaniSilver™ (for datasheet see Figure C.2)</p>	<p data-bbox="715 898 831 965">Laser engraving</p>	<p data-bbox="901 898 975 931">NIMs</p>	<p data-bbox="1085 898 1355 1178">Although the process was slow (c.30 min for one row), the results were a clear image and high conductivity. Samples were fragile and had to be handled carefully or backed with a thin cotton lining.</p>

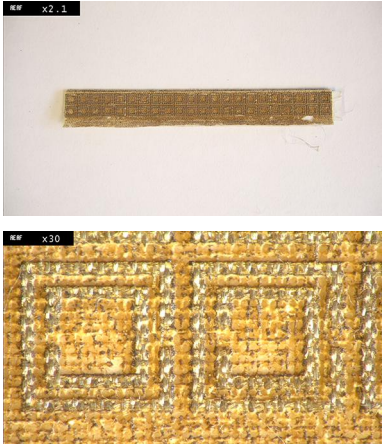
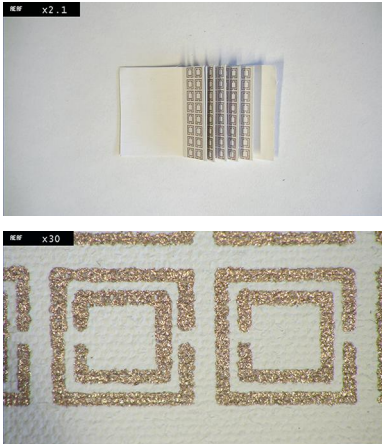
Photo	Main Technique	Intended Use	Notes
 <p data-bbox="316 770 678 837">Laser engraved SaniSilver™ (for datasheet see Figure C.2)</p>	Laser engraving	NIMs	Card strips were inserted to previous sample type to stabilise the structure. Although this resulted in a robust three-dimensional structure, it also lost its 'textile-ness', and thus was not further pursued.
 <p data-bbox="316 1352 691 1451">Screen printed CuPro-Cote™ on cotton that was first screen printed with TiO<sub>2</sub> in before.</p> <p data-bbox="316 1464 644 1496">(For datasheet see Figure C.7)</p>	Screen print copper ink	NIMs	Geometric structures were sharp and conductive. As the cotton was coated with TiO <sub>2</sub> ink beforehand, it was easy to fold and maintained its three-dimensional shape.

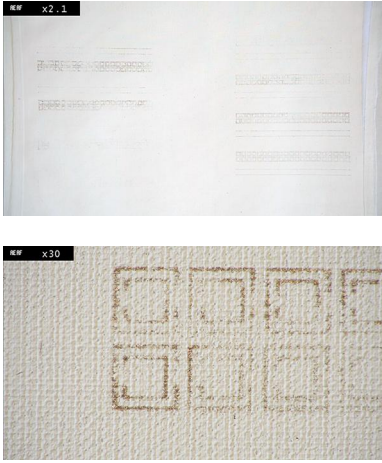
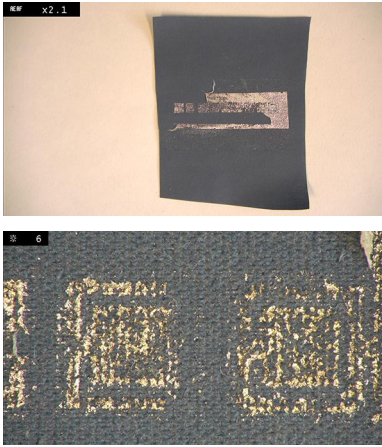
Photo	Main Technique	Intended Use	Notes
 <p data-bbox="316 786 699 931">Screen printed CuPro-Cote™ on cotton that was screen printed with TiO<sub>2</sub> in before. (For datasheet see Figure C.7)</p>	Screen print copper ink	NIMs	To test whether smaller SRRs could be printed with a finer screen mesh (100T), however copper particles did not pass through the screen.
 <p data-bbox="316 1413 699 1480">Silver leaf on Navy Blue Waterproof Coated Polycotton</p>	Silver leafing	NIMs	The screen printed adhesive did not fully adhere to the substrate, and was too thin to stick to the silver leaf when brushed on.

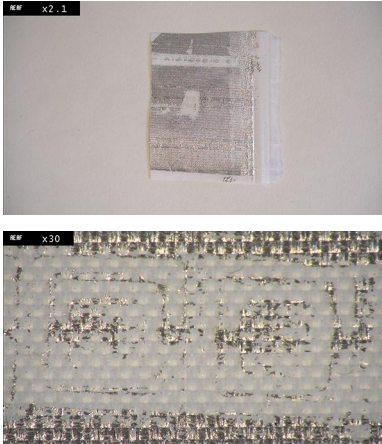
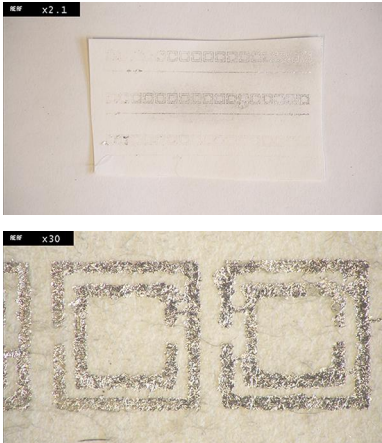
Photo	Main Technique	Intended Use	Notes
 <p data-bbox="316 772 699 835">Silver leaf on White Waterproof Cover Fabric</p>	Silver leafing	NIMs	The screen printed adhesive did not adhere to the substrate, and peeled off when brushing on the silver leaf.
 <p data-bbox="316 1355 699 1395">Silver leaf on technical filter paper</p>	Silver leafing	NIMs	The adhesive and silver leaf adhered well to the surface. The surface was too rough for the silver leaf to be conductive.



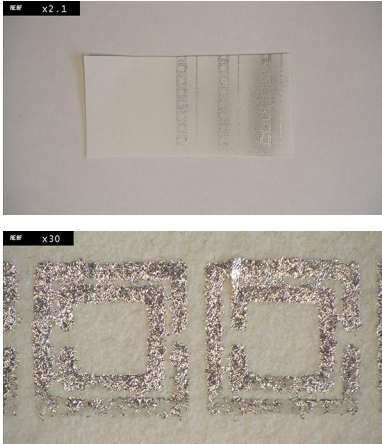

Photo	Main Technique	Intended Use	Notes
 <p data-bbox="316 775 699 808">Silver leaf on technical filter paper</p>	Silver leafing	NIMs	The adhesive and silver leaf adhered well to the surface. The surface was too rough for the silver leaf to be conductive. When attempting to smooth the silver leaf, the silver was distributed.
 <p data-bbox="316 1361 699 1451">Silver leaf on Navy Blue Waterproof Coated Polycotton (smooth side)</p>	Silver leafing	NIMs	Testing of larger surface area of SRR and wire design. SRRs were partially incomplete or not conductive.

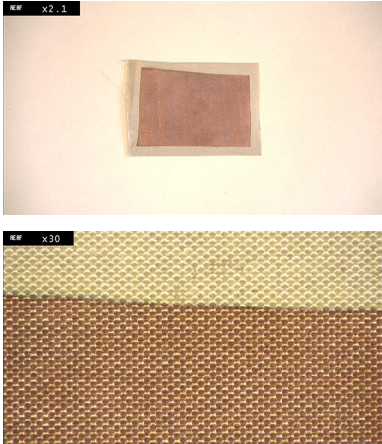
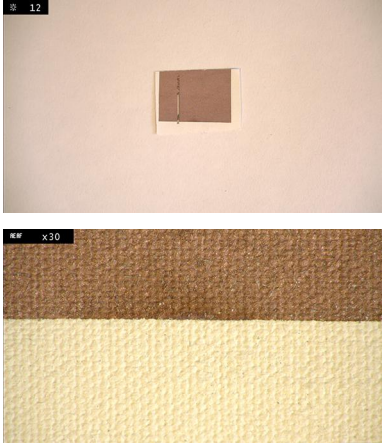
Photo	Main Technique	Intended Use	Notes
 <p data-bbox="316 775 639 835">Vacuum deposition on woven polyester</p>	<p data-bbox="715 315 879 562">Vacuum deposition, screen printed with TiO<sub>2</sub> and sandwiched between two layers of polyester</p>	<p data-bbox="901 315 1066 443">Conductive fabric with high permittivity</p>	<p data-bbox="1085 315 1342 622">Two hours in vacuum depositioner. Highly conductive and scratch resistant. Permittivity was measured prior the copper coating, and determined to be 2.3. Sample was very flexible and had a textile feel.</p>
 <p data-bbox="316 1361 624 1422">Vacuum deposition on TiO<sub>2</sub> printed cotton</p>	<p data-bbox="715 900 879 1028">Vacuum deposition, screen printed with TiO<sub>2</sub></p>	<p data-bbox="901 900 1066 1028">Conductive fabric with high permittivity</p>	<p data-bbox="1085 900 1326 994">Two hours in vacuum depositioner. Low conductivity.</p>

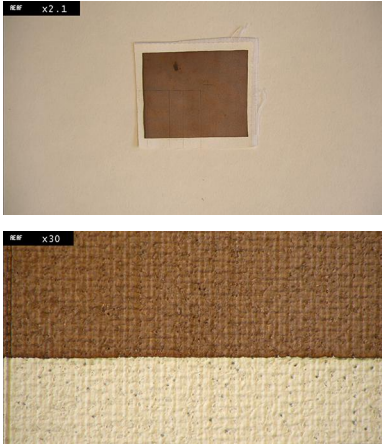
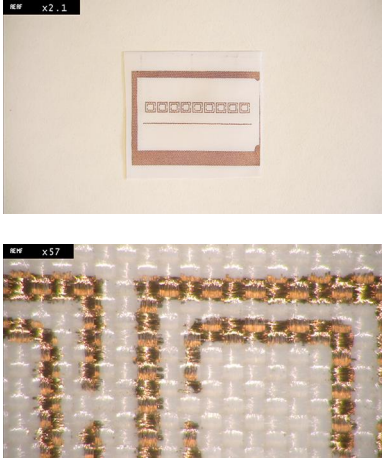
Photo	Main Technique	Intended Use	Notes
 <p data-bbox="316 775 624 835">Vacuum deposition on TiO<sub>2</sub> printed cotton</p>	<p data-bbox="715 315 879 562">Vacuum deposition, screen printed with TiO<sub>2</sub> and sandwiched between two layers of cotton</p>	<p data-bbox="901 315 1066 443">Conductive fabric with high permittivity</p>	<p data-bbox="1085 315 1326 409">Two hours in vacuum depositer. No conductivity.</p>
 <p data-bbox="316 1373 694 1433">Vacuum deposition of copper onto White Waterproof Cover Fabric</p>	<p data-bbox="715 900 879 1028">Screen printed mask with latex, vacuum deposition</p>	<p data-bbox="901 900 975 929">NIMs</p>	<p data-bbox="1085 900 1347 1207">The latex printed well and dried fully. Depositing copper and carefully removing the mask was possible. The SRRs were not scratch resistant, making the technique unusable for larger surfaces and further processing.</p>

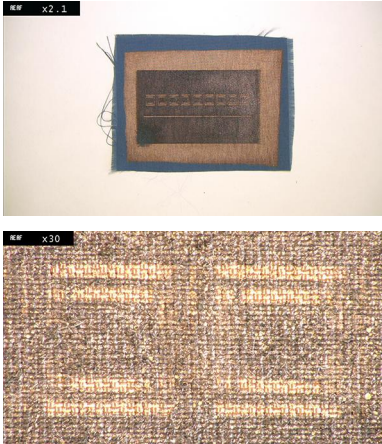
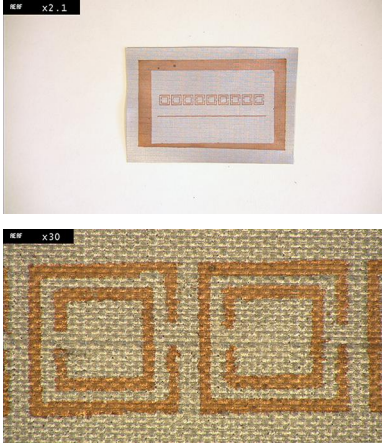
Photo	Main Technique	Intended Use	Notes
 <p data-bbox="316 775 699 864">Vacuum deposition of copper onto Air Force Blue Water Repellent Polycotton Chintz</p>	<p data-bbox="715 315 884 439">Screen printed mask with latex, vacuum deposition</p>	<p data-bbox="900 315 973 344">NIMs</p>	<p data-bbox="1082 315 1353 528">The latex printed well and dried fully. The copper deposited and was highly conductive where the latex was printed. The mask was not removable.</p>
 <p data-bbox="316 1359 699 1420">Vacuum deposition of copper onto Grey Waterproof Ripstop</p>	<p data-bbox="715 900 884 1023">Screen printed mask with latex, vacuum deposition</p>	<p data-bbox="900 900 973 929">NIMs</p>	<p data-bbox="1082 900 1353 1144">The latex printed well and dried fully. Depositing copper and carefully removing the mask was possible. The SRRs were not conductive or scratch resistant.</p>


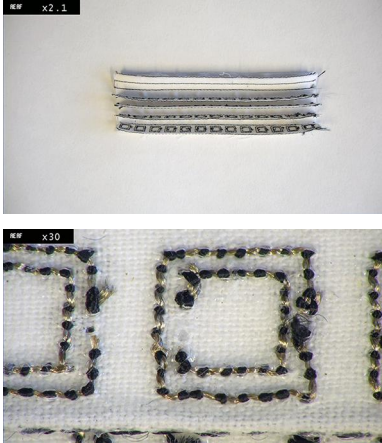
Photo	Main Technique	Intended Use	Notes
 <p data-bbox="316 775 699 864">Vacuum deposition of copper onto Cream Waterproof Breathable Coated Microfibre</p>	<p data-bbox="715 315 884 439">Screen printed mask with latex, vacuum deposition</p>	<p data-bbox="900 315 975 344">NIMs</p>	<p data-bbox="1082 315 1353 528">The latex printed well and dried fully. The copper deposited and was highly conductive where the latex was printed. The mask was not removable.</p>
 <p data-bbox="316 1359 675 1464">Statex silver thread 234/34 4-ply on cotton (For datasheet see Figure C.4)</p>	<p data-bbox="715 900 884 1084">Digital embroidery, screen printed TiO<sub>2</sub>, pleated and fixed with iron-on fabric</p>	<p data-bbox="900 900 975 929">NIMs</p>	<p data-bbox="1082 900 1353 994">The form of the SRR was maintained. High conductivity.</p>

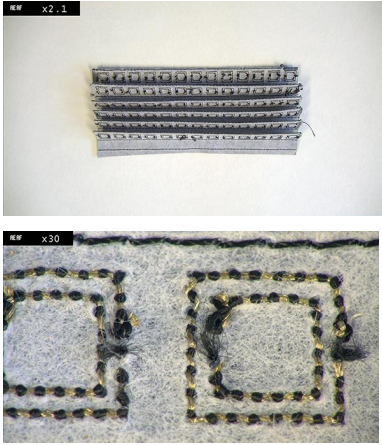

Photo	Main Technique	Intended Use	Notes
 <p data-bbox="316 775 671 882">Statex silver thread 234/34 4-ply on cotton (For datasheet see Figure C.4)</p>	<p data-bbox="715 315 879 499">Digital embroidery, screen printed TiO<sub>2</sub>, pleated and fixed with iron-on fabric.</p>	<p data-bbox="901 315 970 342">NIMs</p>	<p data-bbox="1085 315 1334 409">The form of the SRR was maintained. High conductivity.</p>
 <p data-bbox="316 1373 644 1458">Laser engraved SaniSilver™ (For datasheet see Figure C.2)</p>	<p data-bbox="715 913 879 1097">Laser engraved, screen printed TiO<sub>2</sub>, pleated and fixed with iron-on fabric</p>	<p data-bbox="901 913 970 940">NIMs</p>	<p data-bbox="1085 913 1350 1249">Very slow laser engraving process, sample took 12 hours to laser. The structures were highly conductive, but inconsistent. In some parts, the background cotton was burnt off completely, so SRRs fell away from the sample.</p>

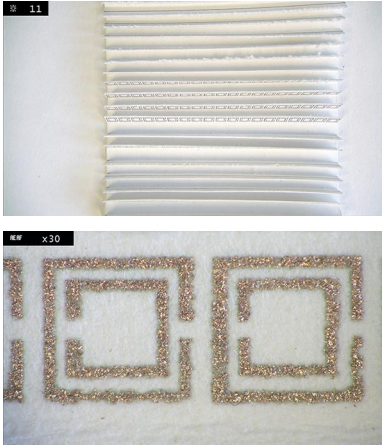
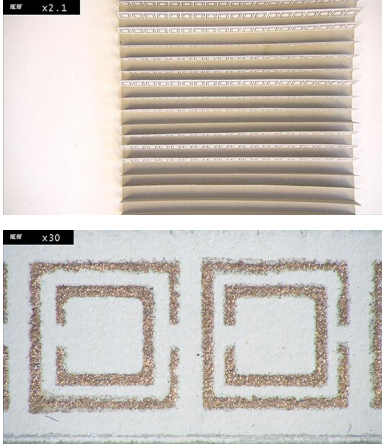
Photo	Main Technique	Intended Use	Notes
 <p data-bbox="316 772 687 864">Screen printed CuPro-Cote™ on white card that was screen printed with TiO<sub>2</sub> first.</p> <p data-bbox="316 882 643 911">(For datasheet see Figure C.7)</p>	Screen print	NIMs	Medium shape accuracy as not much copper ink passed through the screen. Conductivity was high at the beginning, but decreased over time.
 <p data-bbox="316 1402 687 1494">Screen printed CuPro-Cote™ on polycotton that was screen printed with TiO<sub>2</sub> first.</p> <p data-bbox="316 1512 643 1541">(For datasheet see Figure C.7)</p>	Screen print	NIMs	Medium shape accuracy as not much copper ink passed through the screen. Conductivity was high at the beginning, but decreased over time.

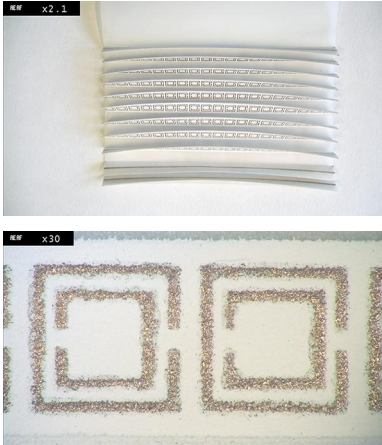

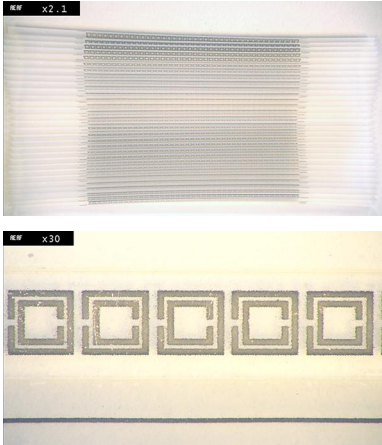
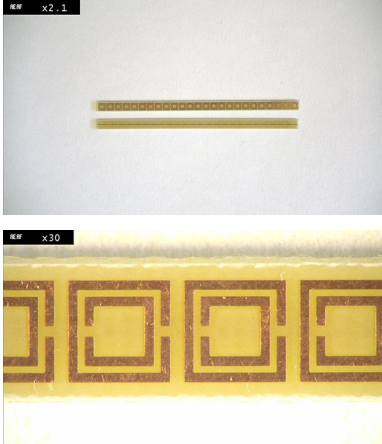
Photo	Main Technique	Intended Use	Notes
 <p>Screen printed C CuPro-Cote™ on technical filter paper that was screen printed with TiO<sub>2</sub> first. (For datasheet see Figure C.7)</p>	Screen print	NIMs	Medium shape accuracy as not much copper ink passed through the screen. Conductivity was high at the beginning, but decreased over time.
 <p>Liberator 20 thread on polycotton (both photos show non-conductive side of embroidery)</p>	Digital embroidery, screen printed with TiO <sub>2</sub> , pleated and fixed with smocking	NIMs	High geometric accuracy and conductivity. When pleated, strips deformed slightly. Sewing the side parts to the opposite side balanced this effect.



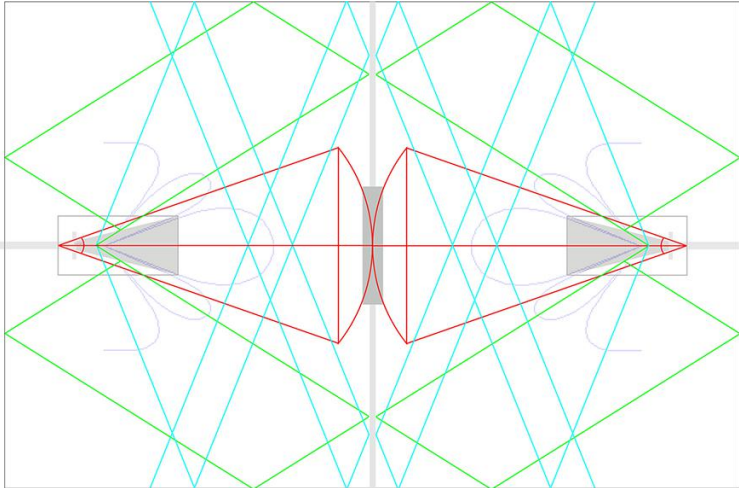
Photo	Main Technique	Intended Use	Notes
 <p data-bbox="316 775 691 913">Silver nano ink inkjet printed onto PET film. (For datasheets see Figure C.3 and Figure C.8)</p>	<p data-bbox="715 320 884 409">Inkjet printing on nano-coated film</p>	<p data-bbox="900 320 975 342">NIMs</p>	<p data-bbox="1082 320 1353 383">High accuracy, medium conductivity.</p>
 <p data-bbox="316 1404 671 1435">PCB etched in industrial facility.</p>	<p data-bbox="715 949 863 1039">PCB etching industrial process</p>	<p data-bbox="900 949 975 972">NIMs</p>	<p data-bbox="1082 949 1345 1070">Produced off-site in industrial facility. High geometric accuracy and conductivity of copper.</p>

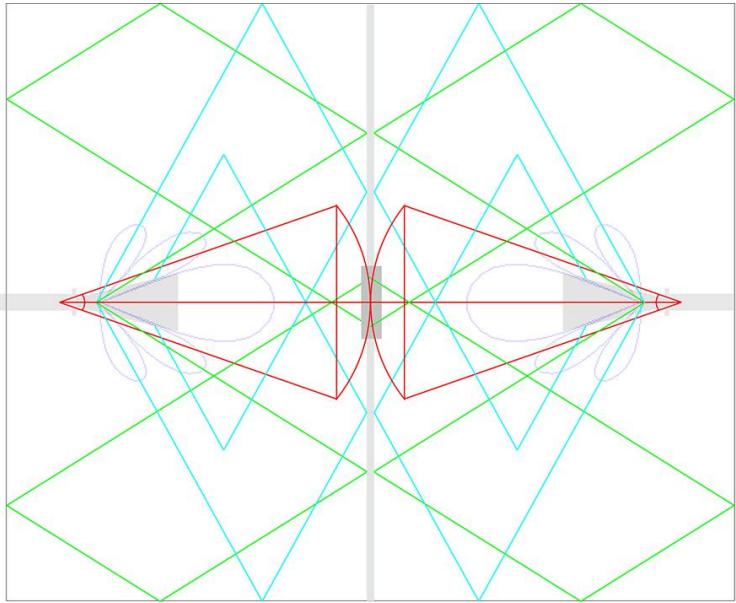
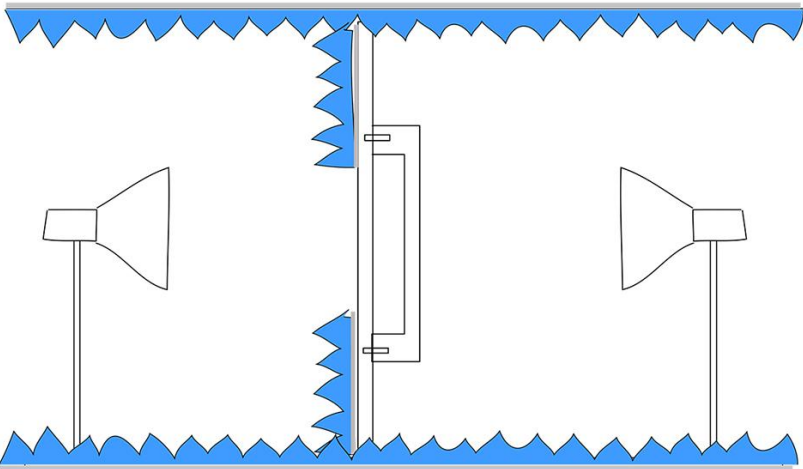
# Appendix E

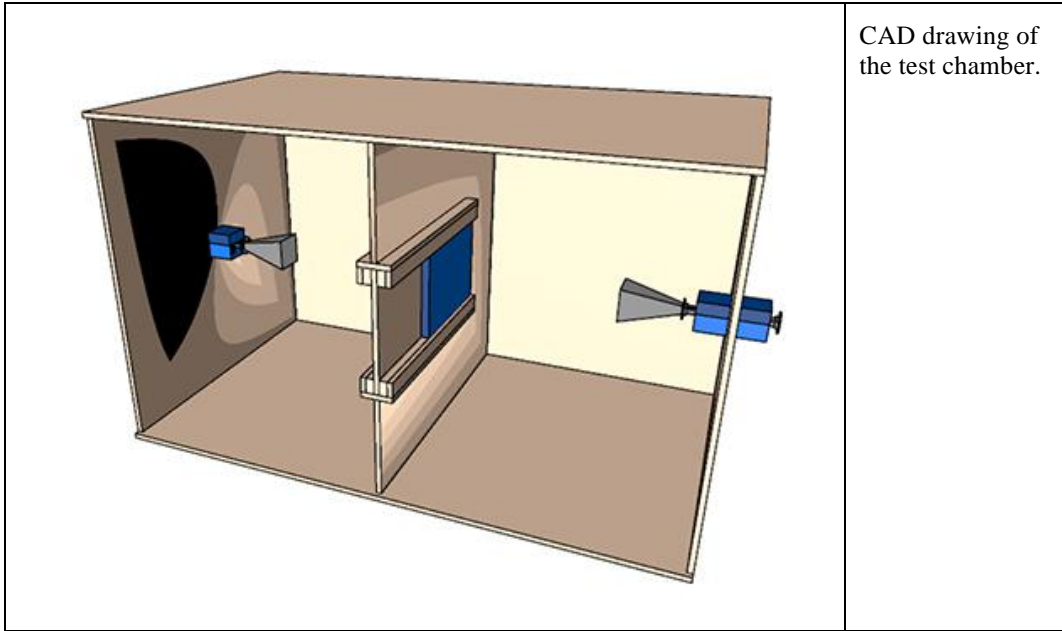
## E.1 Anechoic Chamber Design Documentation

The design and building process of the anechoic chamber was an important part of this work, as it aided understanding of practical measurement requirements and issues in electromagnetic engineering. While commonly, for this kind of work, wave theory is applied in algorithms to find design solutions in a short time, the process used here shows the visual approach which was the driving force for acquiring technical knowledge and design solutions. Illustrations were produced that traced the path of waves within confined spaces to identify the optimum dimensions of the anechoic chamber.

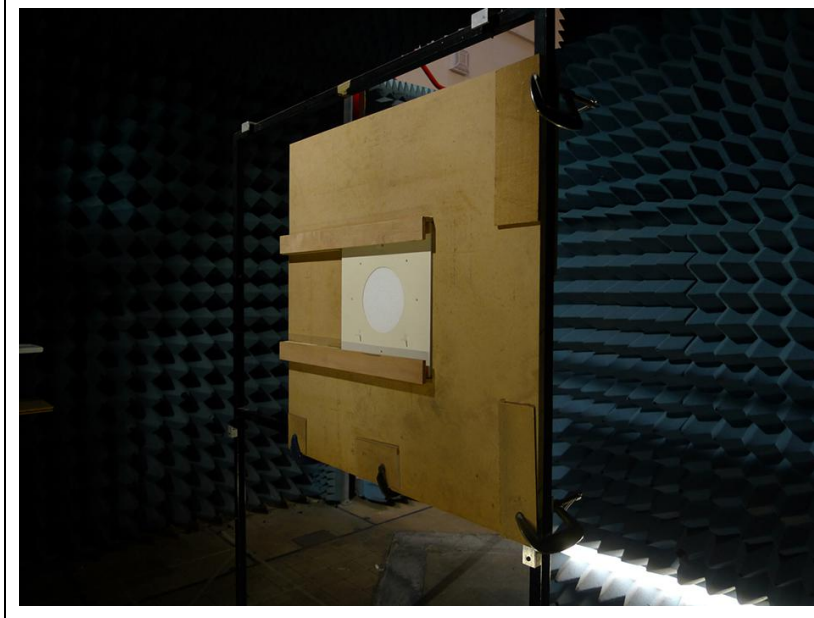
Table E.1: Anechoic chamber design process

Process step of Anechoic Chamber design	Description
	Exploring refractions within the dimensions of the anechoic chamber with drawings.  Software: Adobe Illustrator CS6

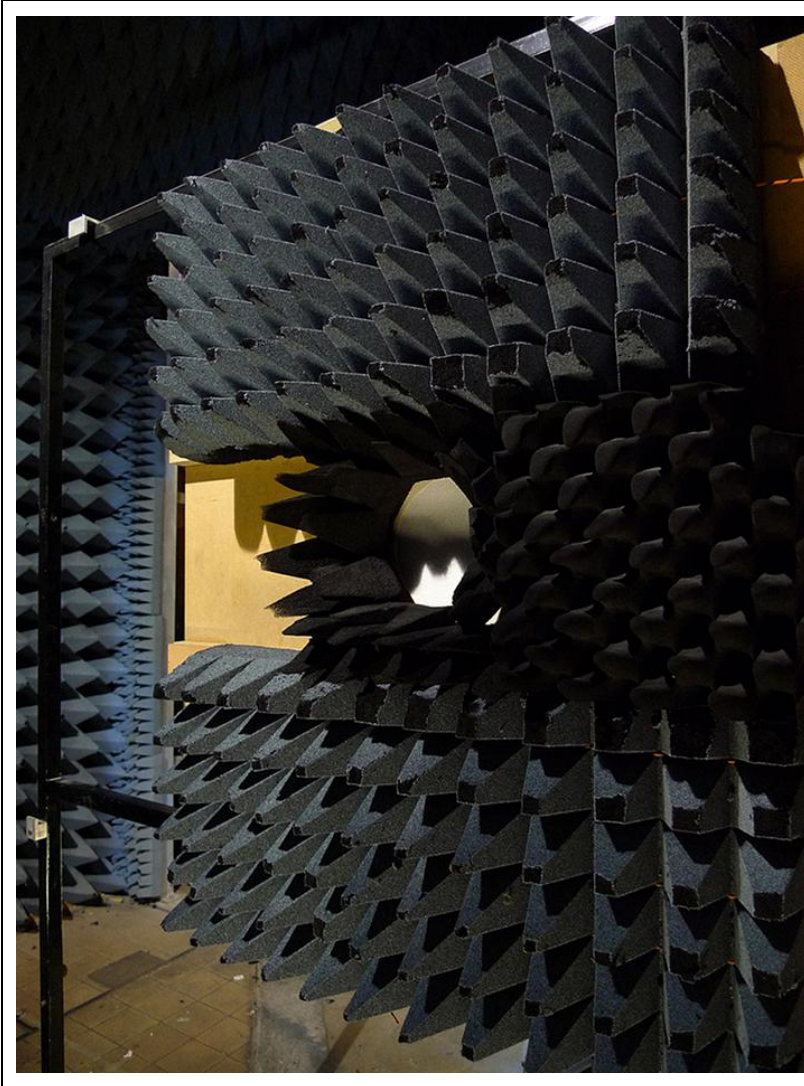
	<p>Exploring refractions within the dimensions of the anechoic chamber with drawings.</p> <p>Software: Adobe Illustrator CS6</p>
<p>MEASUREMENT SET UP, FREE SPACE JULY 2012</p>  <p>BERIT GREINKE, MEDIA &amp; ARTS TECHNOLOGY, QUEEN MARY UNIVERSITY OF LONDON</p>	<p>Conceptual drawing of anechoic chamber.</p>



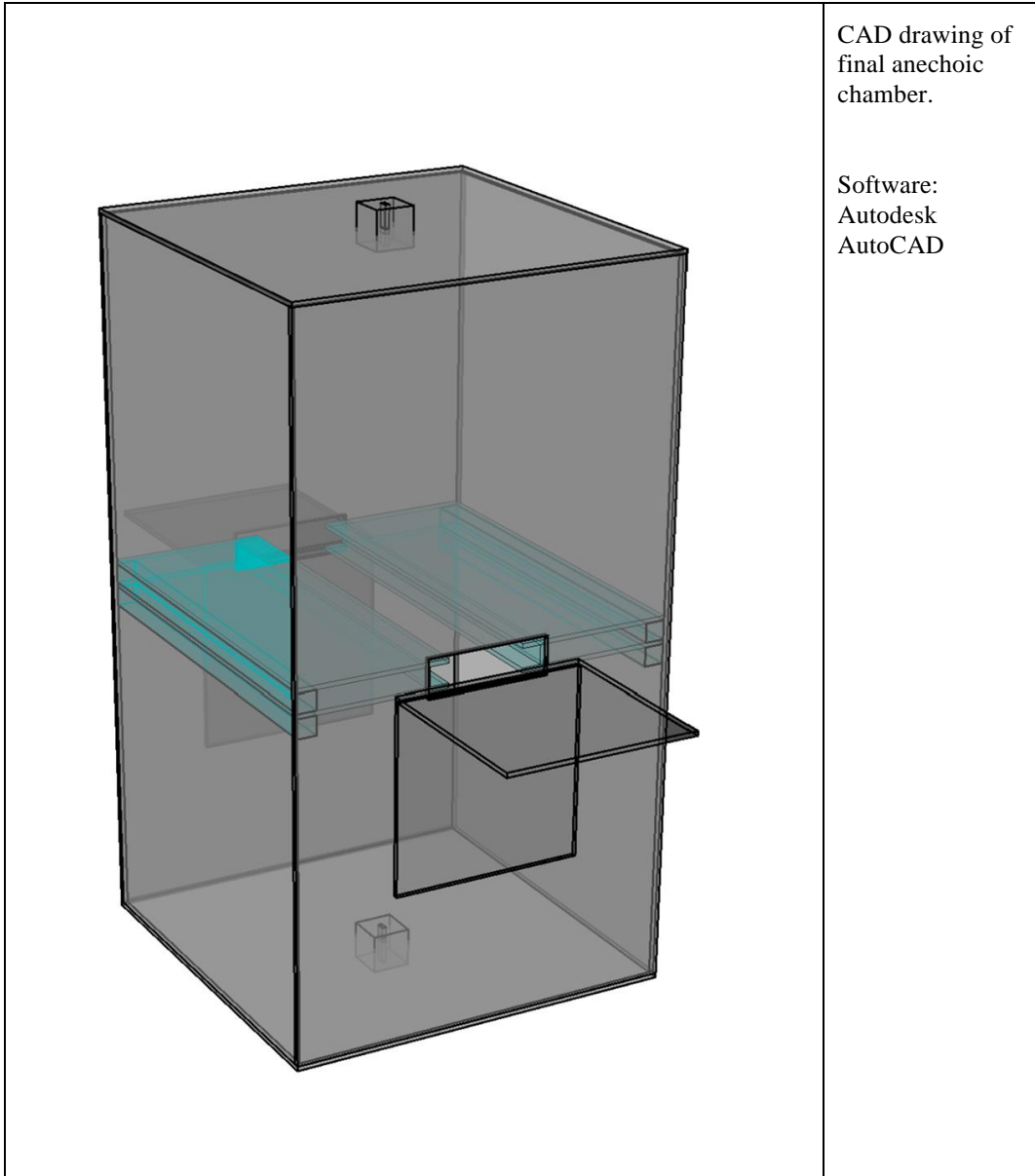
CAD drawing of the test chamber.



Test set up in the anechoic chamber. Assembling the sample holder and dividing wall.



Test set up in the anechoic chamber. Assembling the sample holder and dividing wall.





Building the anechoic chamber.



Building the anechoic chamber.



Completed anechoic chamber.

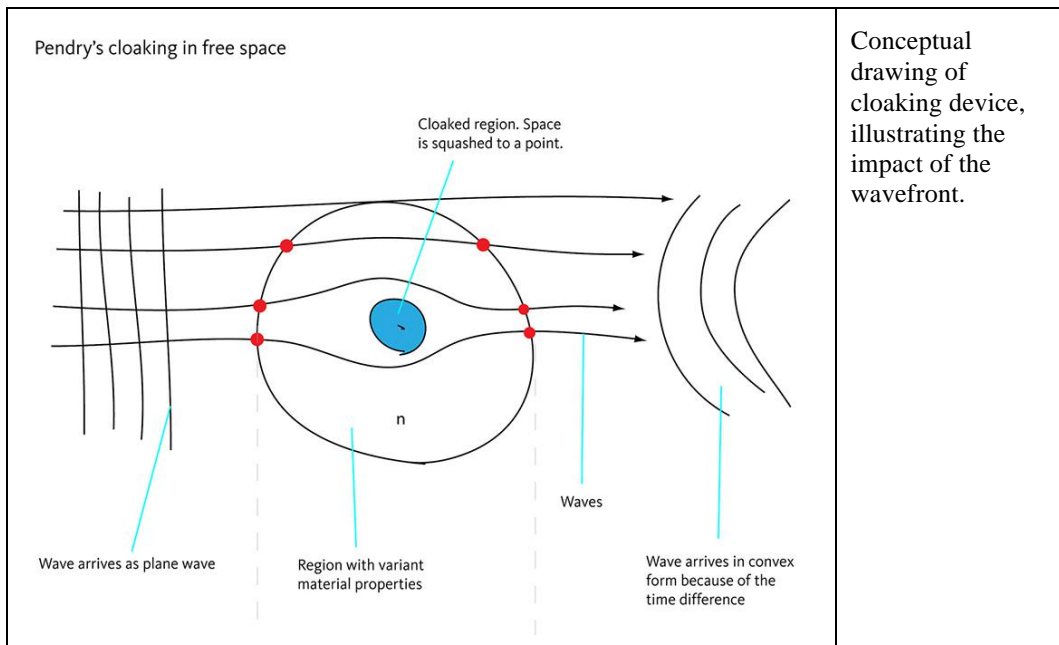


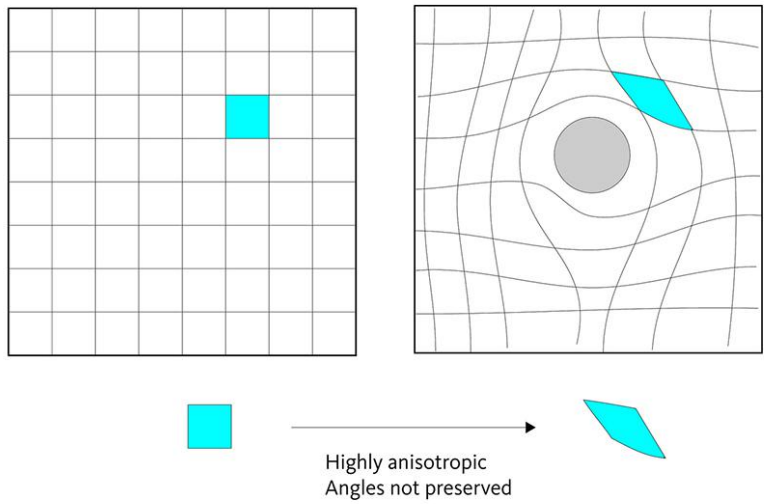
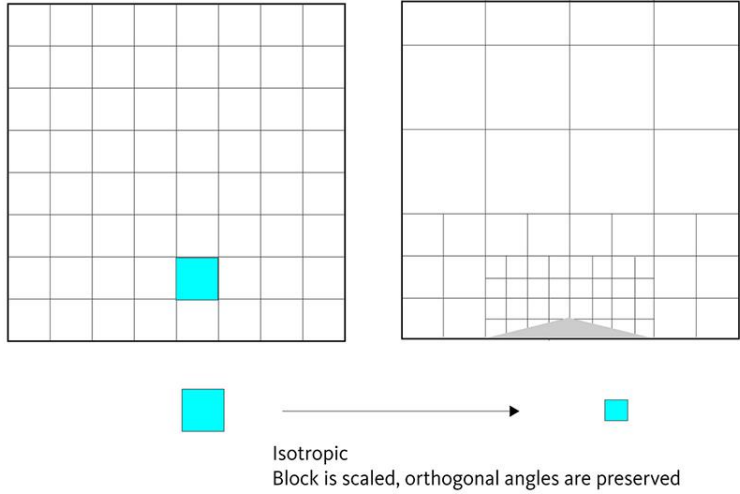
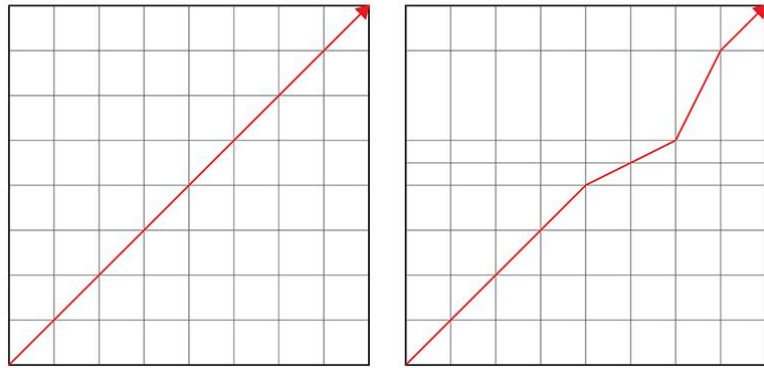
# Appendix F

## F.1 Conceptual Drawings of Cloaking Mechanisms

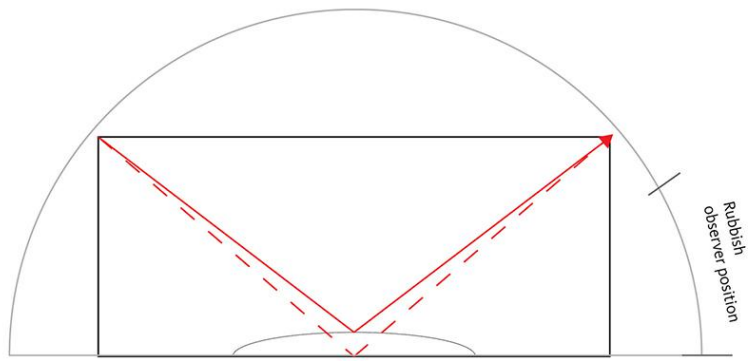
Drawings were used to understand the technical concepts behind metamaterials and Transformation Optics theory, as well as to find bridges to textile design. Following illustrations resulted from initial meeting with various researchers in the Antennas Group at QMUL.

Table F.1: Conceptual drawings of cloaking mechanisms



<p>Analytical transformation (metamaterials with refractive index &lt; 1)</p>  <p>Highly anisotropic Angles not preserved</p>	<p>Conceptual drawing of cloaking with metamaterials. Negative refractive index metamaterials.</p>
<p>Carpet cloaks: Discrete coordinate transformation (dielectrics)</p>  <p>Isotropic Block is scaled, orthogonal angles are preserved</p>	<p>Conceptual drawing of cloaking with metamaterials. Dielectric metamaterials.</p>
<p>Redirecting waves by compressing space (material)</p> 	<p>Conceptual drawing of cloaking with metamaterials.</p>

Carpet Cloak



- - - - - Original reflection without cloak
- Reflection with cloak

Conceptual drawing of ground plane cloaking with all-dielectric metamaterials.

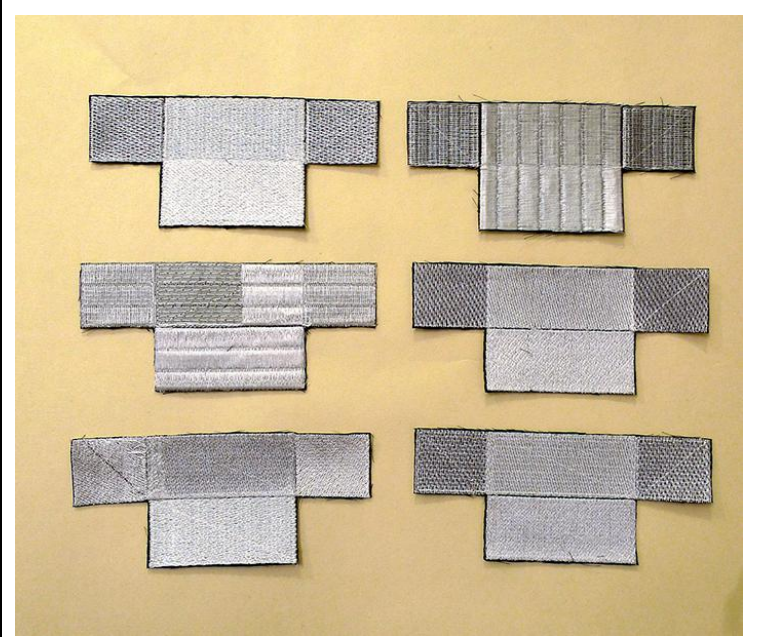
# Appendix G

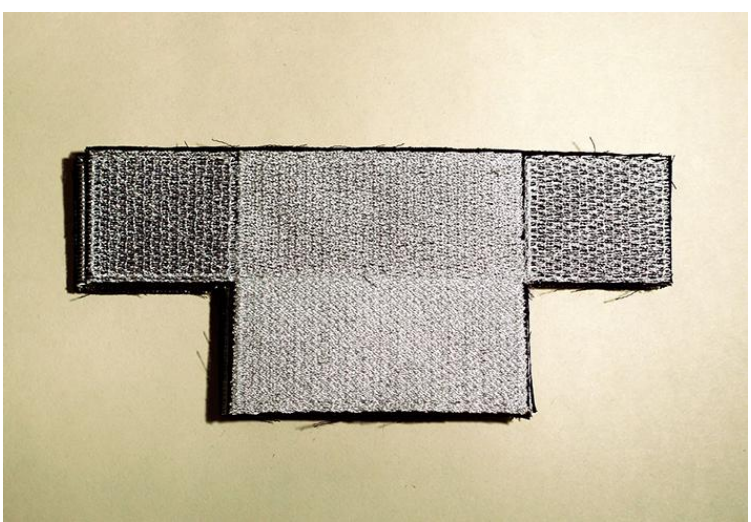
## G.1 Conceptual Samples for the Purpose of Illustration

Non-functional samples, drawings, illustrations and paper models were produced throughout the thesis. This was done for three reasons:

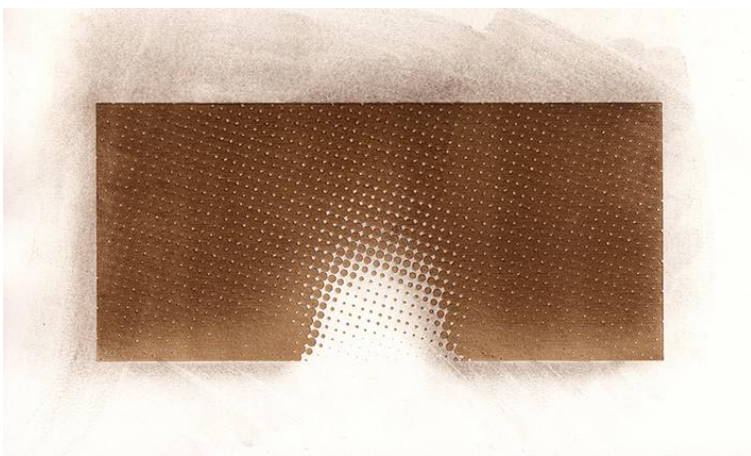
- Drawings and paper models were repeatedly used to clarify technical questions between supervisors, technical staff and author.
- The concept and technical functionality was communicated and demonstrated to the public on many occasions. In most cases, the audience was non-expert.
- The process of conceptual sampling (producing samples to illustrate an idea) helped the author in developing ideas and understanding the workings of metamaterials and cloaking devices. In addition, it served the purpose of demonstrating early stage ideas of how textile-based techniques could be beneficial for the fabrication of metamaterial and cloaking.

Table G.1: List of conceptual samples.

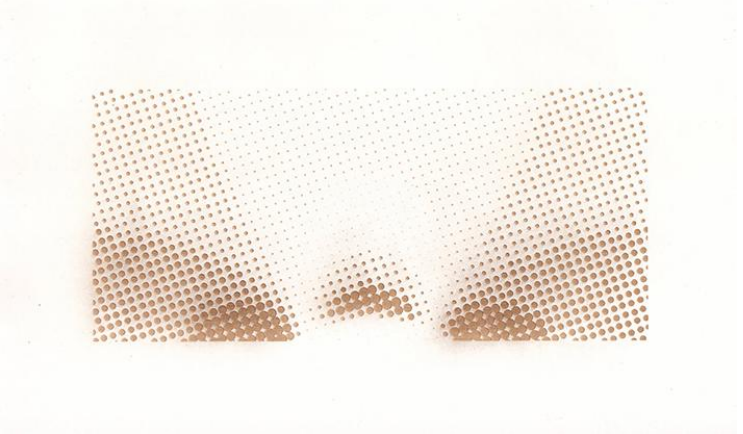
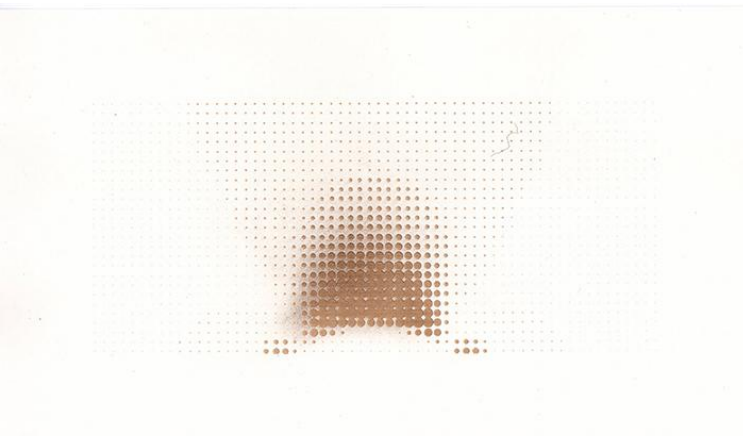
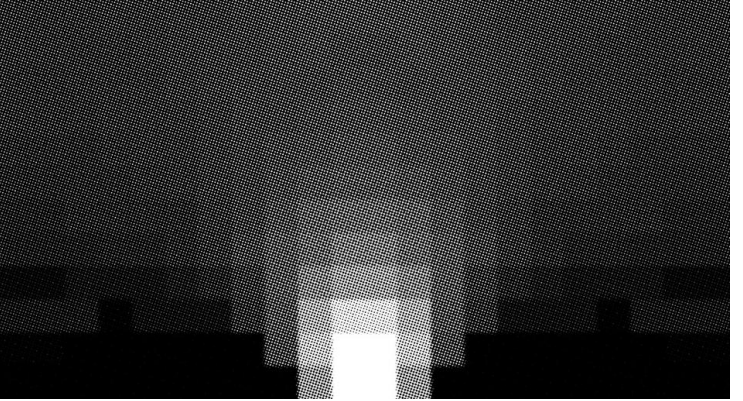
	<p>First samples produced, to test if and how various types of embroidery could create different permittivities and tactile structures.</p>
--	---

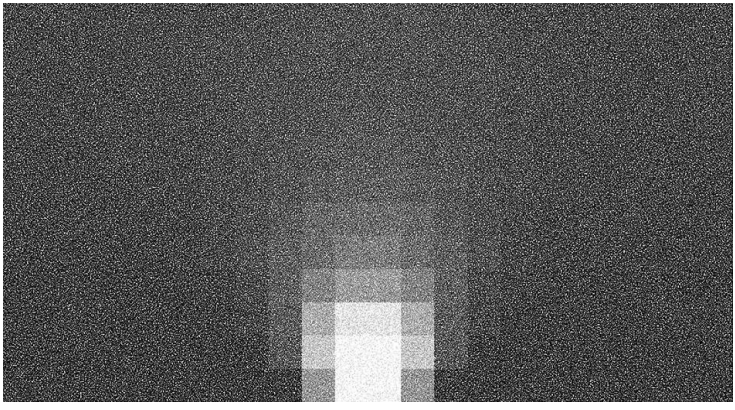
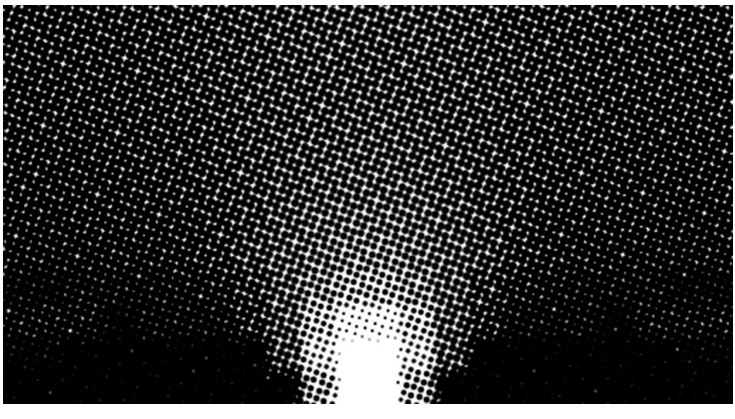


First sample produced, to question how and if various types of embroidery could create different permittivities and tactile structures.



Drawing of a laser engraved paper surface with a gradually varying density, illustrating a map of permittivity building blocks as laid out in Bao (2011). Lighter areas represent higher permittivity areas; darker areas show lower permittivity areas. Although not a functional ground plane cloak, the illustration has been rendered from the values of Bao's (2011) design, aiming to depict the possible construction of textile printed ground plane cloaks. A simple rastering process was used to translate permittivity values into engraving strength.

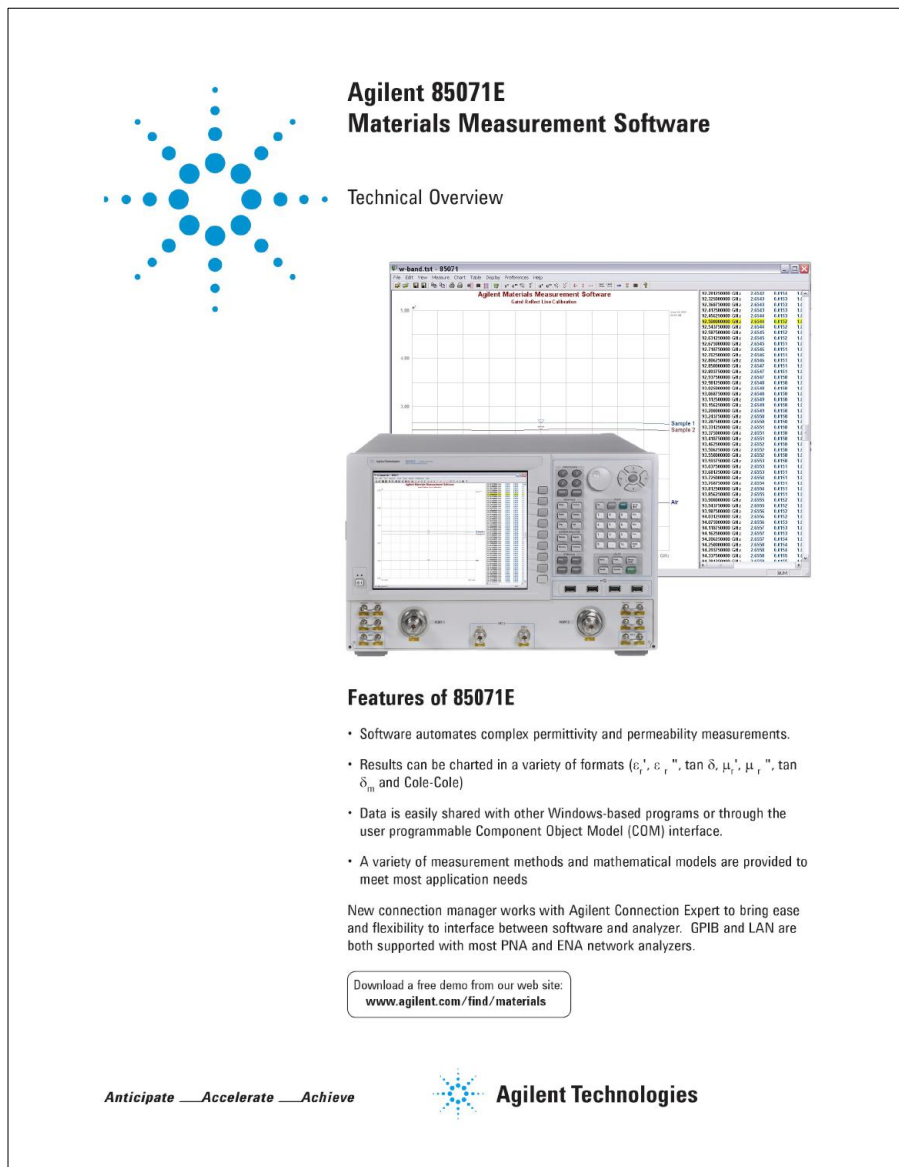
	<p>Drawing to illustrate graded cloak materials.</p>
	<p>Drawing to illustrate graded cloak materials.</p>
	<p>Drawing to illustrate graded cloak materials.</p>

	<p>Drawing to illustrate graded cloak materials.</p>
	<p>Drawing to illustrate graded cloak materials.</p>

# Appendix H

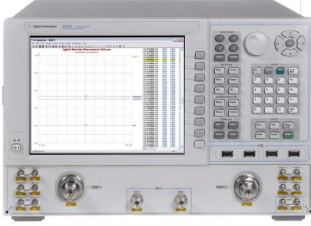
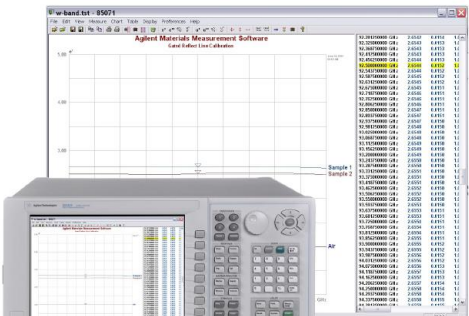
## H.1 Agilent 85071E Materials Measurement Software: Technical Overview

The Agilent 85071E Materials Measurement Software has been discontinued. A document which has repeatedly provided useful information, and which is now unavailable, is included and referenced throughout the thesis.



**Agilent 85071E  
Materials Measurement Software**

Technical Overview




**Features of 85071E**

- Software automates complex permittivity and permeability measurements.
- Results can be charted in a variety of formats ( $\epsilon_r'$ ,  $\epsilon_r''$ ,  $\tan \delta$ ,  $\mu_r'$ ,  $\mu_r''$ ,  $\tan \delta_m$  and Cole-Cole)
- Data is easily shared with other Windows-based programs or through the user programmable Component Object Model (COM) interface.
- A variety of measurement methods and mathematical models are provided to meet most application needs

New connection manager works with Agilent Connection Expert to bring ease and flexibility to interface between software and analyzer. GPIB and LAN are both supported with most PNA and ENA network analyzers.

Download a free demo from our web site:  
[www.agilent.com/find/materials](http://www.agilent.com/find/materials)

*Anticipate — Accelerate — Achieve*



**Agilent Technologies**



# Automate complex permittivity and permeability measurements with Agilent's 85071E materials measurement software

## Measure $\epsilon_r^*$ and $\mu_r^*$ over a wide frequency range

The Agilent Technologies 85071E materials measurement software determines the intrinsic electromagnetic properties of many dielectric and magnetic materials. The complete system is based on a versatile Agilent network analyzer which measures the material's response to RF or microwave energy.

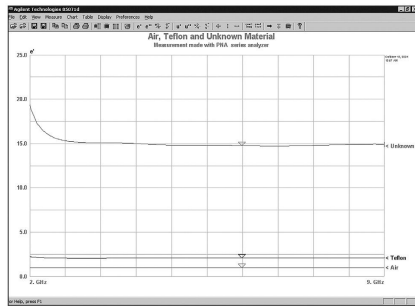


Figure 1. Examine the properties of materials across the RF and microwave frequency spectrum.

The 85071E software controls the network analyzer and calculates the complex permittivity  $\epsilon_r^*$  (or dielectric constant) and permeability  $\mu_r^*$ , including the loss factor or loss tangent. Results are displayed as a function of frequency, with 1 to 2% accuracy (typical). Depending on the Agilent network analyzer and fixture used, frequencies can extend into mm and sub mm wavelengths.

## Display Data to Aid Analysis

The split screen window and markers aid in data analysis. Simply click on a point in the chart or table to activate and move the marker. Charts can be generated in a variety of formats:  $\epsilon_r'$ ,  $\epsilon_r''$ ,  $\tan \delta$ ,  $\mu_r'$ ,  $\mu_r''$ ,  $\tan \delta_m$ , and Cole-Cole.

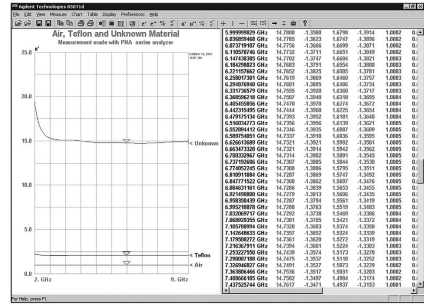


Figure 2. Display data in chart form, table form, or both!

## Connect to other programs

Data charts and tables can easily be copied and pasted into any Windows-based application for further analysis or report generation.

The component object model (COM) interface allows the measurement to be setup, triggered and read from a user written program. This is particularly valuable for analyzing material changes over time. Example Visual Basic® and C++ projects are included to aid program development.

## Measurement Methods

### Transmission Line Method

Coaxial airlines or rectangular waveguide transmission lines are used as sample holders. The transmission line method works best for materials that can be precisely machined to fit inside the sample holder. The 85071E features an algorithm that corrects for the effects of air gap between the sample and holder, considerably reducing the largest source of error with the transmission line technique.

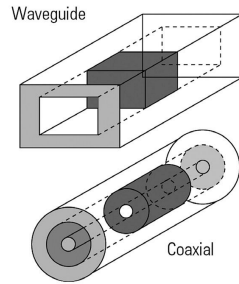


Figure 3. Simple coaxial or waveguide transmission lines hold the samples of material under test.

### Free Space Method

In this method, materials are placed between antennas for a non-contacting measurement. The free space method works best for large flat solid materials, but granular and powdered materials can also be measured in a fixture. It is very useful for many applications such as non-destructive testing, measuring materials that must be heated to very high temperatures, or measuring a large area of material that is non-uniform such as honeycomb or a composite. Calibration and gating techniques performed in the network analyzer can be used to reduce measurement errors.

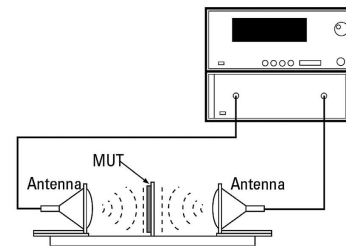


Figure 4. Antennas direct beams of microwave energy at or through a material, without enclosing it in a fixture.

### Free Space Calibration (Option 100)

The Free Space Calibration Option increases ease of use and reduces the costs associated with TRM and TRL calibration methods. The Gated Reflect Line (GRL) calibration technique converts a coaxial/waveguide 2-port calibration into a full 2-port freespace calibration. Use of this option requires an 8510 or a PNA Series network analyzer with the time domain option, an appropriate freespace fixture and a metal calibration plate. This option also includes a gated isolation/ response calibration, which reduces errors from diffraction effects at the sample edges, and multiple residual reflections between the antennas.

Accurate free space measurements are now possible without expensive spot focusing antennas, micro positioning fixturing or direct receiver access. The software automatically sets up all the free space calibration definitions and network analyzer parameters, saving engineering time. In the PNA, additional ease and timesaving is provided with the use of ECal, electronic calibration, which features a guided calibration wizard that steps you through a fast and easy calibration process.

Table 1. Models in the 85071E Materials Measurement Software

85071E Name	Alternate Name(s)	S-parameters measured	Result	Description
Reflection/Transmission Mu and Epsilon	Nicholson-Ross -Weir, NRW	S11, S21, S12, S22	$\epsilon_r, \mu_r$	Originally developed by Nicholson and Ross, and later adapted to automatic network analyzers by Weir to calculate permittivity and permeability from transmission and reflection coefficients. Can have discontinuities for low loss samples with thickness of $> \frac{1}{2}$ wavelength.
Reflection/Transmission Epsilon Precision	NIST Precision	S11, S21, S12, S22	$\epsilon_r$	Developed by NIST to calculate permittivity from transmission and reflection coefficients.
Transmission Epsilon Fast	Fast Transmission	S21, S12	$\epsilon_r$	An iterative technique that estimates permittivity and then minimizes the difference between the S-parameter value calculated from that permittivity and the measured values until the error is less than the expected system performance. Uses only transmission parameters S21, S12, or the average of S21 and S12
Reflection/Transmission Mu and Epsilon Polynomial Fit	Poly Fit, Bartley-Begley, BB	S11, S21, S12, S22	$\epsilon_r, \mu_r$	Uses an iterative technique to fit material properties to a polynomial, incrementing the order of the polynomial until the difference between S-parameters calculated from the polynomial and the measured S-parameters is less than the expected system performance, or the maximum order specified by the user is reached. Best for magnetic samples. Not recommended for meta or left handed materials.
Transmission Epsilon Polynomial Fit	Poly Fit, Bartley-Begley, BB	S21, S12	$\epsilon_r$	Similar to Reflection / Transmission Mu and Epsilon Polynomial Fit. Uses an iterative technique to fit material properties to a polynomial, incrementing the order of the polynomial until the difference between S-parameters calculated from the polynomial and the measured S-parameters is less than the expected system performance, or the maximum order specified by the user is reached. For non-magnetic materials. Not recommended for meta or left handed materials.
Stack Transmission Mu and Epsilon	Stack Two Transmission	S21, S12 (2 samples)	$\epsilon_r, \mu_r$	An iterative technique that uses two transmission measurements. One measurement is of the sample which optionally may be backed by a known dielectric. The second is of the sample, backing and another known dielectric. The model is useful for free space measurements. It requires a full 2-port or a two-port transmission resp/isol cal.
Reflection Only Epsilon Short-Backed	Short Backed	S11	$\epsilon_r$	An iterative technique that minimizes the difference between the measured and calculated reflection coefficient of a material backed by a short. The idea of measuring a material backed by a short was published by Von Hippel. Although, Von Hippel uses tables to determine the value of permittivity instead of iteration.
Reflection Only Epsilon Arbitrary- Backed	Arbitrary Backed	S11	$\epsilon_r$	An iterative technique that minimizes the difference between the measured and calculated reflection coefficient of a material backed by a separately measured backing. This model is an extension of method proposed by Von Hippel. It is useful when the material is electrically short such that the voltage across the material is effectively zero when backed by a short.
Reflection Only Mu and Epsilon Single/Double Thickness	Single/Double Thickness	S11 (2 samples)	$\epsilon_r, \mu_r$	Uses two reflection coefficient measurements to calculate S11 and S21 of the material. The measurements are a sample and a sample that is twice the length as the original. After doing so the Nicolson Ross model is used to determine the material properties.

## Mathematical Models

The 85071E has eight different algorithms to choose from, each with specific benefits:

The traditional method, as described by Nicolson and Ross, is best for magnetic materials such as ferrites and absorbers. It calculates both  $\epsilon^*$  and  $\mu^*$  (including loss) from a two-port measurement of a single sample, producing results quickly and easily.

The 85071E also includes two additional two-port algorithms for non-magnetic materials ( $\mu^*=1$ ). These models do not suffer from discontinuities at frequencies where the sample length is a multiple of half-wavelengths and are best for long, low-loss materials.

While the two-port algorithms are best for most solid materials, one-port algorithms provide a simple calibration and measurement and can be better suited to measurements of liquids and powders. For example, a shorted waveguide can be turned on end and filled with a material for a one-port measurement. One-port fixtures are also better suited for high-temperature measurements where one end of the fixture can be heated, while cooling mechanisms at the other end protect the network analyzer.

Although one-port fixtures are usually terminated with a short circuit, the 85071E also accommodates an arbitrary termination which produces more reliable results for thin samples.

## New Feature: De-embedding

De-embedding allows a sample to be backed with a dielectric backing. It mathematically removes the effects of the backing, so the electromagnetic properties of just the sample are reported. This is useful when a sample is not stiff or thick enough to stand up by itself, or it cannot be removed from a substrate. The backing must have a known permittivity and thickness. If the permittivity of the backing is not known, it can be measured separately first. The backing material cannot be magnetic and it must allow the microwave signal to transmit through it so that S21 and S12 can be measured.

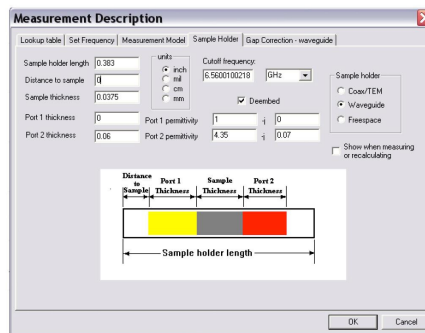


Figure 5. Example of the De-embed user interface for a sample backed on the port 2 side.

De-embedding feature works with the following transmission models:

- Reflection/Transmission Mu and Epsilon
- Transmission Epsilon Fast
- Polynomial Fit.

## Performance Characteristics

Specifications describe the warranted performance over the temperature range 0 to 55 °C. Supplemental characteristics are intended to provide information useful in applying the instrument, by giving typical but non-warranted performance parameters. These are denoted as “typical,” “nominal,” or “approximate.”

### Frequency range (typical)

100 MHz to 325 GHz depending on network analyzer, fixture and material.<sup>1</sup>

### Accuracy (typical)

1 to 2 percent

### Transmission line fixtures

Coaxial fixtures (beadless airlines) are broadband but require a sample shaped into a flat-faced torus. Waveguide fixtures are band-limited but operate at higher frequencies and accept a simpler rectangular shape.

Samples must completely fill the cross section of the transmission line without gaps at the fixture walls. Faces at either end must be flat, smooth and perpendicular to the long axis.

### Free space systems

Large, flat, thin, parallel-faced samples are placed between antennas and measured under free space conditions. Antennas should maintain a planar “far-field” wavefront to the sample.<sup>2</sup>

### Material under test assumptions

Material is homogeneous (uniform composition) with no layers.<sup>3</sup> Non-isotropic (uniform orientation) materials can be measured in waveguide.

## Software Menu Items

### File

Save or recall measurement setups or previous measurement results. Print copies of the measurement results in a tabular or graphical format.

### Edit

Copy the measurement results to the clipboard. Either graph or the tabular listing can be copied. This allows your measurements results to be pasted into other applications.

### View

Select what you want to view. Selections include the toolbar, status bar, table of the measurement data and chart of the measurement data.

### Measure

Trigger a measurement; recalculate without re-measuring the MUT; set measurement model; define sample holder; set measurement attributes and perform a GRL calibration.

### Chart

Select the format to be displayed on the chart. Choices include  $\epsilon_r'$ ,  $\epsilon_r''$ ,  $\tan \delta$ ,  $\mu_r'$ ,  $\mu_r''$ ,  $\tan \delta_m$  and Cole-Cole. Set scale factors or “autoscale.” Select from linear, semi-log, or log-log representations.

### Table

Choose between a tabular formatting of real and imaginary or real and  $\tan \delta$ .

### Display

Display current measurement data; save/display up to 3 memory traces; compare data to reference trace with trace math. Turn the marker on or off.

### Preferences

Select your preferences of fonts, colors, and annotations used to plot and list the measurement data.

### Help

On line help including the product manual.

### ToolBar

Provides single click access to the most important menu items.

1. Minimum frequency is set by the maximum practical sample length (L):  $f$  (in GHz)  $> \frac{1}{\sqrt{\epsilon_r \mu_r}} \frac{30 \text{ cm}}{L(\text{in cm})} \frac{20}{300}$

2. Antenna should be placed  $\approx 2d/\lambda$  from the sample, where  $d$  is the larger of the antenna or sample diameter.

3. If the material is not homogeneous through the length of the sample (i.e., layers), the reflection from the front ( $S_{11}$ ) and back ( $S_{22}$ ) face will be different and will lead to a potentially erroneous result. If the material is not homogeneous across the face of the sample, the result is an average value over the cross section that is exposed to the EM field (weighted by the intensity).

## Additional Measurement Methods

### NRL Arch Free Space Method

First developed by the U.S. Naval Research Lab, the NRL arch measurement method is a useful technique to test angular dependent absorptive characteristics of a material. The typical setup involves a network analyzer connected to two horn antennas fixed to an arch armature above (or below) a flat piece of the material under test. One antenna operates as the transmitting antenna while the second one receives the reflected signal to complete a one-port measurement. Sample should be in "far field."

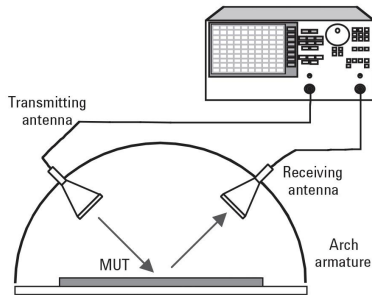


Figure 6. In the NRL arch method, one antenna transmits energy onto the MUT and the second antenna receives the reflected portion.

### Arch Reflectivity Software (Option 200)

Now you can automate your NRL arch measurements with the new Arch Reflectivity Software addition.

Option 200 provides a separate software program that automates NRL arch measurements. The program guides you through the complete process of setup, calibration and measurement of material absorption. Measurements are displayed in both a graphical and tabular form — with up to four measurements displayed simultaneously for comparison. The software includes markers to aid in measurement analysis, and complete measurement results and setup can be saved and recalled. Also, data can be saved in a spreadsheet compatible file format or copied into other applications for further analysis.

Agilent's Arch Reflectivity Software makes it possible to instantly update any NRL arch system to state-of-the-art hardware and measurement techniques.

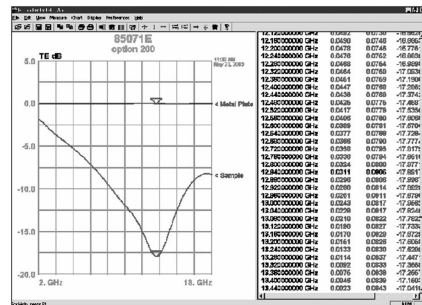


Figure 7. Example of arch reflectivity measurement results.

## Additional Measurement Methods *continued...*

### Resonant Cavity Method

Choose the Resonant Cavity method, for thin films, substrate materials, and other low loss materials. The resonant cavity method uses a network analyzer to measure resonant frequency and Q of a resonant cavity fixture, first empty and then loaded with the sample under test. Permittivity can then be calculated from these measurements, knowing the volume of the sample, and some other parameters about the resonant cavity. Because it is a resonant method, only one frequency point is reported. However, it is much more sensitive and has better resolution than the other techniques. Typical resolution for this method is  $10^{-4}$  where the broadband methods is  $10^{-2}$ .

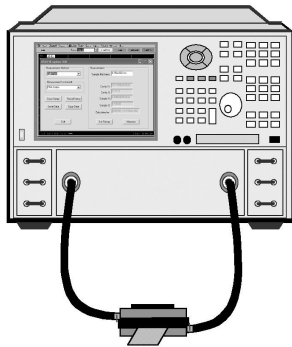


Figure 7. Resonant Cavity connected between ports.

### New! Resonant Cavity Software (Option 300)

Agilent's new Resonant Cavity software controls an Agilent vector network analyzer to measure the resonant frequency of the loaded and unloaded resonant cavity. A least squares circle fitting technique is used to calculate Q, which uses both magnitude and phase information and is more repeatable than other Q calculation methods. The software then calculates  $\epsilon_1'$ ,  $\epsilon_2''$  and loss tangent and displays them in its easy to use interface.

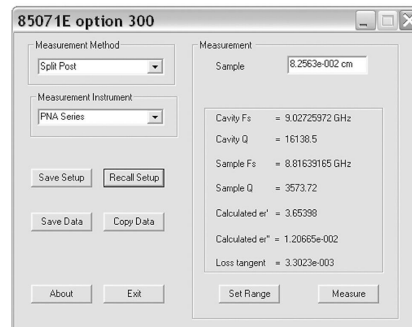


Figure 8. Resonant Cavity Software User Interface

Resonant Cavity Software has a COM applications interface, allowing users to automate measurements easily.

Resonant Cavity Software supports Split Post Dielectric Resonators from QWED. These resonators are high quality and are available in frequencies from 1 GHz to 20 GHz. For more information, please email [info@qwed.com.pl](mailto:info@qwed.com.pl) or visit <http://www.qwed.com.pl/hardware.html>

Resonant Cavity Software also supports ASTM D2520 standard resonators and Agilent 85072A Split Cylinder Resonator.

## Ordering Information

### 85071E Materials Measurement Software

#### Required, but not included:

- Network analyzer (see compatible network analyzers)
- PC (see PC requirements)
- Appropriate fixture for chosen measurement method

#### Required Security Key

- Option UL8 USB Software Security Key

#### Option 100<sup>1</sup>

**Free Space Calibration Option:** Provides Gated Reflect Line calibration technique for free space measurement method.

#### Option 200<sup>1</sup>

**Arch Reflectivity Software:** Provides a separate software program that automates the use of any NRL Arch measurements.

#### Option 300

**Resonant Cavity Software:** Provides a separate software program that automates the resonant cavity measurement technique.

## Upgrades

### 85071EU-071

Upgrade from any older version of 85071 software

### 85071EU-100<sup>1</sup>

Add Free Space calibration option to existing software

### 85071EU-200<sup>1</sup>

Add Arch Reflectivity option to existing software

### 85071EU-300

Add Resonant Cavity option to existing software

## Compatible Network Analyzers

A list of compatible network analyzers can be found on the 8507xE Series Support site at:

<http://na.tm.agilent.com/materials/SupportedVNAs.pdf>

## PC Requirements

- Windows® XP, Windows 7
- Agilent IO Libraries
- DVD Drive or internet connection to load software.

PC is optional for PNA and newer ENA series network analyzers where software can be installed directly on the analyzer. All other analyzers require a PC with a GPIB or LAN interface card. LAN is supported with PNA, newer ENA, and FieldFox models. GPIB is supported with newer PNA and ENA models. Please see: <http://na.tm.agilent.com/materials/SupportedVNAs.pdf> for model number and firmware requirements.

<sup>1</sup>. Requires time domain option installed on network analyzer



## **Ordering Information *continued...***

### **Transmission Line Method Sample Holders**

#### **Waveguide**

Agilent 11644A Series waveguide calibration kits contain a 1/4 wavelength line and a straight section which can be used as sample holders. There are many third-party suppliers as well. Contact Agilent for information on choosing appropriate waveguide sample holders.

#### **Coaxial**

Agilent 8505x Series verification kits contain airlines that can be used as sample holders. There are many third party suppliers as well. Contact Agilent for information on choosing appropriate coax sample holders.

### **Antennas and Fixtures for Free Space and NRL Arch Methods**

Contact Agilent for information on third-party suppliers of free space antennas and fixtures.

### **Cables and Adapters**

Cables and adapters may also be needed to attach sample holders or antennas to the network analyzer. Agilent offers a wide variety of cables and adapters. For more information, visit: [www.agilent.com/find/accessories](http://www.agilent.com/find/accessories)

### **Calibration Kits**

Electronic Calibration (ECal) modules are highly recommended, especially for the PNA Series network analyzer with the 85071E-100 Free Space Calibration Option. For more information about ECal, visit [www.agilent.com/find/ecal](http://www.agilent.com/find/ecal). Agilent also offers a wide variety of mechanical coax and waveguide calibration kits. Contact Agilent for more information and assistance to choose an appropriate calibration technique.

### **Free Trial Demo**

Evaluate a demo version of 85071E Materials Measurement Software for up to two weeks. Visit the Agilent Technologies Web site at [www.agilent.com/find/materials](http://www.agilent.com/find/materials) to download this demo program.

For more information on materials measurement products such as our Dielectric Probe kit, visit us at [www.agilent.com/find/materials](http://www.agilent.com/find/materials)

 **Agilent Email Updates**

[www.agilent.com/find/emailupdates](http://www.agilent.com/find/emailupdates)  
Get the latest information on the products and applications you select.

**Agilent Channel Partners**

[www.agilent.com/find/channelpartners](http://www.agilent.com/find/channelpartners)  
Get the best of both worlds: Agilent's measurement expertise and product breadth, combined with channel partner convenience.



Agilent Advantage Services is committed to your success throughout your equipment's lifetime. To keep you competitive, we continually invest in tools and processes that speed up calibration and repair and reduce your cost of ownership. You can also use Infoline Web Services to manage equipment and services more effectively. By sharing our measurement and service expertise, we help you create the products that change our world.

[www.agilent.com/find/advantageservices](http://www.agilent.com/find/advantageservices)



[www.agilent.com/quality](http://www.agilent.com/quality)

[www.agilent.com](http://www.agilent.com)  
[www.agilent.com/find/materials](http://www.agilent.com/find/materials)  
[www.agilent.com/find/na](http://www.agilent.com/find/na)  
[www.agilent.com/find/ecal](http://www.agilent.com/find/ecal)

For more information on Agilent Technologies' products, applications or services, please contact your local Agilent office. The complete list is available at:

[www.agilent.com/find/contactus](http://www.agilent.com/find/contactus)

**Americas**

Canada	(877) 894 4414
Brazil	(11) 4197 3600
Mexico	01800 5064 800
United States	(800) 829 4444

**Asia Pacific**

Australia	1 800 629 485
China	800 810 0189
Hong Kong	800 938 693
India	1 800 112 929
Japan	0120 (421) 345
Korea	080 769 0800
Malaysia	1 800 888 848
Singapore	1 800 375 8100
Taiwan	0800 047 866
Other AP Countries	(65) 375 8100

**Europe & Middle East**

Belgium	32 (0) 2 404 93 40
Denmark	45 45 80 12 15
Finland	358 (0) 10 855 2100
France	0825 010 700*
	*0.125 €/minute
Germany	49 (0) 7031 464 6333
Ireland	1890 924 204
Israel	972-3-9288-504/544
Italy	39 02 92 60 8484
Netherlands	31 (0) 20 547 2111
Spain	34 (91) 631 3300
Sweden	0200-88 22 55
United Kingdom	44 (0) 118 927 6201

For other unlisted countries:

[www.agilent.com/find/contactus](http://www.agilent.com/find/contactus)

Revised: January 6, 2012

© Agilent Technologies, Inc. 2006, 2011, 2012  
Published in USA, June 14, 2012  
5988-9472EN

